Factors governing rain chemistry and wet deposition at a regional background site in South Africa

L Kok

orcid.org 0000-0003-1695-5963

Thesis accepted in fulfilment of the requirements for the degree *Doctor of Philosophy in Science with Atmospheric Chemistry* at the North-West University

Promoter:	Prof PG van Zyl
Co-promoter:	Prof JP Beukes
Assistant Promoter:	Prof RP Burger

Graduation May 2020

22907149

Water

Is oxygen and hydrogen the divine idea of water?
God put the two together only that man might separate and find them out?
He allows His child to pull his toys to pieces:
but were they made that he might pull them to pieces? ...
A school examiner might see therein the best use of a toy, but not a father!
Find for us what in the constitution of the two gases makes them fit and capable to be thus honored in forming the lovely thing,
and you will give us a revelation about more than water,
namely, about the God who made oxygen and hydrogen.
There is no water in oxygen, there is no water in hydrogen;
it comes bubbling fresh from the imagination of the living God,
rushing from under the great white throne of the glacier.
The very thought of it makes one gasp
with an elemental joy no metaphysician can analyse.
The water itself, that dances and sings, and slakes the wonderful thirst –
symbol and picture of that draught
for which the woman of Samaria made her prayer to Jesus –
this lovely thing itself, whose very witness is a delight to every inch of the human body in its embrace –
this live thing which, if I might, I would have running through my room,
yea, babbling along my table –
this water is its own self, its own truth, and is therein a truth of God.
Let him who would know the truth of the Maker, become sorely athirst,
and drink of the brook by the way –
then lift up his heart –
not at that moment to the Maker of oxygen and hydrogen,
but to the Inventor and Mediator of thirst and water,
that man might foresee a little of what his soul might find in God.
Let a man go to the hillside and let the brook sing to him till he loves it,
and he will find himself far nearer the fountain of truth...
He will draw from the brook the water of joyous tears,
and worship him that made heaven, and earth, and the sea,
and the fountains of waters.

George MacDonald

Unspoken sermons. 3rd Series. 1889

Acknowledgements

My deepest gratitude to my parents, you have been there in every season and in every step, cultivating passion and truth in me with strength, love, and compassion. Dad, thank you for being the mountain you are, my hero. For instilling courage in me, for showing me that nothing is impossible, to find joy and wonder in life and creation, to pursue excellence, to show kindness and to serve where there is a need. Mom, you are my anchor, thank you for always pointing me back to truth and hope. Your love, grace, comfort and strength gives me courage to reach for the sky, knowing there will always be a soft place should I fall. Nandi, my sister and best friend, you inspire me through every season of life. Your determination, perseverance and courage strengthen me to find my own. Thank you for believing in me and for our adventures that fill my heart with much needed love, beauty and nature. To ouma Lulu, oupa Cliff and ouma Byb, thank you for your constant prayers and love that always cover us. May your legacy live on. Thank you to my pastors and church family, you have taught me to keep a Kingdom perspective through it all.

Thank you to my supervisors – Professors Pieter van Zyl and Paul Beukes for the opportunity and funding to pursue my postgraduate studies under your guidance. The Ph.D. journey has been a gift and has shaped me in ways I will continue to discover later in life. Prof. Roelof Burger, thank you for your support and valuable insights.

To my friends and colleagues at the Atmospheric Chemistry Research Group, I will always look back on this time with fond memories shared with you. Dr. Ville Vakkari, thank you for your passionate inputs at Welgegund, encouragement and visits around the braai.

Sincere thank you to Prof. Suria Ellis, I am truly grateful for your kind and patient help with the statistics.

Thank you, Diederik and Jackie Hattingh, for your dedication with the rain sampling.

To the many friends and family who have walked with me in this chapter of life, and to those who have cared for my heart in the seasons leading up to this moment. I am forever grateful for the friends and family God has placed in my life.

My greatest thank you to my Father God, Jesus and the Holy Spirit. Science has always been a passion of mine because I always learn something about You and Your love for me in and through creation. I am learning that Your will is not a map, but a match that sets one on fire. And in finding passion for life, that's where I am most alive and most aware of Your love for me. This Ph.D. journey has taught me so much about surrender, living life for today, seeking You first, and responding to Your love. You have always been right there with me on the mountains and in the valleys.

Your love is so extravagant, it reaches higher than the heavens!

Your faithfulness is so astonishing, it stretches to the skies!

Psalm 108:4

Abstract

Wet deposition is an atmospheric sink that is essential to sustain the Earth-atmosphere biogeochemical balance. Deposited species can either be introduced as nutrients or toxins into a surface environment, which can be either beneficial or detrimental to the health of an ecosystem. Anthropogenic emissions of sulfur- and nitrogen oxides, for example, have been shown to acidify rainwater, which leads to acidification of surface water bodies, leaching of essential nutrients and mobilisation of heavy metals. Rainwater chemistry is generally considered to reflect the impacts of global and regional atmospheric pollution on the environment. The removal of atmospheric species through precipitation is influenced by various factors, which include emission source strengths, ecosystem-specific factors, atmospheric transport, chemical reactivity and physical processes. In-cloud scavenging of gaseous species and particulates in the atmosphere occurs during cloud nucleation and other in-cloud processes, while below-cloud scavenging of atmospheric species takes place during a rain event. The deposition measurements have been identified as a key priority in future atmospheric chemistry research.

South Africa is an important source region of atmospheric pollutants. As the largest industrialised economy in Africa, South Africa contributes 2.5% to global coal consumption, is the 9th largest S-emitting country, has a large NO_2 hotspot over the Mpumalanga Highveld, and is characterised by wide-spread open biomass burning. A few studies have been conducted on the chemical composition of wet deposition in South Africa through the Deposition of Biogeochemically Important Trace Species (DEBITS) project endorsed by the International Global Atmospheric Chemistry (IGAC) project of the Global Atmospheric Watch (GAW) programme of the World Meteorological Organisation (WMO). In this study, rain samples were collected at the Welgegund atmospheric research station, a regional background site in the North-West Province of South Africa. Welgegund was recently included into the renamed African component of DEBITS, i.e. the International Network to study Deposition and Atmospheric chemistry in Africa (INDAAF). Welgegund is situated on a commercial farm on the Highveld of South Africa, approximately 100 km west of the Johannesburg-Pretoria megacity. The site is impacted by air masses passing over the major source regions in the South African interior, as well as a relatively clean region to the west where no large point sources are located. The aim of this study was to identify and determine the major factors governing the chemical composition of rainwater and wet deposition at this regional background site in South Africa, while a novel technique for relating rain chemistry to air mass history was explored. In addition, rain chemistry at Welgegund was also contextualised with the four other DEBITS sites located in the north-eastern interior of South Africa.

A custom-made automated wet-only rain sampler was used to collect rain samples on an event basis. Rain sampling at Welgegund complied with the field protocols of the WMO for precipitation chemistry measurements. Collected rain samples were analysed with a *Dionex* ICS

3000 suppressed ion chromatograph system. Data quality was ensured by complying with the WMO Data Quality Objectives for precipitation chemistry. All analytical techniques were also verified through participation in the bi-annual inter-laboratory comparison study managed by the WMO. Cloud base height (CBH) during the onset of a rain event was measured with a ceilometer, which was related to air mass history by performing back trajectory analyses. In addition, rain intensity was also monitored, while other ancillary measurements continuously performed at Welgegund were also used to assist in elucidating factors influencing the chemical composition of rain. In total, 119 rain samples collected from December 2014 to April 2018 at Welgegund complied with the data quality objectives of the WMO, which represented 89% of all rain events occurring during the sampling period.

Rainwater chemistry and wet deposition fluxes of ionic species determined in rain samples collected at Welgegund indicated that the total ionic concentration of rainwater was similar to two background sites located within proximity of industrial activities. However, the pH of rainwater (4.80) indicated increased neutralisation and was comparable to that determined at two rural background sites. Lower S- and N fluxes at Welgegund compared to the industrially influenced sites were attributed to lower annual average rainfall (573.3 mm). Similar to the four other South African sites, SO_4^{2-} was the most abundant species in rain, with concentrations thereof in the same order determined at the two industrially influenced sites The major source groups influencing rainwater ionic content identified with empirical calculations and explorative statistical analyses included anthropogenic- (industrial), crustal-, marine-, agricultural- and biomass burning sources. A large anthropogenic (industrial) source group contribution to wet deposition chemical composition signified the influence of major source regions in the South African interior impacting Welgegund. Relatively large contributions were also calculated from marine and crustal sources. The influence of agricultural activities was also evident, while biomass burning had the lowest contribution due to open biomass burning occurring mainly during the dry season.

An advanced assessment on large-scale factors influencing the chemical composition of rain in the South African interior was conducted by relating rain events at Welgegund to air mass history at CBH and at arrival heights below clouds (100 m a.g.l.). Air mass histories at CBH reflected the influence of the region where cloud formation occurred on rain chemistry, while 100 m a.g.l. air mass histories indicated the influence of below-cloud scavenging. Hierarchical clustering analyses (HCA) were performed during which two different approaches were followed, i.e. (1) clustering according to the chemical composition of rain that was related to air mass histories at the two air mass arrival heights, and (2) grouping based on air mass histories at 100 m a.g.l. and CBH arrival heights that was associated with chemical composition. In each of these approaches, the optimum solutions yielded three clusters.

Clustering according to the ionic composition of rain events grouped the events together in relation to their total VWM concentrations, i.e. from high to low VWM concentrations. Correlation of air mass histories to the three clusters did indicate, to an extent, that higher VWM concentrations of ionic species in rain were associated with air masses at 100 m a.g.l. passing over anthropogenic source regions. Clustering of air mass histories grouped air masses passing predominantly over pre-defined source regions together, i.e. air masses passing over anthropogenic source regions, a clean western background region and oceans. The rain chemistry associated with clusters determined for air masses at 100 m a.g.l. arrival heights could be related to the influence of different source regions, with, especially, the influence of large point sources, the clean western background sector and oceans evident. Clustering according to the chemical composition of rain and air masses at an arrival height of 100 m a.g.l. did reflect the regional impact of anthropogenic activities in the north-eastern part of South Africa on rain chemistry, while the influence of household combustion was also evident. In addition, these two clustering approaches also indicated higher VWM concentrations of ionic species associated with increased rain intensity. Although air masses arriving at CBH could partially be related to rain chemistry, no significant correlations between air mass histories at CBH and ionic composition of rain were evident. Therefore, it seemed that below-cloud scavenging was more important to the chemical composition of rain samples in this part of South Africa. Although clustering analysis revealed some correlations between air mass history and chemical composition, it emphasised the complexity associated with correlating rain chemistry to sources of atmospheric species.

Rain events were also categorised according to three main synoptic patterns, namely tropical-temperate surface troughs, surface troughs with coastal low pressures, and surface troughs with temperate westerly wave disturbances, in order to investigate the mesoscale influence of the type of convection on rainwater chemistry. Although some association between the type of uplift and the rainwater chemistry was evident, surface flow patterns varied significantly in the specific groups identified.

Case studies were conducted in order to further explore the advantages associated with the availability of CBH height measurements in conjunction with rain sampling. These case studies were chosen in order to support the clustering analyses conducted and illustrate other factors influencing the chemical composition of rain in this part of South Africa that were not clearly indicated by the clustering analyses. These case studies included exploring the influences of anthropogenic source regions, below-cloud scavenging and rain intensity as revealed by statistical analysis, as well as the impacts of pollution build-up and open biomass burning on rain chemistry. The influence of anthropogenic activities in the north-eastern interior of South Africa on the rainwater chemistry was evident and substantiated in these case studies. The influence of below-cloud scavenging on rain chemistry at Welgegund was also signified by investigating the chemical composition of two successive rain events associated with similar air mass histories. In addition,

higher VWM concentrations of ionic species in rain events associated with increased rain intensity, suggested by statistical analysis, were also supported by case studies comparing the rain events with the maximum and highest average rain intensities to the rain event with the lowest average rain intensity. The impact of pollution build-up during winter was also illustrated, with rainfall associated with this period corresponding to higher loading of ionic species. The impact of open biomass burning was also indicated, although the peak open biomass burning and wet seasons in South Africa do not coincide. In addition, it was also shown that long-range transport of species associated with open biomass burning could influence rain chemistry in the South African interior.

Keywords: atmospheric scavenging; cloud base height; rain intensity; hierarchical cluster analyses; grazed-savannah-grassland; Welgegund

Table of Contents

List of Figures

Chapter 2

Chapter 3

Chapter 4

Chapter 5

Chapter 6

Appendix A

Appendix B

Appendix C

List of Tables

Chapter 4

Chapter 5

Chapter 6

Abbreviations

ACRG	Atmospheric Chemistry Research Group
ACSM	Aerosol Chemical Specification Monitor
AE	Anionic equivalents
AF	Amersfoort
a.g.l.	Above ground level
Al	Aluminium
APD	Avalanche photodiode
AQ	Air quality
ARL	Air Resource Laboratory
Ca^{2+}	Calcium
$CaCO_3$	Calcium carbonate/Calcite
CBH	Cloud base height
CCN	Cloud condensation nuclei
Cd	Cadmium
CE	Cationic equivalents
CE'	Coalescence efficiency
CEC	Cation exchange capacity
CFCs	Chlorofluorocarbons
CH_3COO^-	Acetic acid
$C_3H_5O_2^-$	Propionic acid
CH_3SH	Methyl mercaptan
CIESIN	Centre for International Earth Science Information Network
CL	Coastal low pressure
Cl^-	Chloride
CN	Condensation nuclei
CO_2	Carbon dioxide
$C_2O_4^-$	Oxalic acid
CO	Carbon monoxide
COOH	Carboxylic acid
COS	Carbonyl sulfide
CS_2	Carbon disulphide
DAAC	Distributed Active Archive Centers
DEBITS	Deposition of Biogeochemically Important Trace Species
DMS	Dimethyl sulfide
E	Collision efficiency
EBC	Eastern Busveld Complex
eBC	Equivalent black carbon
EC	Electrical conductivity
E_c	Collecting efficiency
EF	Enrichment factor

EOS	Earth Observation System
FMI	Finnish Meteorological Institute
GAW	Global Atmospheric Watch
GAW-PCP	Global Atmospheric Watch- Precipitation Chemistry Program
GCCN	Giant cloud condensation nuclei
GDAS	Global Data Assimilation System
HCA	Hierarchical cluster analysis
HCO_3^-	Bicarbonate
H_2CO_3	Carbonic acid
$HCOO^-$	Formic acid
HDPE	High-density polyethelyne
Hg	Mercury
HNO_3	Nitric acid
H_2O_2	Hydrogen peroxide
HONO	Nitrous acid
H_2S	Hydrogen sulfide
H_2SO_4	Sulphuric acid
HYSPLIT	Hybrid Single-Particle Lagrangian Integrated Trajectory
IC	Ion chromatography
ID	Ion difference
IGAC	International Global Atmospheric Chemistry
IN	Ice nuclei
INDAAF	International Network to study Deposition and Atmospheric chemistry in Africa
InGaAs	Indium gallium arsenide
IR	Infrared
IQR	Interquartile range
IVOC	Intermediate volatility organic compound
JHB-PTA	Johannesburg-Pretoria Metropolitan
K^+	Potassium
KCl	Potassium chloride
KOH	Potassium hydroxide
Lidar	Light detection and ranging
LIS	Inter-laboratory comparison study
LT	Louis Trichardt
LWC	Liquid water content
mA	Measured acidity
megaC	Johannesburg-Pretoria megacity
Mg^{2+}	Magnesium
MODIS	Moderate Resolution Imaging Spectrometer
MpHV	Mpumalanga Highveld
MSA	Methane sulfonic acid
N	Nitrogen
Na^+	Sodium

NASA	National Aeronautics and Space Administration
NCEP	National Centre for Environmental Prediction
NF	Neutralisation factor
NH_2	Amide
NH_3	Ammonia
NH_4^+	Ammonium
$(NH_4)_2SO_4$	Ammonium sulfate
NH_4HSO_4	Ammonium bisulphate
NH_4NO_3	Ammonium nitrate
NO_3^-	Nitrate
NO	Nitric oxide
NO_2	Nitrogen dioxide
N_2O_5	Dinitrogen pentoxide
NO·	Nitrate radical
NOx	Nitrogen oxides
NOAA	National Oceanic and Atmospheric Administration
nSSF	Non-sea salt fraction
NUE	Nitrogen use efficiency
NWU	North-West University
O_3	Ozone
OA	Organic acids
OA*	Dissociated organic acids
OH·	Hydroxyl radical
P	Pressure
pA	Acidic potential
Pb	Lead
PBL	Planetary boundary layer
PCA	Principal component analysis
PCL	Precipitation covering length
PM	Particulate matter
PO_4^{2-}	Phosphate
ppb	Parts per billion
RF	Radiative forcing
RH	Relative humidity
S	Sulfur
SAWS	South African Weather Service
Sb	Antimony
SK	Skukuza
SO_4^{2-}	Sulfate
SO_2	Sulfur dioxide
SOx	Sulfur oxides
SOA	Secondary organic aerosol
SSF	Sea salt fraction

ST	Surface trough
T	Temperature
tOA/tOA*	Total organic acids/Total dissociated organic acids
TiO_2	Titanium oxide
TOC	Total organic carbon
TP	Total precipitation
UH	University of Helsinki
$\mu eq.L^{-1}$	Micro-equivalents per litre
VOC	Volatile organic compound
VT	Vaal Triangle
VWM	Volume weighted mean
WBC	Western Bushveld Complex
WHO	World Health Organization
WMO	World Meteorological Organization
WD	Wind direction
Wr	Washout ratio
WS	Wind speed
WW	Westerly waves

Chapter 1

Introduction, Motivation & Objectives

In this chapter, a brief introduction and motivation are presented in order to contextualise this study in relation to wet deposition studies in southern Africa. Precipitation processes and the associated scavenging processes that lead to rainwater composition are spread over a vast scale ranging from the microscopic (10^{-6} m) to the synoptic scale (10^{6} m). An overview of the processes that typically influence rainwater composition in this region, together with existing uncertainties associated with rain chemistry in southern Africa, is given. The Welgegund atmospheric research station, recently included in the International Network to study Deposition and Atmospheric chemistry in Africa (INDAAF), is also introduced as a unique background site to assess rain chemistry in the South African interior, while the benefits of comprehensive ancillary measurements conducted at this site are indicated. Finally, in view of the background and motivation presented for this study, the general aim and specific objectives are also listed.

1.1 Introduction

Deposition of chemical species onto the surface of the Earth through wet and dry processes are essential to sustain the earth-atmosphere biogeochemical balance by removing aerosols and gaseous species from the atmosphere (Galy-Lacaux et al., 2009; Laouali et al., 2012; Akpo et al., 2015). During wet deposition, atmospheric species are taken up into moisture and clouds in the atmosphere and are returned to the Earth's surface through precipitation processes (WMO, 2004; Galy-Lacaux et al., 2009). Precipitation chemistry plays an integral role in understanding the temporal and spatial evolution of atmospheric processes, as well as the influence of anthropogenic activities on the atmospheric composition. In addition, it also reflects impacts associated with global environmental threats such as climate change and acidification (Galy-Lacaux et al., 2009; Laouali et al., 2012, Vet et al., 2014). A recent comprehensive assessment of atmospheric deposition of biogeochemically important compounds and precipitation chemistry placed new emphasis on the importance of deposition measurements (Vet et al., 2014), which is also identified by the National Academies of Sciences, Engineering and Medicine in the United States as one of the key priorities for future atmospheric chemistry research (National Academies of Sciences Engineering and Medicine, 2016).

Deposition of atmospheric species can be beneficial or detrimental to ecosystems, since nutrients or toxic compounds affecting the nutrient levels, the pH, fertility and general health of the environment can be introduced into terrestrial and aquatic ecosystems (Mphepya et al., 2006; Pauliquevis et al., 2012; Vet et al., 2014). Certain pollutants have an acidifying effect on rainwater through the formation of acidic species, which mainly include sulfuric- (H_2SO_4), nitric- (HNO_3), hydrochloric- (HCl) and organic acids (Evans et al., 2011). In general, the main cause of acid rain formation has been the emission of sulfur (S) and nitrogen (N) compounds such as S- and N oxides (SO_x and NO_x) into the atmosphere from anthropogenic sources, which include fossil fuel combustion, transport, industry and agriculture. Globally, sulfuric acid is considered the most important acidifying species (Rodhe et al., 2002; Conradie et al., 2016), while the influence of nitric acid on rainwater acidity has also increased in China and Northern America in recent years (Vet et al., 2014; Xiao, 2016). Acid rain contributes to acidification of surface water bodies, soil and vegetation (Bravo et al., 2000), which could lead to leaching of essential nutrients and the mobilisation of heavy metals (Krug and Frink, 1983; Schindler, 1988; Eby, 2004). Basic atmospheric species such as calcium (Ca), magnesium (Mg) and ammonium (NH_4^+) are, however, capable of neutralising acidic precipitation or even favour alkaline rainwater composition (Galy-Lacaux et al., 2009; Conradie et al., 2016).

The chemical composition of precipitation is affected by physical and chemical factors on different scales ranging from the dynamic synoptic framework, the mesoscale characteristics of a storm or rainfall event, and the microscopic processes in the atmosphere and clouds. Rainwater composition is controlled by various ecosystem-specific and complex factors. Locally, ecosystem-specific characteristics, which contribute to the available nuclei, and geographical features, such as the soil type and distance from the ocean will affect the ionic content of precipitation (Garstang et al., 1996; Galy-Lacaux et al., 2009; Li et al., 2011). In addition, several aerosols can undergo long-range transportation and act as condensation nuclei in a region other than where they were emitted (Garstang et al., 1996; McGranahan and Murray, 2003). Precipitation chemistry is also influenced by various complex processes in the earth-atmosphere water cycle (Hall, 2003; Pauliquevis et al., 2012), while the temporal and spatial evolution of air masses also influences the chemical composition of rain (Lutgens and Tarbuck, 1982; Akpo et al., 2015; Fedkin et al., 2019; Uchiyama et al., 2019). These processes include factors on various scales - emissions, chemical reactions and transport of species, as well as droplet and cloud nucleation, microphysical droplet interactions, cloud mechanics and scavenging during the precipitation event (Al-Khashman, 2009; Zhang et al., 2012).

Water-soluble chemical compounds can be introduced into droplets during nucleation, cloud formation or during the precipitation event. Typical condensation nuclei (CN) include dust, sea salt, sulfates (SO_4^{2-}) and organic species (Wallace and Hobbs, 2006b; Christner et al., 2008; Feltracco et al., 2019; Uchiyama et al., 2019). These CN species can either be primarily emitted from local sources or can be formed as secondary particulates in the atmosphere (e.g. gas-to-particle conversion), which can be associated with long-range transport of air masses (Seinfeld and Pandis, 2006; Wallace and Hobbs, 2006b; Orué et al., 2019). After a cloud is formed, in-cloud mixing occurs between different droplets, while various aqueous reactions take place that can be catalysed by species in interstitial cloud air (Brimblecombe, 2003; Hall, 2003; Pauliquevis et al., 2012). In-cloud reactions such as the formation of SO_4^{2-} increase the average aerosol size, which can increase the droplet size distribution (Schmeller and Geresdi, 2019). The inclusion of particulates or gaseous species into a cloud or rain droplet is referred to as scavenging, which can occur through various processes. In-cloud scavenging entails the absorption of species into the droplet during droplet formation (rainout) and from the interstitial atmosphere (washout), which is dependent on the droplet size spectra and total droplet surface area, as well as on the solubility, concentration, size and size distribution of the species being scavenged. Typical below-cloud scavenging processes include collision-coalescence, sweep-out, and wake capture (which are influenced by Brownian and turbulent shear diffusion, as well as the Bernoulli Effect), and the chemical scavenging processes of diffusio- and thermophoresis (Urone, 2001; Hall, 2003). Scavenging efficiency depends on numerous factors, which include terminal velocity of the raindrops, collision efficiency, diffusivity, raindrop and particle size distributions, solubility and concentration of the particle or gas being scavenged, the electric field and polarisation, and rain intensity. Smaller droplets, for instance, will scavenge more efficiently due to slower terminal velocities and larger mass transfer coefficients (Lutgens and Tarbuck, 1982; Preston-Whyte and Tyson, 1988; Hall, 2003; Chate and Pranesha, 2004; Bae et al., 2006; Pauliquevis et al., 2012; Xu et al., 2017), while higher scavenging ratios are also associated with larger particles and increased rain intensity (Kulshrestha et al., 2009; González and Aristizábal, 2012). Modelling studies have shown that an increase in in-cloud turbulence increases rainfall rate, which then increases particle-droplet collision rates (Lynn et al., 2005b; González and Aristizábal, 2012). In light of the above mentioned importance of wet deposition studies and the complex factors that influence rainwater chemistry, the motivation for this study is discussed in the following section.

1.2 Motivation

South Africa has the largest industrialised economy in Africa and is an important source region of atmospheric pollutants (Meth, 2018; UNIDO, 2018). It is estimated that South Africa contributes approximately 2.5% to global coal consumption (Yao et al., 2015), while it is also regarded as the 9th largest emitter of S (Stern, 2006). Satellite images also reveal a clear nitrogen dioxide (NO_2) hotspot over the Mpumalanga Highveld, which is mainly attributed to a cluster of 12 coal-fired power stations located in this region (Lourens et al., 2012). Recent satellite images retrieved from TROPOMI on the European Space Agency's Sentinel 5P satellite again highlighted the extent of pollution in this region (Meth, 2018). High S- and N- emissions in South Africa stem from most industries not employing de-SO_x and de-NO_x abatement technologies (Scorgie, 2012; Tiitta et al., 2014). Southern Africa is also characterised by the occurrence of widespread open biomass burning, which is an important source of atmospheric pollutants in this region. Chiloane et al. (2017) recently indicated the significant contribution of open biomass burning to atmospheric organic species in the north-eastern part of the South African Highveld.

Limited studies have been conducted on the chemical composition of wet deposition for South Africa. A recent study by Conradie et al. (2016) reported on the chemical composition of rainwater collected from 2009 to 2014 at four regional background sites considered to be representative of the north-eastern interior of South Africa, i.e. two sites within proximity of industrial activities (Amersfoort and Vaal Triangle) and two rural sites (Louis Trichardt and Skukuza). Measurements at these sites were conducted within the framework of the long-term monitoring of biogeochemical species in the subtropics network established through the Deposition of Biogeochemically Important Trace Species (DEBITS) task, which is endorsed by the International Global Atmospheric Chemistry (IGAC) programme of the Global Atmosphere Watch (GAW) network of the World Meteorological Organisation (WMO) (Lacaux et al., 2003). Conradie et al. (2016) also compared rainwater composition and wet deposition fluxes to a previous study conducted by Mphepya et al. (2004, 2006) at three of these South African DEBITS sites, which indicated an increase in S- and N- wet deposition fluxes as well as rain events with lower pH from 1986 to 2014. Conradie et al. (2016) and Mphepya et al. (2004, 2006) also identified five main source groups influencing rainwater composition at the South African DEBITS sites, i.e. marine sources, terrigenous sources, fossil fuels, agriculture and biomass burning.

Rainwater collection was discontinued at the four South African DEBITS sites in 2015 due to financial constraints. However, in 2014, Welgegund – a comprehensively equipped regional background atmospheric measurement station impacted by the major source regions in the South African interior – was included in the DEBITS network under the

renamed African component of the DEBITS task, i.e. the International Network to study Deposition and Atmospheric chemistry in Africa (INDAAF) network (Swartz, 2019). The Welgegund atmospheric monitoring station is a regional background site located in the Highveld of South Africa, approximately 100 km west of the Johannesburg-Pretoria conurbation. It is located on a commercial farm with no large local point sources in the proximity. It is, however, impacted by air masses passing over the major source regions in the South African interior. These source regions include: (1) the western Bushveld Igneous Complex, where a large number of pyrometallurgical smelters are located; (2) the Mpumalanga Highveld, where 12 coal-fired power stations, a large petrochemical industry and other industries are located; (3) the Johannesburg-Pretoria conurbation with a population of > 10 million people; and (4) the densely populated and highly industrialised Vaal Triangle, holding numerous industries including a large petrochemical smelter. In addition, Welgegund is also influenced by a relatively clean region to the west where no large point sources are located (Beukes et al., 2013; Tiitta et al., 2014). Air masses impacting Welgegund are considered to be aged air masses in which atmospheric pollutants had sufficient time to be oxidised or react (Tiitta et al., 2014) through the anticyclonic recirculation of air masses over the South African Highveld (Preston-Whyte and Tyson, 1988; Zunckel et al., 2000).

Although back trajectory analyses were conducted by Conradie et al. (2016) to substantiate the influences of sources on rain chemistry at the four sites, back trajectories could not be optimally utilised to determine the influence of air mass histories on individual rain events due to logistical constraints. These four sites were remote, with site operators only logging dates when rain samples were collected with the wet-only samplers and not the exact beginning/end times of rain events. In addition, these sites were also only equipped with the basic logistically feasible instrumentation required for deposition studies, which included measurements of monthly concentrations of inorganic gaseous species (SO_2, NO_2, O_3 and NH_3) with passive samplers, while aerosol samples were collected once a month. However, Welgegund is a comprehensively equipped atmospheric monitoring station where *in situ* measurements of several atmospheric parameters are conducted, which allows advanced assessment of precipitation chemistry (Beukes et al., 2015; welgegund.org). Relating the chemical composition of rain samples to air mass history can be improved by specific measurements including vertical profiling of the atmosphere and a rain intensity meter. Vertical profiles can be used to determine cloud base height during the onset of a rain event, which can be associated with air mass history in order to evaluate the influence of source regions on specific rain events. In addition, other ancillary measurements could also assist with an improved understanding of the chemical composition of rain. These

include measurements of gaseous species and particulate matter, as well as meteorological parameters.

1.3 Aim & Objectives

The general aim of this study is to identify and determine the influence of large-scale factors governing the chemical composition of rainwater and wet deposition at a regional background site in South Africa. A novel technique for relating rain chemistry to air mass history will be explored in this study. The general aim of the study will be met through the following specific objectives:

- Determine the chemical composition of rainwater, as well as sulfur- (S) and nitrogen (N) wet deposition fluxes at the Welgegund atmospheric monitoring station over the period of three rain seasons, while also relating wet deposition chemistry at Welgegund to the other South African sites where wet deposition studies have been conducted.
- Determine the major sources of ionic species at Welgegund through empirical and explorative statistical methods
- Develop a novel method to relate below-cloud air mass history and air mass history associated with precipitating clouds to the rainwater chemistry at Welgegund.
- Conduct an advanced assessment of large-scale factors influencing chemical composition of rain in the South African interior by relating individual rain events to *in situ* measurements conducted at Welgegund and to air mass histories associated with precipitating clouds and with the below-cloud air masses through statistical clustering analyses; and determine whether using crude back trajectories is a viable method to relate air mass history to the variability in rainwater chemistry.
- Relate the rainwater chemistry to rain event day synoptic patterns.
- Perform specific case studies of rain events in order to further assess the influence of air mass histories at cloud base height (in-cloud scavenging) and below clouds (below-cloud scavenging) on rain chemistry.

1.4 Thesis Outline

This thesis comprises the following chapters:

Chapter 1

Introduction, motivation, aim and objectives.

Chapter 2

A thorough literature study on rainwater chemistry and wet deposition will be conducted with the main topics including condensation nuclei properties, in-cloud chemical and physical processes, precipitation and below-cloud scavenging processes, fundamental chemical reactions of ionic species in rain, rainwater acidity, as well as the South African context in terms of meteorology, precipitation studies and air quality.

Chapter 3

A sampling site description and the main experimental methods used in this study are presented. Empirical and statistical methods employed in this study are also discussed, while calculation of air mass histories is also described.

Chapter 4

This is the first results chapter presenting the general chemical composition of rainwater, as well as S and N wet deposition fluxes at Welgegund over the period of three rain seasons, while wet deposition chemistry at Welgegund is also contextualised with other South African sites. Source contributions determined with empirical and explorative statistical methods are also presented.

Chapter 5

This second results chapter presents an advanced assessment of large-scale factors influencing chemical composition of rain in the South African interior by relating individual rain events at Welgegund to air mass histories at cloud base height and below-cloud arrival height through statistical clustering, while also evaluating the relationship between ancillary measurements and synoptic patterns on ionic composition.

Chapter 6

The third results chapter presents specific case studies of rain events in order to substantiate the influence of anthropogenic source regions and below-cloud scavenging on rain chemistry, as well as to indicate the influence of pollution build-up, open biomass burning and rain intensity on the chemical composition of rain.

Chapter 7

An evaluation of the successes and shortcomings of the study is presented, while a few future perspectives are also indicated.

Chapter 2

Literature Review

This literature review chapter aims to present a thorough review of the literature on the processes that ultimately lead to the rainwater chemical composition and wet deposition fluxes. The relationship between atmospheric moisture and the dissolute chemical components therein is explored as it develops throughout the physical and chemical transformation of atmospheric moisture. The concept of scavenging as the physical and chemical pathway through which atmospheric moisture collects chemical components and scrubs the lower atmosphere is discussed in the literature review. Scavenging processes are categorised into nucleation-, in-cloud and below-cloud scavenging. The formation of water droplets through condensation and the subsequent formation of clouds are explored with a perspective on the chemical properties of the cloud condensation nuclei (CCN). In-cloud scavenging is discussed next, while recognising the complex role of cloud microphysics and droplet growth in different cloud environments. Scavenging of interstitial gases and aqueous reactions further develop the cloud water chemistry. Aqueous and oxidation reactions are promoted in the cloud environment. The size and nature of the droplets and of the chemical species determine the scavenging efficiency through warm and cold cloud processes. The below-cloud scavenging efficiency is dependent on the physical properties of the falling rain such as rain intensity, -drop size and -drop size distributions, as well as on the physical and chemical properties of the below-cloud atmosphere. The composition of the below-cloud atmosphere is influenced by emissions from natural and anthropogenic sources and air mass history. The properties of various chemical components have been found to not only affect the efficiency whereby the component can be scavenged by droplets but also affect cloud lifetimes, -mixing, -saturation, -droplet size distributions etc. The chemistry of prominent species contributing to rainwater composition and acidity investigated in this study is discussed in terms of common emission sources. These species are sulfate (SO_4^{2-}), nitrate (NO_3^-), ammonium (NH_4^+), calcium (Ca^{2+}), potassium (K^+), magnesium (Mg^{2+}), sodium (Na^+), chloride (Cl^-), and oxalic- ($C_2O_4^-$), formic- ($HCOO^-$), acetic- (CH_3COO^-), and propionic ($C_3H_5O_2^-$) acids. South Africa has distinct wet and dry seasons. Anticyclonic recirculation and ageing of air masses, as well as stable inversion layers influence the chemical composition of the atmosphere and scavenging efficiency over the plateau. Tropical-Temperate troughs play a dominant role in rainfall formation over the Highveld and rain is mostly convective with thunderstorms and relatively high rain intensities.

2.1 Introduction to Scavenging

The removal of biogeochemical compounds from the atmosphere through deposition during precipitation, together with dry deposition of gaseous species and aerosols, balances the biogeochemical budget in the atmosphere (Laouali et al., 2012). Dry deposition is the dry removal of gaseous compounds and aerosols, while wet deposition indicates the scavenging of species from the atmosphere through moisture. Scavenging is the process whereby particles and gases in the atmosphere are included in a water droplet (Hall, 2003; Pauliquevis et al., 2012). Chemical species deposited through rain are scavenged during droplet nucleation, in the cloud environment and through precipitation (Hall, 2003; WMO, 2004). Scavenging describes the processes whereby precipitation acts as a significant atmospheric sink and contributes to maintaining the earth-atmosphere balance. The removal of chemical species through deposition is directly related to the ambient concentration of those species. Therefore, deposition can give an indication of the current chemical state of the atmosphere, as well as the anthropogenic contribution to it (Özsoy et al., 2008; Yang et al., 2012), with rainwater chemistry and wet deposition fluxes being measurable endpoints of the scavenging processes of atmospheric moisture (Hall, 2003; Pauliquevis et al., 2012). Scavenging is dependent on various physical and chemical properties of both the water droplet and the particle or gas being scavenged. Hall (2003) described scavenging processes as a function of space, time, precipitation characteristics, the concentration, distribution and solubility of the gas- and aerosol species being scavenged.

The stages of scavenging can be classified as nucleation, in-cloud and below-cloud scavenging. Nucleation scavenging or rainout includes the process of moisture condensation around a particle or cloud condensation nuclei (CCN). Throughout this study, the terms condensation nuclei (CN) and cloud condensation nuclei (CCN) are used interchangeably to refer to the process of moisture condensation onto a particle. Aerosols play a central role in the nucleation of cloud drops. The in-cloud scavenging of chemical species in the interstitial air of the cloud is termed washout (Johnson, 1982; Critchfield, 1983; Brimblecombe, 2003; Hall, 2003; Pauliquevis et al., 2012; Uchiyama et al., 2019). Smaller cloud droplets will scavenge gases more efficiently due to larger mass transfer coefficients and total surface area (Lutgens and Tarbuck, 1982; Preston-Whyte and Tyson, 1988; Hall, 2003; Chate and Pranesha, 2004; Bae et al., 2006; Pauliquevis et al., 2012; Xu et al., 2017). Below-cloud scavenging occurs when particles are included in falling raindrops through both physical collision and chemical diffusion. Larger raindrop- and particle sizes are associated with higher below cloud scavenging ratios (Kulshrestha et al., 2009; González and Aristizábal, 2012). Below-cloud scavenging processes include collision-

coalescence, sweepout, and wake capture (Lutgens and Tarbuck, 1982; Preston-Whyte and Tyson, 1988; Hall, 2003). A general depiction of nucleation-, in-cloud and below-cloud scavenging is given in Figure 2.1 (Hall, 2003). Wet deposition, through scavenging processes, contributes the most to the removal of chemical species from the air (GESAMP, 1985; Seinfeld and Pandis, 2006; Orué et al., 2019). The scavenging processes are described in more detail hereafter.

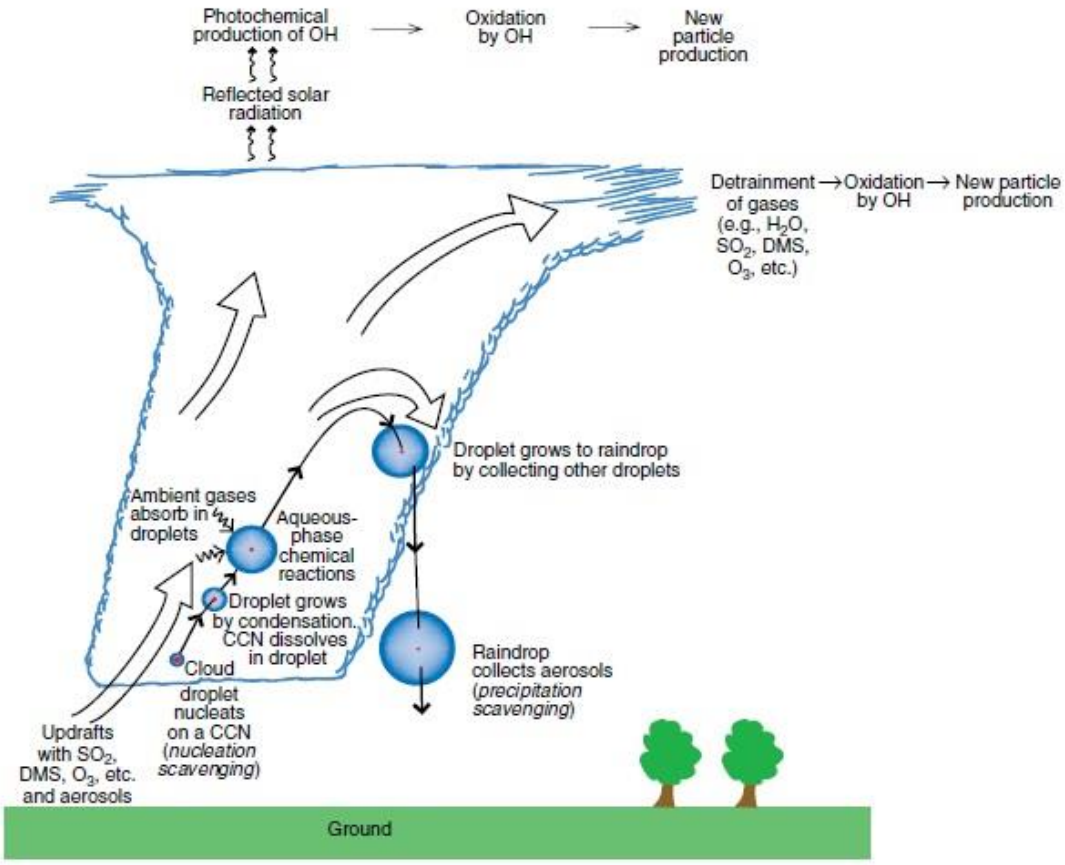

Figure 2.1 The scavenging of atmospheric species through nucleation-, in-cloud and below-cloud scavenging. Droplets nucleate around CCN emitted from various natural and anthropogenic emission sources which determine the initial cloud droplet spectra. In-cloud scavenging includes absorption of gases into droplets through the warm- and cold cloud processes of droplet growth. In the cloud, aqueous reactions are also catalysed. Droplets can evaporate and release scavenged species into the upper atmosphere where photochemical reactions and oxidation can trigger new particle formation and convection. Raindrops further scavenge chemical species from the atmosphere through below-cloud scavenging (Hall, 2003).

2.1.1 Maintaining perspective on scale

The processes that ultimately determine rainwater composition are spread over a vast scale ranging from the microscopic (10^{-6} m) to the synoptic scale (10^{6} m). The synoptic situation presents a dynamic framework for cloud formation. The air mass history is influenced by the progression of synoptic patterns and air flow such as the recirculation of air masses over the interior, which will affect the extent of pollution and pollution build-up in the inflow region of convection processes (Garstang et al., 1996; Ross et al., 2003). The type of convection, wind shear and instability can lead to isolated, multicell, or widespread embedded convection. The temperature and moisture associated with the synoptic patterns will determine the cloud base height (Wallace and Hobbs, 2006b). On the mesoscale, the position of convection and associated rainstorms will determine the inflow and outflow regions, which can interact with other storm systems nearby and can trigger new convection. On the microscale, warm and cold cloud microphysical processes are influenced by the cloud droplet size and spectra, as well as the chemical and physical properties of CCN and interstitial gases (Rauber and Tokay, 1991; 2000; Wallace and Hobbs, 2006b). The chemical and physical properties of the aerosols also have feedback effects on clouds (McFiggans et al., 2005; Rosenfeld et al., 2014). Polluted air masses can influence the droplet nucleation, the initial droplet spectra and can ultimately change the dominant rainfall process (small particles will favour small droplets and ice processes and giant cloud condensation nuclei favour large droplet formation and warm cloud processes). Polluted air masses can directly impact the radiation balance and layers of pollution can even change the thermodynamic structure of the atmosphere, which can impact cloud formation. Aerosols also influence the radiative properties of clouds through altering the droplet spectra. These feedback effects have a confounding effect on rainfall chemistry (Wallace and Hobbs, 2006b; 2006a).

2.2 Nucleation Scavenging

Nucleation scavenging, or rainout, involves the collecting of the nuclei during the initial droplet condensation onto CCN and throughout the cloud during its lifetime (Figure 2.1) (Hall, 2003; Wallace and Hobbs, 2006b; Pauliquevis et al., 2012). Approximately 4% of the total available atmospheric water is contained in clouds at any given moment (Brimblecombe, 2003). Spontaneous nucleation of water droplets from ambient moisture, without the presence of CN, can only occur when the relative humidity (RH) increases by several hundred percent when an air mass rapidly expands. When air parcels rise, expand and cool adiabatically, a super-saturation of the liquid water content of the air is achieved. Hygroscopic aerosols will deliquesce at a high RH. Depending on the updraft velocity and CCN spectra, a certain supersaturation will be reached. Only a fraction of the available CCN population is activated and continues to grow through condensation. Homogenous nucleation rarely occurs in nature (Wallace and Hobbs, 2006b).

CCN are certain types of aerosols that are conducive to droplet formation in clouds with typical supersaturations of 0.1-1%. The CCN composition and characteristics can influence the droplet surface tension and total surface area and either contribute to or inhibit the droplet growth. When CCN exhibit hygroscopic properties, condensation can occur above dew point temperatures and below 100% RH (Preston-Whyte and Tyson, 1988; Roberts, 2003). This is called the solute effect (Critchfield, 1983; Preston-Whyte and Tyson, 1988; Brimblecombe, 2003; Wallace and Hobbs, 2006b). Once the droplets are deliquesced, the droplet growth is dependent on the solute concentration and droplet surface curvature. The surface tension of the water droplet associated with the curvature of its form, influenced by the type of CN, has to be overcome by a sufficient vapour pressure (greater than the saturation vapour pressure for a plane surface) in order for the droplet to grow. The surface energy of a liquid is equal to the value of its surface tension. Energetically, the formation of liquid droplets is not favourable under subsaturated conditions. This is known as the curvature effect (Abraham, 1974; Critchfield, 1983; Preston-Whyte and Tyson, 1988). Hydrophilic CCN allow for a liquid film to condense onto their surface at a much lower supersaturation than nuclei with hydrophobic characteristics (Critchfield, 1983; Rosenfeld et al., 2012). Solution droplets form when condensation occurs around soluble nuclei such as sodium chloride (NaCl) and ammonium sulfate ($(NH_4)_2SO_4$). A solution droplet will have a lower saturation vapour pressure around the droplet than a droplet of pure water, which enhances droplet growth. Raoult's law describes the fractional reduction in vapour pressure adjacent to a solution droplet (Critchfield, 1983; Brimblecombe, 2003; Wallace and Hobbs, 2006b; Wex et al., 2008). The maximum supersaturation depends on the updraft velocity

and the CCN spectra. This will cause droplets larger than the critical size to be activated (Abraham, 1974; Preston-Whyte and Tyson, 1988).

CCN are classified according to their size, which can range from $1x10^{-4}$ to 100 μm, as small or Aitken nuclei, large and giant CCN (GCCN) (Pruppacher and Klett, 1997; Wallace and Hobbs, 2006b). The size of the initial CCN aerosol plays a role in the rate at which a cloud droplet will form and grow into a droplet large enough to fall as precipitation (Johnson, 1982; Yin et al., 2000; Dusek et al., 2006). The larger the CCN particle, the easier the surface is wettable. Atmospheric aerosols require activation to act as CCN (McFiggans et al., 2005). For two particles of equal size, the vapour supersaturation at which they will be activated is dependent on the chemical composition (Dusek et al., 2006). If the particle has a higher solubility, the ambient supersaturation required for it to serve as CCN is lower (Johnson, 1982; Brimblecombe and Dawson, 1984; Brimblecombe, 2003; Wallace and Hobbs, 2006b).

The type and amount of nucleators found in the ambient air are dependent on the local ecosystem and emission sources, long-range transport of air masses, topography, climate, season and existing cloud water chemistry (Christner et al., 2008). Continental air parcels measured near to the Earth's surface have been shown to contain more significant concentrations of CCN and GCCN than marine air masses (Yin et al., 2000; Wallace and Hobbs, 2006b). The CCN concentration remains relatively the same with increasing altitude in marine air masses, whereas the continental concentration has been shown to decrease with height. The continental concentration above the boundary layer is smaller than near the surface of the Earth by approximately a factor of 5. The increased concentrations over continents can be ascribed to soil and dust particles, biomass burning events and anthropogenic activities emitting CCN (Wallace and Hobbs, 2006b).

CCN have feedback effects that influence the droplet- spectra and concentrations of clouds. Cumulus clouds over the ocean, where less CCN is typically present, rarely have droplet concentrations greater than 200 cm^{-3}, in contrast with cumulus clouds over the continent, which can have droplet concentrations of more than 900 cm^{-3}. The liquid water content (LWC) does not differ greatly for these clouds, and the higher droplet concentrations in continental clouds are reflected by much smaller droplet radii and a narrower droplet size distribution. Because of the smaller size of the droplets, they are easily evaporated into non-saturated air at the cloud boundary, which makes the cloud boundaries much better defined than for marine clouds (Wallace and Hobbs, 2006b). Continental and pollutant air masses have been shown to eventually change the dynamical frame of convective storms, leading to stronger updrafts, higher tops, and a shift to cold precipitation processes (Rosenfeld et al., 2014).

During nucleation scavenging, the chemical composition of the droplet is inherently affected. CCN can be organic, inorganic or biochemical. Electrolytic salts are more effective as CCN as they lower the vapour pressure over the droplet, making smaller droplets more resistant to evaporation soon after formation (Brimblecombe, 2003). Common CCN include sulfuric acid (H_2SO_4), ammonium sulfate ($(NH_4)_2SO_4$), sea salt and certain organic species (Brimblecombe, 2003). Dust and other particles, though less hygroscopic, can also act as CCN in more saturated air. Nitric acid (HNO_3) condensation onto dust particles make them more soluble and deposition of these particles become much more efficient. Anthropogenic activities and biomass burning that emit nitrate (NO_3^-) can increase the CCN properties of natural mineral dust (Karydis et al., 2017). Bio-aerosols such as amino acids are released through plankton activity as well as through biomass burning (Feltracco et al., 2019). Amino acids (containing amide ($-NH_2$) and carboxyl (-COOH) functional groups) are hygroscopic and can, therefore, enhance droplet growth (Feltracco et al., 2019). According to Wallace and Hobbs (2006b), 80% of particles emitted from diesel combustion are active as CCN at a 1% supersaturation. A diurnal variation has been noted in CCN concentrations with a maximum measured at around 6 p.m. Particle formation, especially gas to particle conversion through photolytic reactions, can be a contributing factor to the peak in CCN at 6 p.m. (Wallace and Hobbs, 2006b). Particles such as dimethyl sulfide (DMS) and methane sulfonic acid (MSA) are converted to sulfate in the atmosphere and are prominent CCN (Shallcross et al., 2003; Stefels et al., 2007). Hygroscopic particles such as sodium chloride (NaCl), silver iodide, cupric sulfide and metaldehyde have been tested and used for cloud modification or cloud seeding (Wallace and Hobbs, 2006b). In one study by Lompar et al. (2018), the use of the anthropogenic TiO_2/NaCl enhanced precipitation by 30% compared to natural conditions. Many pollutants are hygroscopic and therefore act as CCN, while also having a stabilisation effect on the droplet. When pollutants or CCN particles have an oily nature, they can further stabilise the droplet by deferring dispersion and evaporation (Critchfield, 1983). Salts in the initial droplet decreases the water vapour pressure and thereby increases the droplet stability by preventing evaporation (Brimblecombe, 2003).

The size and type of CCN are possibly also related to the type of rainfall event that follows. The urban environment of Tokyo, Japan, was the location of a recent study that found coarse mineral dust, associated with road dust, was most likely the GCCN that initiated urban heavy rain events (Uchiyama et al., 2019). However, in a study by Rodriguez et al. (2010) in São Paulo, no effect of aerosols on the development of summer thunderstorms could be determined. Some mechanisms have been studied in the subsequent formation of larger droplets from GCCN, which can become efficient collector drops. One of these mechanisms is concerned with the type of CCN. GCCN are hydrophilic or wettable particles with a radius greater than 3 μm. Modelling studies have shown that a

polluted convective cloud with a GCCN concentration of approximately 20 litre^{-1} produces precipitation much more quickly than a cleaner cloud with no GCCN (Feingold et al., 1999; Yin et al., 2000; Wallace and Hobbs, 2006b). Dusek et al. (2006) reported that the size of CCN played a more significant role than the composition of the particle in determining whether it can act as CCN.

The in-cloud environment will eventually consist of activated drops and crystals that are growing through various processes, small drops that were not nucleated and hydrophobic aerosols. The CCN that provided the nuclei for cloud drops would eventually be so diluted that their role in precipitation chemistry is likely not that important. A rise in relative humidity will increase the droplet equilibrium size enabling the droplets to grow further and the remaining aerosols in the in-cloud environment to be scavenged (Wallace and Hobbs, 2006b). The availability of aerosols acting as CCN limits the development of the cloud (Yin et al., 2000; Koren et al., 2014).

2.3 In-cloud Scavenging

The concentration of aerosols that served as CCN in the droplet changes as the droplet grows. When the droplets grow to be larger than 1 μm in radius, the solute and Kelvin curvature effects do not play such significant roles in the further growth of the droplet. As the droplets grow through condensation and collision-coalescence to ~50 μm in diameter, the surrounding additional CCN and gases can diffuse into the droplet (Brimblecombe, 2003; Wallace and Hobbs, 2006b). Smaller droplets with a greater total surface area will more efficiently absorb gases from the interstitial air (Hall, 2003) as described by the gas absorption mechanism (Pruppacher and Klett, 1997). Henry's law and the solubility and concentration of the gas will determine the concentration of the gas that can be dissolved at equilibrium (Brimblecombe and Dawson, 1984; Zhang et al., 2006b). The chemical concentrations in the droplets can thereby be increased (Brimblecombe, 2003). The process of the inclusion of particles and gases in the interstitial cloud air (the air surrounding the droplets within the cloud) into the cloud droplets is referred to as washout (Figure 2.1) (Hall, 2003; Wallace and Hobbs, 2006b; Pauliquevis et al., 2012). Washout of soluble species is an effective equilibrium process, however, the inclusion of interstitial aerosols is not considered to be an effective aerosol removal mechanism as the process is relatively slow (Brimblecombe, 2003; Hall, 2003).

The chemical driving force of scavenging processes is related to the difference between the atmospheric concentration and the gas-phase concentration near the surface of a droplet, which is in equilibrium with the droplet concentration. Scavenging in the cloud itself

occurs rapidly as mass transfer in the equilibrium process is aided by the small size of the droplets and the large total surface area (Hall, 2003). The aqueous solubility of the gas being scavenged affects the effectiveness of the rainout and washout processes. Highly soluble gases beneath the cloud are easily removed through the washout process as well, while aerosols are predominantly scavenged during the nucleation process (Chate and Pranesha, 2004). At lower temperatures, the liquid phase is energetically favoured and more gas will tend to dissolve into liquid drops (Wallace and Hobbs, 2006b). When ice is present in a cloud, the larger surface area contributes to the role of gas absorption in scavenging.

2.3.1 Warm- & cold cloud processes

Clouds can be classified as warm or cold clouds, with warm clouds having temperatures above 0^{o}C (Rauber and Tokay, 1991). Warm clouds occur below the 0^{o}C isotherm and only contain liquid water. In the supersaturated air of warm clouds, droplets grow through collision and coalescence of water droplets (Wallace and Hobbs, 2006b). Cold clouds can have supercooled water droplets (0 to -40^{o}C), ice particles (glaciated cloud) or both (mixed-phase cloud).

Warm cloud droplet collisions contribute to droplet growth. Larger falling drops have greater terminal velocities and collide into and coalesce with smaller, slower falling drops (Lutgens and Tarbuck, 1982). An effective collision, where the larger collector drop collects the liquid volume of the smaller drop, is dependent on the critical distance between the centre fall lines of the two drops as well as the individual radii of the drops. Drops with similar size will have a greater effect on each other's motion. When the sizes differ significantly, the smaller droplet will tend to follow the streamline of motion around the larger collector drop. Drops can collide but not coalesce when a pocket of air is trapped between the two colliding drops, deforming the surface of the drops and causing them to rebound without touching. Particles are also collected into falling raindrops through collision-coalescence. For coalescence to happen, the impact energy needs to overcome the surface energy of the drops. The coalescence efficiency (CE') is defined as the fraction of collisions that result in coalescence between two drops with radii of r_1 and r_2, respectively. The overall collecting efficiency (E_c) is equal to the collision efficiency (E) times the coalescence efficiency (E') (i.e. $E_c = E.E'$) (Wallace and Hobbs, 2006b). The presence of CN in the cloud enlarges the droplet size distribution which increases the collision-coalescence probability within the cloud (Wallace and Hobbs, 2006b). A modelling study by Lamb and Chen (1990) concluded that the removal efficiency of cloud chemical constituents is largely controlled by

the coalescent growth of the droplets. Precipitation from warm clouds commences when the updraught velocity that keeps the cloud in suspension is less than the terminal velocity of the raindrops. The terminal velocity of falling raindrops is dependent on the droplet size and density.

In cold cloud processes, homogenous nucleation of ice particles depends on the temperature of freezing. Laboratory results suggest that, at -41^{o}C, homogenous nucleation will occur for droplets of 1 μm in diameter. However, aerosols such as black carbon can act as ice nuclei (IN), which can contribute to heterogeneous nucleation through deposition, contact and immersion freezing of water vapour or droplets. These particles make freezing possible at much higher temperatures. If supercooled droplets are present with ice crystals, the latter will grow to the expense of the former through the processes described by the Bergeron-Findeison theory, because ice has a lower saturation vapour pressure than water (Rauber et al., 2000; Christner et al., 2008; De Boer et al., 2010; Koch and Del Genio, 2010). Inorganic clay particles (especially kaolinite), plankton and organic material from plants can act as IN, and particles with a hexagonal structure reflecting that of ice are effective IN (Preston-Whyte and Tyson, 1988; Rauber and Tokay, 1991).

Anthropogenic aerosols can affect the crystallisation process either directly or indirectly by inducing heterogeneous freezing, or by changing the temperature required for freezing, respectively (Christner et al., 2008; Ekman et al., 2011). Aerosols in the PM_{10} fraction can predominantly be activated as IN (Santachiara et al., 2010). The local ecosystem largely influences the type of IN in the air, since bacteria, fungi, algae and pollen can act as IN. Biological IN can catalyse freezing processes in clouds at much higher temperatures (-2^{o}C) than inorganic aerosols. These biological nucleating particles, for example different bacteria related to plants (e.g. different *Pseudomonas* species), fungi and algae are pH sensitive and are indicative of the acidic and chemical content of the precipitation (Christner et al., 2008). Christner et al. (2008) determined a directly proportionate relationship between the bicarbonate (HCO_3^-) concentration and the number of biological IN. A positive correlation was also observed between terrigenous total organic carbon (TOC), NH_4^+ and Ca^{2+} aerosol concentrations, and the number of biological nuclei (Christner et al., 2008). IN can therefore also contribute to the ultimate precipitation chemistry. However, there are significant uncertainties associated with the specifics of aerosol particles acting as IN (McFiggans et al., 2005; DeMott et al., 2011).

The ice crystals or snowflakes formed in cold clouds will remain in a solid state or melt into raindrops depending on the ambient temperature of the air when falling (Preston-Whyte and Tyson, 1988). Different stages of the cloud and precipitation formation have different intensities of latent heating, which also plays a significant role in the microphysical processes (Li et al., 2017). Droplets from cold and mixed clouds precipitate following ice formation or aggregation into snowflakes (Preston-Whyte and Tyson, 1988; Rauber et al., 2000).

While all clouds have some degree of electric charge, most thunderstorms are from cold clouds as positive ions move through ice quicker than negative ions. Precipitation gets polarised through the fair weather electric field (the electrosphere is net positive and the Earth's surface is net negative). Precipitation tends to collect positive ions in the air as it falls. 30 positive units $C.km^{-2}.yr^{-1}$ are gained onto the Earth's surface through precipitation (Wallace and Hobbs, 2006b). The type and size of CCN and IN are therefore important factors in cloud formation, the microstructure of the cloud, the growth of the droplets and the precipitation process (Christner et al., 2008). A modelling study showed that an increase in CCN concentration leads to a definite increase in accumulated rain and to a large increase in hail mass and diameter as well as to an increase in the precipitation efficiency of deep convective clouds (Khain et al., 2011).

The droplets grow to a few hundred micrometers with thorough mixing between various droplets creating a constant concentration throughout the cloud droplets, given sufficient time (Brimblecombe, 2003). Droplets can also evaporate in response to growth beyond the equilibrium size or changes in the cloud environment. Gases and aerosols are released through evaporation, and can follow updrafts through the cloud to be emitted at the cloud tops (Figure 2.1). Solar radiation and reflection from the cloud tops enhance photochemical reactions of the detrained gases and aerosols. The formation of the hydroxyl radical ($OH\cdot$) is prominent at these altitudes and serves to oxidise gases such as sulfur dioxide (SO_2), dimethyl sulfide (DMS) and ozone (O_3). In the presence of water vapour along the cloud boundary, new particle formation from the oxidised gases and particles is promoted. Evaporating clouds release particles formed through aqueous reactions which are then generally more soluble than the original particle and act as more efficient CCN at lower supersaturations. These are some of the feedback effects of certain chemical species on clouds, which could be hard to quantify in a deposition analyses. On the mesoscale, detrained species and new CCN in the outflow regions of the cloud can trigger new convection or interact with other storm systems (Wallace and Hobbs, 2006b; Westervelt et al., 2014; Vakkari et al., 2015).

2.4 The Effects of Aerosol Properties on Clouds

Although interstitial aerosols are not easily taken up into the cloud droplets, aerosols do have direct (as mentioned above) and indirect feedback effects on the cloud and droplet properties. Indirect effects include the Twomey and the cloud lifetime effects (McFiggans et al., 2005; Chapman et al., 2009). These effects occur when there is a change in the cloud droplet number, thereby affecting the cloud albedo (reflection of the incoming solar radiation), as well as the persistence of the cloud (McFiggans et al., 2005). The microphysical processes of a cloud are dependent on the droplet size distribution (Lynn et al., 2005b). Aerosols of anthropogenic origin that serve as CCN tend to increase the cloud droplet number by reducing the size of the cloud droplets. An increase in cloud droplet number with constant water content reduces the precipitation capability and increases the evaporation, thereby affecting the cloud lifetime (Chapman et al., 2009; Ekman et al., 2011; Konwar et al., 2012). A semi-direct effect of aerosols on cloud properties is the case of light-absorbing aerosols, such as black carbon, present beneath the cloud layer, which increase the ambient air temperature and stabilise the below-cloud air layer, as well as assist in cloud burn-off (McFiggans et al., 2005; Chapman et al., 2009; Koch and Del Genio, 2010). These light-absorbing aerosols present in the boundary layer decrease the ambient RH, which can reduce the cloud coverage by up to 40% (Koch and Del Genio, 2010).

Aerosol effects on clouds have been shown to be an important factor influencing the type, rate and distribution of convective precipitation (Khain and Sednev, 1999; Rosenfeld and Woodley, 2000; Rosenfeld et al., 2001; Lynn et al., 2005a). Lynn et al. (2005a) noted the importance of aerosol concentration on the cloud dynamics, microphysics and rainfall. Expanding anthropogenic activities in China have been shown to increase the aerosol loading in the atmosphere, which increases the cloud droplet number concentration (Zhao et al., 2017). Initial droplet spectra with increased amounts of smaller drops promote cold cloud processes such as ice formation. In contrast, larger CCN and GCCN promote the formation of larger drops that promotes warm cloud processes. Entrainment of unsaturated ambient air from the free troposphere above the well-mixed boundary layer can take place at the tops of small cumulus clouds. Entrainment from the upper troposphere can also occur at the top of strong convective clouds, introducing aerosols and gases such as mercury (Hg) into the cloud environment (Wallace and Hobbs, 2006b; Holmes et al., 2016). Considering all of the afore-mentioned, it is evident that the characteristics of aerosols, aerosol perturbations and feedback effects largely affect cloud systems.

2.5 Below-cloud Scavenging

For a raindrop to form, a cloud droplet has to increase in mass around one million times (Wallace and Hobbs, 2006b). Precipitation is regarded as the form in which atmospheric moisture returns to the surface of the Earth in a liquid or solid state. However, fog, dew and frost are generally not included in this category. Precipitation is mainly classified according to the physical state of the falling moisture (e.g. rain, hail or snow), or according to the formation processes (e.g. orographic or frontal precipitation) (Preston-Whyte and Tyson, 1988). The below-cloud scavenging processes include collision-coalescence, sweepout and wake capture as raindrops, hail and snow return to the surface of the Earth (Lutgens and Tarbuck, 1982). The precipitation and scavenging processes below the cloud are explored next.

2.5.1 Rainfall – Physical change from cloud to surface

Falling raindrops start out in a spherical shape. The bottom of the drop starts flattening out as it falls and eventually the centre part of drops larger than 2.5 mm is pushed upwards into a jellyfish-like shape and the drops can also burst into smaller drops influencing the raindrop size distribution and scavenging efficiency (Wallace and Hobbs, 2006b). In an unsaturated atmosphere, falling raindrops will evaporate and release the chemical components back into the atmosphere (Gong et al., 2006). More detail on the shape of raindrops and the physical changes as the drops fall and collide with other drops is presented by Beard et al. (2010), Szakáll et al. (2010) and Müller et al. (2013).

As the raindrops fall through the air, collide and coalesce with each other, they also scavenge other particles. Collision-coalescence is the process described above whereby a larger drop collides and coalesces with smaller drops, increasing in size (Lutgens and Tarbuck, 1982). Collision between the earthbound raindrops and ambient aerosols further evolve the rainwater chemistry. Falling raindrops create streamlines of perturbed airflow and Brownian motion around the droplets, sweeping the surrounding particles. The motion of the particles is also subjected to the Bernoulli Effect at this stage. Smaller particles will more likely continue to follow the streamline motion and be swept downward without being collected into the droplet (inertial impaction) (Preston-Whyte and Tyson, 1988; Urone, 2001; Hall, 2003). Removal of particles by this means is called sweepout (Hall, 2003). Occasionally, atmospheric particles (other droplets, gases or aerosols) swept along these streamlines will be collected into the raindrop as determined by the droplet- and particle diameters and temperature gradients (thermophoresis), among others. Particles with a

larger diameter will most likely be collected into the drop (directional interception). This scavenging process, called wake capture, is relatively efficient (Preston-Whyte and Tyson, 1988; Chate et al., 2011).

2.5.2 Raindrop size distribution & rain intensity

The raindrop size distribution is descriptive of the type of rain event, and relationships between different rainfall types and droplet distribution have been noted in previous studies such as those by Campos et al. (2006) and Marzuki et al. (2010). The droplet size distribution is directly related to the microphysical processes in the cloud (Martinez and Gori, 1999). The raindrop size distribution is also the fundamental property of rainfall that relates to rainfall rate, radar reflectivity and kinetic energy flux (Martinez and Gori, 1999; Uijlenhoet and Stricker, 1999). The degree of scavenging that can take place during precipitation largely depends on the droplet size (Hall, 2003). Scavenging is furthermore proportional to the rainfall rate or intensity, which is proportional to droplet size and droplet size distribution (Engelmann, 1965; Chate, 2005). Rainfall rate was also correlated to the raindrop size distribution in a principal component analysis (PCA) study of East Asian monsoon rain (Karev et al., 2010). In Figure 2.2, an illustration of the positive relationship between the scavenging coefficient, a numerical entity that describes the scavenging efficiency, rainfall rate and particle diameter is presented (Chapter 2.7.1) (Engelmann, 1965).

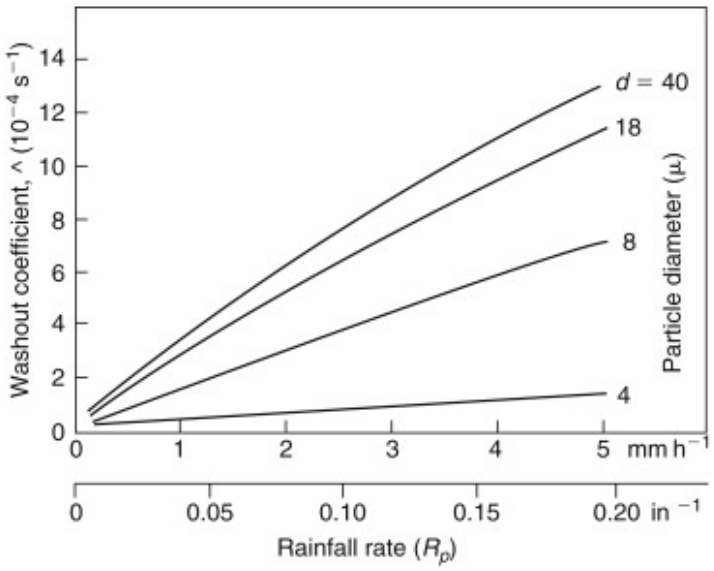

Figure 2.2 Illustration of the washout coefficient as a function of particle diameter and rainfall rate (after Engelmann (1965)).

Models have shown an increase in rainfall rate as a result of in-cloud turbulence that increases the particle and drop collision rates (Lynn et al., 2005b). In warm convective clouds (especially with cloud tops higher than 6 km or at the -8/-10^{o}C isotherm), giant raindrops and high rain intensities are favoured through collision-coalescence in updrafts of air with high humidity (Martinez and Gori, 1999). Scavenging ratios have been calculated to determine the washout of particles through rain events. These ratios, which describe the ratio of the concentration of a species in the rainwater to the concentration thereof in the ambient air, have been found to be higher for coarser particles or particles with a larger diameter (Engelmann, 1971; Galloway et al., 1993; González and Aristizábal, 2012). The rain intensity impacts the below-cloud scavenging ratio depending on the aerosol- and raindrop sizes, and the duration of the event (Kulshrestha et al., 2009). González and Aristizábal (2012) reported a positive relationship between the scavenging ratios of sulfates and nitrates to the rain intensity, particularly in the scavenging of sulfates. The particle dimensions and solubility of sulfate contributes to the scavenging efficiency thereof. However, there seems to be variability in the scavenging ratios between different locations. Rain intensity was determined to be a controlling factor for sulfate scavenging in an urban environment (González and Aristizábal, 2012).

Xu et al. (2017) found that the below-cloud scavenging processes contributed between 47 - 61 % to the SO_4^{2-}, NO_3^- and NH_4^+ concentrations in rainwater. Xu et al. (2017) also reported that the below-cloud scavenging coefficient was related to the rain intensity with an exponential power distribution. It was found that the SO_4^{2-} deposited in the first moments of a rainfall event positively correlated to the ambient air concentrations and the rainwater SO_4^{2-} content was largely ascribed to a strong influence of aerosol concentrations (Xu et al., 2017). NO_3^- in the form of $NaNO_3$ is also more efficiently scavenged than NH_4^+ in the form of $(NH_4)_2SO_4$. It was therefore proposed that the chemical properties of ions should be taken into consideration when considering wet scavenging coefficients (Xu et al., 2017). The scavenging ratios for NH_4^+ and NO_3^- increase with rain intensity up to a point, there after larger aerosols such as Ca^{2+} and SO_4^{2-} have higher scavenging ratios. A longer event with lower rain intensity was reported to remove NO_3^- and NH_4^+ particles effectively, while a shorter, more intensive rainfall removes coarser $CaSO_4$ aerosols. A study on the real-time aerosol concentration and rainwater chemistry by Kulshrestha et al. (2009) reported a smaller atmospheric aerosol concentration of Ca^{2+}, NH_4^+, NO_3^- and SO_4^{2-} during a rain event, indicating the wet scavenging of these species. The largest decreases in aerosol concentrations occurred after a continuous rain event with a long duration and low intensity. They found that Ca^{2+} was most efficiently scavenged through the rain event. Elemental carbon is mostly scavenged below-cloud, with the size and hygroscopicity of the compound

being the determining factor of whether it will be included into a cloud as a CCN (Hadi et al., 1994).

Thunderstorms generally have higher rainfall intensities (Rodriguez et al., 2010). A longer rainfall event will also have an elevated RH for a sustained period. The RH has been shown to impact the scavenging of hygroscopic aerosols (e.g. NaCl and $(NH_4)_2SO_4$) (Kulshrestha et al., 2009). In a similar study in China, Zhao et al. (2015) reported that particles with sizes ranging from 500-1000 nm were effectively scavenged through thunderstorm rain events with higher intensities, whereas smaller particles were effectively scavenged through non-thunderstorm rain events. They also reported that an event with a longer duration and lower raindrop velocity more efficiently scavenged particles with sizes in the range of 10 - 50 nm. In their study, they reported a larger raindrop size distribution in thunderstorm events, which could explain the more effective scavenging. Similarly, Chate (2011) indicated 60 – 80% of initial atmospheric sulfate and organic carbon was washed out through thunderstorm events lasting less than an hour. He also indicated the importance of thunderstorms and lightning in modulating the aerosol distributions in the continental tropical belt through effective scavenging (Chate, 2011). Thunderstorms have also been related to the effective removal of mercury (Hg) from the upper troposphere (Holmes et al., 2016). In contrast, research in Wales found that, when rain falls from high altitude clouds, sub-micron aerosols are not efficiently scavenged in the atmosphere, and therefore the rainwater composition reflects the cloud chemistry more closely (Cape et al., 2015).

Considering the discussion above, below-cloud scavenging is therefore a major removal process in the boundary layer, with the efficiency thereof being dependent on factors such as the particle- diameter and size distribution, as well as the raindrop terminal velocity, collision efficiency, size distributions, and rain intensity (Bae et al., 2006).

2.6 Long-range transportation & the role of air mass history

Sun et al. (2010) found that the chemistry of liquid water in clouds differed from the rainwater chemistry of the related event. It was suggested that air masses arriving from different regions at different heights were the major factor influencing this observation. An air mass refers to a body of air with relatively homogenous composition, temperature and moisture characteristics. In order to have these homogenous characteristics, an air body should be relatively stable over the source region for a time sufficient to achieve equilibrium. As the air mass moves onward, it will tend to keep those characteristics determined by the source region (Critchfield, 1983). Other studies have also associated varying air mass histories arriving at different altitudes with the chemical composition of rainwater. Li et al.

(2011), for instance, determined differences in trace element concentrations and pH levels of rainwater sampled on a mountaintop compared to rainwater samples taken at the base of the same mountain. The authors found that the major ionic concentrations were much higher at the mountain base than at the summit and ascribed these differences to varying air mass histories (Li et al., 2011).

Air masses can carry primary and secondary pollutants over long distances on a synoptic scale. Therefore, distant emission sources can affect the air quality, nucleation capability, precipitation chemistry and deposition at a remote site. Moody and Samson (1989) attributed a variability of up to 40% for certain ionic concentrations measured in rainwater samples to differences in the long-range transportation of air masses. Residence or lifetimes of different chemical species in the atmosphere also vary, from the very reactive OH radical with a lifetime of a few seconds to the moderate lifetime of SO_2, and the long-lived species such as methane (CH_4) and chlorofluorocarbons (CFCs) that have lifetimes of up to 100 years. Figure 2.3, from Wallace and Hobbs (2006a), illustrates the residence times of certain important chemical species in a spatial context. Considering the lifetimes of species measured in the current study, NO_3 has a short residence time, while S-containing species, NO_x, CO, certain aerosols and oxidising agents are species with relatively longer residence times in the boundary layer (~ days to months). These lifetimes enable long-range transport of these species and scavenging thereof through rain at locations distant from the primary emission sources.

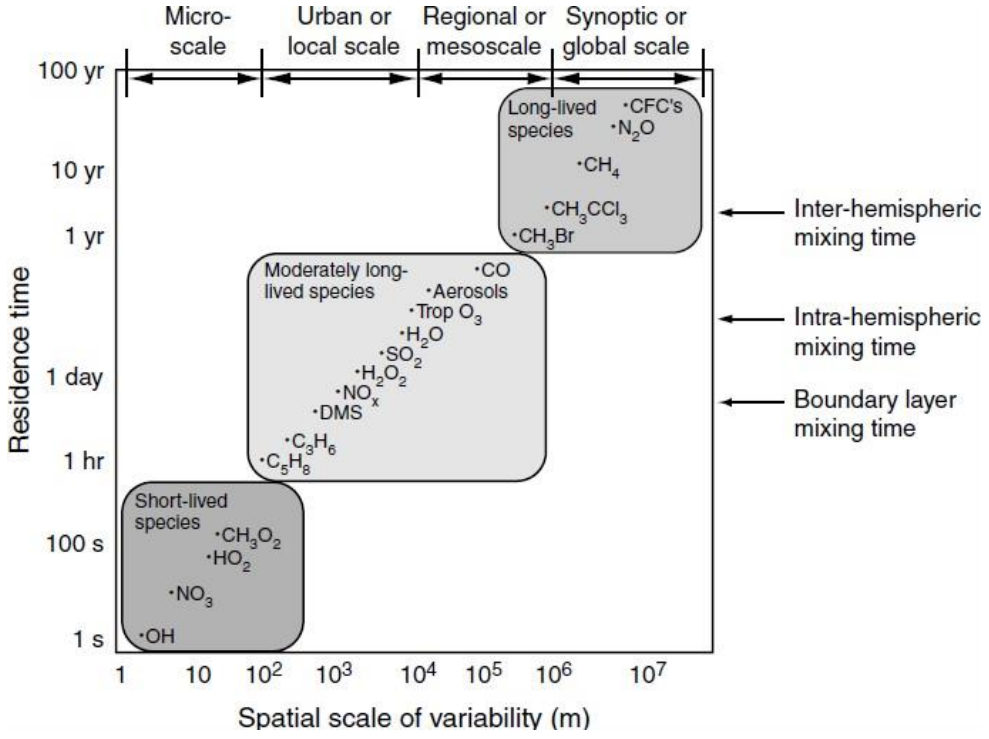

Figure 2.3 Residence times of certain species at different spatial scales (Wallace and Hobbs, 2006a).

The distance of the rainfall event from emission sources, the source strengths, seasonality, turbulent mixing of the atmosphere and the lifetimes of chemically important species determine the effects of long-range transportation of air masses and regional distribution of chemical species on the rain composition (Li et al., 2019). Gas phase sulfate production is estimated to be regionally confined to an area close to the emission site, whereas aqueous phase oxidation to SO_4^{2-} can occur at any time and place inside the cloud as it is transported downwind (Gong et al., 2006). Gong et al. (2006) compared the simulated aqueous phase SO_4^{2-} production to the wet deposition flux thereof and found 50% of the deposited SO_4^{2-} had been oxidised through aqueous reactions in the atmosphere and was influenced by turbulent mixing. In a study by Fedkin et al. (2019), for example, SO_2 oxidised faster in warmer summer months with SO_4^{2-} deposited less than 300 km from the emission source. In contrast, the SO_4^{2-} was deposited over 500 km away during the winter months. Welgegund should therefore experience SO_4^{2-} deposition throughout the year.

In studies at mountainous sites, the importance of cloud water composition and related air mass histories is made evident. It has been found that cloud deposition can be the dominant contributor to the total deposition at high elevation sites. At Whiteface mountain in the USA, approximately 90% of the total soluble sulfur deposition was via cloud water and the deposition of major soluble ions was around 14 to 28 times higher through cloud deposition than through wet deposition (Schwab et al., 2016). Concentrations of major ions in clouds are generally higher than in rainwater. The average ionic concentration measured in clouds at a high elevation site in Wales was double the concentration of rainwater sampled nearby (Cape et al., 2015). However, sampling in studies on cloud water is usually near the base of the cloud where the cloud droplets are usually very small and does not consider most of the liquid water content higher up in the cloud. An increase in cloud liquid water content with height means that the solute concentration decreases with height. Another factor considered in these cloud water chemistry studies is the orographic scavenging factor (Reynolds et al., 1996; Cape et al., 2015).

Concluding from these studies, the air mass history and movement at different altitudes play a significant role in the scavenging processes that establish the rainwater composition. Various previous authors (Sun et al., 2010; Shen et al., 2012; Liu et al., 2013; Aikawa et al., 2014) determined the air mass history of the lower atmosphere and identified different source regions by employing back trajectory analysis calculated at a range of different arrival heights. Some of these studies used statistical methods such as K-means clustering and Ward's method to compute Euclidean distances to analyse the spatial differences in the range of trajectories. Although the importance of determining air mass trajectories when studying cloud and precipitation chemistry has been highlighted by these and other authors, these studies considered a vertical range of arrival heights and did not directly determine the

air mass histories associated with the arrival height of the precipitating cloud. In this study the precipitating cloud base height (CBH) was measured with a ceilometer before the start of a rain event and was used as the arrival height in back trajectory calculations (Chapter 3.2.3.2 and 3.2.4).

2.7 Rainwater Chemistry

Following the above discussion on scavenging, the chemical composition of cloud- or rain droplets are inherently determined by the chemical and physical characteristics of the CCN onto which the droplet originally condensed. This composition changes during the lifetime of the droplet through chemical reactions, as well as through the physical changes the droplet is subjected to. Gases and other particulate matter, from various natural and anthropogenic sources, are also taken up into the droplets during the numerous scavenging processes discussed in the above sections (Sun et al., 2010; Liu et al., 2013). By 1983, more than 1 600 chemical compounds had been identified in the atmosphere. This number reached over 3000 species by 1992 (Critchfield, 1983; Graedel and Crutzen, 1993). Atmospheric moisture in the form of cloud- or rain droplets creates the environment for numerous aqueous chemical reactions to occur and oxidation reactions are promoted, while the rainout and washout processes can catalyse these aqueous reactions in the cloud environment (Brimblecombe, 2003; Sun et al., 2010). The chemical characteristics of the eventual precipitation are the net result of complex microscale processes and interactions of cloud mechanics, microphysical properties of the droplets and chemical reactions occurring during the various scavenging processes (Al-Khashman, 2009; Zhang et al., 2012). This section aims to present some of the fundamental chemical properties and reactions in the lower atmosphere concerning the ionic species investigated in this study.

2.7.1 Chemistry & scavenging

Although there are numerous chemical species in different forms and phases present in the atmosphere, the intrinsic properties of the species will also determine to what extent it could be deposited through wet deposition. For example, the aqueous solubility of a gaseous species contributes to its susceptibility for uptake into the clouds and raindrops, which can be described by Henry's law (Brimblecombe and Dawson, 1984; Finlayson-Pitts and Pitts, 2000; Connell, 2005).

Scavenging ratios, scavenging coefficients and washout ratios are some numerical entities that describe the scavenging efficiency. The rate of change in gaseous concentration due to scavenging in a homogenous air mass can be defined in the following equation (2.1):

$$\frac{dC}{dt} = -\Lambda C \qquad (2.1)$$

where C is the concentration in moles.m^{-3}, t is time in s, and Λ is the scavenging coefficient in s^{-1} (Hall, 2003). The scavenging coefficient is dependent on the solubility of the gaseous species. Mass transfer can occur from the air to the droplet or vice versa, depending on the equilibrium concentration in the ambient air mass and in the droplet. This can especially occur in the cloud environment through in-cloud scavenging, as there is sufficient time for mass transfer to take place. As indicated earlier (Section 2.3), below-cloud scavenging mass transfer coefficients factor in a few more parameters (i.e. diffusivity, droplet diameter, the terminal velocity of the droplet, and rainfall rate). The droplet size distribution also has a large effect on the total scavenging coefficient (Section 2.3.1.3) (Hall, 2003).

The washout ratio (W_r) is a function of the rainwater concentration (C_p) and the ambient concentration. Using the rainwater concentration together with the rainwater rate or intensity (p_o in mm.h^{-1}), the specific flux (F) of the species being deposited can be calculated. (Equations 2.2 - 2.3) (Hall, 2003)

$$W_r = \frac{C_p}{C_{air}} \qquad (2.2)$$

$$F = p_0 C_p \qquad (2.3)$$

Scavenging processes, as described in the above sections, are functions of the concentration and solubility of the gas or particle being scavenged. For example, HNO_3 and hydrogen peroxide (H_2O_2) are efficiently scavenged under equilibrium conditions. Since the concentration difference is the chemical driving force of these processes, a droplet containing a certain concentration of a species, that is deficient in the ambient atmosphere, will undergo mass transfer diffusion out of the droplet into the atmosphere and vice versa. The amount of below-cloud scavenging that can take place mostly depends on the size of the raindrops and the distance they travel to the ground (Hall, 2003).

2.7.2 In-cloud aqueous reactions

The rainout and washout processes can catalyse aqueous reactions in the cloud environment. SO_2 oxidation to SO_4^{2-} is a major reaction that occurs in clouds, which largely contributes to the total SO_4^{2-} in the atmosphere (Hegg and Hobbs, 1981; Gong et al., 2006). Model results from Zhang et al. (2006a) showed that SO_2 oxidation to SO_4^{2-} resulted in a broader cloud droplet size distribution, which made precipitation formation more efficient. SO_4^{2-} formation in the cloud is largely determined by the initial concentration of trace gases. SO_4^{2-} formation through aqueous reactions in the cloud increases the mean aerosol size, thereby affecting the aerosol size distribution. This in turn increases the droplet size distribution and scattering efficiency (Gong et al., 2006; Zhang et al., 2006a; Schmeller and Geresdi, 2019). Both the pH and the concentration of compounds in the water drops depend on the size of the drops (Schmeller and Geresdi, 2019).

The aqueous in-cloud environment promotes oxidation reactions. H_2O_2 rapidly oxidises SO_2 in the cloud environment (Mohnen and Kadlecek, 1989), however, the presence of formaldehyde may inhibit S oxidation (Adewuyi et al., 1984). Recent studies have shown that the aqueous environments are important sources of secondary organic aerosols (Mekic et al., 2019). A recent study by Lu et al. (2019) determined that aqueous atmospheric environments such as fog and clouds are ideal environments for significant secondary organic aerosol (SOA) formation through the oxidation of intermediate volatility organic compounds (IVOCs). IVOCs have been related to diesel combustion and are estimated to contribute to over 50% of the SOA in Eastern China. They reported that the aqueous ageing of the organic aerosols also enhanced the light absorbing ability of the aerosols (Lu et al., 2019). Oxidation in the aqueous cloud environment has also been shown to produce highly oxidized, high molecular weight compounds (Mekic et al., 2019).

Polluted tropospheric environments are favourable to the formation of nitrated aromatic compounds through aqueous phase oxidations of aromatic compounds via the OH radical, O_3 and HO_2 in clouds (Hoffmann et al., 2018). The NO_3 radical ($NO_3\cdot$) is a strong oxidising agent. At night, $NO_3\cdot$ is formed through the reaction between NO_2 and O_3, which is then scavenged by cloud droplets (Equation 2.4 – 2.5). This process may be a significant pathway to introducing the NO_3 radical into cloud water, which can also affect the rate of formation of H_2SO_4 from SO_2 in clouds. Dinitrogen pentoxide (N_2O_5) can then be dissolved in the cloud water producing HNO_3 (Chameides, 1986; Iribarne and Cho, 1989).

$$NO_2 + O_3 \rightarrow NO_3\cdot + O_2 \quad (2.4)$$

$$NO_2 + NO_3\cdot \rightarrow N_2O_5 \quad (2.5)$$

Cloud droplet size and ionic concentration are related, as noted by Bator and Collett Jr (1997), who reported smaller drops being enriched with SO_4^{2-}, NO_3^- and NH_4^+, and larger drops being enriched with coarse aerosol particles. They highlighted that the droplet maintained the properties of the precursor species (CN). Cloud water sampled in Switzerland was reported to have higher SO_4^{2-}, NO_3^- and NH_4^+ concentrations in smaller cloud droplets compared to the related rain samples (Collett Jr et al., 1993). Kaufman and Nakajima (1993) noted a decrease in droplet size and more droplets in ~~-s~~moky" continental clouds. Schwartz et al. (2002) noted a similar relationship between droplet size and number with increases in SO_4^{2-} aerosols.

Aqueous chemical reactions in clouds usually increase the $PM_{2.5}$ concentration through SO_4^{2-} formation, while wet scavenging is known to reduce the $PM_{2.5}$ concentrations. Depending on the season, cloud processes and wet scavenging have varying effects on the $PM_{2.5}$ concentrations. Increased aerosol loading can lead to self-enhancement of the $PM_{2.5}$ concentration by increased cloud formation and enhancing aqueous reactions (Zhao et al., 2017).

On the microscale, detailed cloud chemistry is very difficult to predict and large uncertainties remain on the chemical reactions and compositions of clouds, although more detailed simulations have been carried out in small scale models (Tost et al., 2007). Equilibrium is eventually reached in the cloud droplets and they will at some stage return to the Earth in the form of precipitation (Brimblecombe, 2003). The chemical composition and properties of the droplets are determining factors for not only cloud formation and lifetime, but also the eventual initiation of the precipitation event and its composition. Further discussion on the chemical reactions related to specific ionic species is presented in the following section.

2.7.3 Investigation of rainwater ionic species

Natural and anthropogenic emission sources are the origins of various chemical species found in the troposphere. Ultimately, through scavenging processes, the chemical composition of rainwater can give information on the regional and local tropospheric composition and pollution levels (Mphepya et al., 2004; Vet et al., 2014). Prominent correlations between ionic species have been related to certain emission sources and are discussed here in relation to the characteristics of the species analysed in this study (Conradie et al., 2016). These species are water soluble inorganic and organic ions namely nitrate (NO_3^-), sulfate (SO_4^{2-}), chloride (Cl^-), fluoride (F^-), acetic acid (CH_3COO^-), formic acid ($HCOO^-$), oxalic acid ($C_2O_4^{2-}$), propionic acid ($C_3H_5O_2^-$), ammonium (NH_4^+), calcium (Ca^{2+}), potassium (K^+), magnesium (Mg^{2+}) and sodium (Na^+). The sources of these species are discussed as ions related to common (although not exclusive) emission sources. These sources are anthropogenic and agricultural activities, crustal and marine sources and organic acids. Although not considered in this study, trace metals such as mercury (Hg), antimony (Sb), lead (Pb) and cadmium (Cd), as well as biological species such as algae, pollen, bacteria and fungi can also be present in rainwater (Christner et al., 2008; Li et al., 2011).

2.7.3.1 Anthropogenic & agricultural ions

Sulfur oxides (SO_x)

Sulfur (S) is emitted into the atmosphere in different chemical forms which include sulfur dioxide (SO_2), hydrogen sulfide (H_2S) and dimethyl sulfide (DMS) (Shallcross et al., 2003). SO_2 is predominantly generated through the combustion of S-containing fossil fuels such as coal and oil, as well as smelting of S-containing ores. Anthropogenic emissions of SO_2 through mainly fossil fuel combustion contribute approximately 75% to the total global S emission budget. In addition, SO_2 is emitted naturally through erupting volcanoes and other geochemical sources (Aiuppa et al., 2004; Kanayo et al., 2010). Volcanic eruptions can largely affect the S budget in the atmosphere by a sudden release of a large amount of SO_2. Biogeochemical S emissions include species such as H_2S, DMS and other reduced forms of S (Finlayson-Pitts and Pitts, 2000; González and Aristizábal, 2012).

In a dry atmosphere, SO_2 and SO_4^{2-} will persist for a couple of days and can therefore be subject to long-range transportation (Figure 2.3). SO_4^{2-} is formed when gaseous SO_2 reacts with moisture to form an acidic solution, whereafter H^+ is abstracted from reactive

metals to form H_2SO_4 (McGranahan and Murray, 2003; Adon et al., 2010; Kanayo et al., 2010; Aikawa et al., 2014). Hydroxyl radicals (OH·) also play a significant role in the production of H_2SO_4 (Reactions 2.6 - 2.8) (Shallcross et al., 2003).

$$SO_2 + \mathrm{OH}\cdot \rightarrow HOSO_2 \quad (2.6)$$

$$HOSO_2 + O_2 \rightarrow SO_3 + HO_2 \quad (2.7)$$

$$SO_3 + H_2O \rightarrow H_2SO_4 \quad (2.8)$$

Additionally, there are many redox reactions through which S containing species such as H_2S, DMS, methyl mercaptan (CH_3SH), carbon disulfide (CS_2) and carbonyl sulfide (COS) are oxidised with OH·, nitrate radical (NO_3·), O_3, hydrogen peroxide (H_2O_2), transition metal-catalysed reactions and halogens (Penkett et al., 1978; Brandt and Van Eldik, 1995; Finlayson-Pitts and Pitts, 2000). When the particulate carbon concentration in the cloud water is high and H_2O_2 levels are low, SO_2 can effectively be oxidised by molecular oxygen when catalysed by the carbon (Hadi et al., 1994). High concentrations of non-sea salt fraction (nSSF) SO_4^{2-} and the highest elemental carbon concentrations were found in the same samples in a study on cloud water chemistry by Hadi et al. (1994), although they did not derive a direct relationship. The nSSF is the contribution to the rainwater ionic concentrations by sources other than marine salt and are presented in Chapter 3.2.6.2. An in-depth discussion for the oxidation reactions of SO_2 is given by Brandt and Van Eldik (1995).

In general, SO_4^{2-} comprises the largest fraction of water soluble ions in particulate matter and has the largest concentration in rainwater, even at background sites (Vet et al., 2014; Aurela et al., 2016; Conradie et al., 2016). SO_4^{2-} exhibits a negative radiative forcing (RF) value (Banerjee, 2008), which indicates a cooling effect on the climate (IPCC, 2013). SO_4^{2-} acts as CN in the form of $(NH_4)_2SO_4$ and ammonium bisulphate (NH_4HSO_4) (Kanayo et al., 2010; Aikawa et al., 2014) and affects cloud lifetimes (Smith et al., 2001). A study on the reactivity of SO_2 on the surface of α-Al_2O_3, representing mineral dust, found that in the presence of O_3 or NO_2 and with increased relative humidity (RH), the conversion rate of SO_2 to SO_4^{2-} increases. SO_2 and NO_2 as a coating on mineral dust will more easily convert to SO_4^{2-} and NO_3^- in a high RH environment which can then easily act as CCN (Liu et al., 2017). Kulshrestha et al. (2009) attributed the doubling in the SO_4^{2-} aerosol concentration after a rainfall event to the possibly elevated RH that supported the oxidation of SO_2.

In a polluted environment, cloud droplets can contain high concentrations of chemical species which then undergo fast aqueous chemical reactions. A typical reaction that takes place in cloud water is the conversion of SO_2 to H_2SO_4 (Equations 2.8 – 2.11). The aqueous reactions include the formation of bisulfite (HSO_3^-) from SO_2, which then dissolve into cloud

water to form sulfite (SO_3^-) ions. After the ionisation of SO_2, oxidation rapidly takes place to form SO_4^{2-} (Brandt and Van Eldik, 1995; Wallace and Hobbs, 2006b).

$$SO_2(g) + H_2O(l) \leftrightarrow SO_2.H_2O(aq) \quad (2.9)$$

$$SO_2.H_2O(aq) \leftrightarrow HSO_3^-(aq) + \mathrm{H}^+(aq) \quad (2.10)$$

$$HSO_3^-(aq) \leftrightarrow SO_3^{2-}(aq) + \mathrm{H}^+(aq) \quad (2.11)$$

A recent study on the decreasing trend in SO_2 emission and SO_4^{2-} wet deposition in the United States emphasised the link between the location of the emission sources to the deposition observation site as well as the local seasonal impact on the photochemical reactions of SO_2 (Section 2.6) (Fedkin et al., 2019).

Concerning the environmental and health impacts of sulfur oxides, SO_4^{2-} is not considered by the World Health Organization (WHO) to be very toxic, although elevated levels can irritate the skin and mucous membranes, as well as potentially aggravating heart and respiratory diseases (EPA, 1999; EPA, 2008). Elevated atmospheric SO_2 levels can also lead to respiratory illness in humans and animals (Shallcross et al., 2003). SO_4^{2-} and NO_3^- are mobile in soils and can be taken up by plant systems (Menz and Seip, 2004). SO_4^{2-} deposition can stimulate microbes to methylate mercury (Hg); a process that introduces Hg into the food chain and contributes to bioaccumulation of Hg (Greaver et al., 2012). Increased SO_4^{2-} concentrations also lead to the acidification of surface water bodies (Krug and Frink, 1983).

Nitrogenous components: Nitrogen oxides (NO_x)

Nitrogen oxides (NO_x) are present in the atmosphere mainly as nitric oxide (NO) and nitrogen dioxide (NO_2) together with dinitrogen pentoxide (N_2O_5) and nitrous acid (HONO) (Finlayson-Pitts and Pitts, 2000; Shallcross et al., 2003). These chemical states of NO_x show strong diurnal and seasonal concentration tendencies (Shallcross et al., 2003; Collett et al., 2010; Lourens et al., 2012). NO and NO_2 react with ozone (O_3) in a photochemical reaction to interchange between these two chemical forms (Reactions 2.12 and 2.13).

$$NO + O_3 \rightarrow NO_2 + O_2 \quad (2.12)$$

$$NO_2 \xrightarrow{h\nu} NO + O \quad (2.13)$$

Natural and anthropogenic emissions contribute to continental NO_x levels (Shallcross et al., 2003; Collett et al., 2010; Lourens et al., 2012). NO_x levels are usually more elevated

over continental and polluted areas in comparison with marine environments (Shallcross et al., 2003). NO_x do not have long atmospheric residence times, which are in the order of a few hours (Figure 2.3, Section 2.6). Soil, tilling of fertilised soil, lightning and wildfires (e.g. lightning induced), are examples of natural emission sources. Lightning approximately contributes 10-33 $Tg.y^{-1}$ to the global atmospheric NO_x budget. In addition, stratospheric influx also contributes to tropospheric NO_x (Finlayson-Pitts and Pitts, 2000; Jackson, 2003; Rakov and Uman, 2003).

There is a global increase in anthropogenic emission of NO_x compounds (Shallcross et al., 2003). The main anthropogenic sources of NO_x are vehicular emissions and biomass burning (man-made savannah and grassland fires, as well as household combustion for space heating and cooking, and fossil fuel combustion) (Graedel and Crutzen, 1993; Finlayson-Pitts and Pitts, 2000; Jackson, 2003; Shallcross et al., 2003).

Atmospheric NO_x are furthermore notable pollutant species since tropospheric O_3 can only be formed in the atmosphere from NO_2. The concentration of NO_2 can be enhanced by the presence of other precursor species such as volatile organic compounds (VOCs) and carbon monoxide (CO) (Finlayson-Pitts and Pitts, 2000; Shallcross et al., 2003). Nitric acid (HNO_3), which contributes to the acidic content of precipitation, is formed through the hydrolysis of N_2O_5 (Reaction 2.14). Nitric acid is more soluble than SO_2, making scavenging thereof more efficient (Cape et al., 2015). The reaction of NO_x with hydroxyl radicals to form HNO_3 is part of the removal mechanisms of NO_x (Reaction 2.15). NO and NO_2 are not significantly absorbed into cloud or rainwater, since they are not highly soluble and kinetically the reactions are too slow. However, reactions at the droplet surface exist where NO_2 reacts with water vapour to form HONO through a mechanism not yet well understood (Reaction 2.16) (Finlayson-Pitts and Pitts, 2000).

$$N_2O_5 + H_2O \rightarrow 2HNO_3 \quad (2.14)$$

$$NO_2 + OH^{\cdot} \rightarrow HNO_3 \quad (2.15)$$

$$2NO_2 + H_2O \rightarrow HONO + HNO_3 \quad (2.16)$$

Under high temperature conditions, the equilibrium conditions for nitrate (NO_3) will be towards the gas phase (Cape et al., 2015). NO_3^- is oxidised by dissolved oxygen to nitrite (NO_2^-) when the liquid water freezes. This oxidation takes place more effectively as the pH decreases below 6 (Takenaka et al., 1998). Elevated NO_3^- levels in drinking water are toxic and can cause, among others, a blood disorder called methemoglobinemia (Kanayo et al., 2010).

Nitrogenous components: Ammonium (NH_4^+)

In addition to NO_3^-, further nitrogenous contributions to rainwater chemistry include ammonia (NH_3) emissions (Galy-Lacaux et al., 2009). NH_3 in the atmosphere has a moderate lifetime of approximately 10 days (Shallcross et al., 2003). NH_4^+ is quickly removed through both wet and dry deposition processes and will likely be deposited in an area close to its emission source (Cape et al., 2015). NH_3 levels in the atmosphere are highly variable as their sources are both natural (e.g. soil and ocean emissions, and decomposition and hydrolysis of urea and excreta) and anthropogenic (primarily from the agricultural fertilisation industry). NH_3 is an important basic gas in the atmosphere and therefore plays an important role in neutralising acids such as H_2SO_4 by forming ammonium sulfate ($(NH_4)_2SO_4$) (Shallcross et al., 2003; Galy-Lacaux et al., 2009; Laouali et al., 2012; Conradie et al., 2016). However, $(NH_4)_2SO_4$ has an acidifying effect on soil, which can inhibit plant growth (Shallcross et al., 2003), and on surface water bodies (Krug and Frink, 1983).

Although N is an essential nutrient, an elevated N influx into sensitive ecosystems ultimately has a detrimental effect. The net effect of N deposition is dependent on whether the terrestrial ecosystem is N or P limited. When the system is N limited, an increase in N would increase the growth rate of plants, which would then generate an imbalance in the carbohydrate-protein levels. Other essential minerals such as Mg^{2+}, K^+ and phosphate (PO_4^{2-}) can restore this balance. The excess N then reacts to form toxic substances such as amides and amines, as well as ammonium derivatives. This can lead to increased parasitic activity, dehydration and excess stress on the plants (Aber et al., 1989; Halsall, 2003; Fields, 2004). N cycling and concentrations in soil are directly dependent on the nitrogenous concentration in the precipitation (Sanger et al., 1996). N deposition in excess of critical loads can cause nitrate leaching into surface water bodies leading to acidification and eutrophication of these ecosystems (Aber et al., 1989; Fields, 2004; Josipovic et al., 2011). Recently it was estimated that worldwide 11% of the natural vegetation receives N through deposition exceeding the critical load threshold of 1000 $mg.N.m^{-2}.y^{-1}$ (Dentener et al., 2006). The detrimental effects of eutrophication have been highlighted in various publications, including those referenced in Halsall (2003).

N in excess of the amounts taken up by crops such as maize or the natural vegetation leads to NO_3-N leaching through groundwater (Dhital and Raun, 2016). Increased nitrogen use efficiency (NUE) for cereal crop production and more accurately in-season estimated N fertilisation could not only prove to be cost efficient (a global increase of 1% NUE was estimated to save 234 million USD in 1999), but also decrease NO_3-N leaching and runoff to surface water bodies. It could therefore also be crucial to have an estimated N deposition

value to determine optimum fertilisation time, method and rate to minimise N losses (Dhital and Raun, 2016).

2.7.3.2 Crustal ions

Soil and dust particles lifted into suspension either by natural processes or by direct and indirect anthropogenic activities, e.g. vehicles, tilling and agricultural activities, can affect the atmospheric concentrations of water insoluble species such as aluminium silicates, as well as water soluble species such as K^+, Ca^{2+} and Mg^{2+} carbonates. Ions of these origins are classified as terrigenous or crustal elements. Crustal contributions to the chemical composition are related to the geological properties of the region. A study by Orué et al. (2019) in Argentina, for example, found trace elements in the rainwater associated with polymetallic ore found in local outcroppings. Crustal ionic species that are associated with mineral dust from alkali feldspars, lime rich dolomite, diabase and silicate rich minerals, such as those found in granites, micas and chert, are dominant over southern Africa (Cairncross, 2004; McCarthy and Rubidge, 2005; Jaars et al., 2016). Although dust is a natural contribution to rainwater composition, Chen et al. (2019) showed the relevance of the direct and indirect anthropogenic emission of dust. Most of the Ca^{2+} and K^+ contributions to the cationic content of rainwater are usually attributed to mineral dust or crustal contributions and are especially associated with environments where soil minerals such as K-feldspar are abundant (Yang et al., 2012). The alkalinity of water is influenced by the concentration of Ca- and Mg bicarbonates. These ions therefore act as buffering agents against acidification (Kanayo et al., 2010; González and Aristizábal, 2012).

Dust is not only known to affect cloud lifetimes through the aerosol indirect effect, but can also enhance precipitation at one location while suppressing it at another (Tang et al., 2018; Luo et al., 2019). The aforementioned elements, i.e. Ca, K and Mg, together with dissolved metals, also contribute to the hardness of the rainwater. Hardness is classified according to the equivalent calcium carbonate ($CaCO_3$) concentration in the water with hard water considered to have a concentration greater than 150 $mg.L^{-1}$ (Kanayo et al., 2010). Soft water is corrosive and causes the dissolution of metals such as Pb and Cd, which, when introduced into potable water systems can have detrimental effects on human health (Nishijo et al., 1995; Kanayo et al., 2010).

2.7.3.3 Marine ions

Na^+ and Cl^- are usually well correlated in rainwater, since these ions are considered to be tracers for marine salt influence (Keene et al., 1986; Sun et al., 2010; Yang et al., 2012; Zhang et al., 2012). Sea salt aerosols are very hygroscopic and with their relatively large radii can enhance the precipitation of warm clouds by encouraging the growth of cloud droplets to rain drops (Johnson, 1982; Rosenfeld et al., 2012; Luo et al., 2019). In their study on tropical cyclones, Luo et al. (2019) found that, with higher levels of sea-salt aerosol, more latent heat is released, which can promote convection and precipitation. The amount of sea-salt aerosol being emitted is dependent on the sea surface wind speed.

Marine environments contribute as a natural source of SO_2 as sea salt is released into the atmosphere as ocean spray. This salt is, however, mostly deposited soon after its release back to the ocean (Shallcross et al., 2003). DMS, produced by phytoplankton, is the most abundant source of biogenic marine SO_2 emitted from the ocean (Stefels et al., 2007; Feltracco et al., 2019). Ca^{2+} and Mg^{2+} can also originate from sea salt spray (Kanayo et al., 2010; González and Aristizábal, 2012; Conradie et al., 2016). Sea salt and non-sea salt fractions of ions such as K^+, Mg^{2+}, Ca^{2+}, Cl^- and SO_4^{2-}, can be derived by relating the ratio of these ions to Na^+ in rainwater to the same ratio in seawater (Keene et al., 1986) (Chapter 3.2.6.2).

2.7.3.4 Organic acids

Oxalic acid ($C_2O_4^{2-}$) is the most abundant dicarboxylic acid in the atmosphere (Kawamura et al., 1996; Pauliquevis et al., 2012). Oxalic acid can be formed when natural vegetation emits isoprene, a volatile organic compound (VOC), which is then oxidised to pyruvic acid and methylglyoxal. These two compounds then react further to form oxalic acid in the cloud environment. Oxalic acid is also emitted through biomass and fossil fuel burning (Huang et al., 2019). Furthermore, oxalic acid is prominent in the atmosphere as it is stable, accumulates and is a product of photochemical oxidation reactions involving the hydroxyl radical. Since HNO_3 forms through similar reactions, the rate of formation of oxalic acid is expected to correspond to that of HNO_3 formation and a possible concentration relationship is expected. Precipitation is considered to be the major removal process of oxalic acid. The oxalic acid concentration in rainwater is expected to be higher than the sum of formic ($HCOO^-$) and acetic (CH_3COO^-) acids when pollution levels are elevated (Pauliquevis et al., 2012).

Acetic- and formic acid, which constitute a large fraction of the organic gaseous acidity, have high vapour pressures and are therefore mostly present in the gas phase in the atmosphere (Grosjean, 1989). Acetic- and formic acid are also emitted by anthropogenic and natural sources, which include fossil fuel combustion and biomass burning. There are, however, significant uncertainties with regard to the individual source contributions to these acids (Finlayson-Pitts and Pitts, 2000; Connell, 2005). The volatile propionic acid emitted through industrial waste and hydrocarbon combustion has an approximate half-life of 13 days. Some herbicides commonly used for cereal crops also contain propionic- and acetic acids that can volatilise (Thompson et al., 1984; Bryson, 1988).

Acetic- and formic acid are considered to be major acids, which can even exceed HNO_3 concentrations in certain conditions. These organic acids, as well as propionic acid, are formed when O_3 reacts with alkenes (olefins) in an aqueous environment. Less reactive olefins (e.g. ethylene) will react with the OH or NO_3 radicals, but in a high RH environment, more reactive olefins will undergo an ozone-olefin reaction that produces organic acids (Grosjean, 1989). Formic acid formation has been related to formaldehyde concentrations and may be as a result of an aldehyde-HO_2 reaction or an OH-initiated oxidation in cloud water (Grosjean, 1989). These acids are easily removed through both wet- and dry deposition processes as they have high Henry's law constant values (Finlayson-Pitts and Pitts, 2000; Connell, 2005).

Concentrations of oxalic-, acetic-, formic- and propionic acids can be combined to give a total value for the water soluble organic acid (OA) fraction of the rainwater chemistry. A strong correlation between K^+, Cl^- and OAs has been related to biomass burning, while the OA fraction is regularly used as an estimate for biomass burning contribution to the rainwater chemistry (Helas and Pienaar, 1996; Cheng et al., 2013; Park et al., 2013; Aurela et al., 2016).

2.7.4 Rainwater Acidity

The natural pH of unpolluted rain in equilibrium with CO_2 is approximately 5.7. The reason for the naturally low pH is that rainwater reacts with CO_2 to form the weak carbonic acid (H_2CO_3) (Reaction 2.17). Rainwater acidity is sometimes expressed as the amount of $CaCO_3$ that can be neutralised. An annual rainfall with a pH of 5.6 of 1 meter depth over a surface of one hectare can dissolve about 400-500 kg $CaCO_3.ha^{-1}.y^{-1}$ (Krug and Frink, 1983; Connell, 2005).

$$CO_2 + H_2O \leftrightarrow H_2CO_3 \quad (2.17)$$

Other acidifying compounds such as SO_2 and NO_x, as well as organic acids, can also contribute to the acidity (Schindler, 1988; Eby, 2004; Menz and Seip, 2004; Banerjee, 2008). Acid rain is mainly caused by SO_2 and NO_x, which oxidise to form H_2SO_4 and HNO_3 as shown in Reactions 2.6 to 2.8 and 2.14 to 2.16 (Halsall, 2003; McGranahan and Murray, 2003; Connell, 2005). According to references in Halsall (2003), between 48 and 84% of all the SO_2 conversion to H_2SO_4 in the troposphere occurs within clouds.

The term acid rain was originally used by Angus Smith in 1852 with reference to the anthropogenic influence of industrial emissions on rain quality (Schindler, 1988). Acid rain gained more public interest later when it was identified as the cause of the acidification of surface water bodies and the subsequent decline in fish populations in Scandinavia and the northern United Kingdom in the 1970s, which contributed to the now popular term (Krug and Frink, 1983). Acid rain has been considered an environmental threat as it acidifies natural water bodies and mobilises heavy metals such as iron (Fe) and aluminium (Al), which contribute to leaching of nutrients from the soil (Krug and Frink, 1983).

Acid rain has been known to have detrimental effects not only on water bodies and aquatic life, but also on soil composition and the related biosphere. Acidic rainwater influences the pH of the uppermost horizon of the soil. This layer of soil contains most root growth and facilitates healthy plant life (Krug and Frink, 1983). Humic acids found in topsoil are especially sensitive to acid rain, as their solubility is pH dependent. When the rain pH is too low, the humic acid becomes less soluble and can no longer regulate the acidity and anionic fluxes in the soil. The result is an increase in the SO_4^{2-} concentration and a decrease in organic acid flux through the soil. Al complexation is inhibited in an acidic soil environment (pH <4.5) and leads to elevated Al concentrations in leached water (Krug and Frink, 1983; Likens et al., 1996). Acid rain also precedes an equivalent net loss of cations in the soil. Soils that have high acidity and low nutrient content are generally more susceptible to further acidification due to acid rain. Other soils that are prone to acidification through rainwater are soils with a pH >5 and soils where basic cations are easily exchanged. These are typically course, siliceous soils with a low cation exchange capacity (CEC). In more basic soil environments, Ca^{2+} and Mg^{2+} can also be leached out. The soil type and composition will therefore determine its ability to act as an acid sink or source, as well as the extent of the detrimental influence from acidic precipitation.

Strong alkaline rain can also be detrimental as it can cause nitrification and subsequent acidification of soils (Krug and Frink, 1983). Alkaline species such as NH_3, carbonates, and Ca^{+} and Mg^{2+} containing dust can increase the pH by neutralising the acidic species and can even lead to alkaline rain (Laouali et al., 2012). Gaseous NH_3 can partially neutralise H_2SO_4

and HNO_3 by producing ammonium nitrate (NH_4NO_3) and $(NH_4)_2SO_4$ (Finlayson-Pitts and Pitts, 2000).

Some studies have found a link between the droplet size and pH. These studies suggest that larger drops contain larger neutralising particles such as dust and salts, while smaller droplets contain more acidifying species such as SO_4^{2-} and NH_4^+ (Finlayson-Pitts and Pitts, 2000). Acid rain is not only harmful to ecosystems and the biosphere, but also impacts infrastructure. The negative impacts associated with acid rain have been widely noted as in Banerjee (2008) and other publications.

2.8 South African Context

Rainwater chemistry is not only influenced by the various microphysical and chemical scavenging processes, but also by the air mass history that is influenced by the progression of synoptic patterns over a region, the type of uplift associated with the rainfall event and the regional air quality context where rainwater is sampled. This section presents a brief overview of South African weather systems influencing rainfall on the Highveld.

South Africa is characterised by distinct wet and dry seasons (Held et al., 1996; Rouault et al., 2013). The South African meteorology is influenced by global circulation as flow patterns from the tropic-, subtropic- and temperate regions affect the weather systems over South Africa. The annual average rainfall over subtropical southern Africa is approximately 500 mm (Harrison, 1986). The central South African wet season ranges from mid-October to May, through mostly convective precipitation systems (Harrison, 1986; Mphepya et al., 2004) Autumn rainfall over western southern Africa can most often be attributed to moisture-rich air coming from the tropical north, while summer precipitation is mostly of the convective type (Harrison, 1986; Preston-Whyte and Tyson, 1988). Diurnal patterns are observed in these convective precipitation events as there is diurnal heating and cooling of the land surface. This is partly due to South African soils, which have low heat capacities and therefore contribute to the night-time formation of surface inversions and convective mixing induced during the day (Garstang et al., 1996; Collett et al., 2010; Laakso et al., 2012).

The prevalence of a continental high pressure over the central plateau, that intensifies and moves northward during winter months, generally results in fine, clear weather. Anticyclonic circulation patterns are dominant over the subcontinent (Garstang et al., 1996), which leads to the atmospheric build-up of pollutants and ageing of air masses, especially during winter when low-level stable layers inhibit vertical mixing of the troposphere (Harrison, 1984; Freiman and Tyson, 2000; Collett et al., 2010). This recirculation of air masses can

last for up to 20 days and is expected to increase the scavenging efficiency (see also Section 2.5.2) (Garstang et al., 1996; Tiitta et al., 2014). Subsidence associated with the persistent anticyclonic circulation promotes the formation of stable layers and associated inversion layers (Preston-Whyte and Tyson, 1988; Freiman and Tyson, 2000; Tyson and Preston-Whyte, 2017). These stable inversion layers have the largest influence on the moisture transport over South Africa and low-level inversion layers are common over continental South Africa during the winter (Newell et al., 1972; Garstang et al., 1996; Freiman and Tyson, 2000; Tyson and Preston-Whyte, 2017). The relatively polluted CCN population and its impact on cloud and precipitation processes have also been shown (Terblanche et al., 2000; Ross et al., 2003).

Convective rain events predominantly occur during the afternoon or early evenings. These events are also associated with relatively high rainfall intensities. In more than 7% of storms on the Highveld, the rate was > 10 $mm.h^{-1}$ and it is not uncommon for intensities to reach up to 90 $mm.h^{-1}$ (Tyson and Preston-Whyte, 2017). Hailstorms over the interior are also associated with the convective rain events and the hailstones are classified as hard hail. Hail is most common during late spring or early summer. More severe storms occur early in the wet season (Tyson and Preston-Whyte, 2017). Tropical-Temperate troughs play a dominant role in rainfall formation over the South African interior. A tropical influence in rainfall is therefore common. These systems combine the instability of westerly waves with the low-level moisture of tropical lows over the subcontinent (Harrison, 1986; Preston-Whyte and Tyson, 1988). Westerly waves and cold fronts affecting South Africa are associated with polar maritime air masses. During the austral summer months, the subsidence inversion layer is at an altitude higher than the escarpment on the east of South Africa and warm moist air from the Indian Ocean is able to move in over the interior. A low pressure trough extends over the country from the tropical north. To the east of the trough axis, convergence occurs and to the west, divergence. A moisture front and squall line thunderstorms are usually associated with this convergence as warm moist air from the north-east meets warm dry air from the south-west. Movement of the moisture front is most often from the south-west (Tyson and Preston-Whyte, 2017). The storms over the Highveld can often be scattered and isolated showing little to no spatial organization (Tyson and Preston-Whyte, 2017). The Highveld plateau has an elevation of between 1200 and 1800 m (Nel and Cobbing, 2019). Convective storm bases are therefore already fairly cold and cold cloud processes play an important role in the precipitation formation processes along with warm cloud (Krauss et al., 1987; Mather, 1991). The effects of the global circulation and local disturbances on the seasonal variability in the rainfall over South Africa can be seen in the rainfall maps for the sampling period in Figure 3.4 (Chapter 3.1).

The type of convection associated with a rain event is a mesoscale factor that can influence the rainwater chemistry. A modelling study by Lynn et al. (2005b) has shown the convective processes that form a convective cloud scavenge most of the CCN within the first 30 minutes during the cloud formation. They also determined a removal of more than 60% available CCN (see also Chate (2011) in Section 2.5.2). A study on seeding agent dispersion by Ćurić et al. (2006) showed the importance of the location where seeding agents will be entrained in the inflow regions of a cumulonimbus cloud. They showed that the internal cloud dynamics determine the entrainment of atmospheric species into the convective cloud. Another study by Ćurić et al. (2009) showed that low-level convergence entrained seeding agents that were roughly 20 km away into convective clouds. In multicell convective storms, the self-destructing mechanism of a single cell serves to promote the development of a new cell. Of the water vapour condensed into the convective cloud, only approximately 20% thereof is precipitated onto the Earth's surface. The other 80% either evaporates on its way to the surface during precipitation or remains as cloud debris that eventually evaporates and can act as CCN that trigger new convection (Wallace et al., 2006).

Chapter 3

Experimental Design

In this chapter, the sampling site for this study is introduced, followed by the procedures followed during the sampling and analytical stages to determine the rainwater composition. The in-situ instruments for the measurement of ambient conditions and ancillary data are presented. Furthermore, the empirical and statistical calculations, as well as the methods followed to determine the air mass histories, are presented.

3.1 Site Description

The sampling site for this project was the Welgegund atmospheric measurement station established in 2010 and operated by the North-West University (NWU), in collaboration with the University of Helsinki (UH) and the Finnish Meteorological Institute (FMI) (Welgegund, 2018). The station is situated on a privately owned farm on the Highveld, approximately 25 km north-west of Potchefstroom and 100 km west of the Johannesburg-Pretoria metropolitan area, in the Republic of South Africa. The measurement station is shown in Figure 3.1. Figure 3.2 depicts the geographical location of the measurement site (26°34'10"S, 26°56'21"E) within a regional context with overlaid back-trajectories indicating the predominant air mass movement during the sampling period prior to arrival at Welgegund (Section 3.2.4).

According to the guidelines of the Global Atmospheric Watch - Precipitation Chemistry Programme (GAW-PCP) of the World Meteorological Organization (WMO), the Welgegund site is considered a regional station since it is less remote than a global station, experiences medium pollutant levels and is located in a rural area with few to no local pollution point sources (WMO, 2004). The site does however experience occasional pollution plumes hailing from major source regions in the South African interior (Figure 3.1). These regions include the government declared pollution hotspots, i.e. the Vaal Triangle Airshed (Government Gazette Republic of South Africa, 2009), the Mpumalanga Highveld (Government Gazette Republic of South Africa, 2007), and the Waterberg-Bojanala (Government Gazette Republic of South Africa, 2015) Priority Areas. The main industries in the Vaal Triangle Priority Area include pyrometallurgical smelters and a large petrochemical smelter. A large number of coal-fired power stations are located in the Mpumalanga

Highveld Priority Area (Lourens et al., 2012; Pretorius et al., 2015). The Waterberg-Bojanala Priority Area includes the industrialised Bushveld Igneous Complex, several large pyrometallurgical smelters and two large coal-fired power stations (Hirsikko et al., 2012; Venter et al., 2012). Air masses arriving at Welgegund are also affected by the Johannesburg-Pretoria megacity. The site is also affected by the dominant anticyclonic air mass movement over the South African interior. As a result, air masses analysed at Welgegund have passed over or around the source regions and have substantially aged over the course of movement to the site (Zunckel et al., 2000). In addition, the site is also impacted by relatively clean regional air masses arriving from the north-west to south-west. The terrain surrounding the station is relatively flat and covered with savannah grasslands.

A recent vegetation survey within a 60 km radius from the site was presented by Jaars et al. (2016). The farm is mainly used for cattle grazing and maize cultivation. The soil type of the area, derived from the calcium, magnesium and carbonate rich Ventersdorp Supergroup geological structures, is heterogeneous ranging from sand to clay (Cairncross, 2004; McCarthy and Rubidge, 2005; Jaars et al., 2016).

Figure 3.1 The Welgegund atmospheric measurement station with (a) the *Vaisala* and *Casella* rain intensity instruments indicated along with (b) the *Vaisala* CT25K ceilometer (Photo credit: Prof J.P. Beukes).

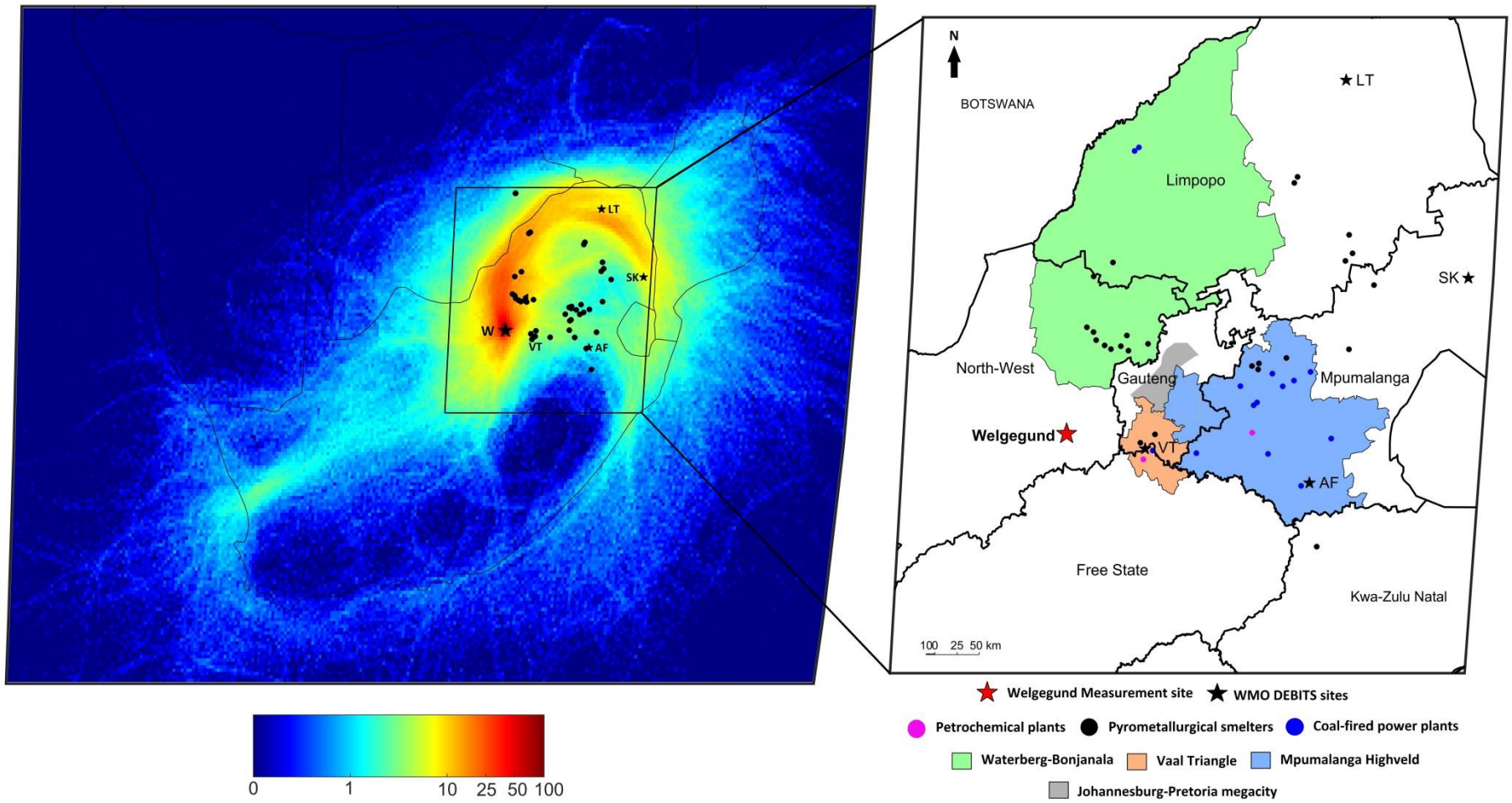

Figure 3.2: Map of southern Africa indicating the Welgegund atmospheric research station relative to major pollution point sources and priority areas, the Johannesburg-Pretoria megacity, and four other South African DEBITS sites (AF: Amersfoort; LT: Louis Trichardt; SK: Skukuza; VT: Vaal Triangle). Overlaid back trajectories for the sampling period are indicated on a percentage colour scale (Section 3.2.4).

Welgegund is located in the Highveld region and the regional meteorology is therefore similar to the description given in Section 2.1.5. A six year measurement record indicates that the temperatures range from -5°C to 36°C with an annual average of 18°C (Jaars et al., 2016; Welgegund, 2018). Seasonal shifts of the continental high pressure controls the meteorology of the South African Highveld. During the austral winter pronounced low-level inversion layers reduce vertical mixing and effectively trap pollutants near the surface (Garstang et al., 1996; Tyson et al., 1996; Laakso et al., 2012). During the austral summer, the high-pressure shifts southwards allowing tropical easterly flow to be prevalent. Low air pressure conditions prevail and are generally associated with unstable conditions and increased dispersion of pollutants. A more detailed description on the meteorology influencing rainfall at Welgegund is presented in Chapter 2.8.

The distinct wet season ranges from mid-October to April with precipitation being mainly of the convective type (Harrison, 1986; Welgegund, 2018). In Figure 3.3, this distinct seasonal precipitation pattern can be seen in the monthly rainfall depths measured at Welgegund during the entire sampling period as well as in the rainfall maps in Figure 3.4 from SAWS (2019). A graduated funnel-shaped rain gauge that limits evaporation was used to measure rainfall depth to the nearest millimetre. Depths below 0.25 mm were regarded as trace amounts. The precipitation covering length (%PCL) or percentage of rain event depths measured was 100%. Significantly lower rainfall depths were recorded for the wet season from October 2015 to May 2016 which corresponded to a severe drought in this region (Simpson and Dyson, 2018). A high rainfall depth was recorded for July 2016 corresponding to an event associated with a low pressure system over the south-eastern coast of South Africa (see also Chapter 6.5) (Tyson and Preston-Whyte, 2017).

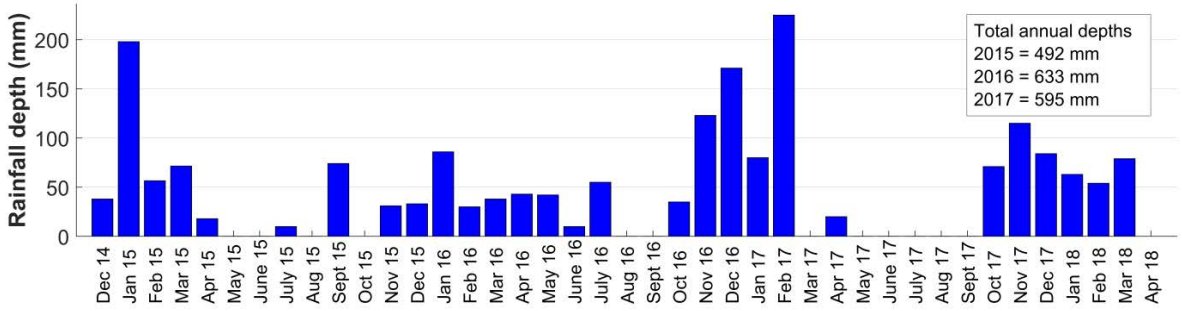

Figure 3.3 Monthly rainfall depths measured during the sampling period with the annual rain depths for 2015 to 2017 also indicated.

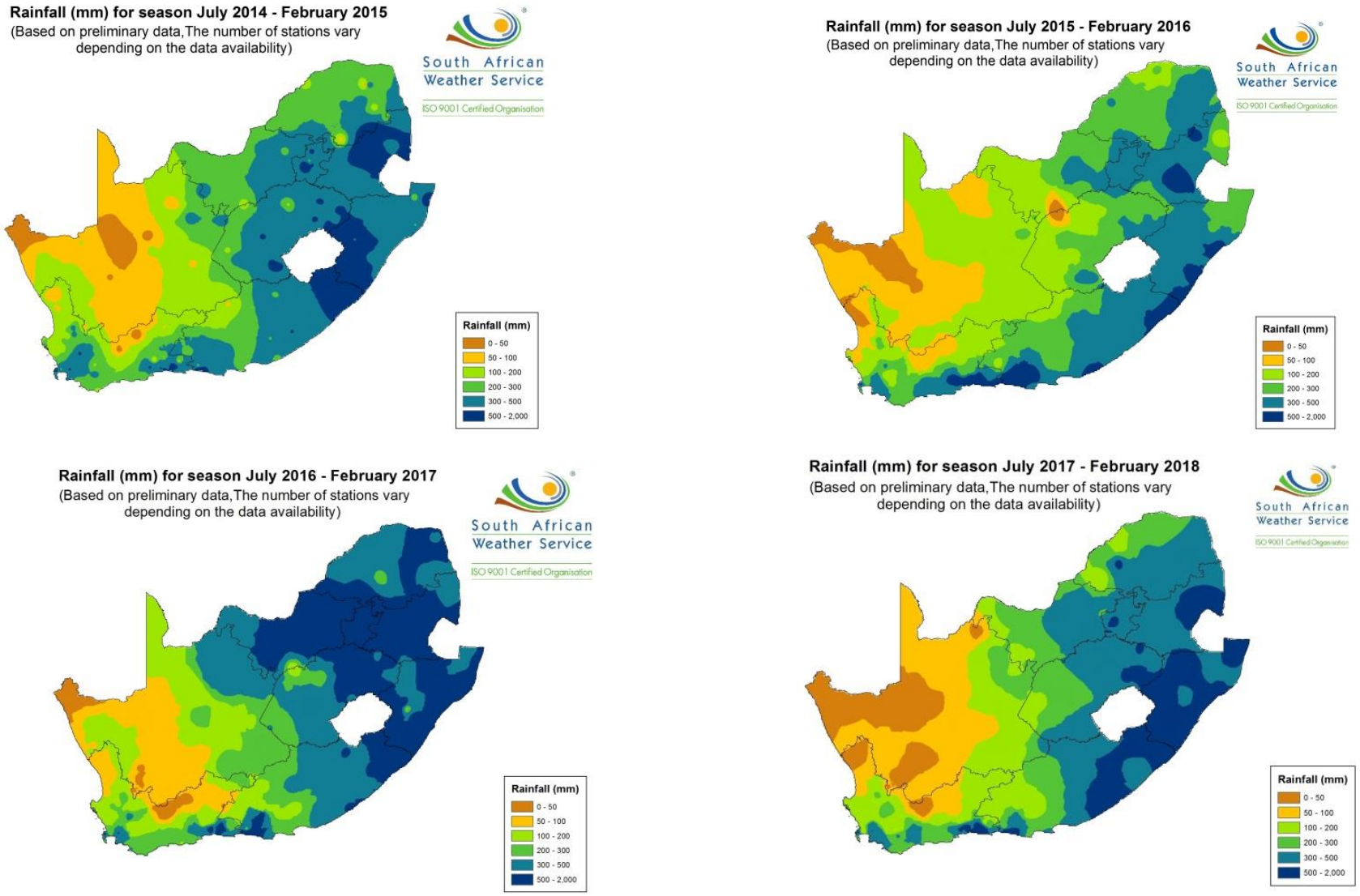

Figure 3.4 Rainfall maps, from left to right, for July 2014 to February 2015; July 2015 to February 2016; July 2016 to February 2017; and July 2017 to February 2018, as published by SAWS (2019).

The measurement site has been described in more detail by several authors including Beukes et al. (2013) and Jaars et al. (2014; 2016). The station is comprehensively equipped with measurements including, but not limited to, rain intensity- and other meteorological measurements, ceilometer lidar, aerosol and ion size distributions, aerosol optical properties, trace gas measurements including carbon dioxide- (CO_2), nitrogen oxides (NO_x) and sulphur dioxide- (SO_2) fluxes, radiation, soil moisture and temperature measurements (Beukes et al., 2013; Welgegund, 2018). The candidate formed part of the ACRG team responsible for general weekly and monthly maintenance, instrument calibrations and data quality procedures.

3.2 Materials and Methods

Various measurement and analytical techniques were used in this study. The methods and their applications are briefly discussed in the following sections. These include on-site measurements (e.g. wet-only sampling, and rain intensity- and ceilometer lidar measurements), as well as laboratory techniques (ion chromatography analyses, pH and electrical conductivity (EC) measurements), empirical and statistical calculations, and modelling of air mass movement.

3.2.1 Rainwater sampling

An automated wet-only sampler derived from the *AeroChemetric* wet-only sampler design, was custom-made by the instrument makers of the NWU (Figure 3.5). The instrument was installed in accordance to the WMO GAW-PCP regulations, and to the guidelines regarding the placement relative to obstructive objects (WMO, 2004), similar to methods used by Mphepya et al. (2004); (2006) and Conradie et al. (2016). The sampler operates using a light-refracting sensor switch that enables the instrument to open the lid of the collection vessel when precipitation starts and to close the lid a few minutes after the rain event has stopped, therefore preventing contamination and further collection of dry deposition. The collection vessel was lined by a high-density polyethylene (HDPE) bag, replaced after every event and weekly during dry periods to minimise contamination. Rain samples were removed from the collection vessel and a field log entry completed by an onsite operator as soon as possible after a rain event (within 24 hours) and frozen immediately in HDPE bottles. The samples were transported in a frozen state in insulated containers to the laboratory where they were kept frozen (at ~-10^{o}C) until chemical analyses commenced.

Figure 3.5: The wet-only sampler (*NWU Instrument Makers*). The open collection vessel is lined with a HDPE bag. The light-refracting sensor is visible at the foremost corner of the instrument. (Photo credit: Dr. M. Josipovic).

3.2.2 Chemical analyses of rainwater

Chemical analysis, quality control and –assurance procedures similar to the methods recently presented by Conradie et al. (2016) were followed by the candidate under guidance from Dr. J. Swarts (ACRG). After the samples were defrosted overnight, the electrical conductivity and pH of 25 mL aliquots were measured using a *Hanna Instruments* HI 255 combined meter (Figure 3.6). The instrument includes in-situ temperature compensation. The electrodes were calibrated using standard buffer solutions with respective pH values of 4.01, 7.01 and 10.01, as well as a potassium chloride (KCl) EC buffer solution all supplied by *Hanna Instruments*. The samples were then filtered using a 0.2 µm *Sigma Aldrich* filter and analysed with a *Dionex* ICS 3000 suppressed IC system (Figure 3.7) to determine the dissolved inorganic and organic content.

For anionic analysis an *IonPac* AS15 (4 mm) analytical column was preceded by an *IonPac* AG15 (4 mm) guard column with an AERS-500 suppressor (4 mm). The potassium hydroxide (KOH) eluent was prepared in-situ with an eluent generator. For the cationic analyses, an *IonPac* CS16 (3 mm) analytical column preceded by an *IonPac* CG16 (3 mm) guard column along with a self-regulating CERS-500 suppressor (4 mm) was used. The methane sulfonic acid (MSA) eluent was generated in-situ. The species measured included the inorganic ions nitrate (NO_3^-), sulfate (SO_4^{2-}), chloride (Cl^-), fluoride (F^-), ammonium (NH_4^+), calcium (Ca^{2+}), potassium (K^+), magnesium (Mg^{2+}) and sodium (Na^+) as well as the water-soluble organic acids (OAs), i.e. acetic- (CH_3COO^-), formic- ($HCOO^-$), oxalic- ($C_2O_4^{2-}$) and propionic acid ($C_3H_5O_2^-$). Standard stock solutions for each ion were obtained from *Industrial Analytical* for a five-point calibration that was performed for each ion within the concentration range expected for rainwater in South Africa. The detection limits of the IC for the species analysed were 28 ppb for NO_3^-, 31 ppb for SO_4^{2-}, 11 ppb for Cl^-, 4 ppb for NH_4^+, 2 ppb for Ca^{2+}, 1 ppb for, K^+, Mg^{2+} and Na^+.

Figure 3.6 The *Hanna Instruments* HI 255 combined EC and pH meter.

Figure 3.7 The *Dionex* ICS-3000 ion chromatographic system used for the ionic content analysis.

3.2.3 Supplementary measurements

The rainwater chemical composition was compared to ancillary measurements continuously performed at Welgegund. These measurements included cloud base height, atmospheric trace gas concentrations (SO_2, O_3, CO and NO/NO_x), PM_{10} concentrations and equivalent black carbon (eBC) measurements, as well as meteorological conditions including temperature, relative humidity, ambient pressure, precipitation intensity, wind speed and wind direction. More details on the ancillary instruments used in this study are given below.

3.2.3.1 Rain intensity measurements

The rainfall intensity was measured with *Vaisala* QMR102 and *Casella* 0.1 mm tipping bucket rain gauges (Figures 3.1 and 3.8) for this study. These instruments have fixed-volume (0.2 mm) buckets that fill with rainwater and are then tipped by a cantilever action. A time stamp is created every time the bucket is tipped out. The volume of rainwater accumulated over the time period between bucket tips is then calculated. The instruments were used to determine the starting times of rain events, rain depth (mm) and rain intensity ($mm.h^{-1}$) (Michaelides et al., 2009).

There is some variability between the different instruments, as well as for the effects of wind speed and precipitation intensity on the instruments (Sevruk, 1996). Wind-induced loss of precipitation volume accumulating in the tipping buckets exceeds the influence of loss due to instrument surface wetting and evaporation. The wind field is furthermore disturbed by the instrument itself being elevated above the ground. Loss of precipitation volume, as measured with the intensity instrument, notably increases with a precipitation rate lower than 2 $mm.h^{-1}$. Wind-induced losses will thus be more pronounced on smaller, non-convective type droplets. The accuracy of the measured precipitation intensity is reduced by higher wind speeds, lower precipitation intensity and non-convective type rainfall (Chvìla et al., 2005). Measurements obtained from both instruments correlated well and were combined in this study.

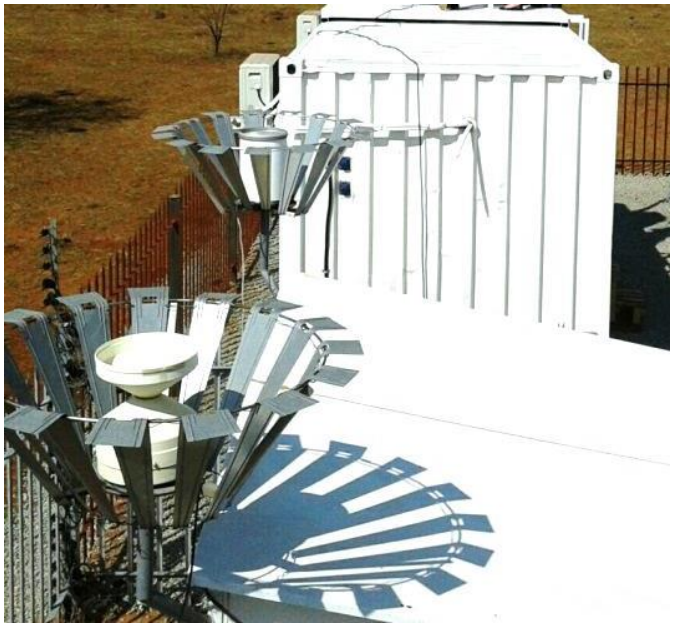

Figure 3.8 The *Vaisala* QMR102 *and Casella* 0.1 mm tipping bucket rain intensity instruments as installed at the Welgegund measurement station (Photo credit: Dr. M. Josipovic).

3.2.3.2 Cloud base height measurements

The cloud base height (CBH) during the onset of a rain event was measured with a *Vaisala* ceilometer CT25K (Figure 3.1 and 3.9). Ceilometer observations were used rather than satellite observations due to the lower time resolution obtained from satellites as there is currently no geostationary satellite covering South Africa (Vaisala, 1999; Costa-Surós et al., 2013). Ceilometers are mainly used to obtain a vertical profile of the atmospheric visibility at airports. The ceilometer is based on light detection and ranging (lidar) principles. A high intensity near-infrared green laser beam is pulsated vertically from a fixed height above the ground into the air as a collimated beam, i.e. a beam that minimally diverges as it propagates. A returning signal is detected as backscattering is caused by atmospheric moisture such as haze, fog, rain, mist and clouds, as well as other particles from which the profile of the attenuated backscatter coefficient (β') can be retrieved (Vaisala, 1999; Emeis et al., 2012; Gierens et al., 2019). This is a stereographic measurement method where the vertical profile and CBH are calculated using the speed of light, the time delay between the laser pulse emissions, and the backscatter signal detection. A vertical profile of the atmospheric backscattering is obtained and visualised as a quantitative signal image. The instrument is equipped with a class 1 laser transmitter source, which is an indium gallium arsenide (InGaAs) diode laser with a centre wavelength of 905 ±5 nm (25^{o}C), as well as a silicon Avalanche Photodiode (APD) detector (Vaisala, 1999). The ceilometer has a 15 s temporal resolution which was averaged to 15 min (Gierens et al., 2019). The instrument was also tilted 4 degrees from the vertical towards the south to avoid reflection from ice clouds.

The CBH is automatically obtained where the backscattering value reaches a maximum. However, precipitation obscures this maximum value. Three respective CBH layers can be obtained from the backscattering values, but clouds can occur in more than three distinct layers, or even in indistinct, merged layers. It is also possible for the layers to obscure each other, in which case only the lowest CBH is detected (Costa-Surós et al., 2013). Therefore, in this study, an assumption was made to only consider the lowest CBH detected by the ceilometer. Other CBH layers, which were not significantly higher than the lowest CBH, were only detected in a few instances. This can be attributed to the merging of cloud layers or other layers being obscured by the lowest layer.

Figure 3.9 The *Vaisala* CT25K ceilometer (Photo credit: Micky Josipovic).

The median CBH was calculated for the 2-hour period prior to the onset of a rain event (as determined by the rain intensity instruments, (Section 3.2.3.1), which enabled calculation of three hourly-arriving back trajectories at the CBH. Since individually calculated trajectories could have errors of up to 15 to 30% (Stohl and Koffi, 1998; Stohl et al., 2002), the use of three instead of only one trajectory significantly reduced such possible error margins (Section 3.2.4).

3.2.3.3 Ancillary measurements

Ancillary measurements continuously performed at Welgegund were used to assist in elucidating factors influencing the chemical composition of rain. General meteorological parameters measured in addition to precipitation included temperature (T), relative humidity (RH), wind speed (WS), wind direction (WD), and atmospheric pressure (P). Atmospheric trace gas measurements at Welgegund included sulfur dioxide (SO_2) (Thermo-Electron 43S SO_2 analyser from *Thermo Fisher Scientific Inc.*, Yokohama-shi, Japan), nitrogen oxides (NO_x) (Teledyne 200AU NO_x analyser from *Advanced Pollution Instrumentation Inc.*, San Diego, Cam USA), carbon monoxide (CO) (Horiba APMA-360 CO analyser from *Horiba*, Kyoto, Japan) and ozone (O_3) (Environment SA 41M O_3 analyser from *Environment SA*, Poissy, France). Particulate measurements included PM_{10} concentrations, measured with a Synchronized Hybrid Ambient Real-time Particulate Monitor (*Thermo Scientific* Model 5030 SHARP), while equivalent black carbon (eBC) measurements were conducted with a Multi-Angle Absorption Photometer (*Thermo Scientific* Model 5012 MAAP). Continuous data was averaged over a 2 hour period before the rain events started. The rain event start times were recorded with the rain intensity meters.

3.2.3.4 Burn scar data

In addition to ancillary measurements conducted at Welgegund, daily fire distribution data were retrieved from the National Aeronautics and Space Administration's (NASA) Distributed Active Archive Centres (DAAC) with assistance from Dr. V. Vakkari (Kaufman et al., 2003). The data is derived from satellite retrievals of the Moderate Resolution Imaging Spectrometer (MODIS) mounted on the polar-orbiting Earth Observation System's (EOS) Terra satellite. Burn scar data were further used by the candidate to present burn scar data for the entire southern Africa for 4 days prior to all rain events in Figure 3.12, to count total burn scars within a 100, 250 and 500 km radius from Welgegund during the sampling period presented in Figure 4.4, and 4 days prior to individual rain events in case studies in Chapter 6.

3.2.3.5 Population density

The South African population density estimate for 2010 was obtained from the Centre for International Earth Science Information Network and plotted by the candidate in

Figure 3.12 (CIESIN, 2010). The population density map is presented with a colour index over a 0.25º by 0.25º resolution (Laakso et al., 2012).

3.2.4 Back trajectory calculations – relating rain events to air mass history

Back trajectories were calculated using the National Oceanic and Atmospheric Administration (NOAA) Air Resource Laboratory's (ARL) Hybrid Single-Particle Lagrangian Integrated Trajectory (HYSPLIT) model (version 4.8) (Fleming et al., 2012; Stein et al., 2015). Meteorological data, obtained from the Global Data Assimilation System (GDAS) archive of the US National Weather Service's National Centre for Environmental Prediction (NCEP), were used in the HYSPLIT model. HYSPLIT is a computer model used globally in atmospheric research applications to calculate and simulate air mass trajectories, dispersion, transformation and temporal history of air masses (Fleming et al., 2012; Stein et al., 2015; Fedkin et al., 2019). The hybrid model integrates the numerical Lagrangian approach and the Eulerian method. These methods differ in their approach to the reference frame or grid, as well as in their methodology in measuring advection and diffusion components.

Three hourly-arriving 96-hour back trajectories were calculated at two arrival heights (i.e. 100m and CBH) for each rain event sampled. A back trajectory was calculated at the starting time of the rain event, with an additional two trajectories calculated one and two hours prior to the onset of the rain event at the two heights indicated. This was done in order to reduce the 15 to 30% uncertainty associated with individual back trajectories (Stohl, 1998; Stohl and Koffi, 1998; Stohl et al., 2002). Following this method, three back trajectories were plotted for individual rain events in selected case studies. Rain events were selected to study specific effects including: the effects of large point sources on rain chemistry; the scavenging efficiency of rain through events on consecutive days and the events with the maximum and minimum rain intensity; winter rainfall events which show the effect of atmospheric pollutant build-up; and events with high tOA concentrations were chosen to explore the effect of biomass burning on rain chemistry.

Back trajectories associated with the 100 m above ground level (a.g.l.) arrival height were considered representative of the air mass history related to below-cloud scavenging. Since orography is not well defined in the HYSPLIT model, arrival heights lower than 100 m a.g.l. also increase the estimated error margins on individual trajectories (Stohl et al., 2002; Draxler and Hess, 2004; Stein et al., 2015). The boundary layer was also considered to be well mixed during the wet season, which is supported by Gierens et al. (2019), who indicated rapid evolution of the boundary layer after sunrise. Their results indicated that a

stable layer at a depth of 200 m or lower traps pollutants during the night and is especially well developed during the colder winter months. After sunrise, a mixed layer rapidly grows with the growth rate being more pronounced in the summer months when the most rain events occur. This mixed layer grows to a depth of approximately 1.75 to 2.25 km, with relatively large standard deviations of around 500 m. These depths stabilise and a residual layer remains after sunset, shrinking as the night passes (Gierens et al., 2019). Three hourly-arriving 96-hour back trajectories at the median CBH 2 hours prior to the onset of rain were calculated for each rain event (Section 3.2.3.2).

In order to generate overlay back trajectories, the individual back trajectories were superimposed on a frequency map with a 0.2º x 0.2º resolution grid to show the statistical distribution. The frequency map has a colour index that indicates the frequency of the trajectories passing over the map grid cells. All calculated trajectories were visualised using *MATLAB* R2019b (www.mathworks.com). The trajectories are constructed using three-dimensional velocity fields, thereby making it an ideal method to incorporate convective motions and the role thereof in the vertical transport of air masses. The overlay back trajectories arriving at 100 m a.g.l. for every day of the sampling period are shown in Figure 3.10.

Although vertical motions are not explicit in synoptic charts (Wallace et al., 2006), surface synoptic weather charts from the *South African Weather Service,* as well as visible- and infrared satellite images from *EUMETSAT* were assessed (SAWS, 2019; EUMETSAT, 2019) in conjunction with the back trajectories in order to determine meteorological systems associated with the rain events. Daily synoptic charts and satellite images was available and was correlated to the rain event timestamps. The maximum CBH measured before an event was 4660 m (or < 5 km), which can still be considered to be in the boundary layer, and therefore surface synoptic maps were a viable information source. Distinct surface pressure features were used to classify rain events into events associated with surface troughs, surface troughs with coastal low pressures, and surface troughs with westerly waves.

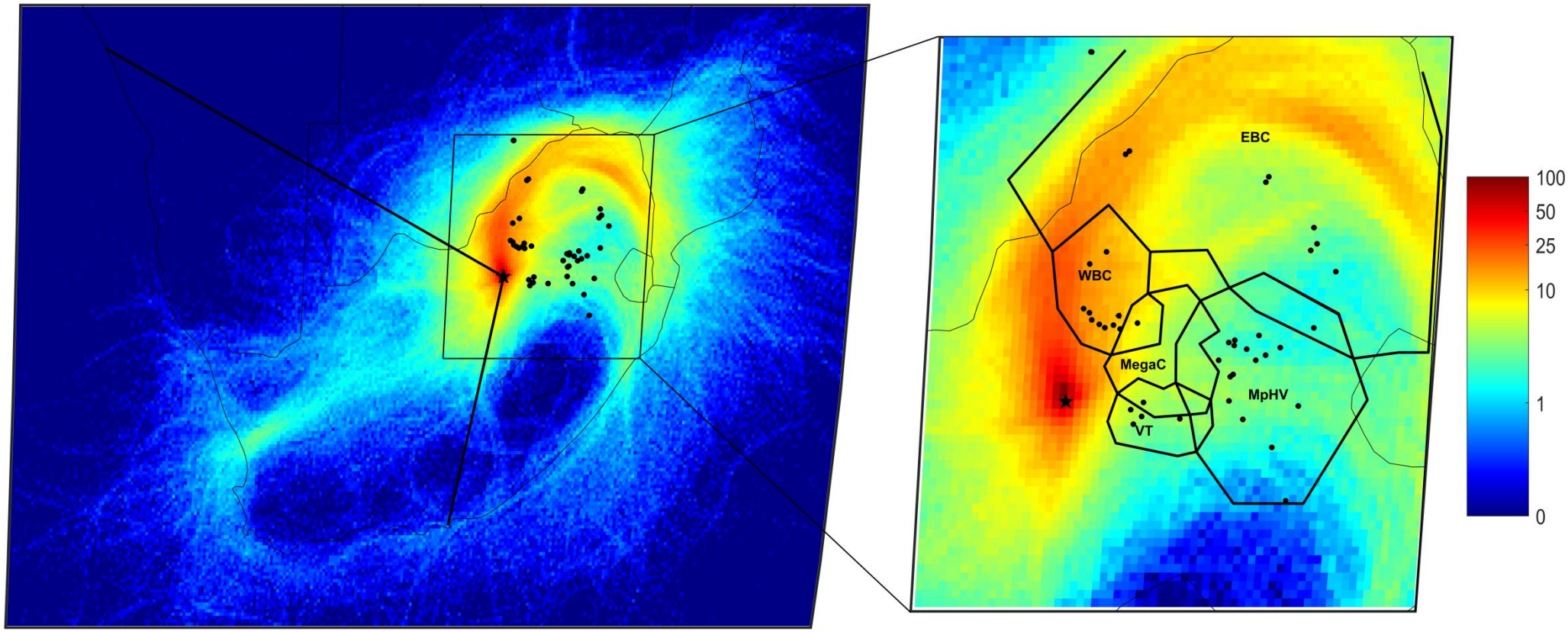

Figure 3.10 Map of South Africa indicating Welgegund (black star), large point sources in the north-eastern interior (black dots) and the major source regions impacting air masses measured at Welgegund (WBC: Western Bushveld Complex; EBC: Eastern Bushveld Complex; MpHV: Mpumalanga Highveld; VT: Vaal Triangle; MegaC: Johannesburg-Pretoria megacity). The black lines stretching from the north-west coast and to the south-west coast from Welgegund demarcate a relatively clean sector to the west of Welgegund with no large point sources. 96-hour overlay back trajectories for the entire sampling period are also presented with the colour scale indicating the percentage of trajectories passing over 0.2° × 0.2° grid cells (blue to yellow to red indicate the lowest to highest frequency of air mass movement).

3.2.5 Data quality of the chemical rainwater analyses

The WMO Data Quality Objectives procedures were followed to determine the ion balance for each sample (WMO, 2004; Conradie et al., 2016). Visible contaminants were reported and removed from the samples by filtration (0.2 mm filter, *Sigma Aldrich*). Ion balances were considered by calculating an ion difference (ID) percentage using the anionic and cationic micro-equivalents (AE and CE respectively in μeq.L^{-1}). Samples with an ID outside of the WMO acceptable ranges were flagged and excluded from further calculations (Equation 3.1-3.2) (WMO, 2004; Laouali et al., 2012).

$$Ion\ Difference\ (\%) = \frac{CE-AE}{CE+AE} \times 100 \quad (3.1)$$

with

$$AE\ (\mu eq.L^{-1}) = [\sum \frac{C_{Ai}}{(EqWt)_{Ai}}] + \left[\frac{5.1}{10^{6-pH}}\right] \times 1000 \quad (3.2)$$

where C_{Ai} is the concentration of the i^{th} anion in mg.L^{-1}, $(EqWt)_{Ai}$ is the equivalent weight of anion i and the second term represents the bicarbonate concentration at 25°C and at a pH above 5.0;

and

$$CE\ (\mu eq.L^{-1}) = \left[\sum \frac{C_{Ci}}{(EqWt)_{Ci}}\right] + 10^{(6-pH)} \times 1000 \quad (3.3)$$

where C_{Ci} is the concentration of the i^{th} cation in mg.L^{-1}, $(EqWt)_{Ci}$ is the equivalent weight of cation i and the second term represents the H^+ concentration in μeq.L^{-1}.

In addition to the above mentioned, accuracy (how close the concentration is to the correct value), precision (how large the standard deviation is), as well as general quality control of IC chemical rainwater analyses were established by the Atmospheric Chemistry Research Group's (ACRG) laboratory of the NWU through participation in the bi-annual inter-laboratory comparison study (LIS) managed by the World Meteorological Organization (WMO) (QA/SAC-Americas, 2018). The results of the 57^{th} LIS study conducted in 2017 are presented in Figure 3.11. The results indicated that the recovery of most ions in standard samples were between 95 and 105%.

Operational procedures to ensure data quality were followed at the research site with weekly and monthly scheduled basic instrument maintenance including filter cleaning, flow rate adjustments and calibrations as well as post hoc data set cleaning to remove irregularities.

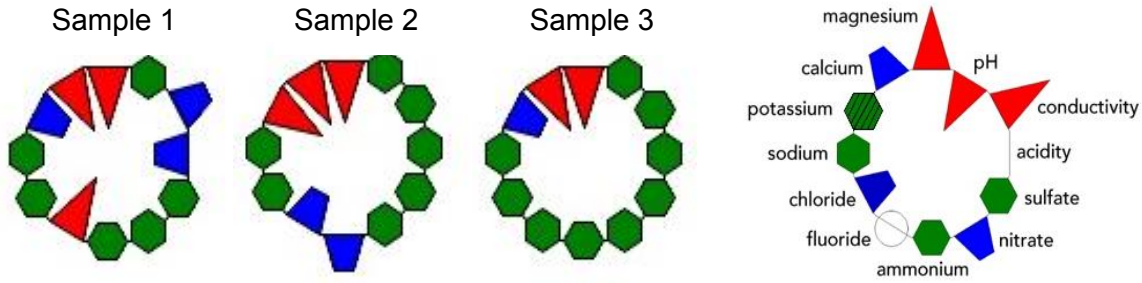

Figure 3.11 Results of the LIS 57 study in 2017 indicated by ring diagrams (legend for the ring diagram also included). Green hexagons indicates that the results are good (measurements are within the interquartile range (IQR), defined as the 25th to 75th percentile or middle half (50%) of the measurements), blue trapezoids indicates that results are satisfactory (measurements are within the range defined by the median ± IQR/1.349) and red triangles indicates that the results are unsatisfactory (measurements are outside the range defined by the median ± IQR/1.349). IQR/1.349 is the non-parametric estimate of the standard deviation, sometimes called the pseudostandard deviation (QA/SAC-Americas, 2018).

3.2.6 Empirical calculations & evaluation

3.2.6.1 Volume weighted mean & wet deposition flux calculations

Ionic concentrations of rainwater samples were determined in ppb with the IC, which were then converted to micro-equivalents per litre (µeq.L^{-1}) by dividing the concentration with the equivalent weight of each of the ionic species. These values were then multiplied with the rainfall event depth ($C_i.P_i$). The C_iP_i values were used in the statistical analyses (Section 3.2.7) and in comparing events in the case studies in Chapter 6. The volume weighted mean (VWM) concentration was calculated for all the ions measured, which was then used to calculate wet deposition fluxes (Equation 3.4 - 3.6).

$$C_{vwm}(\mu eq.L^{-1}) = \sum_{i=1}^{m} \frac{C_i \times P_i}{P_{tot}} \quad (3.4)$$

$$Deposition\ flux\ (kg.ha^{-1}.year^{-1}) = C_{vwm} \times P_{tot} \quad (3.5)$$

with

$$P_{tot}(mm) = \sum_{i=1}^{n} P_i \quad (3.6)$$

C_{vwm} is the volume weighted mean concentration in μeq.L^{-1} and C_i is the analyte concentration in the i^{th} to the m^{th} sample with invalid samples excluded. P_i is the standard gauge precipitation depth for the sample and n is the total number of all rain events that occurred during the entire sampling period (including rain events for which the ionic analysis was excluded) (WMO, 2004). The VWM is calculated to normalise ionic concentrations measured for different rain depths for a sampling period (González and Aristizábal, 2012). The annual wet deposition fluxes (kg.ha^{-1}.year^{-1}) were calculated with Equation 3.7, where Eq.Wt is the equivalent weight of the specific ion (Laouali et al., 2012). The average annual wet deposition fluxes for the sampling period were calculated from the mean annual rainfall from 2015 to 2017, while the total annual rainfall included all rain events during a year and not only rain events passing the WMO data quality criteria (WMO, 2004).

$$Wet\ deposition\ flux\ (kg.ha^{-1}.year^{-1}) = VWM\ \times \sum_{i=1}^{n} P_i \times Eq.Wt\ \times 10^{-5} \quad (3.7)$$

The total VWM was reported in Chapter 4 as calculated for the entire sampling period and the total wet deposition was calculated from 2015-2017.

3.2.6.2 Source contributions and enrichment factor calculations

Conradie et al. (2016) used a combination of empirical calculations and statistical evaluations to estimate source contributions of ionic species in wet deposition, which was also performed in this study. In this study, source groups were classified as being associated with marine-, crustal-, agricultural-, biomass burning-, or fossil fuel combustion sources. A similar approach has been followed in several previous studies where source apportionment of rain chemistry was conducted (Galy-Lacaux et al., 2009; Li et al., 2011; Conradie et al., 2016).

The sea salt and non-sea salt fractions of K^+, Mg^{2+}, Ca^{2+}, Cl^- and SO_4^{2-} were calculated with Equation 3.8 and 3.9,

$$SSF_X = [Na^+]_{rain} \times [\frac{X}{Na^+}]_{seawater} \quad (3.8)$$

$$nSSF_X = [X]_{rain} - SSF_X \quad (3.9)$$

where SSF_x is the sea salt fraction of ion X, $[Na^+]_{rain}$ is the Na^+ concentration in rain, $[X/Na^+]_{seawater}$ is the seawater concentration reference ratio of ion X to Na^+ presented by Keene et al.(1986), $nSSF_x$ the non-sea salt fraction of ion X, and $[X]_{rain}$ the concentration of

ion *X* in the rain sample. In these calculations, it is assumed that all Na^+ in rain is of marine origin (Keene et al., 1986; Laouali et al., 2012; Shen et al., 2012). Enrichment factors of these ions (EF_x) with the regard to $[X/Na^+]_{seawater}$ were calculated with Equation 3.10 (Quiterio et al., 2004)

$$EF_x = [X/Na^+]_{rainwater}/[X/Na^+]_{seawater} \quad (3.10)$$

where $[X/Na^+]_{rainwater}$ is the ratio of ion *X* in relation to Na^+ in rain. When evaluating the EF, a value close to 1 is indicative of marine sources dominating the contribution to that ionic concentration. An indication of the terrigenous source contributions is obtained by considering the EF together with the nSSFs (Keene et al., 1986).

Fossil fuel combustion is related to the anthropogenic SO_4^{2-} and NO_3^- concentrations. In order to estimate the anthropogenic SO_4^{2-} contribution, the marine SO_4^{2-} contribution is subtracted from the total SO_4^{2-} measured in the rain. This nSSF-SO_4^{2-} can then further be distinguished as terrigenous or anthropogenic by two methods (Conradie et al., 2016). The first method uses Ca^{2+} as a reference ion for gypsum ($CaSO_4 \cdot H_2O$). Gypsum is considered to be the reference mineral for continental crust contribution and therefore by determining the excess SO_4^{2-} with regard to gypsum, the anthropogenic contribution can be estimated (Equation 3.11) (Delmas, 1981; Conradie et al., 2016), i.e.

$$[SO_4{}^{2-}]_{anthro} = [SO_4{}^{2-}]_{nSS} - 0.47[Ca^{2+}]_{nSS} \quad (3.11)$$

where $[SO_4^{2-}]_{nss}$ and $[Ca^+]_{nss}$ are the calculated non-sea salt concentrations of SO_4^{2-} and Ca^+. The second method uses an estimate of 7.0 µeq.L^{-1} for background SO_4^{2-} concentrations, which is subtracted from the $[SO_4^{2-}]_{nss}$. This background SO_4^{2-} level was indicated by studies in West Africa (Galy-Lacaux et al., 2009) and agrees with global models.

The agricultural contribution was related to the NH_4^+ concentration and the biomass burning contribution was related to the total dissociated organic acid concentration (Conradie et al., 2016).

3.2.6.3 Acidity

The acidity (H^+ concentration in mol.L^{-1}) was determined from the measured pH with Equation 3.12.

$$pH = -\log[H^+] \quad (3.12)$$

The neutralisation of rainwater is indicated when the actual measured acidity (mA) is less than the acidic potential (pA) of the acidic contributors (i.e. pA is the sum of SO_4^{2-}, NO_3^-

and OA). A neutralisation factor (NF) can be calculated to describe the cation-anion interaction. In Equation 3.13, the relationship of a neutralisation cation *Y* (*Y* = Ca^{2+}, NH_4^+ or Mg^{2+}) with the sum of the potential mineral acids, i.e. H_2SO_4 and HNO_3 is evaluated to calculate the NF with regard to ion *Y* (NF_Y) (Possanzini et al., 1988; Laouali et al., 2012; Yang et al., 2012).

$$NF_Y = \frac{Y}{NO_3^- + SO_4^{2-}{}_{anthro}} \quad (3.13)$$

3.2.7 Statistical evaluation

The statistical analyses were performed in collaboration with the Statistical Consultancy Service of the NWU, Potchefstroom. Multivariate analyses performed on the data included principal component analysis (PCA), Spearman correlations, and hierarchical cluster analysis (HCA). In order to compare the chemical compositions of individual rain events with different rain depths, a standardisation method was applied by dividing the ionic concentration determined in parts per billion (ppb) with the relevant equivalent weight and multiplying by the rain event sample depth (see Section 3.2.2). For non-detected concentrations, half of the detection limit was substituted to prevent inflated mean values.

3.2.7.1 Principal Component Analyses (PCA)

Principal component analyses were performed on the rainwater chemistry as an explorative statistical method as the dataset was not large enough to do a proper source apportionment. PCA and Spearman correlations were calculated to determine similar sources of chemical species in the rainwater. As an explorative method, the PCA was performed on the rainwater chemistry with the ancillary measurements as supplementary variables. A varimax rotation along the principal component axes allowed the best separation so that the ions with the largest contributions to the variance were located at the furthest distance from the origins of the axes. Eigenvalues larger than 1 were considered significant (Hosiokangas et al., 1999). The PCA were performed with *STATISTICA* for *Windows 7* (StatSoft, 2006).

3.2.7.2 Hierarchical Cluster Analyses (HCA)

In contrast to the multi-dimensional space analysis of PCA, HCA is one-dimensional, which simplifies the interpretation of associations of the different samples (Pieters, 2007). The rainwater chemical composition, as well as air mass histories at CBH and 100 m a.g.l., were subjected to a hierarchical cluster analysis (HCA) (*STATISTICA*, (StatSoft, 2006) and *SPSS Statistics*). Ward's method, in which the squared Euclidean linkage distances were determined to reveal optimum cluster solutions, was applied. Samples with strong associations were clustered together based on a minimising loss of information principle (Johnson and Wichern, 2007). Two approaches were followed, i.e. (1) clustering based on the chemical composition of rain and, (2) clustering according to air mass history at 100 m and CBH.

The first approach determined clusters of strong correlations between ionic species in rainwater, which was then related to air mass history at CBH and 100 m a.g.l. as well as to rain intensity and ancillary measurements. Since back trajectories are a type of time series (Pérez et al., 2017), the second approach clustered the average time that back trajectories arriving at Welgegund at CBH and 100 m a.g.l. spent over different source regions (Figure 3.12), which was then associated with ionic composition of rainwater as well as rain intensity and ancillary measurements.

The second HCA approach was based on the air mass histories of the samples. According to Critchfield (1983), a body of air that is relatively stable over a source region will achieve equilibrium with the surrounding environment given sufficient time. The air mass will then tend to keep the characteristics, including homogenous composition, temperature and moisture characteristics that are in equilibrium with the source region, even as it moves onward. The chemical composition of precipitation is also controlled by various ecosystem-specific and complex factors, which include emission source strengths, atmospheric transport, chemical reactivity and other removal processes (Akpo et al., 2015). Long-range transport of aerosols, for example, can affect rainwater composition by acting as condensation nuclei (CN) in a region distant from the original emissions. In addition, the ecosystem characteristics, such as being within proximity of an ocean, will also affect the ionic content of precipitation (Chapter 2.6) (Garstang et al., 1996; Galy-Lacaux et al., 2009; Li et al., 2011). Therefore, the air mass histories were grouped together based on the time spent over different predefined environments. The source regions were defined as: (1) pollution point sources; (2) north/north-eastern continental region; (3) clean western continental sector; and (4) oceanic sources. These regions can be seen in Figure 3.12 (see also Section 3.2.4).

The time that air masses arriving at 100 m a.g.l. and CBH spent over predefined source regions prior to arrival at Welgegund was determined. These regions included an area to the west and a region to the east of Welgegund, which are demarcated by the purple lines in Figure 3.12. The sector to the west represents the relatively clean background region with no large point sources influencing air masses measured at Welgegund. The eastern area includes the major point sources in the interior of South Africa, while this region is also densely populated with extensive biomass burning occurring in this sector (Figure 3.12). This eastern area was further separated into two source regions. The first source region included the major point sources in the interior of South Africa, i.e. coal-fired power stations, pyrometallurgical smelters and petrochemical industries, as well as the JHB-PTA conurbation (indicated by the blue polygon in Figure 3.12) (see also Figure 3.2). The second source region excluded these large point sources and represented the regional impacts associated with major large point sources, i.e. household combustion and open biomass burning. The total time that air masses spent over the oceans was also quantified.

Dendrograms for the three-cluster solutions for the two approaches are presented as: Figure 3.13 chemical approach; Figure 3.14 the 100 m arrival height air mass history approach; and Figure 3.15 the CBH arrival height. Since the ideal cluster solution is subjective and subject to some variability, the agglomerate schedule coefficients – a measure of heterogeneity between groups – were plotted as indicated in Figure 3.16 (Pérez et al., 2017). These plots revealed relatively good cluster solutions, which are descriptive of the data within each group without increasing the degree of detail of each group to an extent where the complexity increases, i.e. meaningful solutions. The most significant decrease in the coefficient differences was considered optimum cluster solutions. Therefore, as indicated in Figure 3.16, three clusters were determined to be optimum solutions for each of the approaches followed in this study. Higher than three-cluster solutions resulted either in increased or negligible changes in heterogeneity. A maximum of three back trajectory clusters are sometimes suggested as they prove simple to explain, while retaining a sufficient degree of detail of the different air masses (Pérez et al., 2017).

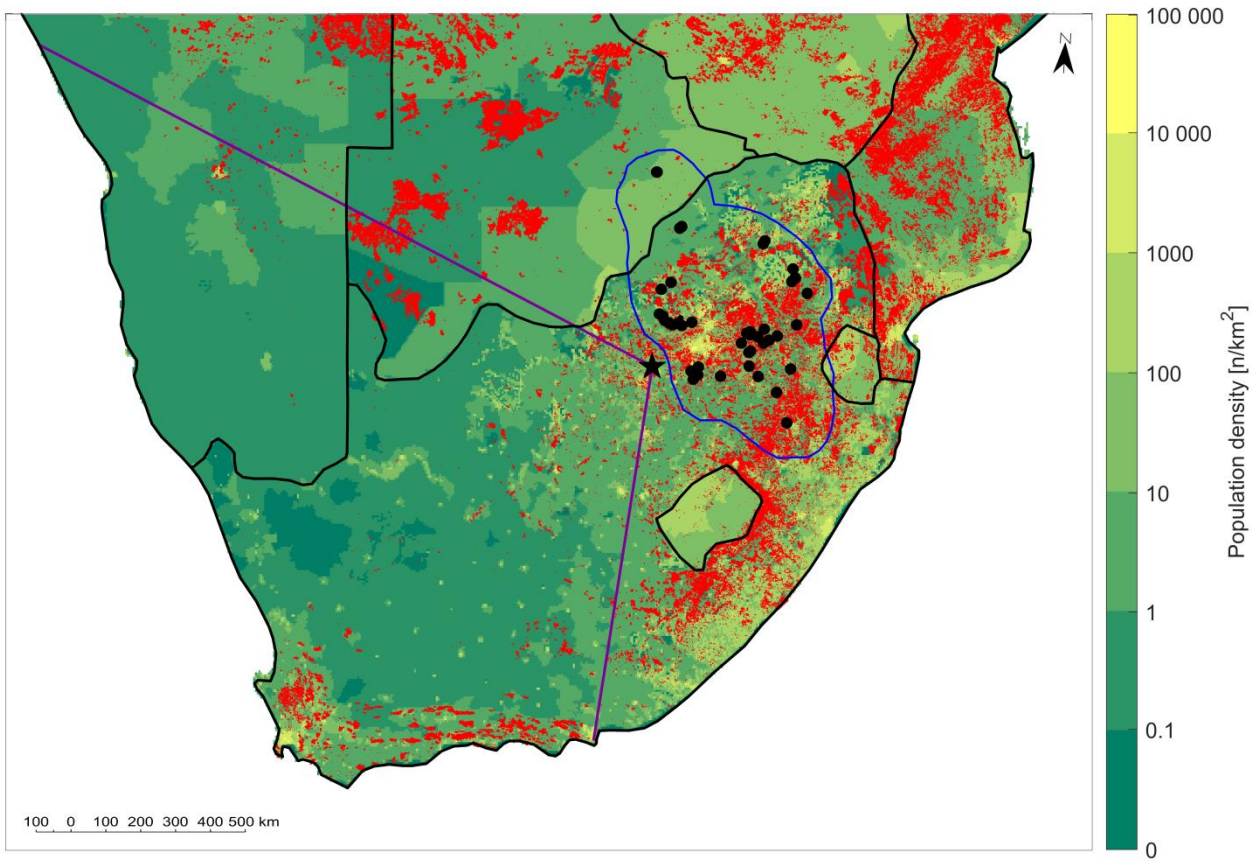

Figure 3.12 A map of southern Africa indicating the 2010 population density estimate for South Africa (CIESIN, 2010), the MODIS burned areas (red areas), major point sources (black dots) impacting Welgegund (black star), and the source regions defined in this study. The purple lines separate the source regions into the relatively clean north-west to south-western sector with no large point sources, and an eastern region that is densely populated, has extensive open biomass burning occurrences and includes major point sources in the South African interior. The blue polygon indicates the source region including only the major point sources and the JHB-PTA conurbation.

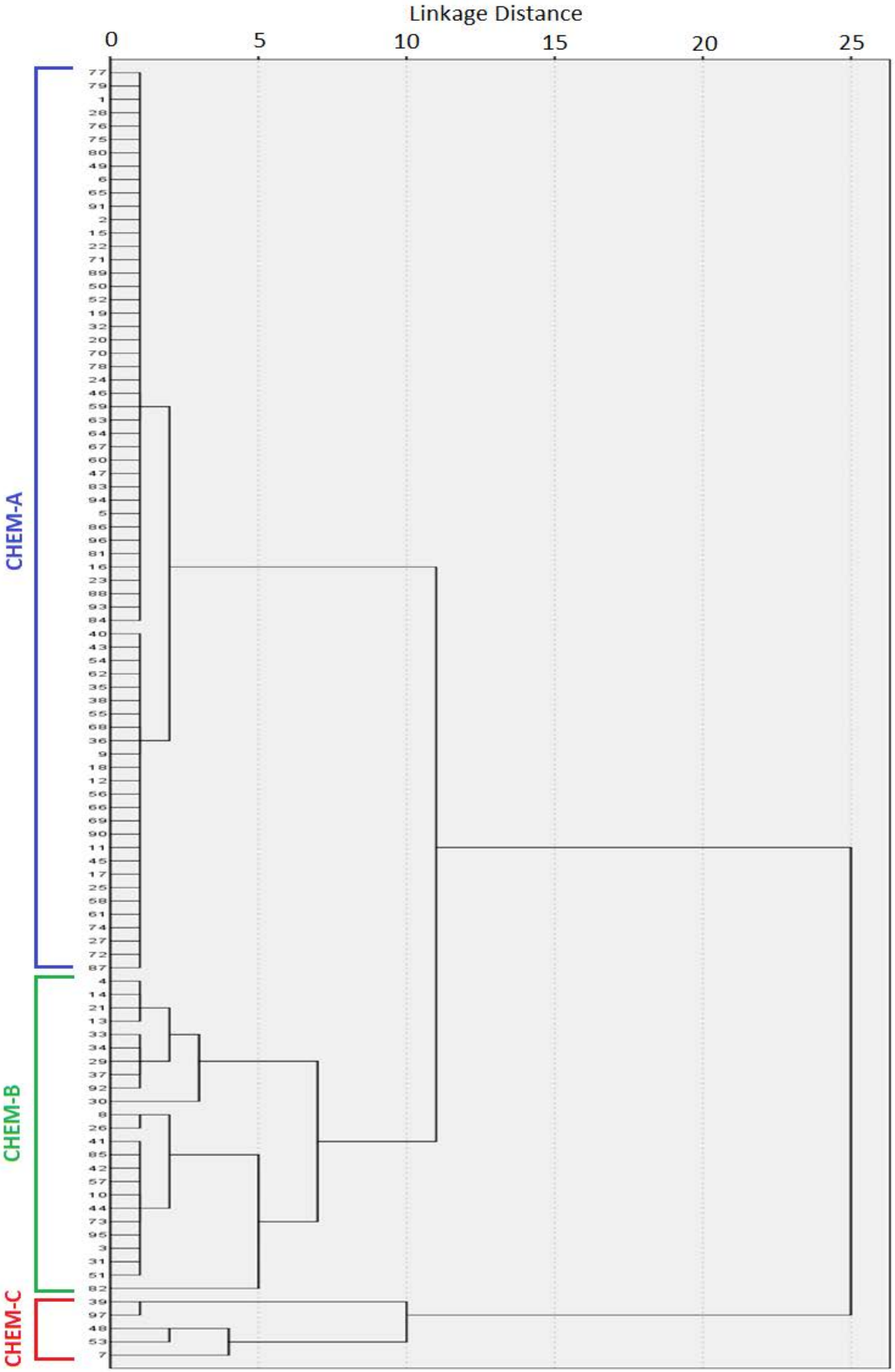

Figure 3.13 Dendrogram for HCA on the ionic composition of rainwater. The y-axis represents individual rainwater samples.

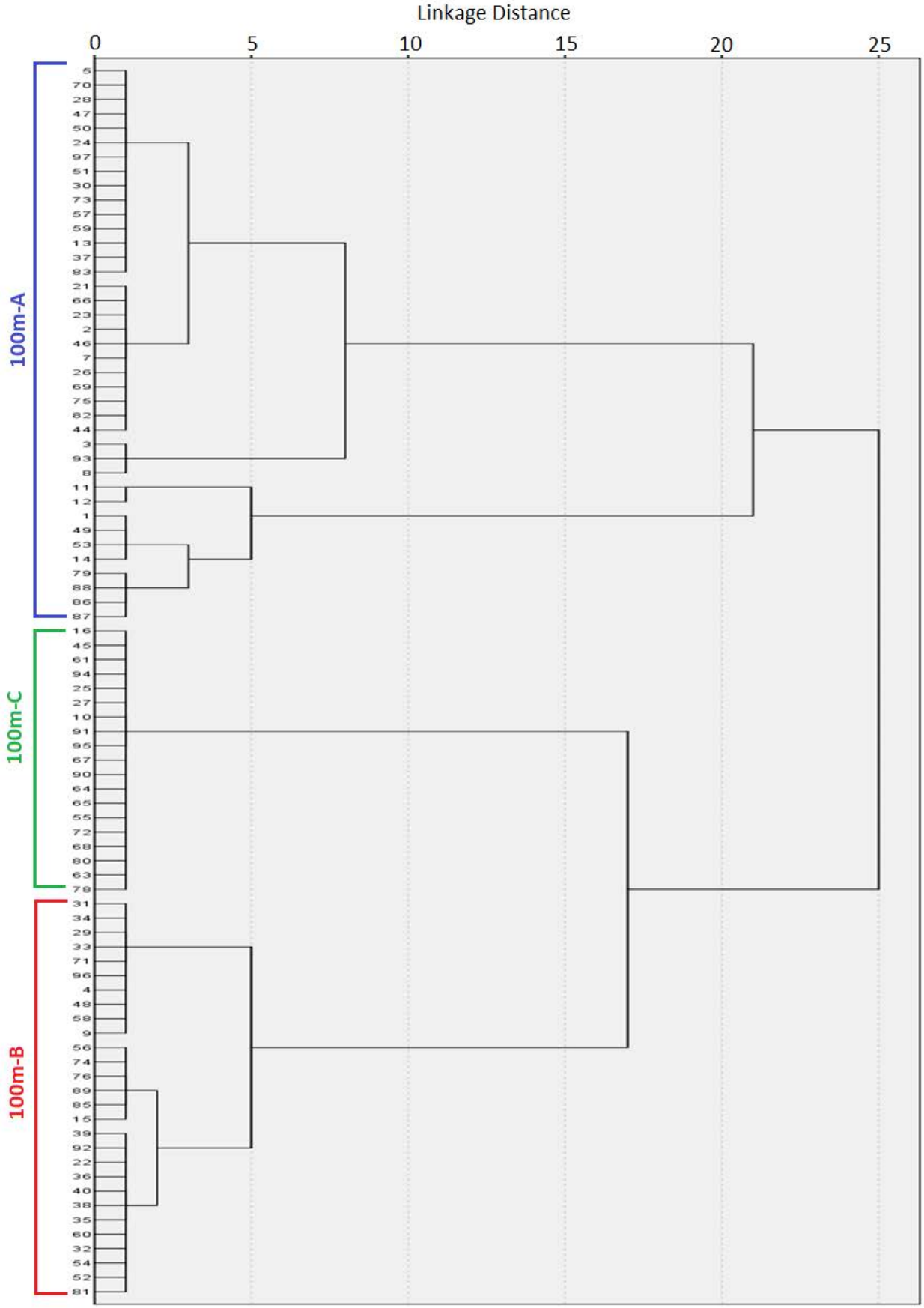

Figure 3.14 Dendrogram for HCA on the time 100m arriving air masses spent over the predefined regions. The y-axis represents individual rainwater samples.

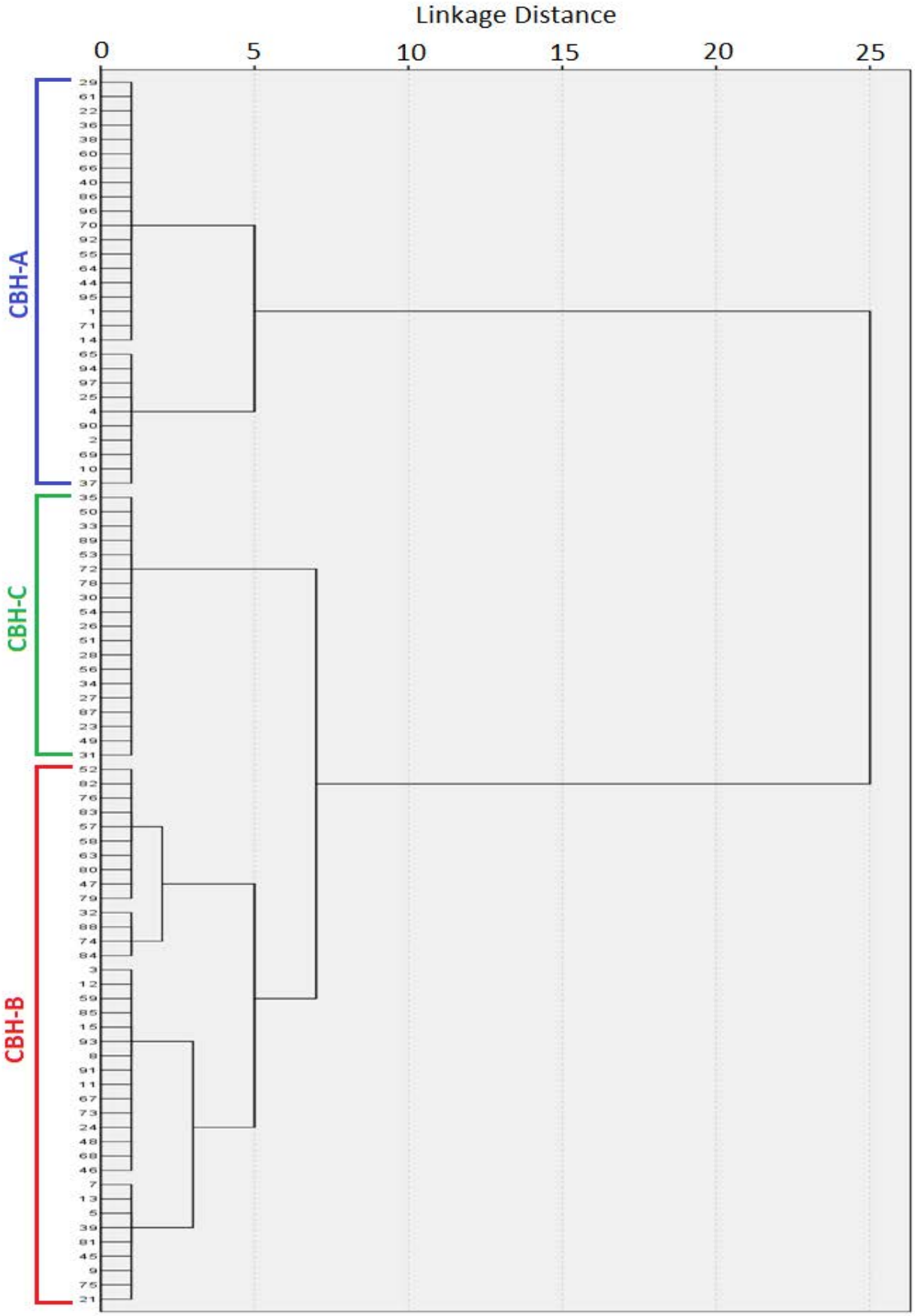

Figure 3.15 Dendrogram for HCA on the time air masses arriving at CBH spent over the predefined regions. The y-axis represents individual rainwater samples.

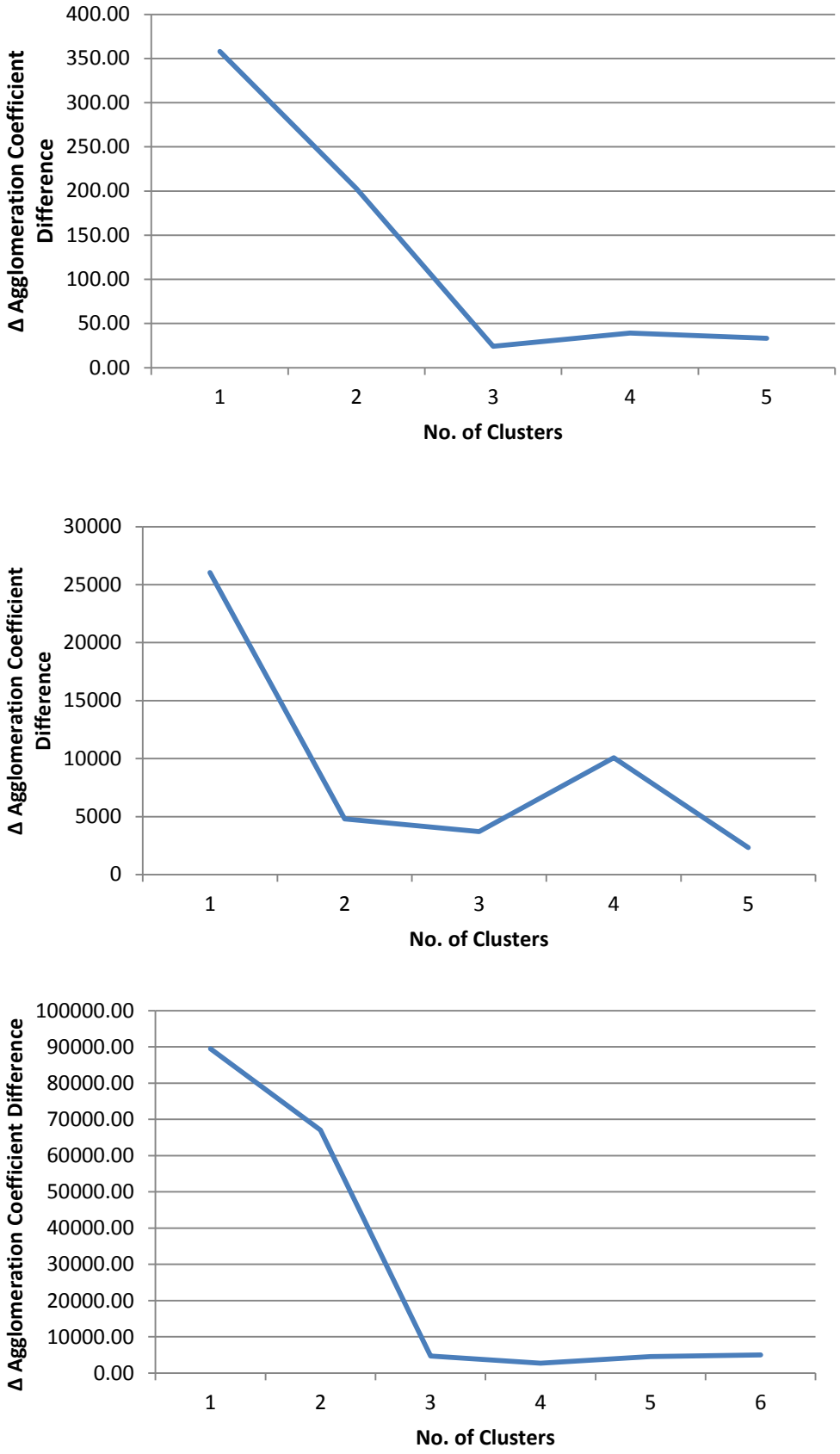

Figure 3.16 Agglomeration schedule coefficient differences that indicate the optimal three-cluster solutions for the chemical approach (top), for the 100 m arriving air masses (middle) and for the CBH arriving air masses (bottom).

An analysis of variance in cluster solutions was conducted by evaluating the statistical and substantive significance of different clusters. When comparing variance of the chemical species, or the ancillary measurements between the different clusters, a p-value of < 0.05 was considered to be a statistically significant difference, with effect sizes also considered. Effect sizes enable a standardised measure regardless of scale, which allows comparisons and identification of relationships between quantities with different units and sizes (Ellis and Steyn, 2003). Furthermore, they limit the possible overestimation associated with only considering statistical significance. In this study, effect sizes were reported as Cohen's d values, which describe the standardised mean difference of the effect as presented in Equation 3.14 (Cohen, 1988; Ellis and Steyn, 2003; Lakens, 2013).

$$d = \frac{|\overline{x_1} - \overline{x_2}|}{s_{max}} \tag{3.14}$$

where d = Cohen's effect size, $\bar{x}_1$ and $\bar{x}_2$ are the means of two samples being compared, and s_{max} is the maximum standard deviation of the two groups. Effect sizes are considered small for $d \leq 0.2$, medium for $0.2 < d \leq 0.5$, and large for $0.5 < d \leq 0.8$ (Cohen, 1988; Ellis and Steyn, 2003; Lakens, 2013). A large effect size implies considerable variances for a variable in different clusters, which is an important factor characterising different clusters. Effect sizes can also be used to determine the significance of overlap between different clusters, and were therefore also used in this study to relate clusters determined with the different approaches to each other.

The HCA clusters from the different approaches were compared through cross-tabulation. Statistically significant overlap between the groups (the same events occurring in the two groups being compared) was indicated when the p-value was < 0.05. Effect sizes can also be defined as the amount of overlap between two groups or the average percentile distribution of one group in comparison to another group. A zero effect size occurs where the mean of one group is at the 50th percentile of another group and there is a complete overlap of the two groups being compared. A small effect size will therefore indicate a small difference between the groups when considering a specific variable. A large effect size (0.8) will have the mean of one group at the 79th percentile of the other group, with an overlap of 53% between the groups (Sullivan and Fein, 2012). By reporting the p-values and effect sizes, relationships between the rainwater composition, air mass histories and ancillary measurements can be established.

Chapter 4

Rain chemistry at a regional background site in the North-West Province of South Africa

This chapter presents the ionic composition and wet deposition of the rainwater sampled at Welgegund atmospheric research station for the period of December 2014 to April 2018. A contextualisation with other South African DEBITS sites is presented. The acidity of the rain, as well as the neutralisation factors, are assessed. Possible apportioned source contribution estimates of the components in the rainwater are determined through Spearman correlations, explorative principal component analyses, and exploring the air mass history through back trajectory calculations. Seasonal variability in the rainwater chemistry and wet deposition is explored.

4.1 Ionic Composition, Wet Deposition Fluxes & Acidity

In Table 4.1, the total number of rain events collected and chemically analysed are presented. The number of events passing the WMO ion difference (ID%) criteria as well as the number of events discarded due to analytical and sampling errors are presented. The samples represent single rain events for all the events where the rain depth was greater than 0.2 mm. The percentage of the samples that passed the WMO ID% criteria and retained for further calculation was in the percentage total precipitation (%TP) acceptance range (i.e. %TP $\geq$ 70%). The %TP (89.2%) can be considered a very good representation of wet deposition (WMO, 2004).

Table 4.1 Summary of rain samples collected from December 2014 to April 2018 at Welgegund.

	2014 (Dec)	2015	2016	2017	2018 (Jan-Apr)	Total
# of events collected	5	37	36	29	12	119
# of events failing WMO ID% criteria	0	3	2	5	5	15
# of events discarded due to sampling and analytical errors	0	0	0	0	1	1
Collected rainfall depth (mm)	38	457	604	499	144	1742
Total rainfall depth (mm)	38	492	633	595	196	1954
Average rainfall depth (mm)						573.33*
%TP	100.00	92.89	95.42	83.87	73.47	89.15

*Calculated for 2015 – 2017

In Table 4.2, the total VWM ionic concentrations ($\mu eq.L^{-1}$) and wet deposition fluxes ($kg.ha^{-1}.year^{-1}$) together with the average pH and mean electrical conductivity (EC) measured at Welgegund for the entire sampling period (VWM: December 2014 – April 2018, wet deposition flux: January 2015 – December 2017) are listed. The VWM and wet deposition fluxes were calculated using the equations (eq. 3.4, 3.5, 3.6) in Chapter 3.2.6. The water-soluble organic acids (OA) (i.e. acetic- (CH_3COO^-), formic- ($HCOO^-$), oxalic- ($C_2O_4^{2-}$) and propionic- ($C_3H_5O_2^-$) acids) were combined and presented as totals. The VWM and wet deposition fluxes of rain samples collected at the four DEBITS sites from 2009 to 2014 by Conradie et al. (2016) are also presented in Table 4.2 for contextualisation.

It is evident that over the sampling period at Welgegund, SO_4^{2-} had the highest VWM concentration, as well as at the other South African DEBITS sites (Conradie et al., 2016). The rainfall at Welgegund as well as the atmosphere on a regional scale is notably influenced by the anthropogenic and industrial activities that contribute to high S- and N-emissions. The VWM SO_4^{2-} concentrations at Welgegund were 3 to 4 times higher when compared to the two rural background sites (Louis Trichardt and Skukuza), but only slightly lower when compared to sites within proximity of industrial sources in two South African priority areas (Vaal Triangle and Amersfoort). The VWM SO_4^{2-} levels at Welgegund were also much higher than VWM SO_4^{2-} measured at other African DEBITS sites (Galy-Lacaux et al., 2009; Conradie et al., 2016), as well as when compared to most other regions globally, with the exception of eastern North America, Eastern Europe and East Asia (Vet et al., 2014).

NO_3^- was the second most abundant species at Welgegund, followed by Ca^{2+} concentrations that were marginally higher than NH_4^+ VWM concentrations. NO_3^- and NH_4^+ were also the second and third most abundant species, respectively at Amersfoort and Vaal Triangle. Similar to these industrially influenced sites, the influence of the anthropogenic source regions on Welgegund is seen in the NO_3^- and NH_4^+ concentrations that were also 2 to 3 times higher compared to levels thereof at the two rural background sites (Figure 3.2, Chapter 3.1). However, the smaller difference in concentrations of the N species compared to that of SO_4^{2-} indicate the nitrogenous contribution of sources other than industry, which can most likely be attributed to the influence of regional household combustion, open biomass burning and agricultural activities.

The VWM concentrations for Ca^+ and Mg^{2+} at Welgegund were higher than all the other South African DEBITS sites, which can most likely be attributed to the influence of wind-blown dust from the relatively clean sector (Figure 3.2, Chapter 3.1) (Venter et al., 2017). Piketh et al. (1999) reported that industrially derived S and wind-blown dust are the main constituents in haze layers over South Africa. A study on the size-resolved characteristics of ionic species in particulate matter (PM) collected at Welgegund by Venter et al. (2017) also indicated that SO_4^{2-} dominated aerosol chemical composition, while NH_4^+ and NO_3^- were the second and third most abundant species, respectively. In addition, aerosol chemical specification monitor (ACSM) measurements of submicron aerosols at Welgegund also revealed higher contributions of SO_4^{2-} and NH_4^+ to the chemical composition of PM_1 (Tiitta et al., 2014). Therefore, the ionic composition of rainwater at Welgegund corresponds to the chemical composition of aerosols measured at Welgegund. Venter et al. (2017) and Tiitta et al. (2014) attributed the chemical composition of aerosols to the influence of SO_2 and NO_2 emissions in source regions impacting air masses measured at Welgegund, as well as the impacts of regional household combustion and open biomass burning.

Table 4.2 The EC, pH, ionic concentrations ($\mu eq.L^{-1}$) and fluxes ($kg.ha^{-1}.yr^{-1}$) of wet deposition at Welgegund from December 2014 to April 2018, as well as at the four South African DEBITS sites from 2009 to 2014 (Conradie et al., 2016).

	Welgegund		Amersfoort		Vaal Triangle		Louis Trichardt		Skukuza	
	Dec 2014 – Apr 2018		2009 – 2014		2009 – 2014		2009 – 2014		2009 – 2014	
	VWM	Flux[a]	VWM	Flux	VWM	Flux	VWM	Flux	VWM	Flux
pH	4.80		4.32		4.51		4.89		4.66	
EC	35.44		42.6		33.6		13.1		22.9	
H^+	28.05	0.16	61.18	0.45	44.64	0.43	15.24	0.11	22.24	0.13
Na^+	18.86	2.52	17.79	2.98	3.50	0.77	7.75	1.30	13.17	1.77
NH_4^+	24.55	2.67	28.50	3.75	29.06	5.01	10.85	1.42	12.80	1.35
(kg $N.ha^{-1}.yr^{-1}$)		2.07		2.91		3.89		1.11		1.04
NO_3^-	30.93	10.65	33.40	15.11	22.97	13.62	7.49	3.38	13.20	4.77
(kg $N.ha^{-1}.yr^{-1}$)		2.41		3.41		3.08		0.76		1.08
K^+	6.45	1.54	7.35	2.10	1.41	0.53	5.12	1.46	2.08	0.48
Mg^{2+}	12.88	0.70	5.54	0.49	4.55	0.53	1.93	0.17	3.27	0.23
Ca^{2+}	24.96	2.74	16.39	2.40	16.18	3.10	6.25	0.91	4.69	0.55
Cl^-	18.60	3.92	17.96	4.65	4.52	1.53	10.83	2.80	15.73	3.25
SO_4^{2-}	48.10	13.11	67.21	23.56	55.0	22.27	12.37	4.33	18.66	5.23
(kg $S.ha^{-1}.yr^{-1}$)		4.38		7.87		8.44		1.44		1.75
F^-	0.56	0.06								
OA	12.98		14.64		12.51		12.14		9.69	
(OA*)	(9.70[b])	4.09	(13.24[b])	5.57	(11.49[b])	6.10	(11.10[b])	4.54	(8.69[b])	2.93
Total VWM and WD	236.6	42.1	283.2	61.1	205.8	62.3	101.1	21.9	124.2	21.7
Total rainfall (mm)	1954		4378.5		5738.6		4369.2		3499.4	
Average annual rainfall (mm)	573.33[a]		729.8		956.4		728.2		583.2	

[a]Calculated for 2015 – 2017
[b]Dissociated fractions of the organic acids

As mentioned previously, although N is an important nutrient in the environment, it can contribute to eutrophication of the environment when it exceeds critical loads (Josipovic et al., 2011). The total wet deposition fluxes of N and S at Welgegund were 4.48 kg $N.ha^{-1}.y^{-1}$ and 4.38 kg $S.ha^{-1}.y^{-1}$, respectively. These wet deposition fluxes of N and S were lower than total N and S wet deposition determined at Amersfoort and Vaal Triangle while being approximately two times higher than wet deposition fluxes of these species determined at Louis Trichardt and Skukuza. The lower N and S deposition at Welgegund compared to the two industrially influenced sites with similar levels of SO_4^{2-}, NO_3^- and NH_4^+ can be attributed to lower average annual rainfall at Welgegund during the respective sampling periods, as well as to the greater distance to the industrial sources from Welgegund.

It is also evident from Table 4.2 that the total VWM ionic concentration at Welgegund was in the same order as the total VWM ionic levels at Amersfoort and Vaal Triangle while being approximately two times higher than total ionic concentrations at Louis Trichardt and Skukuza. The total wet deposition flux at Welgegund was lower than total wet deposition fluxes at the two industrially influenced sites, which can be attributed to lower average annual rainfall at Welgegund during the measurement period as mentioned above. However, total wet deposition flux at Welgegund was approximately two times higher than total wet deposition fluxes at the two rural sites. Ionic concentrations can be considered a better indication of differences in atmospheric chemical composition between these sites since wet deposition fluxes also depend on the rainfall amount (Conradie et al., 2016). The total VWM ionic concentrations and wet deposition fluxes at Welgegund also signify the influence of anthropogenic source regions on air masses measured at Welgegund. In the next section, a source contribution evaluation is explored to further understand the influence of air mass history on the ionic composition of rainwater at Welgegund.

The average pH at Welgegund for the sampling period (4.80) is similar to the average pH values determined for the dry savannah sites Louis Trichardt and Skukuza. The pH was also higher than Amersfoort and Vaal Triangle. Therefore, although VWM concentrations of species associated with acidity in rainwater, i.e. SO_4^{2-} and NO_3^- at Welgegund were similar to levels thereof at the industrially influenced sites, pH levels were comparable to pH values determined at the rural background sites, which suggests increased neutralisation in rainwater collected at Welgegund. The average pH at Welgegund was, however, lower than the natural pH of unpolluted rain in equilibrium with carbon dioxide (5.60), while also being lower than global pH averages (Vet et al., 2014) and pH levels in western African countries (Laouali et al., 2012). In Figure 4.1, the pH frequency distribution at Welgegund is shown (Chapter 3.2.2). 89% of the rain events at Welgegund, compared to 94% of all rain events measured at other South African DEBITS sites, had pH values below 5.6 (Conradie et al., 2016). The majority of rain events

(69%) had pH values between 4.0 and 5.0, with a high frequency of rain events having pH values between 4.4 and 4.8. 3.9% of rain events had pH < 4.0, while 3.9% had pH > 6.0. The maximum and minimum pH measured was 8.08 and 3.55 respectively.

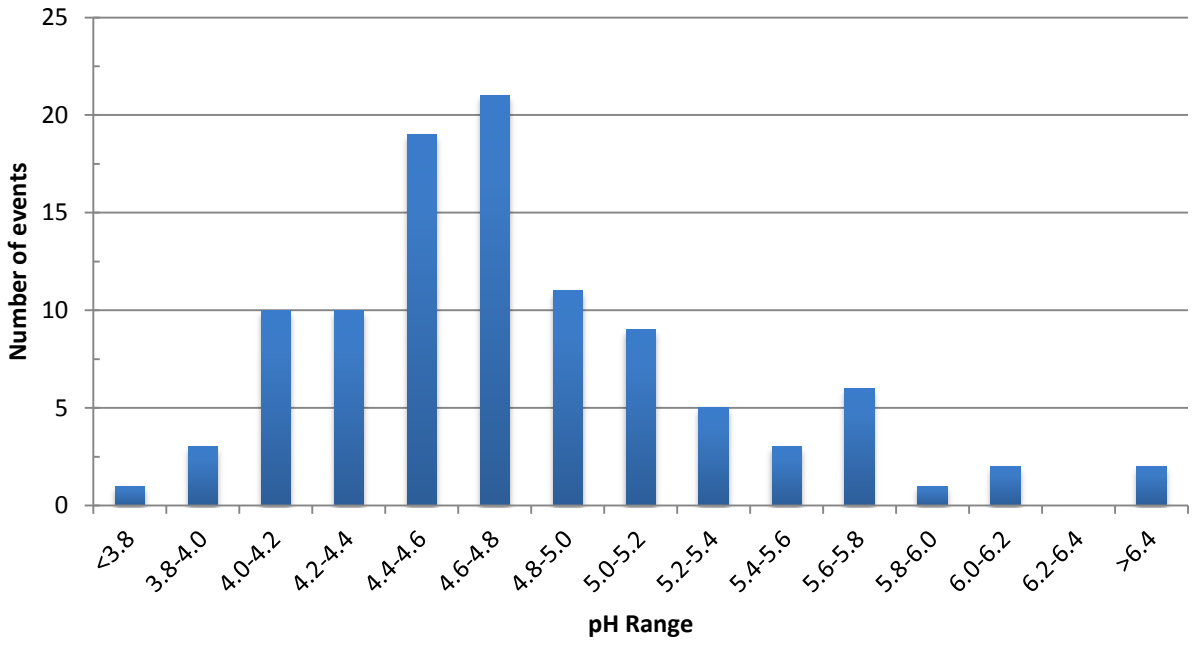

Figure 4.1 The pH distribution of rain samples collected during individual events at Welgegund from 2014 to 2018.

The acidity potential (pA), or the sum of the potential acidic species i.e. (SO_4^{2-}, NO_3^-, and OA) is given in Table 4.3 (Laouali et al., 2012). The potential contribution of mineral acids to free acidity at Welgegund is calculated to be 87%, which is similar to that calculated at Amersfoort and Vaal Triangle (Conradie et al., 2016). However, it is evident that the measured H^+ concentration is considerably lower than the estimated acidity at Welgegund, which is a good indication that neutralisation of acidic species has occurred. In Table 4.3, the neutralisation factors (NF) for the neutralising bases containing the cations NH_4^+, Mg^{2+} and Ca^{2+} calculated using Equation 3.12 is also presented (Chapter 3.2.6.). It is evident that the strong acidic species, sulphuric- and nitric acid, were mainly neutralised by Ca^{2+} and NH_4^+. In contrast to the other South African sites where NH_4^+ was the major NF, Ca^{2+} contributed more significantly to neutralisation at Welgegund.

Table 4.3 Contributions of mineral and organic acids to total acidity, and acid neutralisation factors (NFs) of wet deposition calculated at Welgegund from 2014 to 2018.

	$\mu eq.L^{-1}$	%
Sulphuric acid	34.5	45.9
Nitric acid	30.9	41.2
Organic acids	9.7	12.9
Total estimated H^+ (pA)	75.1	100
Measured H^+ (mA)	28.1	37.4

Neutralisation Factors		
NH_4^+	**Mg^{2+}**	**Ca^{2+}**
0.38	0.20	0.38

4.2 Sources of Ionic Species

4.2.1 Statistical analyses

In order to gain some insight into the source contributions for the ionic content of the rainwater collected at Welgegund, statistical analysis can assist in determining linkages between sources and the ionic composition of rainwater (Xu et al., 2015; Conradie et al., 2016). Therefore principal component analysis (PCA) and Spearman correlations were calculated for all the rain events collected at Welgegund (Figure 4.2) (Chapter 3.2.7.1). The Spearman correlation coefficient is indicated by the colour index ranging from dark blue (< 0) to yellow (1).

Three meaningful factors were identified that explained 84% of the variability in the dataset. These factors identified with PCA (Figure 4.2) corresponded to similar sources of ionic species in rain samples collected at the four other South African DEBITS sites, i.e. marine, crustal, anthropogenic (fossil fuel), agriculture and biomass burning (Conradie et al., 2016), which is also supported by Spearman correlations. The first PCA factor had high loadings of ionic species corresponding to crustal sources (Ca^{2+}, Mg^{2+}), which is also reflected by strong Spearman correlations of these species (0.84). This factor also had a high contribution from NO_3^-, which, in conjunction with strong Spearman correlation between NO_3^- and Ca^{2+} (0.85), also suggests the significant contribution of Ca^{2+} on neutralisation of acidic species at Welgegund. The second factor is mainly related to acidity (H^+), which corresponded to species associated with anthropogenic activities, i.e. NO_3^- and SO_4^+. Spearman correlations also indicate strong linkages between NO_3^- and SO_4^+ (0.74). In addition, this factor also had a relatively high loading of NH_4^+, which is most likely associated with local and regional agricultural activities. The third PCA factor comprised mainly of ionic species associated with biomass burning, i.e. OA, K^+ and Cl^- (Helas and Pienaar, 1996; Aurela et al., 2016), while this factor was also considered to be associated with marine air masses as indicated by high loadings of Na^+ and Cl^-. The species in this factor were also strongly associated in the Spearman correlation analysis. Therefore, according to these two statistical analyses, the major source groups identified as influencing chemical composition of rainwater at Welgegund were marine, crustal, anthropogenic (industrial), agriculture and biomass burning.

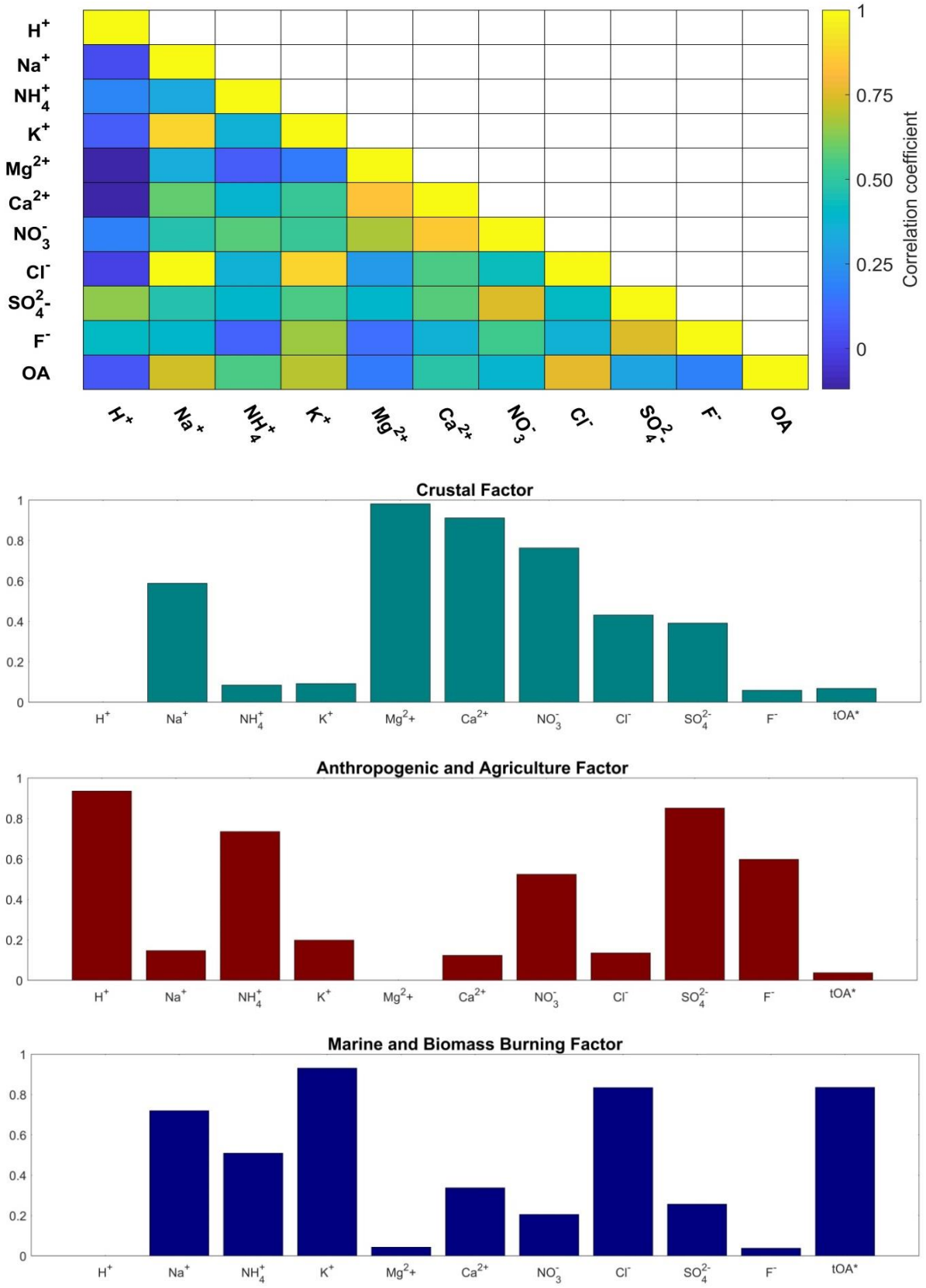

Figure 4.2 Spearman correlations and the three meaningful PCA factors presented with the factor loadings for the ionic species determined in rainwater collected from December 2014 to April 2018 at Welgegund.

4.2.2 Source group contributions

Following the Spearman correlations and the meaningful factors revealed through PCA, the estimated source contributions from the groups identified were calculated. Sea salt and non-sea salt fractions (SSF and nSSF) of Cl^-, SO_4^{2-}, Ca^{2+}, Mg^{2+} and K^+ were determined from which the marine and crustal contributions of these species to the rainwater composition were estimated (Eq. 3.7-3.10, Chapter 3.2.6.1). The nSSF SO_4^{2-} contribution was separated into crustal and anthropogenic contribution with the two methods discussed in Chapter 3.2.6.2. For the other DEBITS sites in South Africa, Conradie et al. (2016) assumed that anthropogenic SO_4^{2-} and total NO_3^- were predominantly associated with fossil fuel combustion. However, since Welgegund is also influenced by other regional sources, such as pyrometallurgical smelters in the western Bushveld Igneous Complex (Figure 3.2, Chapter 3.1), anthropogenic SO_4^{2-} and total NO_3^- at Welgegund were considered to be associated with fossil fuel combustion and other industrial activities, i.e. anthropogenic. NH_4^+ can mainly be related to agriculture in this part of South Africa. Although NO_3^- and NH_4^+ measured in rainwater at Welgegund can be associated with other anthropogenic and natural sources, a much larger contribution from anthropogenic activities indicated here can be assumed. The biomass burning contribution to the chemical composition of rain was estimated by the OA VWM concentrations, which was also estimated by Conradie et al. (2016) for the other South African DEBITS sites in this manner. Estimations of the source group contributions to the chemical composition of rainwater at Welgegund are summarised in Figure 4.3 as percentage of the total ionic composition in equivalent units.

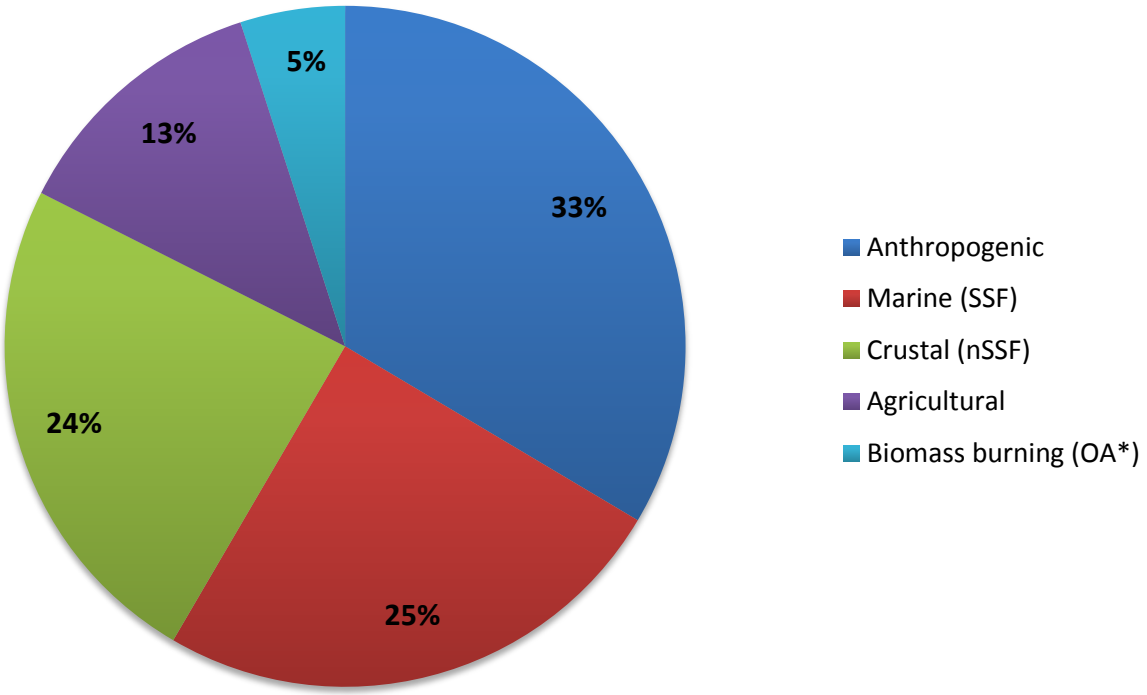

Figure 4.3 Estimations of the source group contributions to the chemical composition of rainwater at Welgegund.

4.2.2.1 Anthropogenic (industrial) contribution

Welgegund is a regional background site impacted by the major source regions in the South African interior (Figure 3.2, Chapter 3.1). Therefore, emissions of gaseous SO_2 and NO_x associated with anthropogenic activities in these source regions would contribute to the occurrence of SO_4^{2-} and NO_3^- in rainwater at Welgegund. Most industries in South Africa do not apply de-SOx and de-NOx technologies, while primary emissions of SO_4^{2-} and NO_3^- are unlikely due to most industries in these regions filtering out particulates in off-gas (Scorgie, 2012; Moganelwa, 2013; Tiitta et al., 2014). The major anthropogenic sources of SO_2 and NO_x in the north-eastern interior of South Africa are coal-fired power plants and petrochemical industries (Schreuder, 2006; Moganelwa, 2013; Papo, 2014; Meth, 2018). In addition, pyrometallurgical smelters are also important sources of SO_2 in this region, while vehicular emissions, open biomass burning and household combustion (for space heating and cooking) also contribute to elevated NO_x (Lourens et al., 2011; Pretorius et al., 2015). The industrialised interior impacting Welgegund is also characterised by anticyclonic recirculation of air masses, which contribute to ageing of SO_2 and NO_2 (Lourens et al., 2012). Although natural emissions of NO_x from e.g. biogenic sources and naturally occurring open biomass burning, could also contribute to NO_3^- in

rainwater at Welgegund, it is expected that anthropogenic sources would make a relatively large contribution (Chan et al., 2005; Ren and Zhao, 2012).

In Table 4.4, the crustal and anthropogenic (industrial) source contributions to non-sea salt SO_4^{2-} calculated with the two methods previously described, i.e. method 1 calculating the excess SO_4^{2-} of that supplied by gypsum (Equation 10) and method 2 where a baseline SO_4^{2-} level is subtracted from the total SO_4^{2-} VWM concentration, are presented. The estimated contributions of anthropogenic (industrial) SO_4^{2-} to the total SO_4^{2-} measured in rainwater at Welgegund calculated with the first and second method is 72 and 81%, respectively. The anthropogenic (industrial) contribution to total SO_4^{2-} calculated with the first method was similar to the anthropogenic contribution calculated at the rural background site Louis Trichardt (72%) with this method. However, the estimated anthropogenic contribution calculated with the second method is slightly lower than the values estimated at the industrially influenced Vaal Triangle and Amersfoort sites (~90%) with the second method, while being significantly higher than the anthropogenic (industrial) contribution calculated at Louis Trichardt (43%) and Skukuza (62%) (Conradie et al., 2016). Notwithstanding the deficiencies associated with these estimations of anthropogenic SO_4^{2-}, both methodologies signify a strong anthropogenic influence on SO_4^{2-} at Welgegund.

Table 4.4 Estimated source contributions to SO_4^{2-} (µeq.L^{-1}). Terrigenous and anthropogenic values calculated with the second method (assumption of background concentration of 7 µeq.L^{-1}) are indicated in brackets, while other values reported were calculated with the first method (excess of that supplied to gypsum).

Total (µeq.L^{-1})	**SSF (µeq.L^{-1})**	**nSSF (µeq.L^{-1})**		**Anthropogenic contribution to total [SO_4^{2-}] (%)**
	Marine	**Terrigenous**	**Anthropogenic**	
49.7	2.7	11.3 (4.7)	34.5 (41.1)	71.7 (80.7)

It is evident from Figure 4.3 that anthropogenic (industrial) activities have a relatively significant influence on rainwater chemical composition at Welgegund, with this source group contributing 33% to the total ionic content. The anthropogenic (industrial) source group contribution at Welgegund is lower than the fossil fuel source group contribution to ionic content in rain at Amersfoort (44%) and Vaal Triangle (47%), but higher than the contribution of fossil fuels at the two rural background sites (24 and 13%) (Conradie et al., 2016). As mentioned previously, Amersfoort and Vaal Triangle are located within two highly industrialised regions declared national priority areas by the South African government, while the impact of air masses passing over these regions is evident at Welgegund (Figure 3.2, Chapter 3.1). Welgegund is also impacted by large point sources in the western Bushveld Complex located within a third South African priority area (Waterberg-Bojanala), as well as the Johannesburg-Pretoria conurbation (Figure 3.2, Chapter 3.1). In addition to large point sources in these source regions, vehicular emissions and household combustion can also contribute to elevated levels of anthropogenic pollutants at Welgegund (Venter et al., 2012; 2017). As previously mentioned, SO_4^{2-} levels dominated the aerosol ionic content in aerosols measured at Welgegund, while NO_3^- had the highest contribution to aerosol ionic composition in the large ($PM_{2.5-10}$) size fraction (Venter et al., 2017). A recent study at Welgegund also indicated the significance of SO_4^{2-} to new particle formation in this region (Vakkari et al., 2015).

4.2.2.2 Marine contribution

The SSF was calculated using the methods described in Chapter 3.2.6.2. The ratio of the ions relative to Na^+ in the rainwater compared to the same ratio in seawater is a good indication of the marine contribution to these specific ionic concentrations measured in the rainwater. The calculated rainwater ratios and reference seawater ratios of Cl^-, SO_4^{2-}, Mg^{2+}, Ca^{2+} and K^+ with respect to Na^+ (Keene et al., 1986), as well as the corresponding enrichment factors (EF) are listed in Table 4.5. The marine source contribution at Welgegund was determined by combining the sea-salt fractions calculated for these species from their measured VWM concentrations (Equation 3.8), which was estimated to be 25% (Figure 4.3). This estimate indicates a relatively substantial contribution from marine air masses on rain chemistry at Welgegund, which is similar to the marine source contribution determined by Conradie et al. (2016) at Amersfoort. The Cl^-/Na^+ ratio was similar to the reference seawater ratio with a corresponding EF close to one, which, together with the strong statistical correlation (Figure 4.2), indicates that air masses passing over marine environments are the major source of these species. As indicated by overlaid back trajectories in Figure 3.2 (Chapter 3.1), Welgegund is impacted by air masses passing over oceans bordering South Africa. Na^+ and Cl^- VWM concentrations were also

relatively high at Welgegund as shown in Table 4.2. The calculated ratios of all other species in relation to Na^+ were higher than the seawater ratio, with SO_4^{2-}/Na^+, Ca^{2+}/Na^+ and K^+/Na^+ being one to two orders of magnitude higher, while Mg^{2+}/Na^+ was three times higher. This can be attributed to other sources of these species associated with the major source regions and the relative clean sector to the west impacting Welgegund. Venter et al. (2017) also attributed the higher contribution of Na^+ and Cl^- in the larger atmospheric aerosols ($PM_{2.5-10}$) at Welgegund to the influence of marine air masses. The Mg^{2+}/Na^+ in aerosols were close to the reference seawater ratio in contrast to the rainwater ratio.

Table 4.5 Comparison of rainwater and seawater ionic ratios, as well as corresponding enrichment factors (EF) in rainfall at Welgegund.

Ion	Seawater*	Rain (2014-2018)	EF
Cl^-/Na^+	1.160	0.986	0.850
SO_4^{2-}/Na^+	0.121	2.551	21.084
Mg^{2+}/Na^+	0.227	0.683	3.008
Ca^{2+}/Na^+	0.044	1.324	30.158
K^+/Na^+	0.022	0.342	15.549

*(Keene et al., 1986)

4.2.2.3 Crustal contribution

The crustal contribution at Welgegund was calculated as the sum of the nSSF of Mg^{2+}, Ca^{2+}, K^+, Cl^-, and SO_4^{2-}. The nSSF was calculated by subtracting the SSF from the VWM concentrations of Cl^-, Mg^{2+}, Ca^{2+} and K^+ (Equation 3.9). The crustal contribution of SO_4^{2-} was determined by subtracting the SSF and the nSSF anthropogenic SO_4^{2-} contribution determined by two methods described in Chapter 3.2.6.2. Ca^{2+}, Mg^{2+} and SO_4^{2-} which were well correlated (Figure 4.2) are indicative of typical southern African soil types that are rich in minerals such as calcite ($CaCO_3$), dolomite ($CaMg(CO_3)_2$), gypsum ($CaSO_4.2H_2O$) and clay minerals (e.g. K-rich illite and smectite micas) (Piketh and Prangley, 1999; McCarthy and Rubidge, 2005; Conradie et al., 2016). The total crustal contribution ranged between 24% and 19% depending on the method applied to estimate anthropogenic SO_4^{2-}contribution (source contribution presented in Figure 4.3 is based on calculations from the first method). A relatively significant crustal contribution is evident at Welgegund, which is similar to that observed at the other South African DEBITS sites (Conradie et al., 2016). As indicated by Conradie et al. (2016), a relatively high contribution from crustal species in rain can be expected for the semi-arid southern African

region with most rainfall events being convective. As previously mentioned, Welgegund is also frequently impacted by air masses moving over a relative clean north to south-western sector in which the Karoo and Kalahari are located (Figure 3.2, Chapter 3.1). Venter et al. (2017) attributed wind-blown dust to be the most important source of certain particulate trace metals in air masses passing over this region, with higher atmospheric levels of Ca, Fe, Na, Mg, Al and Ti associated with the clean sector. Venter et al. (2017) also indicated a considerable contribution of crustal species to the ionic composition in the larger aerosol size fraction ($PM_{2.5-10}$) at Welgegund. Fly ash associated with coal combustion and pyrometallurgical activities could be additional sources of Ca^{2+} and Mg^{+} in rainwater at Welgegund (Mahlaba et al., 2011), which could lead to a slight underestimation of the nSSF anthropogenic SO_4^{2-} concentration.

4.2.2.4 Agricultural contribution

The agricultural source group contribution at Welgegund, mainly related to NH_4^+ at South African DEBITS sites (Conradie et al., 2016), was estimated to be 13% (Figure 4.3), which was similar to the contribution of agricultural activities at Amersfoort, Louis Trichardt and Skukuza. A larger agricultural contribution was determined for Vaal Triangle (20%), which was attributed to the manufacturing of fertilisers in that region. As mentioned in Chapter 3.1, Welgegund is located on a commercial farm, with the immediate area surrounding Welgegund being grazed by livestock, while crop fields cover the remaining area. Jaars et al. (2016) indicated the extent of cultivation in this region through a comprehensive vegetation survey conducted within a 60 km radius from Welgegund. Therefore, gaseous ammonia (NH_3) emissions associated with bacterial decomposition of biological substances such as urea and from soils, together with the use of fertiliser for crop production (Schlesinger and Hartley, 1992), would contribute to NH_4^+ in rain samples collected at Welgegund. The influence of fertilisers on atmospheric NH_4^+ is also signified by the relatively strong statistical correlation between NH_4^+ and NO_3^- (Figure 4.2) (Kelley and Sweeney, 2005; Dambreville et al., 2006). Recent studies on aerosol chemical composition at Welgegund also indicated that NH_4^+ was the second most abundant species in submicron particulates (Tiitta et al., 2014; Venter et al., 2017).

4.2.2.5 Biomass burning contribution

Biomass burning was estimated from the concentrations of total dissociated organic acids (tOA*) to contribute 5% to the total ionic content of rain at Welgegund (Figure 4.3), which was similar to the biomass burning contributions estimated at Amersfoort and Vaal Triangle. The biomass burning source group contribution was higher at the rural background site Louis Trichardt. Although Welgegund is frequently impacted by widespread regional open biomass burning plumes (Vakkari et al., 2014), the open biomass burning period typically occurs at the end of the dry season (June to mid-October) (Roberts et al., 2009). Figure 4.4 depicts the monthly number of fire pixels observed with the MODIS collection 5 burned area product (Roy et al., 2008) within a 100, 250 and 500 km radius from Welgegund together with the number of rain events collected each month (Chapter 3.2.3.4). It is evident that the influence of open biomass burning on rain chemistry will be less pronounced due to the open biomass burning season not coinciding with the wet season. In addition, NO_3^- was estimated to be completely of anthropogenic origin in this study and not considered in biomass burning contribution calculations, which could also contribute to a lower estimate of the biomass burning contribution.

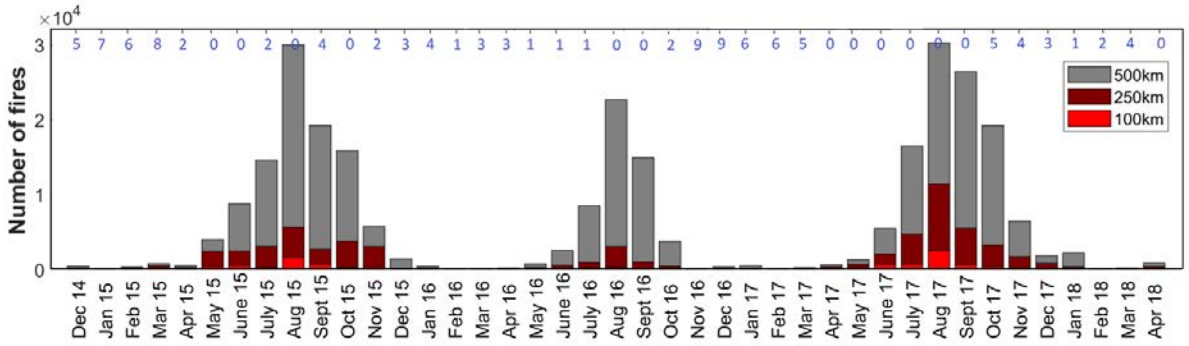

Figure 4.4 Monthly fire frequencies within a 100, 250 and 500 km radius from Welgegund during the sampling period with the number of rain events collected each month indicated on top.

4.3 Seasonal Variability

In Figure 4.5, the seasonal variability in the ionic composition and wet deposition flux determined during the sampling period are presented with the combined monthly rainfall depth summed over the sampling period (VWM: December 2014 - April 2018; wet deposition: January 2015 – December 2017). It is evident that the VWM concentrations and the wet deposition fluxes correspond to rainfall depth, i.e. the dry season is characterised by higher ionic concentrations, while significantly higher wet deposition fluxes occur during the wet season (The South African wet season ranges from mid-October to May; Chapter 2.8). Lower ionic concentrations during the wet season can be attributed to the cleansing of the atmosphere through rain events, while the wet removal rate decreases during the dry season. In addition, the austral winter months, with less frequent rain events, is characterised by increased air mass recirculation and more pronounced low-level inversion layers trapping pollutants near the surface (Garstang et al., 1996). Winter is also associated with additional coal and wood combustion for domestic heating (Venter et al., 2012; Vakkari et al., 2013), which is also reflected by relatively higher OA VWM concentrations during July. A denser particle distribution in the below-cloud atmosphere also promotes the scavenging efficiency of the raindrops and will increase the washout effect of the rain event (Xu et al., 2017). Therefore, the observed temporal variances in chemical composition can be attributed to seasonal changes in meteorological conditions and source strengths (i.e. vegetation cover, biomass burning events, and anthropogenic activities). It is also of interest to note that, similar to the four other South African DEBITS sites, a stronger marine signal is evident during July (higher Na^+ and Cl^-), which could also be attributed to more cold fronts from the southern oceans passing over the region (Conradie et al., 2016).

The pronounced drought between July 2015 to June 2016, when the North-West province received less than 50% of the normal rainfall (SAWS, 2017; Simpson and Dyson, 2018), could affect the seasonal variability and an extended measurement period is advised for determining the regional and temporal norm. During the drier months, the rainfall depth is often smaller than during the wet season, which leads to increased ionic concentrations. The OA concentration and wet deposition peaks in July and remains high through September and October as expected with increased biomass burning during the dry winter months (Figure 4.4). The deposition of SO_4^{2-} and NO_3^- is prominent throughout the year. The agriculturally related NH_4^+ concentration is the highest at the end of the dry season and remains relatively the same over the spring and summer months.

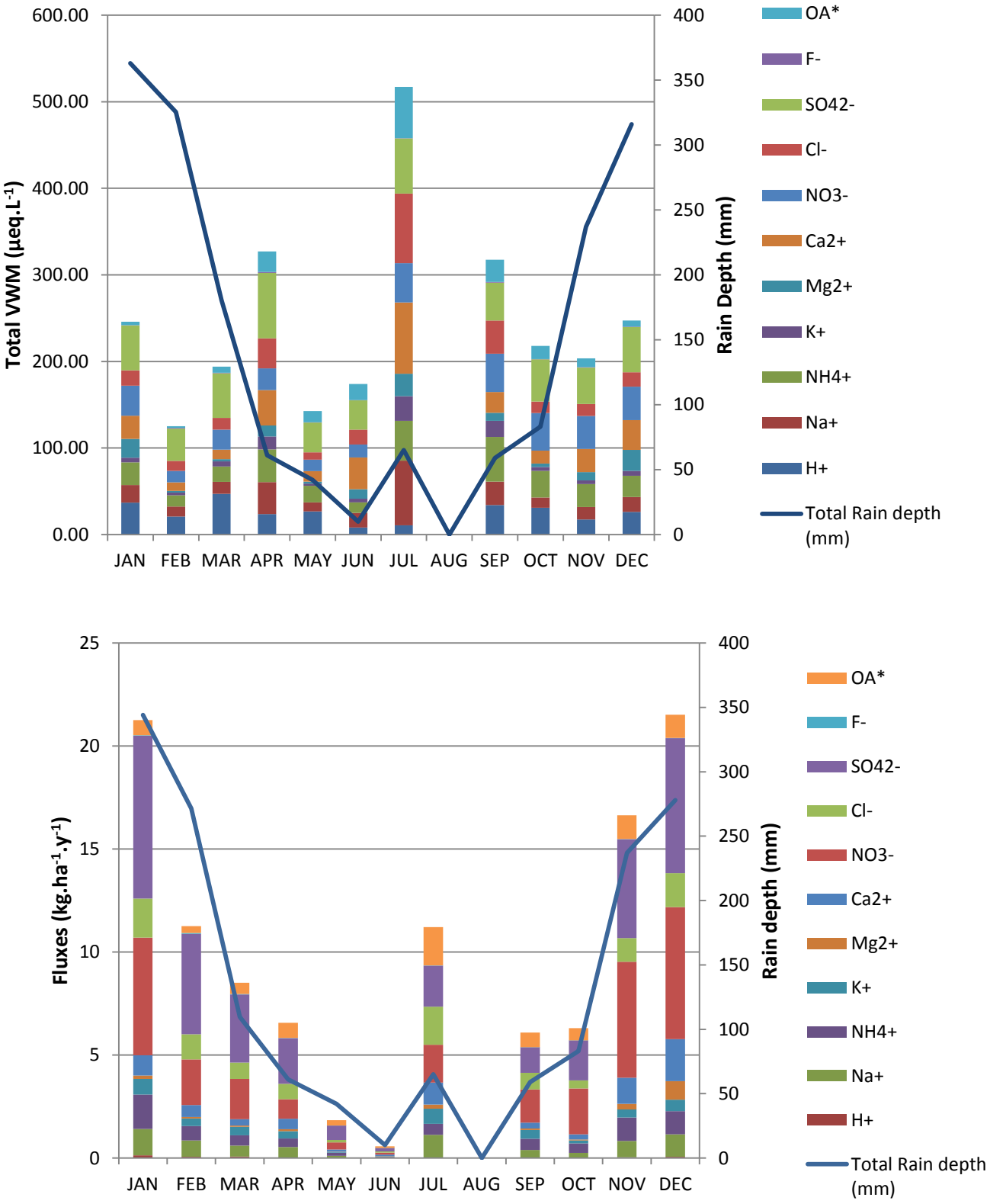

Figure 4.5 Seasonal variations in the (a) ionic concentrations and (b) fluxes of wet deposition at Welgegund between 2015 and 2017. The blue lines present monthly rain depths over the sampling period.

4.4 Summary & Conclusion

The chemical composition of rainwater and the associated wet deposition fluxes were determined for 119 samples collected at the Welgegund atmospheric research station from December 2014 to April 2018. Welgegund was included in the DEBITS network in 2014 under the newly formed INDAAF network, which comprises the African component of the DEBITS task. The ionic composition and wet deposition fluxes determined for the regional background site, Welgegund, was therefore contextualised with four other South African DEBITS sites located in the north-eastern interior.

Similar to the four other South African DEBITS sites, SO_4^{2-} was the most abundant species at Welgegund. The SO_4^{2-} VWM concentration at Welgegund was in the same order than SO_4^{2-} levels determined at two regional background sites within proximity of industrial sources in the Mpumalanga Highveld and the Vaal Triangle, which had SO_4^{2-} VWM concentrations 3 to 4 times higher compared to levels thereof at two rural background sites. NO_3^- was the second most abundant species at Welgegund, with a VWM concentration similar to industrially impacted sites with concentrations 2 to 3 times higher compared to NO_3^- VWM concentrations at rural background sites. In addition, the total ionic VWM concentrations at Welgegund were similar to the total VWM concentrations of ionic species at the two industrially impacted sites. S and N wet deposition fluxes were 4.38 S kg.ha^{-1}.y^{-1} and 4.48 N kg.ha^{-1}.y^{-1}, respectively, which were lower than S and N deposition determined at the industrially influenced sites due to lower average annual rainfall at Welgegund. The pH of rainwater at Welgegund, i.e. 4.80, was below the natural pH of rain and comparable to pH levels at the rural background sites, which suggested increased neutralisation of acidic species at Welgegund. Acidic potential calculations indicated that 63% of the acidity was neutralised, mainly by Ca^{2+} and NH_4^+.

Statistical analysis and empirical calculations revealed the same major sources of ionic species in rainwater at Welgegund as that identified for the other South African DEBITS sites, i.e. marine, crustal, anthropogenic (industrial), agriculture and biomass burning. The anthropogenic (industrial) source group had the largest contribution on ionic content at Welgegund, which indicated the significant regional influence of major source areas in the north-eastern South African interior and anticyclonic recirculation of air masses over this region. Although the region experienced a severe drought from July 2015 to June 2016, the seasonal variability in ionic content in rainwater also reflected the influence of changes in meteorology and source strength. Crustal species made a relatively significant contribution to ionic content, which was attributed to air mass movement over an arid region in South Africa. A relatively high contribution was also determined from marine sources, which reflected the influence of air masses moving over the oceans bordering South Africa. As expected, the influence of agricultural activities was also

evident at Welgegund. A relatively small contribution was estimated for biomass burning, which was ascribed to the open biomass burning season not corresponding to the wet season. The estimated contributions of different source groups to ionic content in rainwater at Welgegund were similar than that determined at the industrially impacted Amersfoort site.

Chapter 5

Large scale factors influencing rain chemistry at a regional background site in South Africa

In Chapter 4, detailed discussions on the chemical composition and pH of rain water, as well as wet deposition fluxes at Welgegund were presented. Explorative statistical evaluations and empirical calculations were used to determine different source contributions to the ionic content of rainwater. Rainwater chemistry at Welgegund was contextualised with other sites in the South African interior. In this chapter, the chemical composition of rainwater at Welgegund is further explored in view of in-depth correlation between the chemical composition and air mass history at 100 m a.g.l. and cloud base height (CBH), together with ancillary measurements at Welgegund. Air masses with a 100 m a.g.l. arrival height are considered in order to determine the influence of below-cloud scavenging on rain chemistry. The impacts of air mass history related to cloud formation and of in-cloud processes on rain chemistry are investigated by relating the chemical composition of rainwater to air masses at CBH. The rainwater composition of events with different synoptic weather systems is also compared. An inter-comparison of the different groups is performed through cross-tabulation, followed by a brief summary of the results. Statistical analyses were performed in collaboration with the Statistical Consultancy Service of the NWU, Potchefstroom.

5.1 Air Mass History

Sun et al. (2010) indicated that the chemistry in cloud water differed from the rainwater chemistry of a related rain event and suggested that air mass history at different heights was the major factor influencing this observation. In addition, Xu et al. (2017) showed that the below-cloud scavenging processes contributed to between 47 and 61 % of the levels of SO_4^{2-}, NO_3^- and NH_4^+ in rain samples collected in Beijing (Chapter 2.5). The hourly-arriving 96-hour air mass back trajectories calculated for Welgegund at 100 m above ground level (a.g.l.) and CBH for each rain event during the sampling period are overlaid in Figure 5.1 on a colour percentage scale (Chapter 3.2.4). Only rain events for which collected samples passed the WMO DQO

criteria were considered. In addition, rain events coinciding with instrumental errors at Welgegund (e.g. power failures), as well as for which no back trajectories were available, were also excluded. In total, 86 rain events were considered. The total time that air masses at both arrival heights spent over the defined source regions (Figure 3.12, Chapter 3.2.7) prior to a rain event is also shown in Figure 5.1. It is evident that air masses arriving at both arrival heights at Welgegund spent the most time over the eastern sector, excluding the large point sources. A larger fraction of air masses associated with the well-mixed boundary layer (100 m a.g.l.) passed over the source region wherein the large point sources are located compared to CBH air mass arrival heights. More air masses associated with the precipitating clouds (CBH) passed over the western background region. Furthermore, air masses arriving at CBH spent relatively more time over oceanic regions compared to air masses at an arrival height of 100 m a.g.l.

Throughout this chapter, boxplots present the total time that air masses at the two arrival heights spent over the defined regions with the median (red line), average (black dot), 25th and 75th percentiles (blue box), and ± 2.7 times the standard deviation (whiskers) indicated.

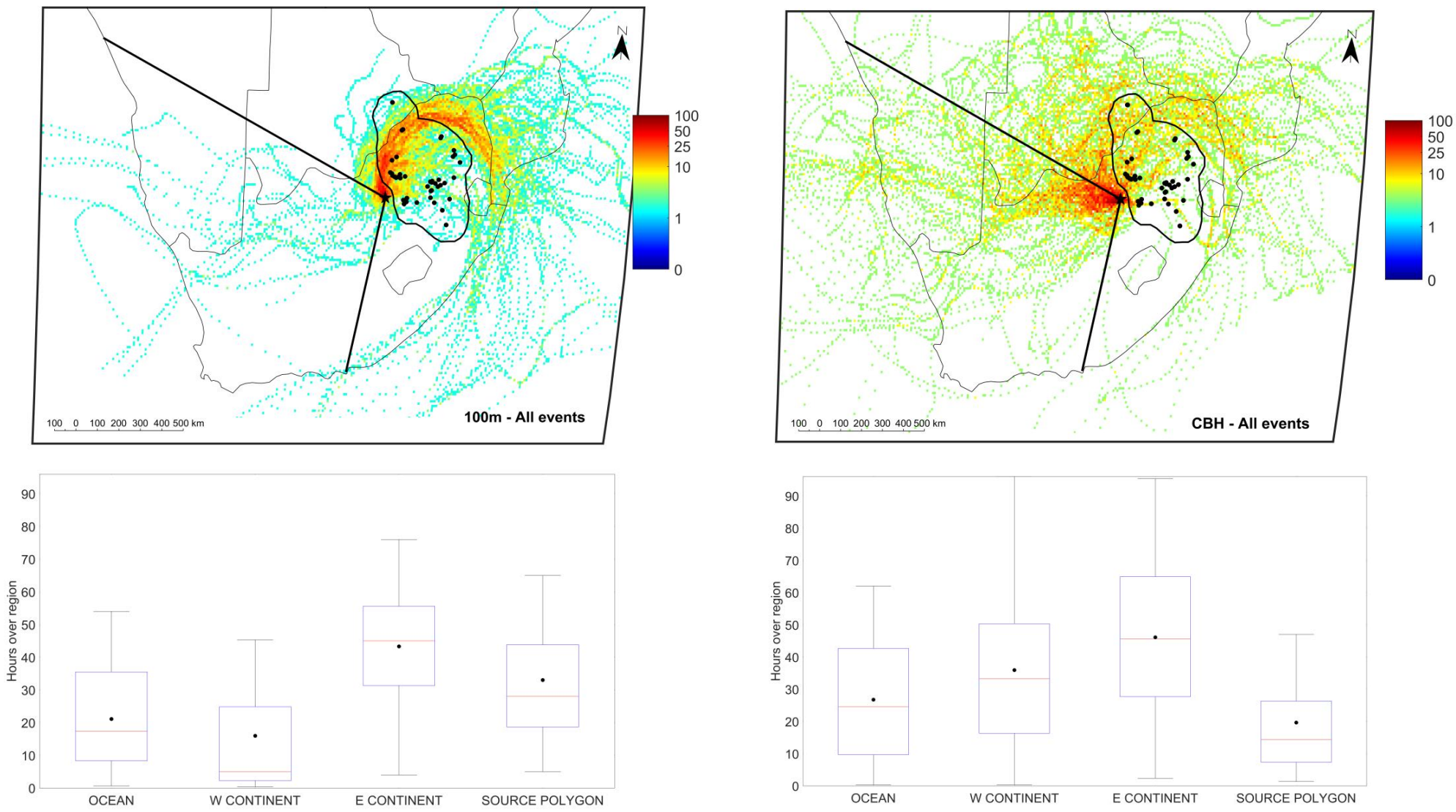

Figure 5.1 96-hour overlay back trajectories for air masses arriving at 100m a.g.l. (left) and CBH (right) for each rain event at Welgegund, with boxplots indicating the total time that air masses at the two arrival heights spent over the defined regions.

5.2 Clustering Chemical Composition of Rain

Clustering analyses based on the ionic composition of rainwater revealed three significant clusters (Figure 3.13 and 3.16, Chapter 3.2.7.2). In Table 5.1, the VWM concentrations of ionic species in each of these clusters are presented, while pH, electrical conductivity (EC), rainfall depth and ancillary measurements at Welgegund associated with each cluster are also included. These clusters, i.e. CHEM-A, CHEM-B and CHEM-C represented 70, 25 and 5% of all rain samples, respectively.

It is evident from Table 5.1 that the optimum three clusters determined represent varying levels of VWM concentrations of ionic species, i.e. VWM concentrations of species in cluster CHEM-A were the lowest with the corresponding lowest total VWM concentration, while the VWM concentrations of ionic compounds in cluster CHEM-C were the highest (with the exception of H^+) with a resultant highest total VWM concentration. Furthermore, as expected, cluster CHEM-C also had the highest EC value. Cluster CHEM-A represented the largest number of rain events, while cluster CHEM-C comprised the lowest number of events. Cluster CHEM-B had higher H^+ levels (and lowest pH) compared to that of CHEM-C, which can be attributed to decreased neutralisation of acidic species by Ca^{2+} in this cluster. The ratios of Ca^{2+} levels compared to concentrations of other species in cluster CHEM-C were significantly higher compared to similar ratios in the other two clusters. The extent of neutralisation of acidic species through Ca^{2+} in rain samples collected at Welgegund was indicated in Chapter 4.1. Cluster CHEM-A is associated with the highest rainfall depth, while cluster CHEM-C corresponds to the lowest rainfall depth. In Chapter 4.3 and in Conradie et al. (2016), the lower rainfall depths were associated with higher VWM concentrations at Welgegund and other sites in the interior of South Africa. Cluster analyses according to ionic composition of rainwater did not reveal any significant chemical compositional differences between clusters, with the exception of proportionally higher Ca^{2+} and Mg^{2+} concentrations in cluster CHEM-C compared to other species. The cluster analyses simply grouped rain events in relation to total VWM concentrations of ionic species from high to low.

Table 5.1 Chemical clustering approach: VWM concentrations (µeq.L^{-1}) of ionic species in each cluster determined, as well as average pH, electrical conductivity (EC), total rainfall depth over the sampling period, average rainfall depth per rain event, and average ancillary measurements in a 2-hour period before the rain event. The standard deviations are indicated in block brackets.

	CHEM-A		CHEM-B		CHEM-C	
# of samples	68		24		5	
H^+	20.38	[23.35]	39.06	[25.51]	31.04	[23.35]
Na^+	11.48	[19.09]	22.69	[57.60]	47.37	[19.09]
NH_4^+	22.28	[16.60]	28.07	[22.74]	34.85	[16.60]
K^+	4.26	[6.87]	8.88	[22.91]	11.68	[6.87]
Mg^{2+}	4.79	[7.11]	5.92	[12.05]	76.60	[7.11]
Ca^{2+}	15.84	[17.15]	21.98	[35.57]	85.08	[17.15]
NO_3^-	24.91	[19.04]	33.54	[28.47]	58.24	[19.04]
Cl^-	11.71	[18.26]	24.16	[60.36]	39.38	[18.26]
SO_4^{2-}	33.8	[24.11]	57.59	[32.22]	86.41	[24.11]
F^-	0.30	[0.24]	0.87	[1.01]	0.84	[0.24]
tOA*	8.89	[13.38]	9.21	[22.50]	20.35	[13.38]
Total VWM	158.64		251.96		491.84	
pH	4.8	[0.52]	4.59	[1.94]	5.96	[1.94]
EC	25.04	[20.37]	55.81	[57.85]	59.64	[42.97]
SO_2 (ppb)	0.5	[0.68]	1.91	[3.64]	0.97	[0.81]
NO (ppb)	0.12	[0.29]	0.00	[0.20]	-0.01	[0.17]
NO_x (ppb)	2.72	[2.09]	3.15	[3.83]	1.91	[1.30]
O_3 (ppb)	32.17	[11.76]	34.38	[11.08]	34.58	[7.74]
CO (ppb)	123.39	[36.70]	129.00	[40.99]	145.92	[25.93]
eBC (ug.m^{-3})	0.26	[0.27]	0.49	[0.68]	0.40	[0.27]
PM_{10} (ug.m^{-3})	14.5	[11.79]	18.03	[9.49]	23.40	[12.17]
RH (%)	65.1	[21.70]	59.88	[20.08]	64.94	[19.00]
Average (max) rain intensity (mm.h^{-1})	4.04 (12.27)	[3.10] [7.80]	5.27 (20.88)	[4.62] [19.00]	7.22 (43.36)	[4.22] [27.78]
Total (avg) rainfall (mm)	809.50 (11.9)	[9.40]	614.50 (25.60)	[18.90]	193.00 (38.6)	[23.54]
CBH_{2hr} (m)	2284.84	[1032.47]	2263.18	[735.43]	2394	[669.09]
$CBH_{15\ min}$ (m)	1961.72	[893.66]	1870.91	[751.40]	1412	[563.27]

Comparison of the ancillary measurements in each of the clusters indicated that the concentrations of most pollutant species (e.g. SO_2, CO, eBC, PM_{10}) were higher in CHEM-B and CHEM-C. Although it is difficult to directly quantify the influence of primary emitted species on rain chemistry, these measurements reflect the influence of the eastern pollution source regions on rain chemistry at Welgegund. In addition, higher PM_{10} concentrations could have a more direct influence on the chemical composition of rain. In Table 5.1, a distinct correlation is observed between the VWM concentrations of ionic species and rain intensity. CHEM-C, with the higher VWM concentrations and the highest rainfall intensity, also corresponded to lower average CBH 15 minutes prior to a rain event, as well as to the greatest difference between the 2 hour and 15 minute CBH averages and the lowest RH. CHEM-A had the smallest difference in CBH averages as well as the lowest rainfall intensity, lowest average pressure and the highest RH. A synoptic comparison between the clusters is further explored in Section 5.4.

An analysis of variance on the levels of each of these ancillary measurements, as well as pH and EC in the three clusters was also conducted to establish statistical and substantive significance. The p-values and size effect (Cohen's d-value) for measurements for which significant differences between different clusters were calculated are listed in Table 5.2 (Chapter 3.2.7.2). The effect sizes reported here indicate the effect of the variable on the distinction between events of different clusters.

Table 5.2 Analyses of variance of ancillary measurements in the three cluster solutions based on ionic composition of rain.

Ancillary measurements	p-Value	Effect Sizes		
		A with B	A with C	B with C
pH	0.000	0.37	0.60	0.71
EC	0.001	0.53	0.81	0.07
SO_2	0.016	0.39	0.58	0.26
Intensity Max	0.000	0.45	1.12	0.81

The pH, EC, SO_2, maximum rainfall intensity and pressure showed statistically significant differences between all three clusters. Large effect sizes were observed between CHEM-A and CHEM-C for all the ancillary measurements which showed statistically significant differences. Between CHEM-A and CHEM-B, the EC and pressure showed large effect sizes, with pH and SO_2 showing substantive differences. The pH and rain intensity differed significantly when comparing cluster CHEM-B and CHEM-C, with the SO_2 and pressure differences also being substantive. Positive correlation between rain intensity and rainwater chemistry can be attributed to increased below-cloud scavenging efficiency (Hall, 2003; Bae et al., 2006; Kulshrestha et al., 2009; Karev et al., 2010; González and Aristizábal, 2012). It is worth noting that the NO/NO_x, PM_{10}, eBC, O_3 and CO concentrations that can also be associated with anthropogenic emission sources, did not present statistically significant covariance with the rainfall chemistry.

In Figures 5.2, 5.3 and 5.4, air mass histories at 100 m a.g.l. and CBH for the events in each of the rainwater chemistry HCA clusters are presented. It is evident that air masses with a 100 m a.g.l. arrival height at Welgegund for rain events associated with cluster CHEM-B and CHEM-C spent similar periods over the source region containing the large point sources, while air masses determined for cluster CHEM-A spent relatively less time over this source region. All air masses arriving at 100 m a.g.l. spent similar times over the eastern source region excluding the large point sources, while a relatively higher percentage of these air masses passed over oceans for cluster CHEM-C.

The main difference between air masses arriving at Welgegund at 100 m a.g.l. in the three clusters relates to the time spent over the clean western sector. Air masses with an arrival height of 100 m a.g.l. in cluster CHEM-C spent significantly more time over the western source region compared to cluster CHEM-B, and relatively more time than that of cluster CHEM-A. The 100 m a.g.l. back trajectories for CHEM-C spent significantly more time over the western source region compared to cluster CHEM-B and relatively more time than that of cluster CHEM-A. The air mass history at 100 m a.g.l. arrival height can therefore explain the significantly higher Ca^{2+} and Mg^{2+} in cluster CHEM-C in relation to the other species. In Chapter 4.1, the increased neutralisation of rain water at Welgegund compared to other sites in the South African interior was attributed to air masses passing over this background region west of Welgegund where areas such as the Karoo and Kalahari are located. Back trajectory calculations, especially at 100 m a.g.l. arrival height, proved to be a good method to relate the residence time of air masses over source regions to the variability in rainwater chemistry.

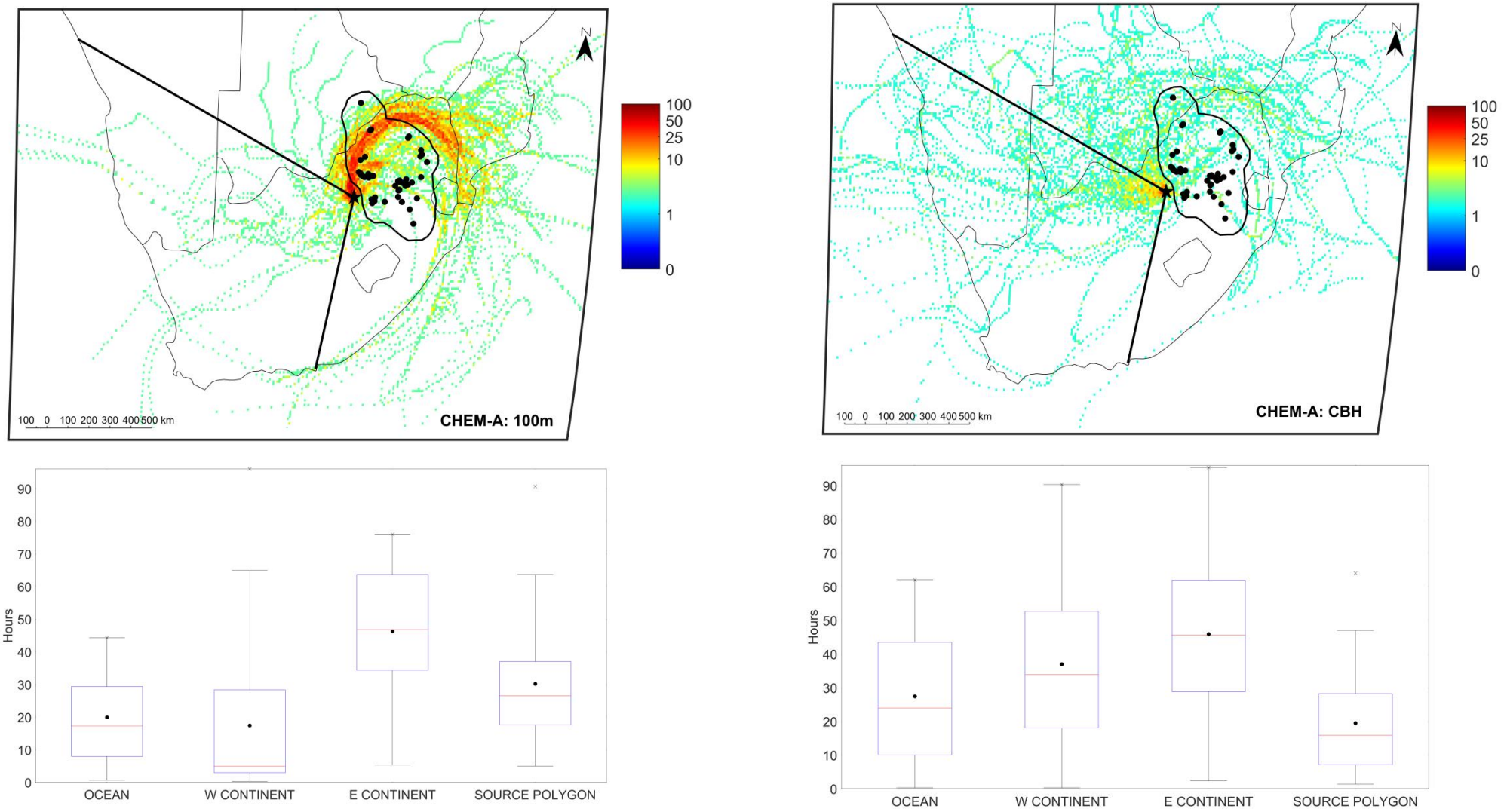

Figure 5.2 96-hour overlay back trajectories for air masses arriving at 100m a.g.l. (left) and CBH (right) for each rain event in cluster CHEM-A at Welgegund, with boxplots indicating the total time that air masses at the two arrival heights spent over the defined regions.

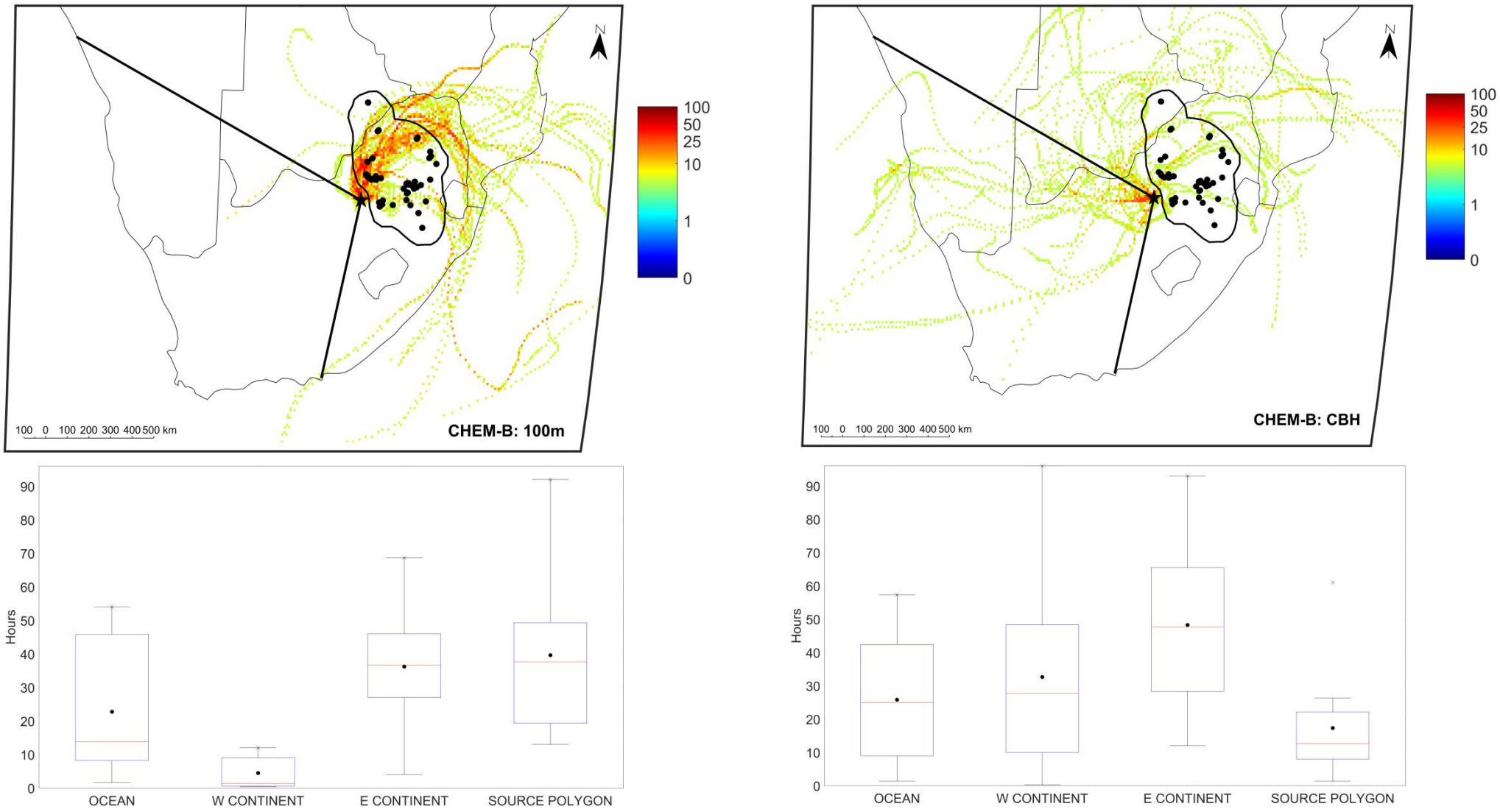

Figure 5.3 96-hour overlay back trajectories for air masses arriving at 100m a.g.l. (left) and CBH (right) for each rain event in cluster CHEM-B at Welgegund, with boxplots indicating the total time that air masses at the two arrival heights spent over the defined regions.

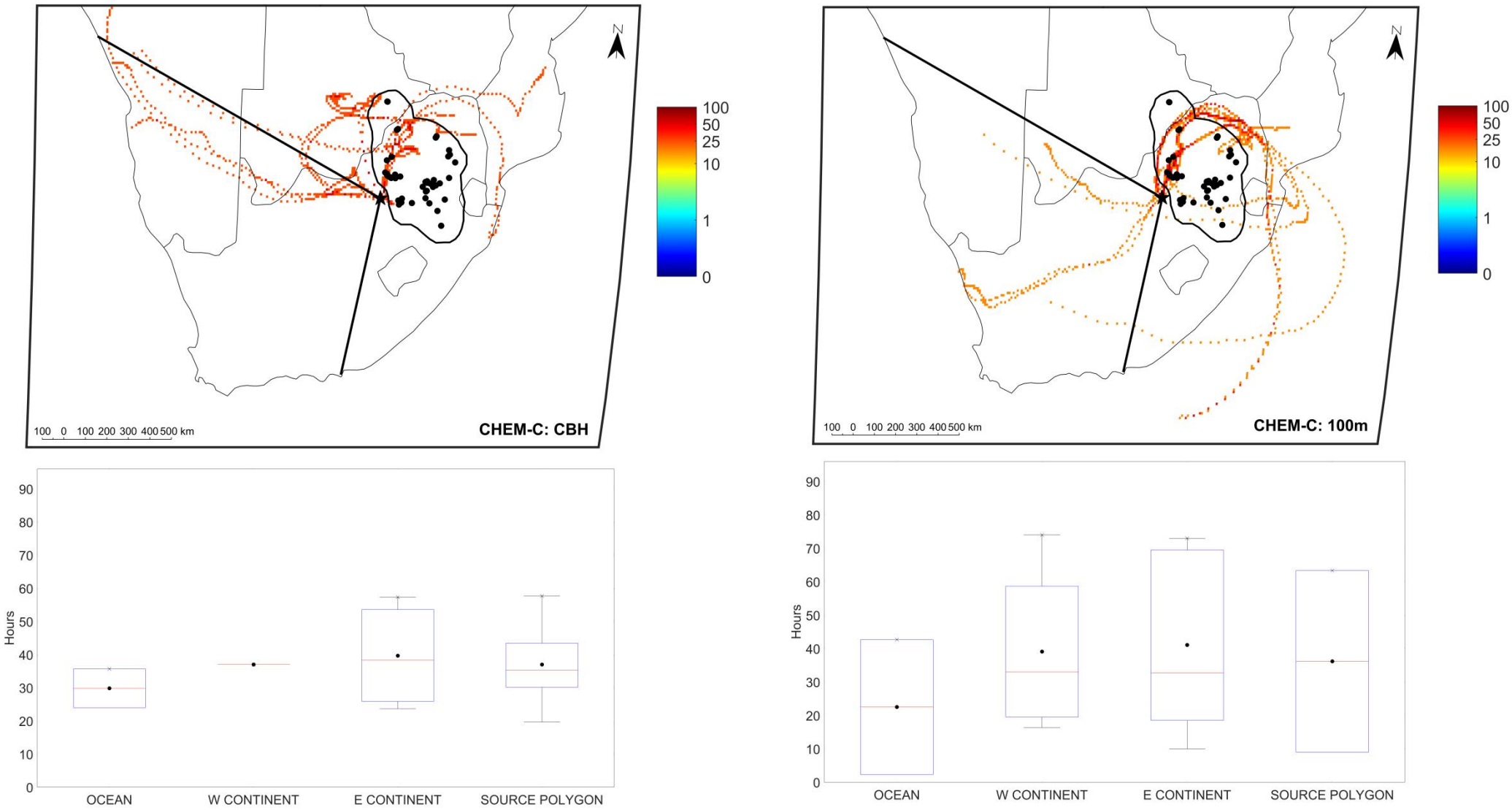

Figure 5.4 96-hour overlay back trajectories for air masses arriving at 100m a.g.l. (left) and CBH (right) for each rain event in cluster CHEM-C at Welgegund, with boxplots indicating the total time that air masses at the two arrival heights spent over the defined regions.

No significant differences are observed between the time air masses arriving at CBH at Welgegund spent for the three clusters, with the exception of air masses arriving at CBH determined for CHEM-C spending more time over the source region containing large point sources. Therefore, this could partially contribute to higher VWM concentrations of ionic species in the cluster.

Although air mass histories and ancillary measurements explain some variances between the clusters to a certain extent, the total rainfall depth associated with each of these clusters seems to be the major factor contributing to the observed differences in the VWM concentrations. Although the total rainfall depth decreased from cluster CHEM-A to CHEM-C, the average event rainfall depth, which could also contribute to higher scavenging, increased. In addition, increased rain intensity also corresponded to higher VWM concentrations. It has been indicated that scavenging ratios, which describe the ratios of concentrations of species in rainwater to levels thereof in the ambient air, are usually higher for larger atmospheric particles (Engelmann, 1971; Galloway et al., 1993; González and Aristizábal, 2012). Kulshrestha et al. (2009), for example, reported that a shorter, more intensive rainfall event more effectively removed coarser particles such as $CaSO_4$ from the atmosphere. González and Aristizábal (2012) indicated a positive correlation between scavenging ratios of SO_4^{2-} and NO_3^- and rain intensity, which was attributed to the high aqueous solubility of these species. In a study conducted in China by Zhao et al. (2015), it was shown that larger particles (500-1000 nm) were effectively scavenged through thunderstorms, whereas smaller particles (10- 50 nm) were more effectively scavenged through rain events with longer durations and lower raindrop velocities. Thunderstorms are commonly associated with larger raindrop size distribution and higher rainfall intensities and could explain the more efficient scavenging (Chate, 2011; Zhao et al., 2015). Xu et al. (2017) reported an exponential power distribution when relating the below-cloud scavenging coefficient with rain intensity (see also Chapter 2.5). As indicated above, the surface air flow, influenced by the progression of synoptic patterns over southern Africa, the type and strength of uplift, and rainfall properties may contribute to the below-cloud scavenging efficiency. A synoptic comparison between the clusters is explored in Section 5.4.

5.3 Clustering Air Mass History

Clustering according to the ionic composition of rainwater did not distinctly reveal the influences of sources on rain chemistry. Therefore, a different approach was followed where air mass history was clustered and possible differences in the chemical composition of rainwater were assessed. Determining back trajectories for four days prior to the rain event allows comparison of the rainwater chemistry with the synoptic scale that influences the air flow. As discussed in Chapter 3.2.7.2, clustering according to air mass history at 100 m a.g.l. and CBH also revealed three meaningful clusters for each arrival height. The average time that air masses arriving at Welgegund at 100 m a.g.l. and CBH spent over different defined source regions (Figure 3.12) was clustered in this approach.

5.3.1 100 m a.g.l. arrival height

In Figure 5.5, clustering according to the time that air masses arriving at 100 m a.g.l. spent over the defined source regions prior to arrival at Welgegund are presented (Chapter 3.2.7.2). The three clusters, i.e. 100m-A, 100m-B and 100m-C comprised 43, 34 and 23% of all rain events, respectively. Clusters 100m-B and 100m-C represented air masses spending significantly more time over the eastern source regions, with air masses in cluster 100m-B spending more time over the eastern source region including the large point sources, and 100m-C spending more time over the eastern source region excluding the large point sources. Air masses in these two clusters spent very little time over the oceans and the clean western background region. Cluster 100m-A represents air masses spending more time over oceans and the clean western background regions, and less time over the eastern source region in comparison to clusters 100m-B and 100m-C. In Figure 5.6, overlaid back trajectories of air mass movements in each of these clusters are presented.

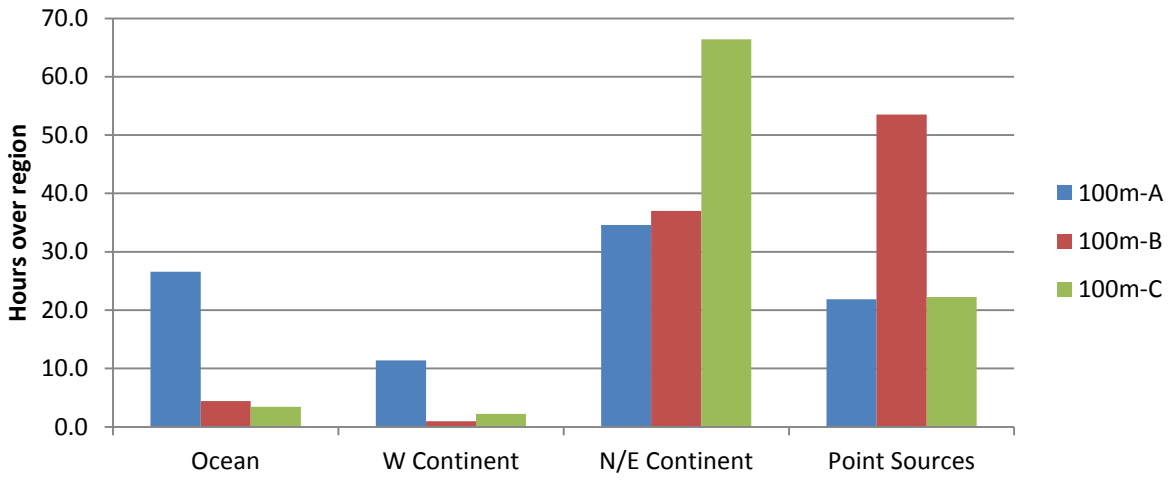

Figure 5.5 Time air masses at a 100 m a.g.l. arrival height in each cluster spent over defined source regions.

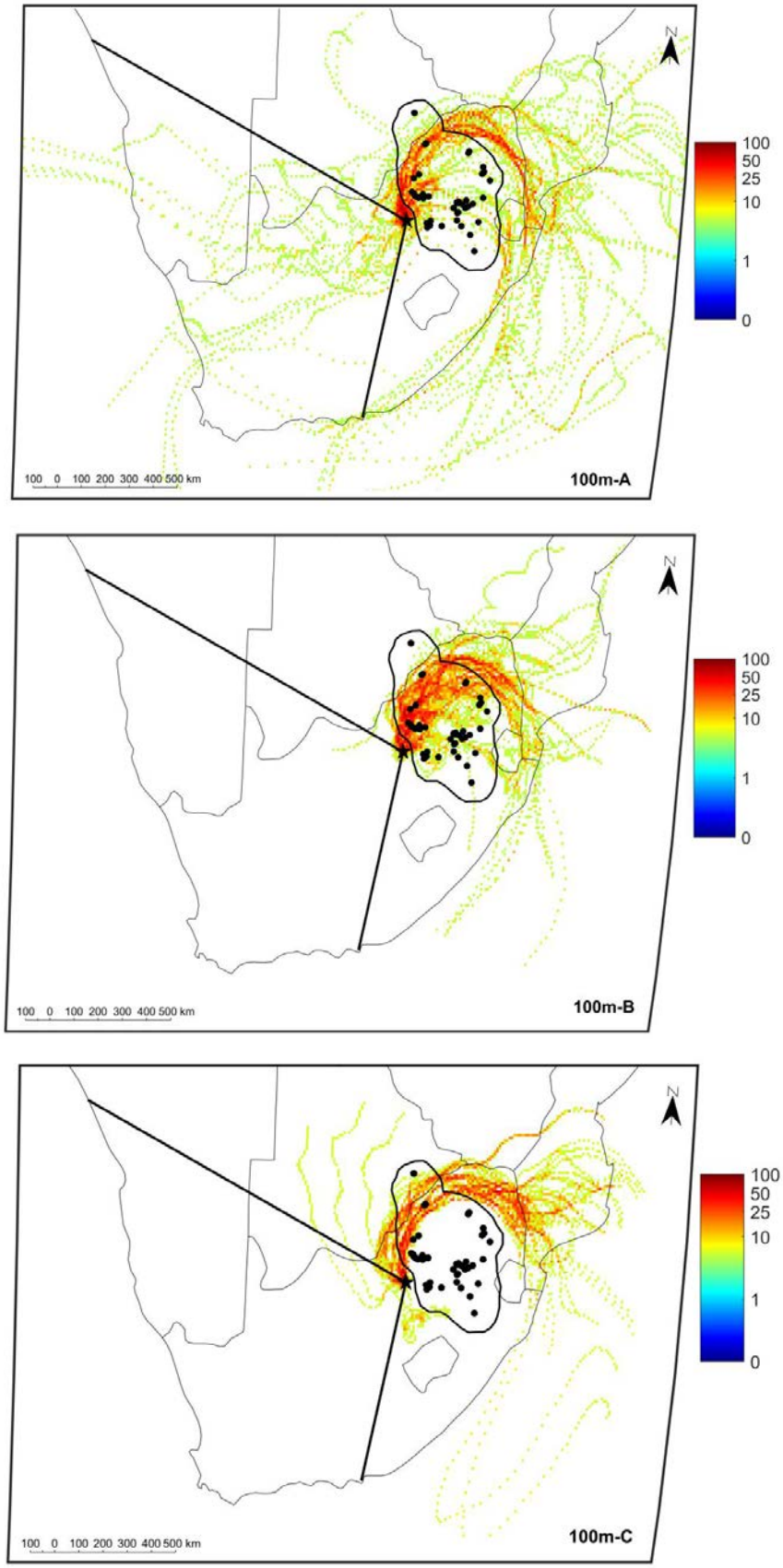

Figure 5.6 96-hour overlay back trajectories for air masses clustered according to the time the air masses at 100 m a.g.l. arrival height spent over defined source regions.

The chemical composition of rain samples in each of the three clusters obtained for air mass history at 100 m a.g.l. arrival height is presented in Table 5.3 together with the pH, EC and ancillary measurements associated with each cluster. Cluster 100m-A had the highest total VWM concentrations of ionic species. It is also of interest to note that cluster 100m-A and 100m-B had similar total rain depths, which indicate that observed differences in VWM concentrations of ionic species in rainwater were indicative of the influence of different sources. Furthermore, cluster 100m-C had the lowest total VWM concentrations associated with the lowest rainfall depth.

VWM concentrations of Na^+ and Cl^-, generally associated with oceanic air masses, were the highest in cluster 100m-A. Ca^{2+} and Mg^{2+} levels were also significantly higher in this cluster, which can indicate the influence of crustal sources from the clean western background region, as can be seen in Figure 5.6 above. VWM concentrations of Mg^{2+} and K^+ that are mainly associated with oceanic or crustal sources were also higher in cluster 100m-A (Chapter 2.7.3) (Kanayo et al., 2010; Sun et al., 2010; Yang et al., 2012; Conradie et al., 2016). Relatively higher Ca^{2+} and Mg^{2+} concentrations in cluster 100m-B can possibly be attributed to fly ash emissions from industrial activities (Laakso et al., 2012). Cluster 100m-B had the highest H^+ levels, which is indicative of the influence of large point sources on rain chemistry, as well as decreased neutralisation of acidic species by Ca^{2+} for air masses associated with this cluster. However, relatively small differences in the average pH of rain events in the three clusters were evident. Furthermore, the VWM concentrations of anthropogenic acidic species, i.e. SO_4^{2-} and NO_3^-, were similar in all three clusters, which signify the regional impacts of anthropogenic activities in the north-eastern interior on rain chemistry as discussed in Chapter 4. SO_4^{2-} levels were, however, marginally higher in cluster 100m-B. NO_3^- levels were higher in clusters 100m-A and 100m-C, which also point to the regional impacts of household combustion for space heating and cooking. Cluster 100m-A also had the highest VWM concentrations of species typically associated with biomass burning, i.e. OAs, K^+ and Cl^-, while CO and eBC levels were also slightly higher in cluster 100m-A. 21% of the rain events in cluster 100m-A coincided with the biomass burning season (May to November, Chapter 4.2.2.5). NH_4^+ levels in all three clusters reflect the influence of local and regional agricultural activities on atmospheric processes in this part of South Africa (Chapter 2.7.3.1 and Chapter 3.1).

No really significant differences were observed between the ancillary measurements in each of the back trajectory clusters. Mean SO_2 concentrations in cluster 100m-B were marginally higher than levels thereof associated with the other two clusters. Similar concentrations of NO_x in all three air mass clusters also emphasise the influence of household combustion on air quality in this region. In contrast to the clustering according to ionic composition of rain, rain intensity had no significant correlation to observed differences

in the three 100 m a.g.l. air mass arrival height clusters. The lowest average CBH 15 min prior to a rain event in cluster 100m-A also corresponded to higher total VWM concentrations than observed for cluster CHEM-C (Section 4.2). Analysis of variances of the ionic composition and ancillary measurements in these three clusters only revealed statistically significant variances and effect sizes concerning H^+ concentrations between cluster 100m-B and the other two clusters.

Using crude trajectory analyses at an arrival height of 100 m a.g.l. confirmed the influence of residence time of air masses over source regions on the variability in rainwater chemistry. Movement of air masses over the major point sources in 100m-B, similar to that of CHEM-B, are related to higher SO_4^{2-} concentrations and low pH, which are associated with anthropogenic activities. An inter-comparison of the different cluster methods is presented in Section 5.5.

Table 5.3 Air mass history clustering at 100m arrival height: VWM concentrations (μeq.L^{-1}) of ionic species in each cluster, as well as average pH, electrical conductivity (EC), rainfall depth and ancillary measurements. The standard deviations are indicated in block brackets.

	100m-A		100m-B		100m-C	
# of samples	37		29		20	
H^+	20.68	[16.07]	36.49	[30.67]	28.77	[29.78]
Na^+	25.82	[35.98]	19.7	[55.23]	11.12	[10.47]
NH_4^+	28.14	[23.80]	23.76	[15.77]	29.02	[16.26]
K^+	9.8	[14.67]	5.77	[19.48]	4.73	[4.44]
Mg^{2+}	19.95	[65.15]	14.43	[59.53]	4.64	[3.77]
Ca^{2+}	38.63	[64.28]	22.96	[46.59]	17.03	[10.63]
NO_3^-	35.81	[59.45]	30	[32.50]	34.66	[17.09]
Cl^-	25.75	[32.63]	19	[56.38]	11.18	[8.59]
SO_4^{2-}	50.85	[37.23]	52.28	[32.51]	46.47	[29.14]
F^-	0.51	[0.64]	0.79	[0.93]	0.47	[0.30]
tOA*	16.8	[20.57]	6.26	[19.53]	7.4	[8.89]
Total VWM	272.75		231.45		195.49	
pH	4.87	[0.71]	4.81	[0.88]	4.76	[0.53]
EC (μS)	33.19	[26.94]	46.53	[55.52]	26.34	[24.28]
O_3 (ppb)	32.47	[11.93]	32.82	[10.65]	31.54	[9.45]
SO_2 (ppb)	0.8	[1.64]	1.25	[2.85]	0.44	[0.66]
NO (ppb)	0.06	[0.16]	0.04	[0.21]	0.1	[0.34]
No_x (ppb)	2.72	[2.62]	2.76	[2.65]	2.85	[1.96]
CO (ppb)	135.99	[41.97]	124.25	[32.59]	116.66	[34.95]
PM_{10} (μg.m^{-3})	16.6	[10.06]	14.34	[9.79]	16.93	[16.33]
eBC (μg.m^{-3})	0.4	[0.38]	0.3	[0.52]	0.26	[0.37]
Total rain depth (avg) (mm)	570 (15.41)	[14.27]	631 (21.74)	[19.32]	240 (11.98)	[7.03]
Intensity average (max) (mm.h^{-1})	4.92 (15.10)	[4.00] [12.36]	4.92 (19.92)	[4.24] [20.21]	3.62 (13.66)	[11.46] [2.43]
CBH_{2hr} (m)	2332.3	[1081.42]	2075	[835.49]	2632.5	[791.08]
CBH_{15min} (m)	1835.14	[785.13]	1735.17	[899.97]	2358.95	[814.11]

5.3.2 Cloud base arrival height

Cluster solutions according to the time that air masses arriving at CBH spent over the defined source regions prior to a rain event at Welgegund are presented in Figure 5.7. As mentioned in Chapter 3.2.7.2, three clusters labelled CBH-A, CBH-B and CBH-C were determined which contained 34, 43 and 23% of all rain events. Cluster CBH-A contained air masses predominantly passing over the clean western background region and western oceans, with < 8% of back trajectories passing over the eastern source regions and no back trajectories passing over the region wherein the large point sources are located. Air masses in cluster CBH-B spent significantly more time over the eastern source region, excluding the large point sources, with very few air masses passing over oceans. Cluster CBH-C represents air masses passing predominantly over the eastern continent (including and excluding large point sources), while air masses also spent time over oceanic regions. In Figure 5.8, overlaid back trajectories of these air masses at CBH in the three different clusters are presented.

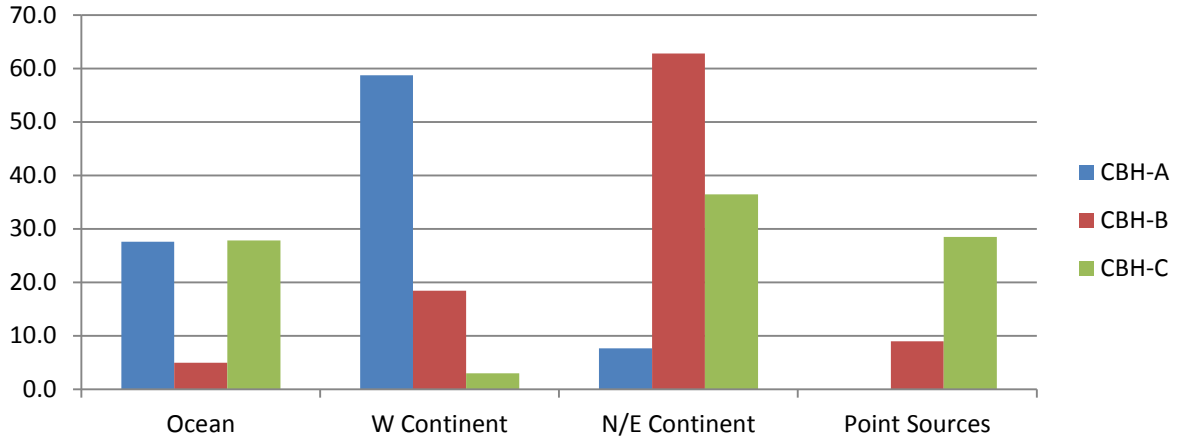

Figure 5.7 Time air masses at CBH spent over defined source regions in each cluster.

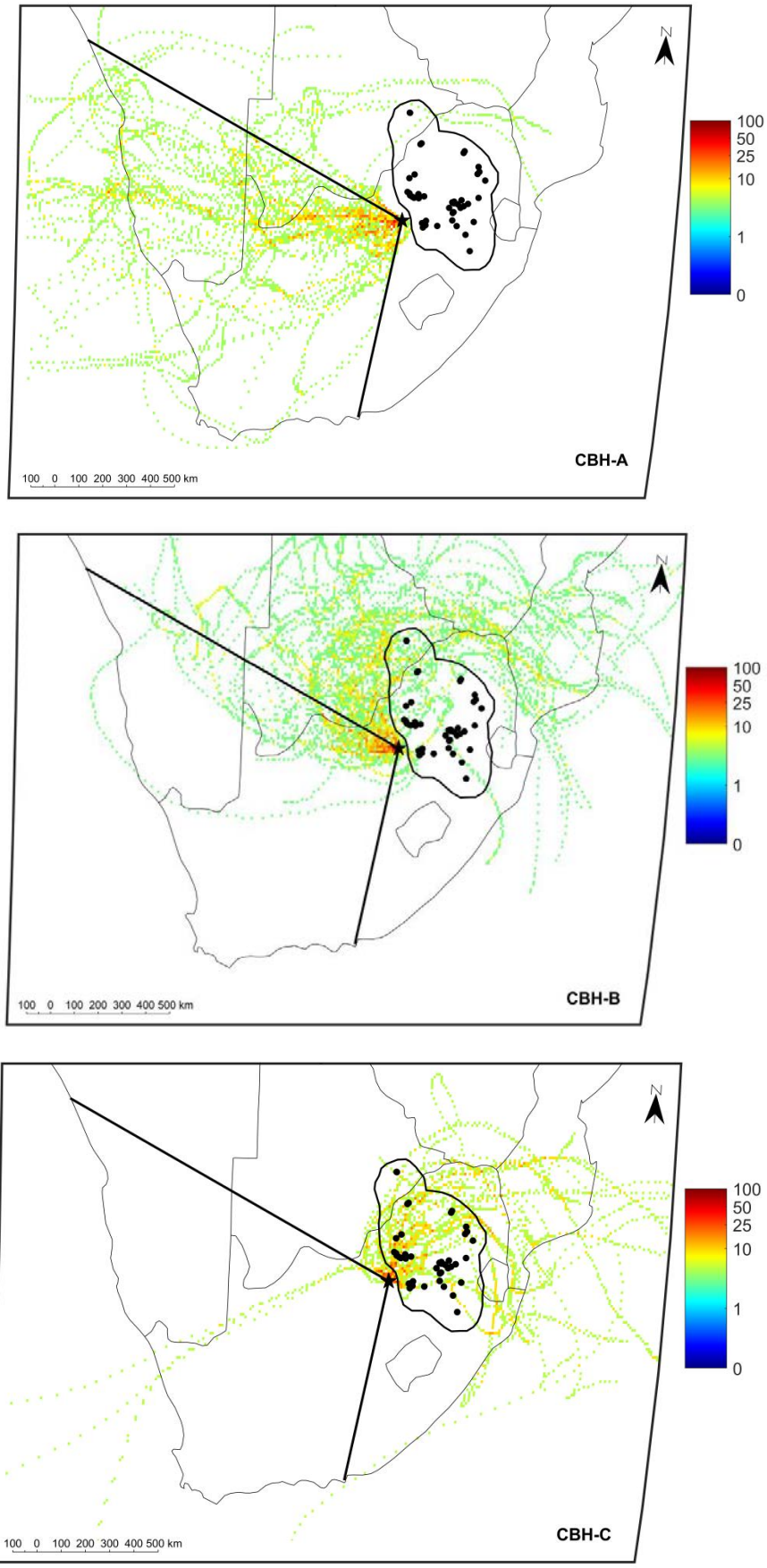

Figure 5.8 96-hour overlay back trajectories for air masses clustered according the time air masses at CBH spent over defined source regions.

The chemical composition of rain samples in each of the three clusters obtained for air mass history at CBH are presented in Table 5.4 together with the pH, EC and ancillary measurements associated with each cluster. Based on the clustering according to air masses arriving at CBH, CBH-A, representing air masses spending most time over the clean western background region, had the highest total VWM concentrations of ionic species. However, the total VWM concentrations of ions in cluster CBH-B were marginally lower, which could be attributed to higher rainfall depth recorded for rain events in this cluster compared to cluster CBH-A. Cluster CBH-C had the lowest total VWM concentrations associated with rainfall depth, similar to that of cluster CBH-A.

VWM concentrations of Na^+, Cl^-, Mg^{2+}, Ca^{2+}, NO_3^- and SO_4^{2-} were the highest for rain events grouped in cluster CBH-A, with Ca^{2+} levels being significantly higher. Rain events in CBH-B had the highest H^+ and corresponding lowest pH, which are most likely due to significantly lower Ca^{2+} in comparison to levels thereof in rain grouped in cluster CBH-A. The extent of neutralisation of rain at Welgegund by Ca^{2+} is also signified by clustering of these air masses. Although the concentrations of species typically associated with oceanic air masses, i.e. Na^+ and Cl^-, were higher in cluster CBH-A, no noteworthy difference was observed compared to levels thereof in the other clusters. Higher concentrations of Cl^- and K^+ in cluster CBH-B, which had the least impact from oceanic air masses, together with the highest total OA VWM concentrations in this cluster, are indicative of the influence of biomass burning to the north and east of the sampling site on rain chemistry (Figure 3.12). Higher concentrations of anthropogenic acidic species, i.e. SO_4^{2-} and NO_3^- in cluster CBH-A and CBH-B in comparison to cluster CBH-C, which represents air masses at CBH spending more time over the point sources, points to the regional influence of anthropogenic activities in this region. Since higher concentrations of these anthropogenic species are associated with air masses at CBH passing over a relatively clean background region prior to a rain event, below-cloud scavenging can be considered more important in influencing the chemical composition of rain in this part of South Africa. Xu et al. (2017) showed that SO_4^{2-} deposited during the initial moments of a rain event corresponded to concentrations thereof in ambient aerosols. Furthermore, higher concentrations of Na^{2+} and Cl^- in cluster CBH-B, representing air masses spending < 8% over oceans, also point to the more prominent influence of below-cloud air mass movement and below-cloud scavenging.

Table 5.4 Air mass history clustering at CBH arrival height: VWM concentrations (μeq.L^{-1}) of ionic species in each cluster, as well as average pH, electrical conductivity (EC), rainfall depth and ancillary measurements. The standard deviations are indicated in block brackets.

	CBH-A		CBH-B		CBH-C	
# of samples	29		37		20	
H^+	19.7	[17.41]	36.67	[27.77]	24.93	[22.60]
Na^+	24.58	[38.44]	19.12	[50.10]	17.3	[35.94]
NH_4^+	26.97	[21.22]	31.73	[19.53]	16.09	[13.46]
K^+	7.65	[16.50]	8.15	[15.82]	4.81	[15.40]
Mg^{2+}	23.59	[71.68]	6.65	[10.52]	16.94	[74.72]
Ca^{2+}	39.79	[62.66]	21.88	[21.22]	23.42	[65.61]
NO_3^-	41.41	[40.71]	31.94	[18.98]	23.37	[36.45]
Cl^-	23.32	[37.43]	20.59	[52.70]	15.5	[29.11]
SO_4^{2-}	53.68	[37.22]	52.02	[24.13]	43.13	[38.70]
F^-	0.47	[0.49]	0.6	[0.57]	0.77	[1.09]
tOA*	9.84	[20.62]	15.58	[22.30]	3.57	[5.97]
Total VWM	271.01		244.94		189.83	
pH	5.04	[0.80]	4.65	[0.50]	4.91	[0.87]
EC (μS)	35.62	[36.37]	34.9	[39.54]	33.99	[40.31]
O_3 (ppb)	35.68	[8.99]	34.07	[10.14]	23.99	[11.61]
SO_2 (ppb)	0.55	[0.72]	0.79	[1.64]	1.67	[3.46]
NO (ppb)	0	[0.13]	0.06	[0.17]	0.24	[0.48]
No_x (ppb)	2.05	[1.57]	2.97	[2.24]	3.86	[3.98]
CO (ppb)	117.07	[37.47]	129.39	[36.42]	140.12	[37.16]
PM_{10} (μg.m^{-3})	15.56	[11.76]	16.31	[11.34]	15.75	[12.06]
eBC (μg.m^{-3})	0.25	[0.28]	0.39	[0.37]	0.38	[0.66]
Total rainfall depth (avg) (mm)	424.00 (14.62)	[13.01]	611.50 (16.53)	[14.82]	442.50 (22.13)	[19.11]
Intensity average (max) (mm.h^{-1})	5.88 (18.30)	[4.91] [16.77]		[3.00] [10.05]	3.55 (18.40)	[2.73] [20.42]
CBH_{2hr} (m)	2741.72	[861.62]	2296.22	[776.03]	1606.5	[1060.65]
CBH_{15min} (m)	2189.29	[905.68]	1930	[739.44]	1415.26	[878.01]

Comparison of ancillary measurements associated with rain events in these clusters, obtained for air masses arriving at CBH, indicates that mean concentrations of species associated with anthropogenic activities, i.e. SO_2, NO_x and CO, were higher in cluster CBH-C. However, average PM_{10} and eBC concentrations were similar in all three clusters although the time air masses spent over point sources differed, which could rather signify the influence of below-cloud scavenging on rain chemistry measured at Welgegund. It is generally considered that between 48% and 84% of all the SO_2 conversion to H_2SO_4 in the

troposphere occurs within clouds (Halsall, 2003). The CBH clusters with the highest SO_4^{2-} rainwater concentrations are also associated with the lowest ambient concentrations of SO_2, which could indicate the contribution of in-cloud oxidation reactions to rain chemistry. Furthermore, NO_x are not highly water-soluble and are not easily absorbed into cloud water (Finlayson-Pitts and Pitts, 2000). The CBH clusters with the lowest NO_3^- concentrations corresponded to the highest ambient concentrations of NO_x, indicating that below-cloud air mass history and scavenging could contribute more to NO_3^- in rain than air mass history associated with CBH. Similarly to that observed for cluster analysis according to the chemical composition of rain, average rain intensities in the three clusters determined for air masses arriving at CBH corresponded to total VWM concentrations of ionic species in each cluster, with the average rain intensity being the highest in cluster CBH-A. Lower O_3 concentrations in cluster CBH-C, are also expected due to titration of atmospheric O_3 within proximity of NO_x sources (Laban et al., 2018). EC measurements of rain events in each cluster correspond to the total VWM concentrations. Analysis of variance of ancillary measurements in these three clusters only revealed significant statistical and substantive variances for O_3 and NO concentrations in cluster CBH-C compared to the other two clusters (Table 5.5).

Table 5.5 Analyses of variance of ancillary measurements in the three cluster solutions based on air mass history arriving at CBH

Ancillary measurement	p-Value	Effect Sizes		
		A with B	A with C	B with C
O_3	0.001	0.16	1.01	0.87
NO	0.019	0.32	0.50	0.38
T	0.012	0.68	0.62	0.06
WS	0.036	0.41	0.73	0.28
RH	0.000	0.74	1.16	0.45
CBH_{2hr}	0.000	0.52	1.07	0.65
CBH_{15min}	0.009	0.29	0.85	0.59

Similarly to the clustering of the chemical composition of rain events, although some differences in ionic composition could be observed in the three clusters determined for air masses arriving at 100 m a.g.l. and CBH, statistical analysis did not explicitly reveal distinct differences between the ionic compositions associated with air masses passing over different source regions. However, the important influence of below-cloud scavenging on rain chemistry in this region was evident as indicated by relating air masses arriving at 100 m a.g.l. to the chemical composition of rain.

5.4 Comparing Synoptic Patterns

This section aims to explore the relationship between rain events associated with different synoptic systems at the mesoscale. Analysing the synoptic charts could give some indication of the type of convection on the rain event day, in contrast with the 96h-back trajectories determined in the previous sections which incorporated the progression of synoptic patterns and the influence thereof on surface flow. The highest CBH measured during this study was 4660m (< 5km), therefore surface synoptic maps were used (SAWS, 2019). The rainfall over the South African interior is influenced through the global circulation patterns and disturbances as described in Chapter 2.8. Rain event day surface synoptic charts as well as infrared (IR) and satellite images from EUMETSAT (2019) were analysed for all rain events that passed the WMO DQO criteria and events with available data (Chapter 3.2.4 and 3.2.5).

All of the events were characterized by a surface trough (ST) extending from the north. As described in Chapter 2.8, the surface troughs associated with tropical disturbances can be related to strong convective rainfall, and are often associated with high rainfall intensities and large rainfall depths over the plateau in the austral summer. These rainfall events are often associated with thunderstorms, lightning and high rainfall depth on the Highveld (Mogale and Dyson, 2017; Tyson and Preston-Whyte, 2017). Lynn et al. (2005a) have reported that convective clouds scavenge 60% of the available CCN, with the most CCN scavenged within the first 30 minutes of cloud formation. Ćurić et al. (2009) showed that cloud seeding agents were entrained into convective clouds from roughly less than 20 km away. Some rainy days showed a coastal low pressure (CL) in addition to the surface trough (34 coastal lows were on the east coast, 12 to the south and 4 to the west). Coastal lows have been known to cause flooding further inland (Tyson and Preston-Whyte, 2017). Coastal lows and westerly waves (WW), with associated cold fronts, are temperate perturbations to the stable conditions that prevail over continental South Africa. Another group of events was identified with a cold front passing over the country from the south-west to the south-east. These westerly waves associated with cold fronts, typically advect polar maritime air from behind the cold front, and cloud bands commonly form through convection. Rainfall associated with these types of temperate westerly waves has relatively low rainfall intensities (Chapter 2.8) (Tyson and Preston-Whyte, 2017). Examples of the three synoptic conditions that rain events were grouped into are given in Appendix A. The events related to surface troughs, coastal low pressures and westerly waves disturbances represented 49, 33 and 17% of the rainfall events collected at Welgegund, respectively.

In Table 5.6, the VWM concentrations for the three synoptic groups are listed. In Figure 5.9 (a-d), boxplots are presented for the pH, EC, ancillary measurements, rainfall depth and intensity, and CBH averages. Events associated with coastal low pressures, and westerly waves had the highest and lowest total VWM respectively. The coastal low events had the highest VWM concentrations of neutralising, crustal and agricultural species i.e. Ca^{2+}, Mg^{2+} and NH_4^+, as well as the highest NO_3^-, and biomass burning related K^+ and total OAs concentrations. The events related to coastal low pressures had the highest average CO, O_3 and eBC concentrations, as well as the largest PM_{10} concentration range that can again be associated with biomass burning emissions (Figure 5.9 (a) and (b)). These events had the greatest pressure range and highest average pressure, as well as the greatest difference between CBH 2 hour and 15 minute averages (Figure 5.9 (c) and (d)). However, these events also had the smallest rainfall depth (Figure 5.9 (c)), which can relate to the higher VWM concentrations.

The events related to westerly wave disturbances and cold fronts did not show substantial differences in the acidifying SO_4^{2-} concentrations. However, these events had the highest H^+, which can be attributed to the exceptionally lower Ca^{2+} and Mg^{2+} concentrations. The westerly wave related events would be expected to have higher crustal ion concentrations associated with movement over the Kalahari and Karoo (Section 5.3.1 and Chapter 4.2). However, these events also had the lowest rain intensity, average wind speed, and PM_{10} concentrations (Figure 5.9 (d)). As mentioned above, higher rain intensity has been related to the effective scavenging of larger aerosols such as $CaSO_4$, while NO_3^- and NH_4^+ can still be efficiently scavenged at lower intensities (see also Chapter 2.5) (Xu et al., 2017). These events would most likely not follow dusty conditions as the wind speed would lack the energy to lift the dust into suspension (Uchiyama et al., 2019). The westerly wave related events had the highest RH that can also contribute to the scavenging of hygroscopic aerosols such as $(NH_4)SO_4$ (Kulshrestha et al., 2009), which could explain why the NH_4^+ and SO_4^{2-} VWMs were still comparable to the other groups, even though the rain intensity and rain depth was lower. Although NaCl is very hygroscopic (Kulshrestha et al., 2009), westerly waves mostly advect moisture from the polar regions to the south-west of South Africa. The lower Na^+ and Cl^- VWMs could be attributed to the marine air masses being transported vast distances over the continent to reach Welgegund. These events were also related to the lowest average SO_2, NO_x, CO, and eBC concentrations, but the highest O_3 concentration (Figure 5.9(a) and (b)). Frontal rainfall associated with westerly waves typically comprises low intensity events with longer duration. The large scale cloud bands associated with this type of rainfall are reflected in the small difference between the 2 hour and 15 minute CBH averages and narrow pressure range (Figure 5.9 (c) and (d)).

The events related to surface troughs had the highest SO_4^{2-} VWM, but the neutralisation through the high concentrations of Ca^{2+} and NH_4^+ is evident by the low H^+ VWM and the high pH. These events were also related to the highest measured EC, and SO_2 and NO_x concentrations (Figure 5.9 (a) and (b)). The highest wind speed average and range was measured for these events, most likely associated with heavy precipitating cumulonimbus clouds, and can also relate to the higher crustal (dust) components (Chapter 2.7.3). Although these events had the highest rainfall intensities which is normally associated with more effective scavenging, these events also had the greatest rainfall depth, which dilutes the components being scavenged, confirming the relatively lower VWM concentrations (Mogale and Dyson, 2017). Hart et al. (2010) reported that convective processes dominated in rain formation over the subtropical regions of southern Africa. Although not investigated in this study, Holmes et al. (2016) also reported 50% more effective Hg washout through thunderstorm related rain compared to stratiform systems. The synoptic groups are compared to the rainwater chemistry and air mass history clusters in Section 5.5.

Table 5.6 Synoptic comparison: VWM concentrations ($\mu eq.L^{-1}$) for rain events grouped according to the dominant synoptic patterns. The weighted standard deviations are indicated in block brackets.

	Surface Troughs		Coastal Lows		Westerly Waves	
# of samples	47		32		17	
H^+	28.00	[26.00]	25.97	[15.25]	36.10	[36.51]
Na^+	20.85	[51.85]	21.66	[24.77]	14.99	[20.05]
NH_4^+	23.87	[18.39]	31.66	[21.98]	22.75	[11.85]
K^+	6.93	[18.63]	8.18	[11.69]	4.87	[4.47]
Mg^{2+}	12.86	[53.18]	22.19	[68.77]	3.44	[5.12]
Ca^{2+}	27.05	[54.66]	32.38	[50.04]	15.30	[16.29]
NO_3^-	29.96	[31.62]	40.03	[35.27]	26.66	[20.43]
Cl^-	20.29	[31.62]	21.41	[35.27]	15.43	[20.43]
SO_4^{2-}	51.50	[35.05]	47.75	[30.50]	43.46	[31.52]
F^-	0.69	[0.87]	0.47	[0.57]	0.40	[0.34]
tOA*	9.00	[21.90]	15.11	[14.14]	7.42	[8.98]
Total VWM	231.02		266.80		190.83	

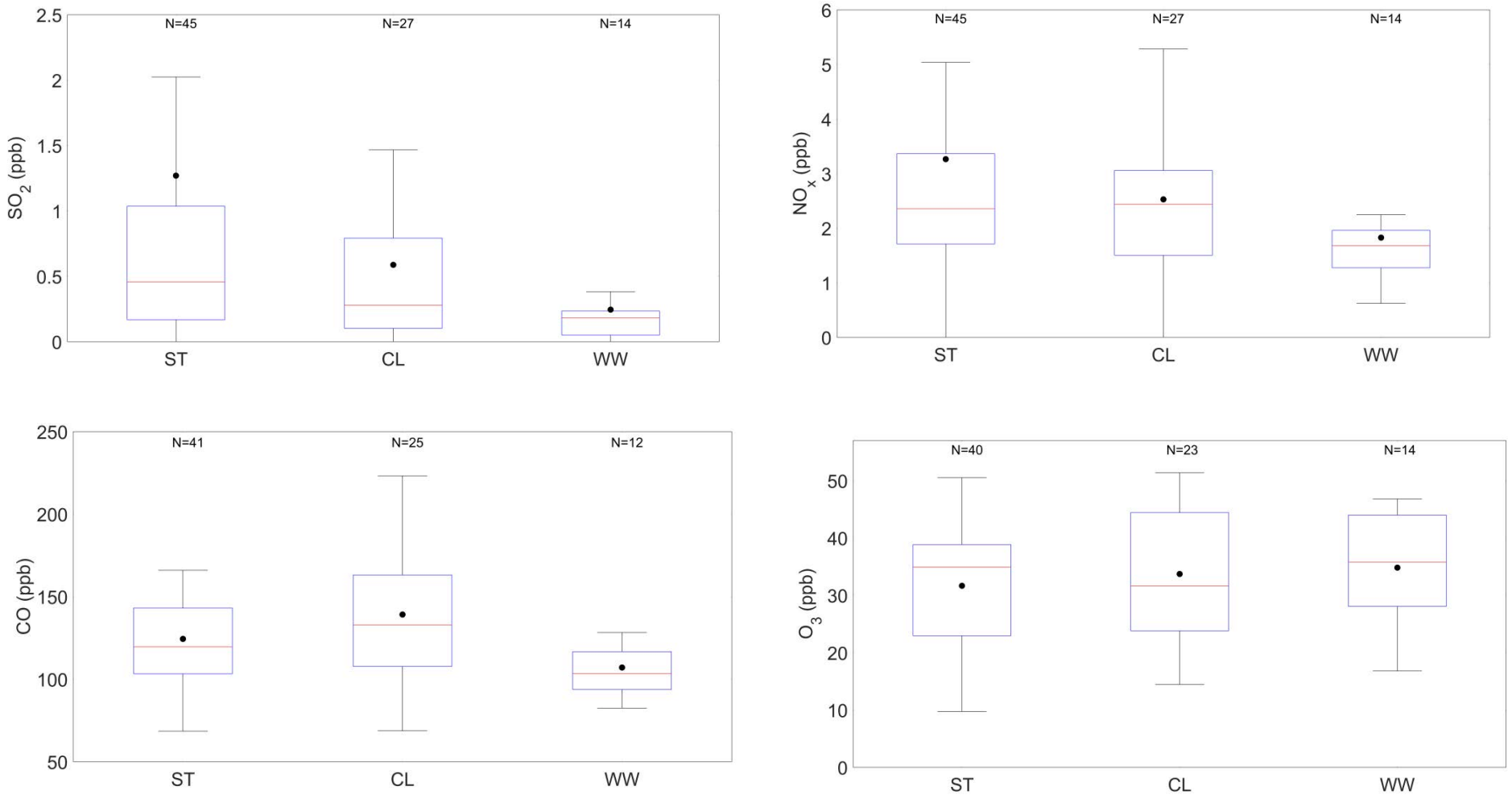

Figure 5.9 (a) Average gaseous concentrations measured before rain events as grouped into the dominant surface flow indicated by synoptic charts. (ST: Surface Trough; CL: Coastal Low Pressure; WW: Westerly Waves).

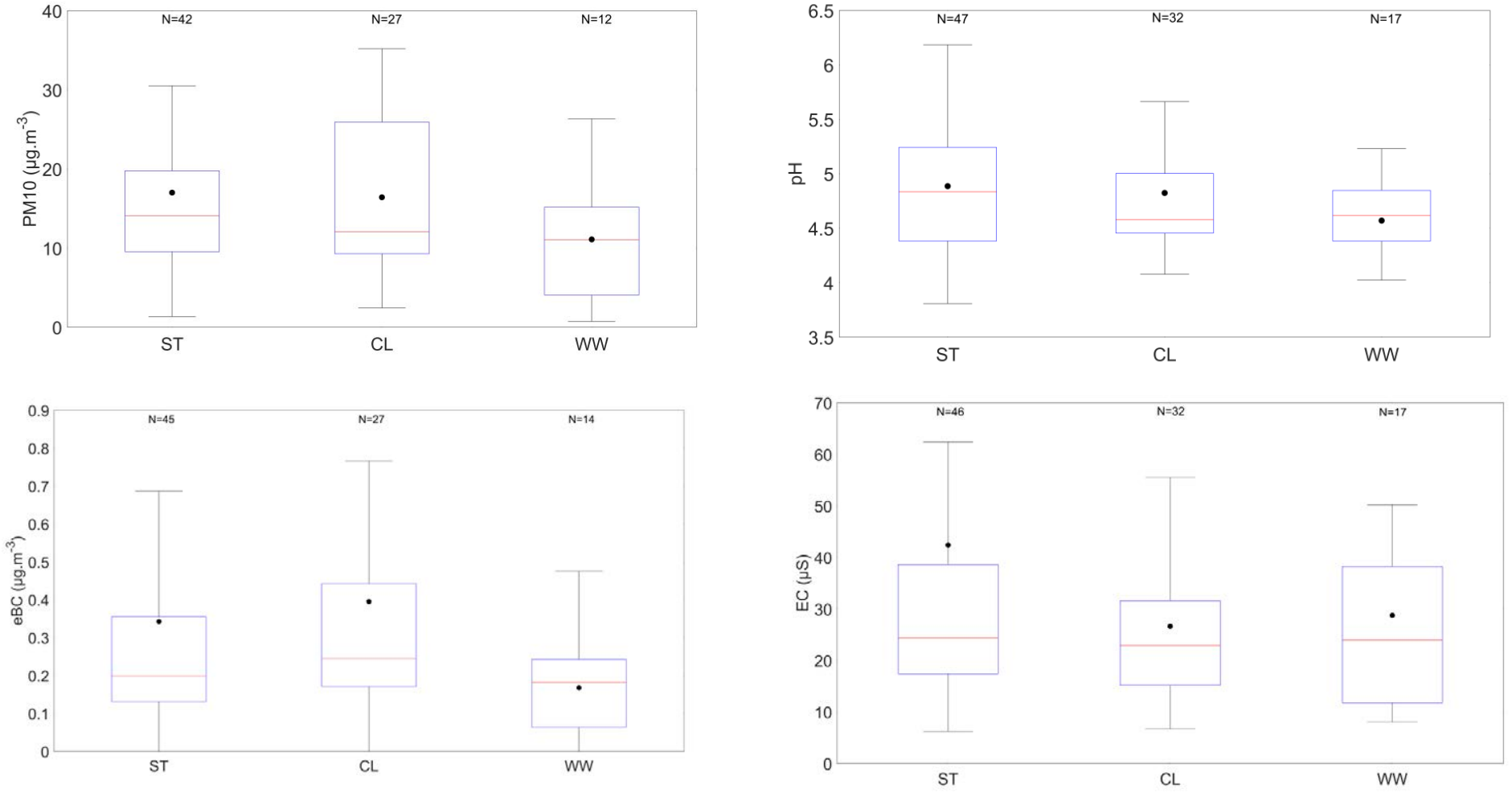

Figure 5.9 (b) Average PM_{10} and eBC concentrations measured before rain events, and pH and EC measurements for events as grouped into the dominant surface flow indicated by synoptic charts. (ST: Surface Trough; CL: Coastal Low Pressure; WW: Westerly Waves).

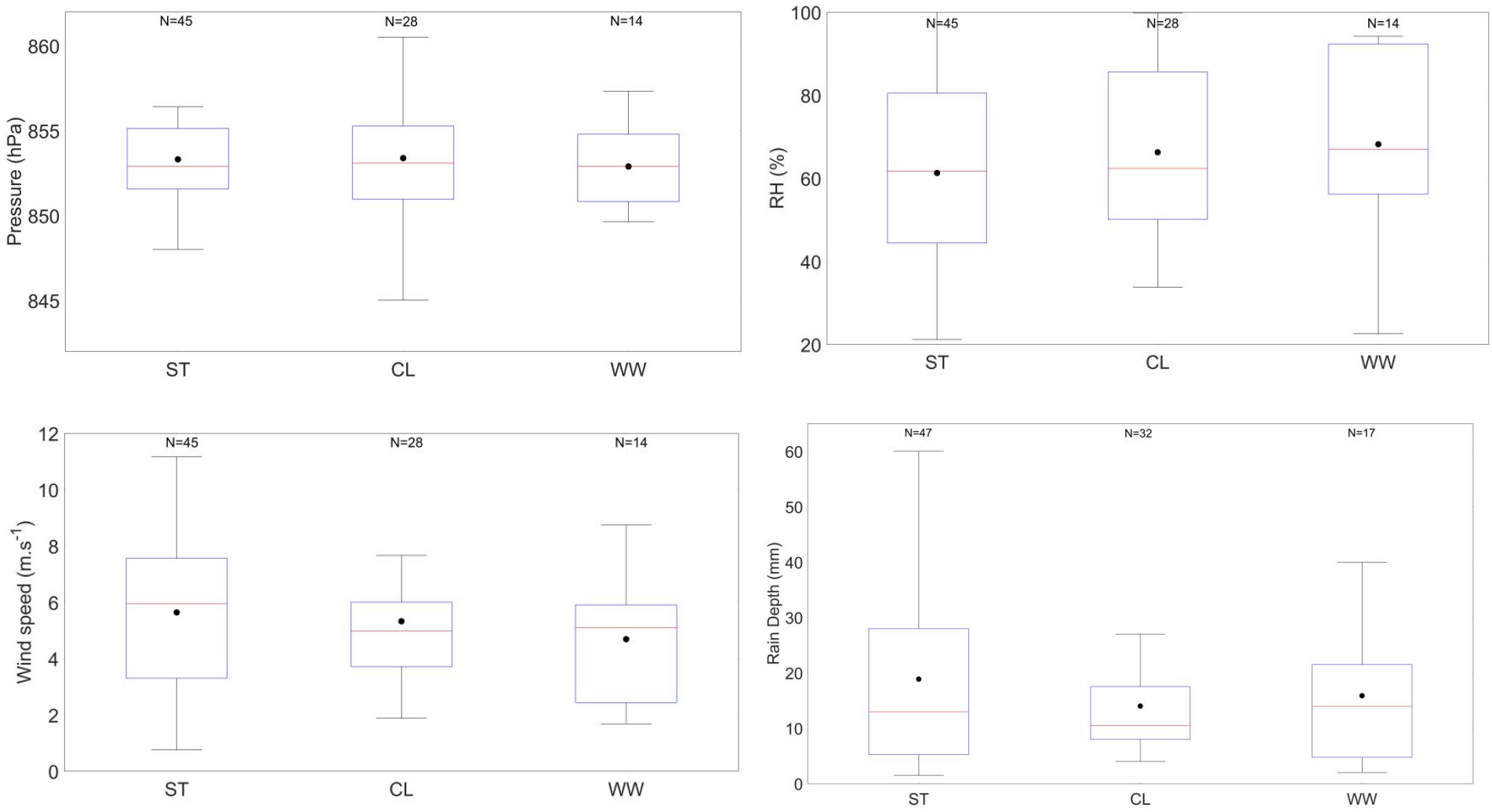

Figure 5.9 (c) Average pressure, RH and wind speed measured before rain events as grouped into the dominant surface flow indicated by synoptic charts, as well as the rain depths. (ST: Surface Trough; CL: Coastal Low Pressure; WW: Westerly Waves).

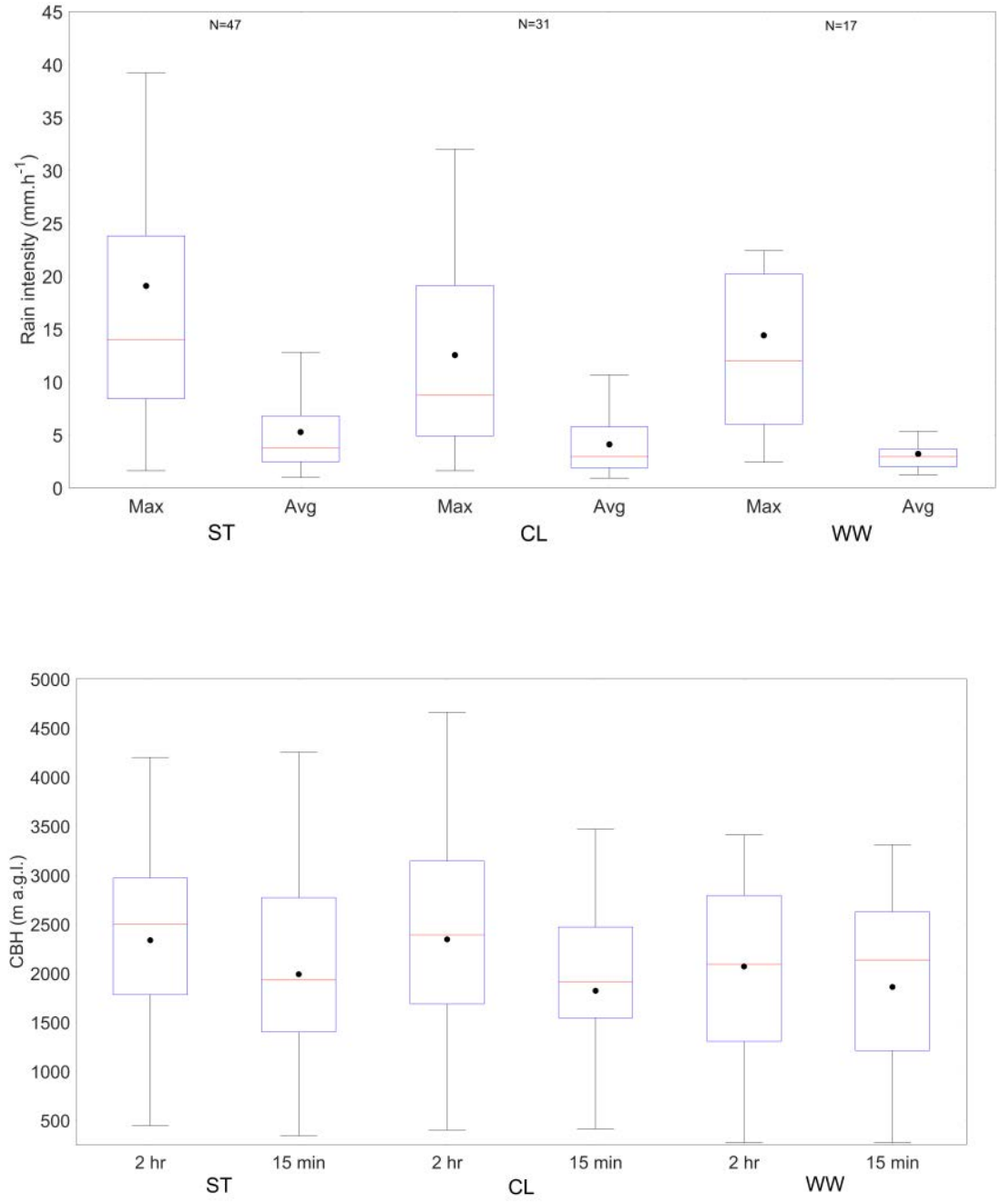

Figure 5.9 (d) Maximum and average rain intensity, and 2 hour and 15 min CBH average measured for rain events as grouped into the dominant surface flow indicated by synoptic charts. (ST: Surface Trough; CL: Coastal Low Pressure; WW: Westerly Waves).

5.5 Inter-comparison of Rain Event Clustering

From the different approaches taken in this study, the cluster solutions were inter-related by establishing whether rain events grouped in one cluster according to a specific approach also occurs in a cluster determined with another approach. Clusters determined by grouping of the air masses at 100 m a.g.l. arrival heights indicated statistically significant overlap with clusters obtained by grouping according to the ionic composition of rain, i.e. $p = 0.059$. Therefore, rain events grouped together according to ionic composition of rain events are likely also to be clustered together when events are clustered according to air mass history at an arrival height of 100 m a.g.l. (Section 5.2 to 5.3.1 and Chapter 3.2.7.2). However, the clusters determined for air masses at CBH did not statistically correspond to any clusters determined for air masses arriving at 100 m a.g.l. or with clusters determined for the chemical composition of rain events, i.e. $p = 0.239$ and 0.874, respectively. Therefore, inter-comparison between different clustering approaches also reflects the significance of below-cloud scavenging on chemical composition of rain samples collected at Welgegund.

The events in the three synoptic groups were also compared to the clusters determined for the ionic composition (Section 5.4). The amount of overlap between the compositional and 100 m a.g.l. air mass history clusters showed noteworthy similarities to the amount of overlap between the compositional and synoptic groups. This could indicate the influence of convection type on rainwater chemistry (Chapter 2.8). The overlap between the chemical clusters and synoptic patterns could signify the relationship of certain ancillary measurements, which showed statistically significant differences between the groups within the HCA clusters, with the rainfall type or type of uplift associated with the precipitating cloud (Section 5.2). These included maximum rainfall intensity, pressure, average CBH, RH, wind speed and temperature. However, the mesoscale factors influencing rain chemistry are complex and a definitive relationship between the type of convection and rainwater chemistry could not be established in the scope of this study. Modelling studies or field measurement studies of convection processes such as those by Tost et al., 2010 and Fuentes et al., 2016 could be more appropriate to determine these relationships. The nuances between the synoptic pattern progression and surface flow determined through trajectories appear to be a better method to link surface air flow and rainwater chemistry.

In an explorative principal component analyses performed on the rainwater ionic composition with the ancillary measurements as supplementary variables, high loadings of the anthropogenic (H^+, SO_4^{2-}, NO_3^- and F^-) and agricultural (NH_4^+) related ions confirmed a positive correlation to rain intensity, wind speed and SO_2 concentrations, and an inverse correlation to relative humidity. The marine, crustal and biomass burning related ions (Na^+, Cl^-, Ca^{2+}, Mg^{2+}, K^+ and tOA*) showed

positive correlation to O_3, CO, eBC and PM_{10} concentrations as well as to the pressure and 2 hour average CBH. The explorative PCA can be seen in Appendix B.

5.6 Summary & Conclusion

The aim of this chapter was to conduct an advanced assessment on large scale factors influencing chemical composition of rain in the South African interior by relating rain events at Welgegund to air mass history at arrival heights below clouds and at cloud base height. HCA were performed following two different approaches, i.e. clustering based on the chemical composition of rain that was related to air mass histories at the two arrival heights, as well as grouping based on air masses arriving at 100 m a.g.l. and CBH that was then associated with chemical composition. Cluster solutions were also related to ancillary measurements conducted at Welgegund. Statistical analyses of back trajectories were performed in order to relate the synoptic scale influence of air flow on rainwater chemistry. The influence of CBH on rain composition was evaluated in order to establish the impacts of the possible region where cloud formation occurred on rain chemistry (microscale in-cloud scavenging), while 100 m a.g.l. air mass histories were related to rain chemistry in order to assess the influence of below-cloud atmospheric chemistry on rain composition through below-cloud scavenging. In each of the approaches in this study, the optimum solutions yielded three clusters. Rain chemistry was also compared between events relating to three different prevailing surface synoptic conditions in order to relate the mesoscale effects such as convection type on rainwater chemistry.

Statistical analyses highlighted the complexity associated with correlating rain chemistry to sources of chemical species. However, clustering analysis was useful in establishing some correlations between rain chemistry and the source regions that air masses pass over prior to a rain event. Clustering conducted according to the ionic composition of rain events grouped rain events together in relation to their total VWM concentrations, i.e. from high to low VWM concentrations. Correlation of air mass histories to the three clusters indicated to an extent that higher VWM concentrations were associated with air masses at 100 m a.g.l. passing over anthropogenic source regions. A statistically significant positive correlation between rain intensity and rain chemistry was determined which could be attributed to increased scavenging efficiency (Hall, 2003; Bae et al., 2006; Kulshrestha et al., 2009; Karev et al., 2010; González and Aristizábal, 2012). SO_2 concentrations and pH also showed covariance with rain chemistry.

Air mass history clustering grouped air masses passing predominantly over predefined source regions, i.e. air masses passing over anthropogenic source regions, a clean western background region and oceans. Air masses arriving at 100 m a.g.l. were considered to be representative of the well-mixed boundary layer. The rain chemistry of clusters determined for air masses at 100 m a.g.l. arrival heights could be related to the influence of different source regions, with the influence of large point sources, the clean western background sector and oceans especially evident. Clustering according to chemical composition and air masses with an arrival height of 100 m a.g.l. also reflected the regional impact of anthropogenic activities in the north-eastern part of South Africa, while the influence of household combustion was also evident. Due to the nuances between 96h back trajectories and the air flow influenced by the progression of synoptic patterns, back trajectories arriving at 100 m a.g.l. were determined to be a useful method in order to evaluate the influence of the synoptic scale air flow over source regions on rainwater chemistry. This method confirmed the influence of residence time over source regions on the variability in rainwater chemistry. Air mass movement over major source regions in the interior for both the chemical and 100m a.g.l. clusters, was related to higher SO_4^{2-} concentrations and low pH. Although air masses arriving at CBH did partially contribute to rain chemistry, no significant correlations between air mass histories at CBH and ionic composition were evident. Therefore, it could be concluded from the statistical analysis according the different approaches followed in this study that below-cloud atmospheric chemical composition was more significant in contributing to the chemical composition of rain samples in this part of South Africa.

Considering the surface synoptic charts and satellite imagery of the rain event days, rain events were categorised according to three main synoptic patterns relating to rain events at Welgegund, namely tropical-temperate surface troughs, surface troughs with coastal low pressures, and surface troughs with temperate westerly wave disturbances. The highest total VWM was measured for events relating coastal low pressures, while the lowest VWM was measured for rain events related to westerly wave conditions. Some association between the type of uplift associated with the rain event and the rainwater chemistry was evident. Events related to strong convective uplift, high rain intensity and depth, and wind speed had the highest SO_4^{2-} concentrations and neutralisation through high concentrations of Ca^{2+} and NH_4^+. Events related to moderate frontal uplift associated with westerly waves, had the highest RH, and the lowest pressure, rain intensity and rain depth relating to the lowest rainwater VWM concentrations. A comparison between the clustering approaches suggests the influence of below-cloud air mass history and meteorological conditions on the rainwater chemistry. Surface flow patterns vary greatly even in the specific groups identified, therefore, it is determined that surface flow trajectories are a more reliable method to relate air mass history to rainwater chemistry.

In view of the results of the clustering analysis of rain chemistry and air mass history at Welgegund, the influences of different source regions, below-cloud scavenging, rain intensity and pollution build-up were further explored in the subsequent section by conducting case studies of specific rain events. Here the advantages associated with the availability of CBH height measurements in conjunction with rain sampling is further explored and presented.

Chapter 6

Case studies on certain rain events

In the previous chapter, statistical analysis of rain events at Welgegund explored the relationships between rainwater chemistry and the air mass history at different arrival heights. Although statistical analysis proved useful in relating rain chemistry to air mass history, some limitations were evident, mainly due to the complexity of factors influencing rain chemistry. Rain events, for instance, that are grouped together in one of the statistical clusters could relate to different air mass histories or synoptic conditions. Events on consecutive days of the same synoptic system and with similar air mass histories could present significantly different chemical compositions, depending on the scavenging efficiency of the rain events and thus be grouped into different statistical clusters. This chapter, therefore, aims to further assess the influence of air mass history and the role of in-cloud and below-cloud scavenging on rain chemistry by presenting a selection of case studies for specific rain events. The rain events are assessed by presenting the ionic composition and the event air mass histories arriving at Welgegund at 100 m .a.g.l. and cloud base height.

6.1 Introduction to Case Studies

Throughout this chapter, back trajectories, as calculated through the methods described in Chapter 3.2.4, are presented. The trajectories were plotted at two arrival heights for each event (100 m a.g.l. and cloud base height (CBH)). For each arrival height, three individual, hourly arriving trajectories were calculated for 2 hours prior to the rain event in order to minimise the 15 to 30% uncertainty associated with individual back trajectories (Chapter 3.2.4) (Stohl, 1998; Stohl and Koffi, 1998). In the back trajectory maps presented in this chapter, the 96-hour back trajectories were plotted in gold for the arrival height at the median CBH and in blue for the 100 m a.g.l. arrival height. The event median CBH measured with the ceilometer (Chapter 3.2.3.2) is indicated. The Welgegund atmospheric research station is represented as a black star, the large pollution point sources as black dots, the Johannesburg-Pretoria conurbation as an area shaded in grey, and the burn scar areas four days prior to the rain events shaded in red (Chapter 3.2.3.4). For each rain event, the ionic concentrations in $\mu eq.L^{-1}$ (Chapter 3.2.2) were normalised by multiplying with the respective rainfall depth and reported here (Chapter 3.2.6.1). The event rainfall depth (mm) and rain intensity ($mm.h^{-1}$) are also listed (Chapter 3.2.1 and 3.2.3.1).

6.2 Anthropogenic Sources

The influence of the densely populated eastern source region, where the major pollution point sources in the interior of South Africa are located, on rain chemistry determined at Welgegund is supported in two examples presented in this case study. In Figure 6.1, back trajectories at CBH and 100 m a.g.l. calculated for rain events on 7 and 9 January 2015 are presented, while Table 6.1 lists the concentrations of ionic species associated with these rain events. It is evident from Figure 6.1 that below-cloud air masses passed over the eastern source region prior to both rain events. The air masses associated with the CBH only passed over this source region on 7 January 2015, while air masses at CBH bypassed most of the eastern source region on 9 January 2015. Both rain events illustrate the influence of anthropogenic sources on the chemical composition, especially as indicated by the elevated levels of SO_4^{2-} and NO_3^- (Chapter 3.2.6.2). Although the statistical analyses discussed in Chapter 5 did not point to a significant contribution of CBH on rain chemistry, this case study shows that air mass history associated with the precipitating cloud could contribute to the chemical composition as indicated by the higher SO_4^{2-} and NO_3^- concentrations in the event of 7 January 2015. These elevated concentrations are possibly related to both in-cloud scavenging processes and to the below-cloud pollutant scavenging that is explored in a following case study.

Table 6.1 Rainwater ionic concentrations, rain depth and -intensity associated with rain events on 7 and 9 January 2015.

	7 January 2015	**9 January 2015**
Rain depth (mm)	70.0	40.0
Max (avg) Intensity ($mm.h^{-1}$)	92 (12.8)	51.2 (10.4)
pH	4.20	4.10
SO_4^{2-}	5285	3024
NO_3^-	2453	1444
NH_4^+	2442	1386
Ca^{2+}	1221	514
Mg^{2+}	442	68
Na^+	1670	95
Cl^-	1439	112
K^+	510	32
tOA*	17	14

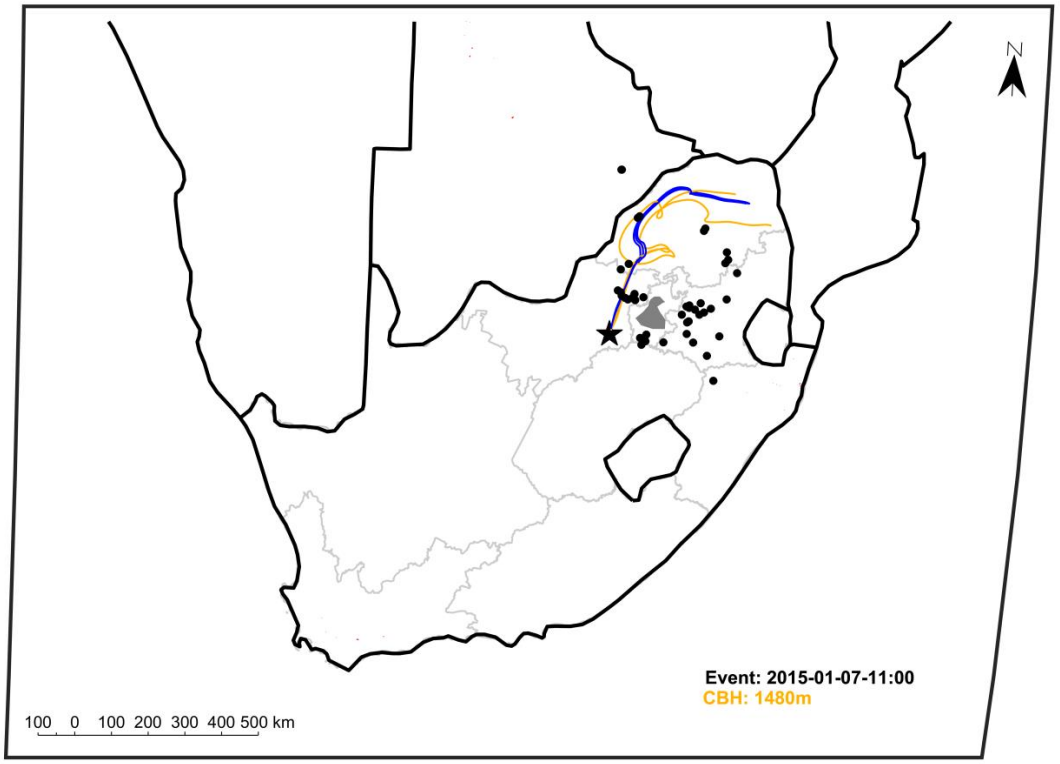

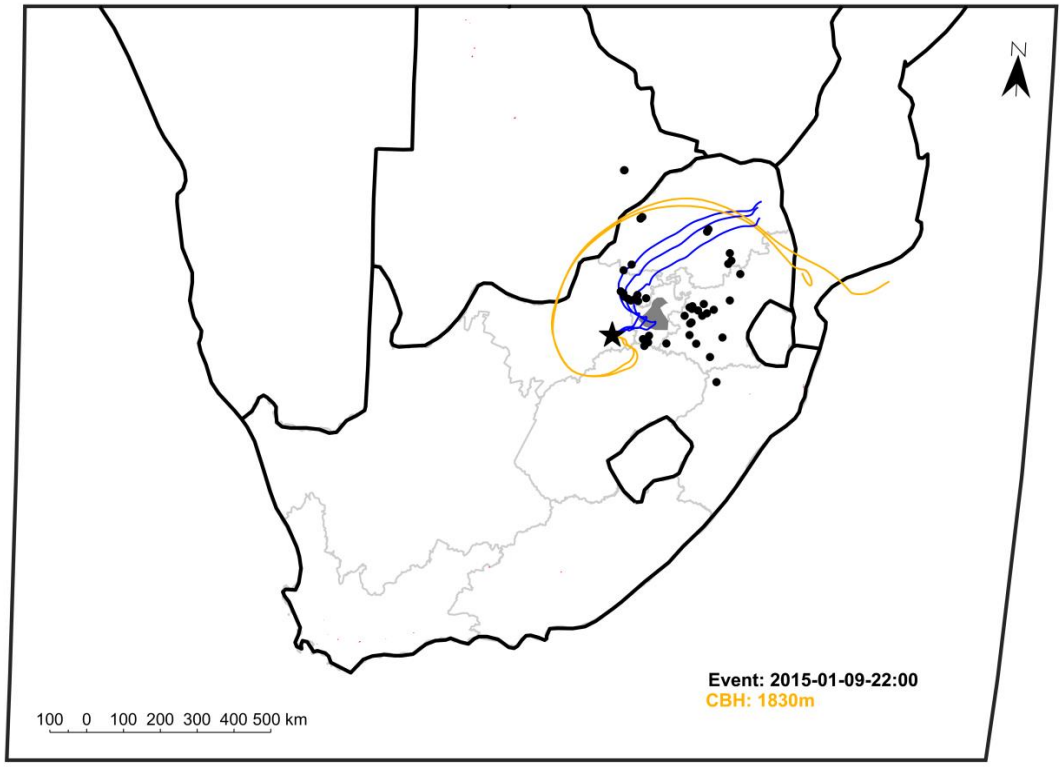

Figure 6.1 96-hour back trajectories at CBH and 100 m a.g.l. indicating air mass movement over anthropogenic sources for rain events occurring on 7 January 2015 (top) and on 9 January 2015 (bottom).

The influence of anthropogenic sources can be seen in another case study comparing a rain event when air mass histories at both arrival heights passed over the eastern source region, large pollution point sources and the JHB-PTA conurbation (21 March 2015), in contrast to an event when air masses at both heights came mainly from the cleaner western region (30 January 2017) as indicated in Figure 6.2(a). Comparing the ionic concentrations of these rain events in Table 6.2, significantly higher concentrations were measured for the event on 21 March 2015 than for the rain samples collected on 30 January 2017. The SO_4^{2-} and total OA concentrations were especially higher, which clearly reflect the influence of air mass movement over anthropogenic sources on the rainwater chemistry. The VWM concentrations of ionic species in the rain event on 30 January 2017 can also be considered representative of the chemical composition of rain minimally influenced by the source regions defined in this study.

A rain sample collected on 18 April 2016 (Figure 6.2(b)) is representative of a rain event with air mass history at both arrival heights following the anticyclonic recirculation pattern, but bypassing most of the large eastern pollution point sources. The ionic concentrations corresponded to similar levels of ionic species for the rain event on 30 January 2017, substantiating the relationship between air masses passing over point sources and higher ionic concentrations (Table 6.2). The significant contribution of below-cloud air masses to ionic concentrations in rainwater through below-cloud scavenging can also be seen in the event on 24 November 2017, when the below-cloud air masses arriving at 100 m .a.g.l. passed over the large pollution point sources as they arrived from the eastern source region. In contrast, the CBH air masses for this event arrived from the cleaner western region (Figure 6.2(b)). The ionic concentrations for this event were notably high, corresponding to the concentrations of the rain event on 21 March 2015 and to the below-cloud air mass movement over the major point sources. The elevated levels of OAs for the events on 21 March 2015 and 18 April 2016 are most likely attributed to the contribution of household combustion for space heating and cooking on the air quality in southern Africa (Laban et al., 2018). The prominent effect of below-cloud air mass movement on the rainwater composition is investigated further by investigating the effects of below-cloud scavenging in the case studies presented in the following section.

Table 6.2 Rainwater ionic concentrations, rain depth and -intensity for the rain events indicating the anthropogenic influence, 21 March 2015 and 24 November 2017, and the background air quality, 30 January 2017 and 18 April 2016.

	21 March 2015	30 January 2017	18 April 2016	24 November 2017
Rain depth (mm)	28	5	2	63
Max (avg) Intensity ($mm.h^{-1}$)	17.6 (3.0)	2.4 (1.3)	14.4 (7.6)	60.8 (13.3)
pH	4.02	5.48	5.8	5.10
SO_4^{2-}	2763	67	156	2832
NO_3^-	979	58	100	1586
NH_4^+	743	63	94	744
Ca^{2+}	292	46	187	1886
Mg^{2+}	2	9	41	323
Na^+	301	16	72	1427
Cl^-	252	45	69	1313
K^+	134	15	22	284
tOA*	119	1	57	19

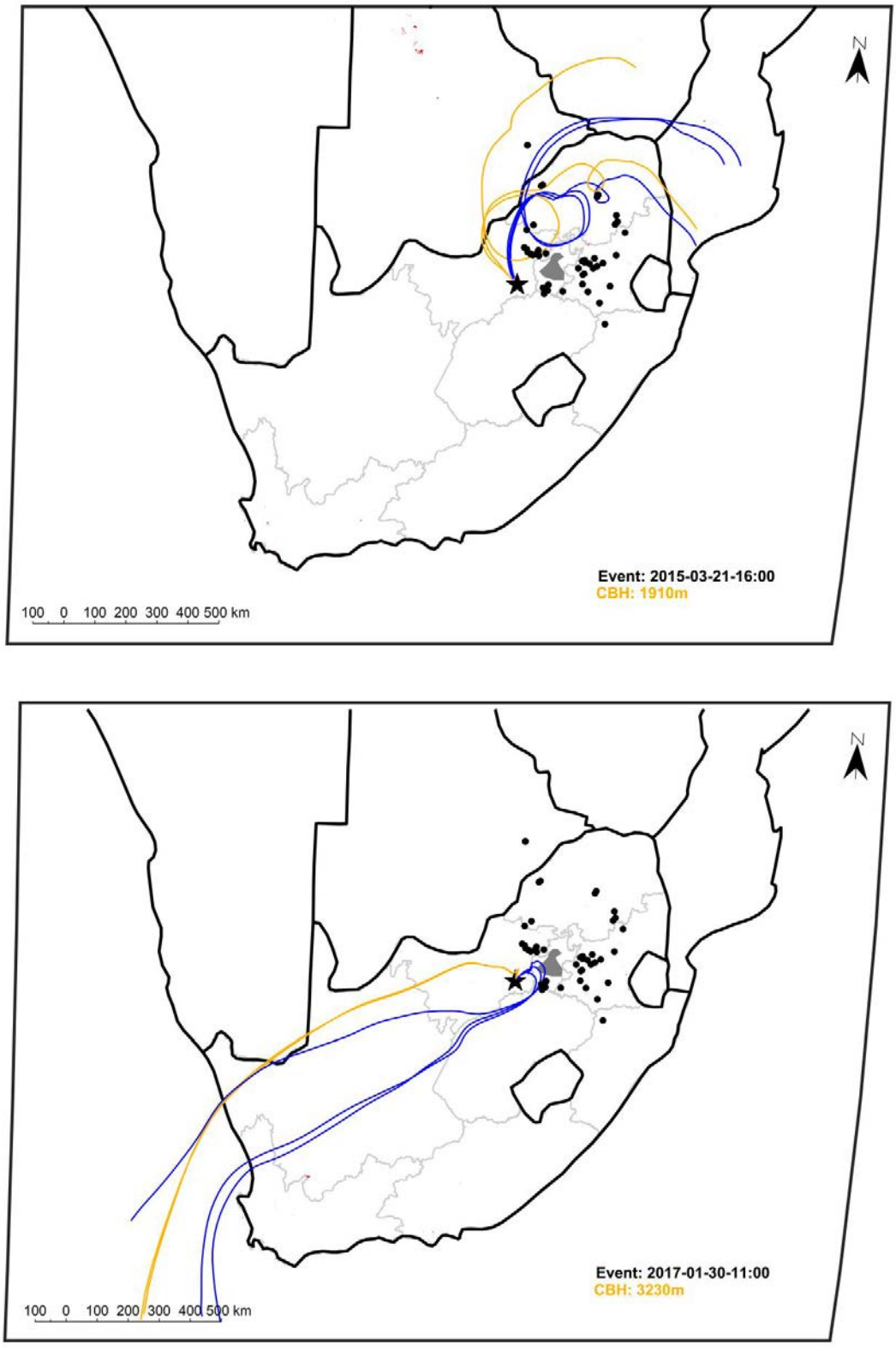

Figure 6.2(a) Back trajectories at CBH and 100 m a.g.l. for a rain event occurring on 21 March 2015, indicating the influence of air mass movement over anthropogenic sources (top), in contrast to the rain event on 30 January 2017, indicating the regional background influence on rainwater chemistry (bottom).

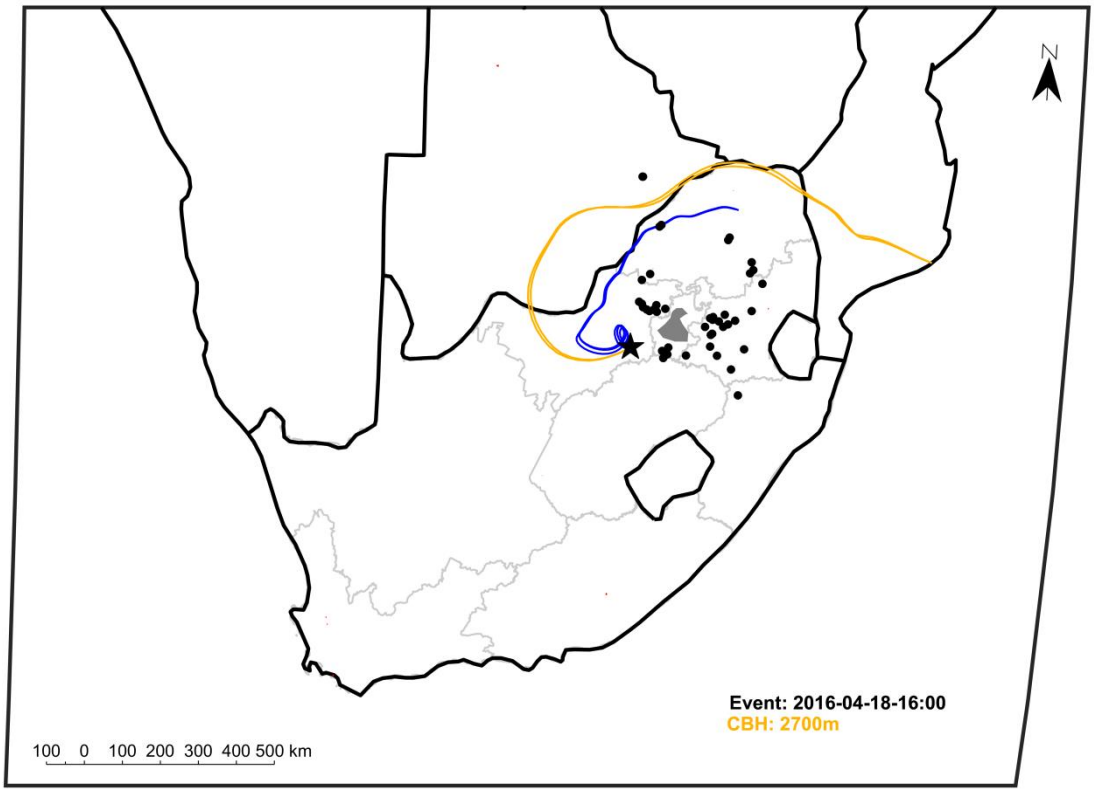

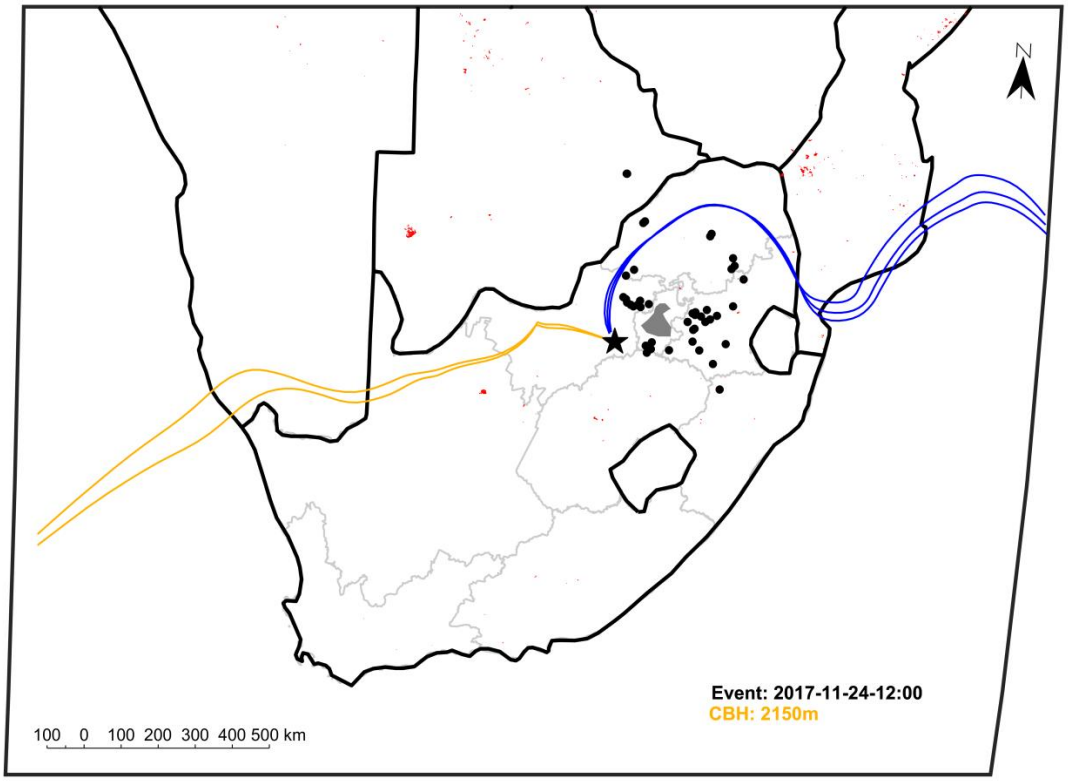

Figure 6.2(b) Back trajectories at CBH and 100 m a.g.l. for rain events occurring on 18 April 2016 and 24 November 2017, indicating the role of background air quality and pollution point sources on the levels of ionic species in rain.

6.3 Below-cloud Scavenging Efficiency

A good example of the scavenging efficiency through below-cloud processes, where in essence the air is being scrubbed, can be seen in the following two case studies for rain events occurring on consecutive days (Chapter 2.3). The events on 20 and 21 February 2017 that both started in the early morning had a relatively large rain depth, high rainfall intensity and similar air mass histories showing movement over the eastern pollution source regions for both arrival heights (Figure 6.3). The ionic concentrations for the events are presented in Table 6.3.

Table 6.3 Rainwater ionic concentrations, rain depth and -intensity for the rain events on 20 and 21 February 2017.

	20 February 2017	**21 February 2017**
Rain depth (mm)	60	38
Max (avg) Intensity ($mm.h^{-1}$)	29.6 (5.6)	29.6 (3.8)
pH	4.99	5.07
SO_4^{2-}	1319	932
NO_3^-	350	270
NH_4^+	229	225
Ca^{2+}	285	289
Mg^{2+}	50	20
Na^+	136	118
Cl^-	141	128
K^+	56	14
tOA*	3	43

Both of these event trajectories show air mass movement arriving from the east, with prominent movement over the pollution point sources and dense population areas (Figure 6.3). However, it is evident that the concentrations of anthropogenic-related ionic species such as SO_4^{2-}, NO_3^- and NH_4^+ were lower in the second rain event on 21 February 2017 compared to the first event on 20 February 2017. The statistical approach clustered these events into different chemical composition clusters (CHEM-B and CHEM-A, respectively), and into the same air mass history clusters for both arrival heights (100m-B and CBH-C). Most of the successive events during the sampling period presented distinctively higher concentrations for the first event when compared to the sequential event.

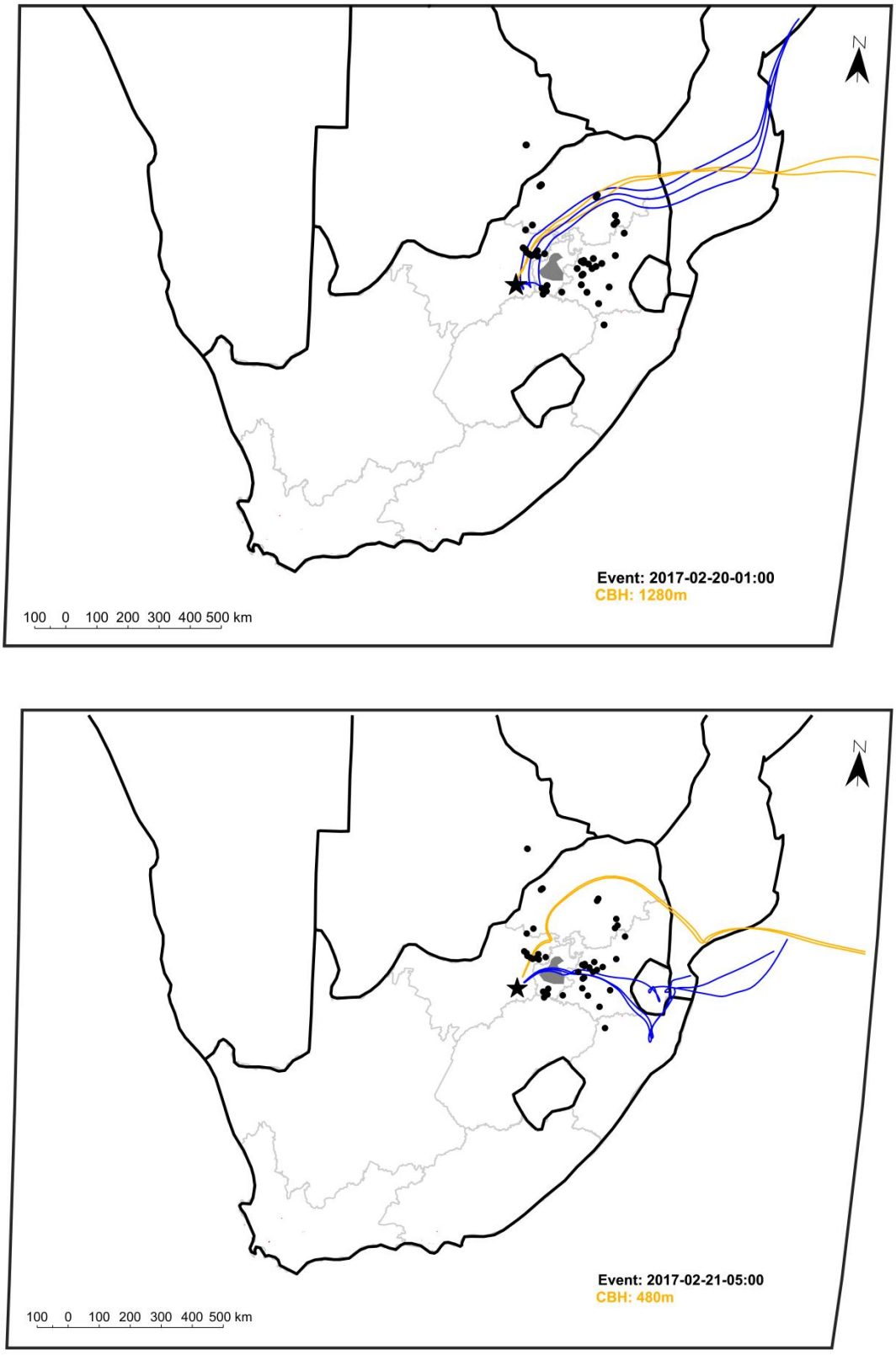

Figure 6.3 The back trajectories at CBH and 100 m a.g.l. for the events on 20 February 2017 (top) and 21 February 2017 (bottom), indicating effective below-cloud scavenging of pollutants.

The influence of the effective below-cloud scavenging of pollutants is also illustrated by two successive rain events on 4 and 5 September 2015. The event on 5 September 2015 had remarkably lower ionic concentrations than the event on the previous day, especially for concentrations of SO_4^{2-}, NO_3^- and NH_4^+ (Table 6.4). This is quite notable when considering the trajectories in Figure 6.4, which show very similar air mass histories for both events at both arrival heights. Both these trajectory maps show movement along the anticyclonic recirculation pattern with distinct movement over the pollution point sources and dense population areas, especially for the 100 m arrival height. Some biomass burning is evident along the CBH trajectory path, which possibly contributes to the total OA concentration. The event on 5 September had a very low average rain intensity, which can also decrease the scavenging efficiency and further explain the lower concentrations of this event (Section 6.5 and Chapter 2.3). This case study of successive rain events also presents examples of rain events that were grouped into different clusters according to chemical composition and CBH air mass history, while clustering according to air mass history at 100 m a.g.l. grouped these events together. This also signifies the complexity associated with factors influencing rain chemistry, and substantiates the suitability of the different statistical clustering approaches followed in this study.

Table 6.4 Rainwater ionic concentrations, rain depth and -intensity for the event on 4 September 2015 and a follow-up event on 5 September 2015.

	4 September 2015	**5 September 2015**
Rain depth (mm)	30	5
Max (avg) Intensity ($mm.h^{-1}$)	4.8 (2.1)	1.6 (0.9)
pH	4.43	4.50
SO_4^{2-}	1273	211
NO_3^-	502	147
NH_4^+	559	97
Ca^{2+}	419	119
Mg^{2+}	138	46
Na^+	117	173
Cl^-	166	173
K^+	51	89
tOA*	456	197

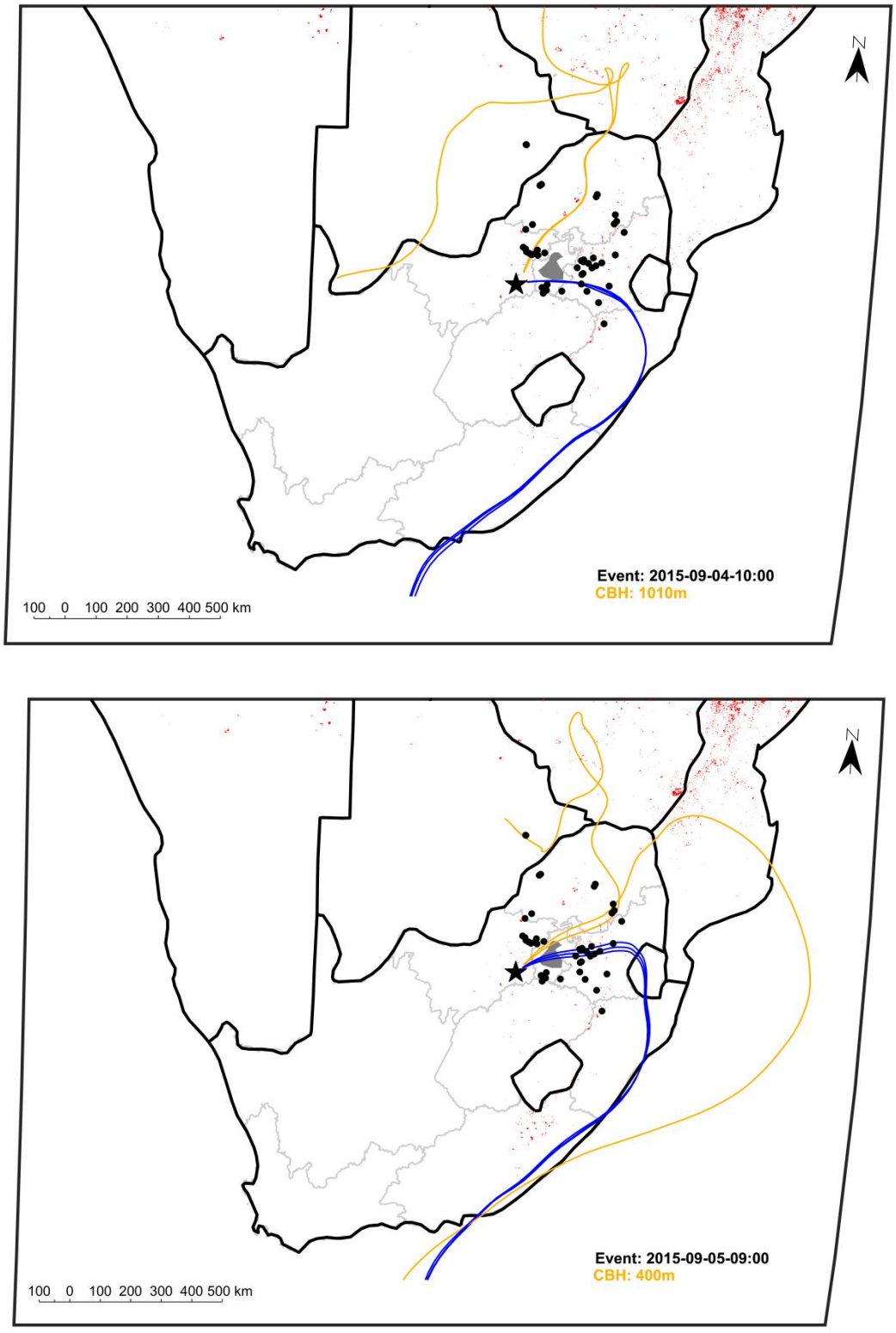

Figure 6.4 The CBH and 100 m a.g.l. back trajectories for the rain events on 4 September 2015 (top) and the day after on 5 September 2015 (bottom), indicating effective below-cloud scavenging of pollutants.

6.4 Rain Intensity

In the statistical analyses discussed in Chapter 5, it was found that the difference in rain intensity between the clusters was statistically significant with higher rain intensities relating to higher VWM concentrations (Chapter 5.2.1). The increased VWM associated with increased rain intensity was attributed to effective collision-coalescence more effectively removing coarser particulates (Engelmann, 1971; Galloway et al., 1993; Kulshrestha et al., 2009). The high aqueous solubility of SO_4^{2-} and NO_3^- have also been shown to contribute to a positive relationship between rain intensity and scavenging ratios (González and Aristizábal, 2012; Xu et al., 2017). Therefore, in this case study, the rain events that had the highest average and maximum rain intensities are compared to the rain event with the lowest rain intensity. In Table 6.5, the VWM concentrations of ionic species in the rain event that recorded the highest maximum rain intensity (7 January 2015), as well as the rain events with the highest (28 February 2016) and lowest (5 September 2015 and 18 December 2014) average rain intensities during the sampling campaign are presented.

Table 6.5 Rainwater ionic concentrations, rain depth and -intensity associated with the rain events with the highest maximum intensity (7 January 2015), as well as the rain events with the highest average intensity (28 February 2016) and lowest average intensity (18 December 2014 and 5 September 2016).

	7 January 2015	28 February 2016	18 December 2014	5 September 2015
Rain depth (mm)	70	30	5	5
Max (avg) Intensity ($mm.h^{-1}$)	92 (12.8)	66.4 (20.5)	1.6 (0.9)	1.6 (0.9)
pH	4.20	4.37	4.08	4.50
SO_4^{2-}	5285	2449	767	211
NO_3^-	2453	1173	503	147
NH_4^+	2442	1570	409	97
Ca^{2+}	1221	770	325	119
Mg^{2+}	442	187	112	46
Na^+	1670	481	490	173
Cl^-	1439	536	389	173
K^+	510	154	304	89
tOA*	17	221	14	93

It is evident that the rain events associated with higher rain intensities had significantly higher loadings of ionic species compared to the events related to lower rain intensities. The rain event with the highest maximum rain intensity recorded also had the highest measured rainfall depth of all rain events collected during this study. Walker and Tsubo (2003) found the rainfall intensity and rain depth to peak in the wet season with shorter event durations at different sites in South Africa. Furthermore, it is also apparent that air masses passed over the anthropogenic eastern source region prior to each of these rain events. Therefore, observed differences in chemical composition of rain cannot be attributed to different air mass histories (Figure 6.5). The overall ionic concentration of the maximum intensity event on 7 January 2015 was high, with an acidic pH. Both the events with the highest maximum and highest average rain intensities were associated with tropical-temperate surface trough conditions (Appendix C). Strong convective rainfall over the Highveld often associated with high rain intensity, large rain depths, hail and thunderstorms has been related to increased scavenging (Wallace et al., 2006; Chate, 2011; Hart et al., 2013; Zhao et al., 2015; Mogale and Dyson, 2017). The movement of both arrival height trajectories over the pollution point sources, along with the high rainfall intensity, could contribute to the high concentrations of this event. The OAs of this event were low in comparison to the other ions, which can be ascribed to the absence of open biomass burning during January (Figure 4.4, Chapter 4.2.2.5). Similarly, the effect of rainfall intensity on the below-cloud scavenging can be seen in the events with the highest and lowest average intensity (28 February 2016, and 18 December 2014 and 5 September 2015, respectively). Even though in both the highest and lowest intensity events the 100 m a.g.l. back trajectories move in from the east/northeast over the pollution source regions, the difference in ionic concentrations is significant. The concentrations for the event on 5 September 2016 were less than the event on 18 December 2014, possibly due to the scavenging of a rainfall event on the previous day (Section 6.3).

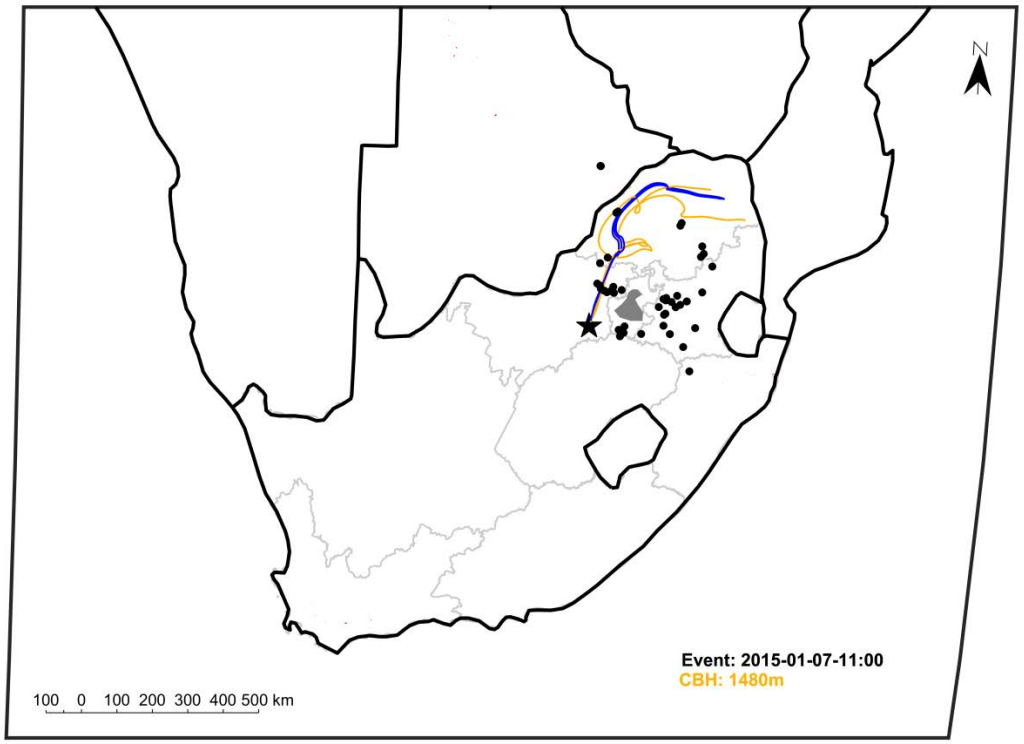

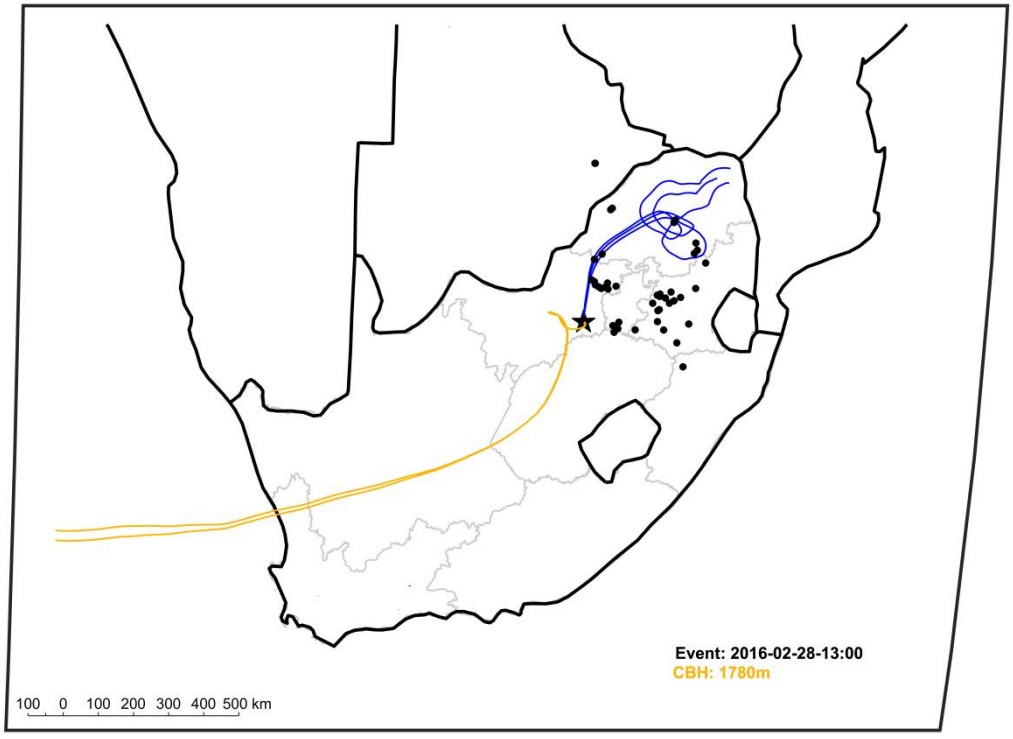

Figure 6.5(a) Back trajectories at CBH and 100 m a.g.l. for rain events with the highest maximum and highest average rainfall intensity on 7 January 2015 (top) and 28 February 2016 (bottom), respectively.

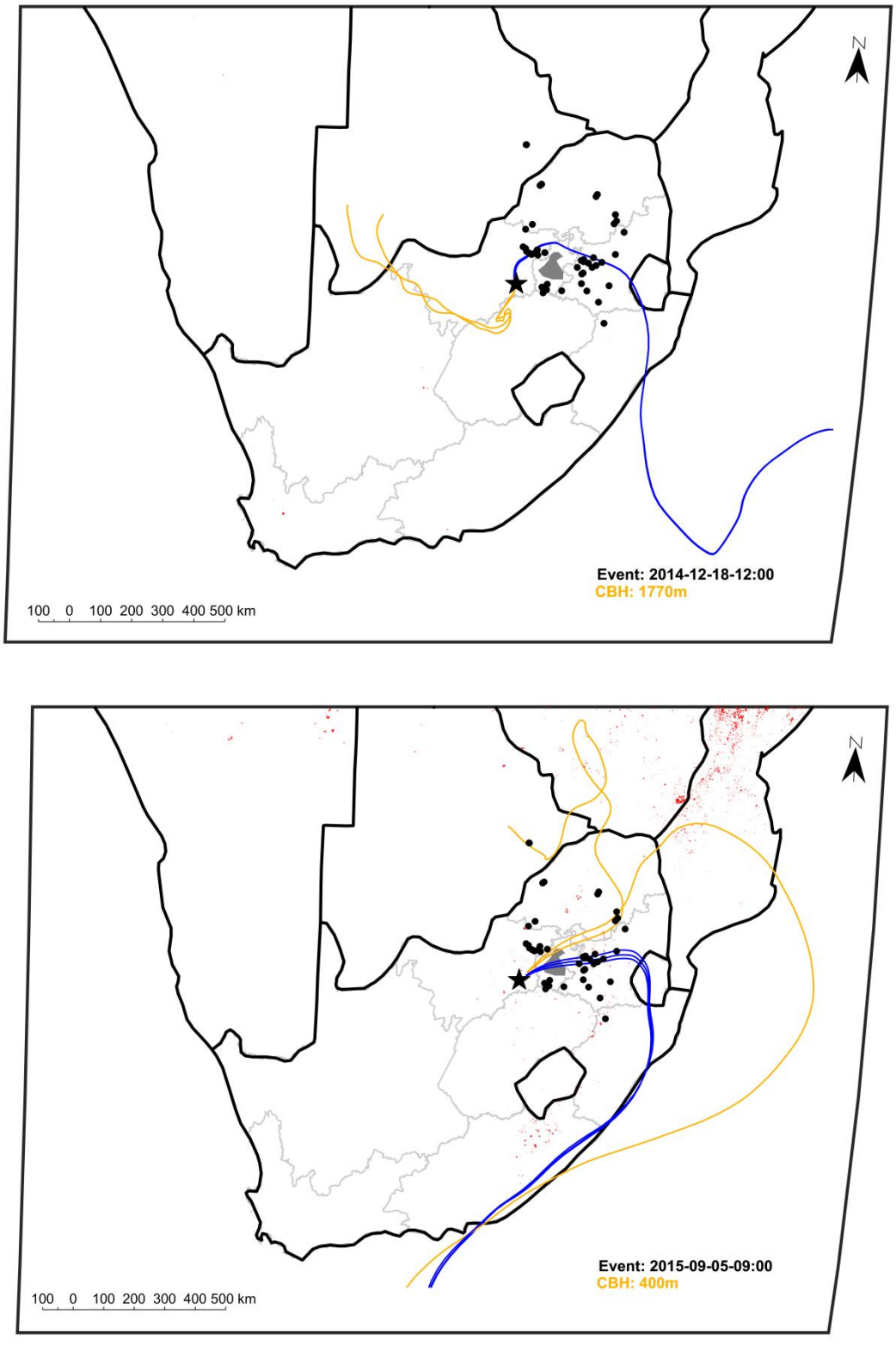

Figure 6.5(b) Back trajectories at CBH and 100 m a.g.l. for rain events with the lowest average rainfall intensity on 18 December 2014 (top) and 5 September 2015 (bottom).

6.5 Atmospheric Pollutant Build-up

South Africa is prone to experience low-level inversion layers during the winter months, which trap aerosols and pollutants over the continent, preventing dispersion and mixing with the upper troposphere (Chapter 2.8) (Harrison, 1984; Freiman and Tyson, 2000). This results in a build-up of species in the lower troposphere that can often be seen as smog, particularly over populated areas. In conjunction with the anticyclonic recirculation of air masses due to a persistent high pressure system over the interior of southern Africa, the chemical species concentration in the atmosphere increases (Garstang et al., 1996; Laakso et al., 2012; Tiitta et al., 2014; Tyson and Preston-Whyte, 2017). In addition, increased household combustion for space heating and open biomass burning also contribute to emissions of atmospheric pollutants (Chapter 4.2) (Forbes, 2012; Kulmala et al., 2013; Chafe et al., 2014). Winter rainfall, although rare over the Highveld, can therefore have greater scavenging efficiencies as the particle size and distribution become increasingly favourable for scavenging (Chapter 2.5 and 2.8) (Tyson and Preston-Whyte, 2017). The effective scrubbing action of rainfall can be seen in the higher pollutant load in the two winter rainfall events that occurred on 13 June and 24 July 2016 (Table 6.6 and Figure 6.6).

Table 6.6 Rainwater ionic concentrations, rain depth and -intensity associated with two rain events in winter in 2016.

	13 June 2016	**24 July 2016**
Rain depth (mm)	10	55
Max (avg) Intensity ($mm.h^{-1}$)	8.8 (3.0)	23.2 (4.8)
pH	5.09	4.90
SO_4^{2-}	338	2931
NO_3^-	152	1672
NH_4^+	121	2168
Ca^{2+}	366	3112
Mg^{2+}	111	1137
Na^+	169	1518
Cl^-	171	1667
K^+	42	670
tOA*	184	2470

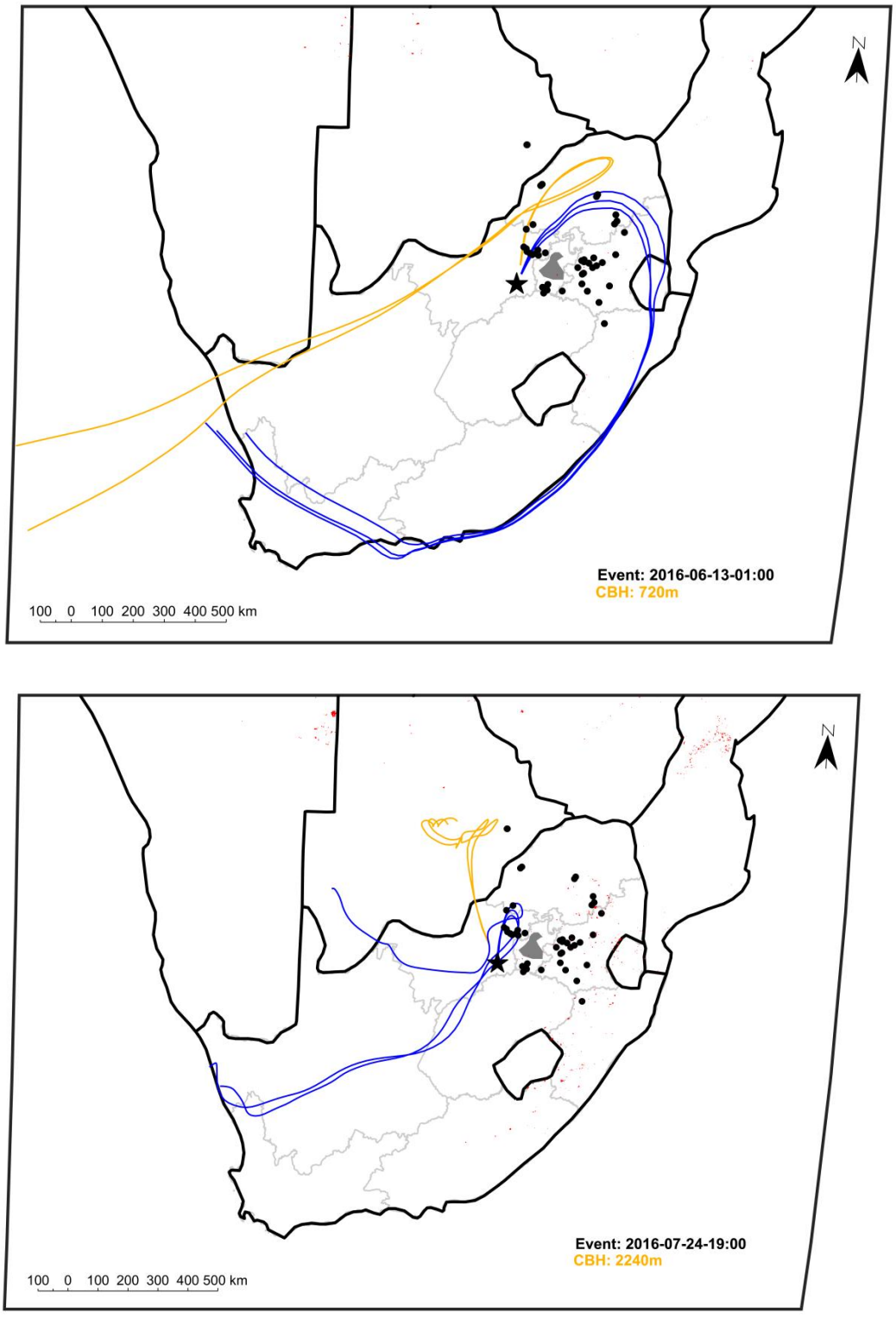

Figure 6.6 Back trajectories at CBH and 100 m a.g.l. for rain events occurring in the South African winter on 13 June 2016 (top) and 24 July 2016 (bottom), showcasing the scavenging efficiency when atmospheric build-up has occurred.

It is evident that, although the 100 m a.g.l. trajectories spent some time over the point sources, the back trajectories appear to mostly move over the ocean and from the cleaner sector to the west for the first event. The high ionic loadings in the rainwater indicate the efficiency of the rain in cleaning the atmospheric build-up through effective scavenging and wet deposition. Another example indicating the influence of pollutant build-up during winter is presented in a previous case study (Section 6.2) for the rain event occurring on 4 September 2015, which was the first rain event at Welgegund after winter and thus had relatively high concentrations of ionic species. Lower concentrations of ionic species in this rain event compared to the event in July can be attributed to less pronounced inversion layers and more turbulent conditions prevailing with heating of the surface in September (Tyson and Preston-Whyte, 2017).

6.6 Open Biomass Burning

In Chapter 4.2.2.5, it was indicated that the influence of open biomass burning on the chemical composition of rainwater was less pronounced due to the open biomass burning season not corresponding with the wet season in this part of South Africa. Piketh et al. (1999) also indicated that biomass burning contribution to the aerosol loading of the background air over South Africa was minimal. The interior of South Africa is characterised by distinct wet and dry seasons, with the dry season occurring from May to mid-October, while the open biomass burning season is typically from June to mid-October (Harrison, 1986; Roberts et al., 2009). However, a case study is presented in order to show the possible influence of open biomass burning on rain chemistry.

Open biomass burning is generally associated with emissions of OAs, while it can also be related to Cl^- and K^+ (Helas and Pienaar, 1996; Galy-Lacaux et al., 2009). In Figure 6.7, the air mass histories associated with two rain events that occurred during the peak burning season on 20 and 22 September 2015 are presented, which indicate air masses passing over open biomass burning prior to these rain events. It is evident from the ionic concentrations determined for these two rain events, presented in Table 6.7, that air masses passing over open biomass burning contributed to increased levels of OAs, Cl^- and K^+ in rainwater. Elevated Cl^- levels from biomass burning are also supported by the Cl^- concentrations being higher than Na^+ levels, since concentrations of Na^+ and Cl^- are mostly similar in rain collected in this part of South Africa (Chapter 4.2.2.2) (Conradie et al., 2016). Air masses at both arrival heights moved within proximity of open biomass burning. Burning vegetation matter emits around 10^{12}-10^{15} CCN per kg material burned (Wallace and Hobbs, 2006b). It is also evident from the air mass histories associated with these two rain events that, when long-range transport of air masses passes over distant fires that do not occur during the open biomass burning season in South Africa, the emissions can have an impact on rainwater chemistry in this region. The NO_3^- concentrations in these events were notably high, which could also be attributed to biomass burning (Chan et al., 2005; Laskin et al., 2009; Ren and Zhao, 2012).

Table 6.7 Rainwater ionic concentrations, rain depth and intensity associated with two rain events during the peak open biomass burning season.

	20 September 2015	21 September 2015
Rain depth (mm)	11	13
Max (avg) Intensity ($mm.h^{-1}$)	5.2 (2.0)	10.4 (4.6)
pH	4.49	4.51
SO_4^{2-}	513	583
NO_3^-	905	1049
NH_4^+	1108	1280
Ca^{2+}	424	452.5
Mg^{2+}	180	196
Na^+	630	680
Cl^-	913	1018
K^+	457	501
tOA*	548	594

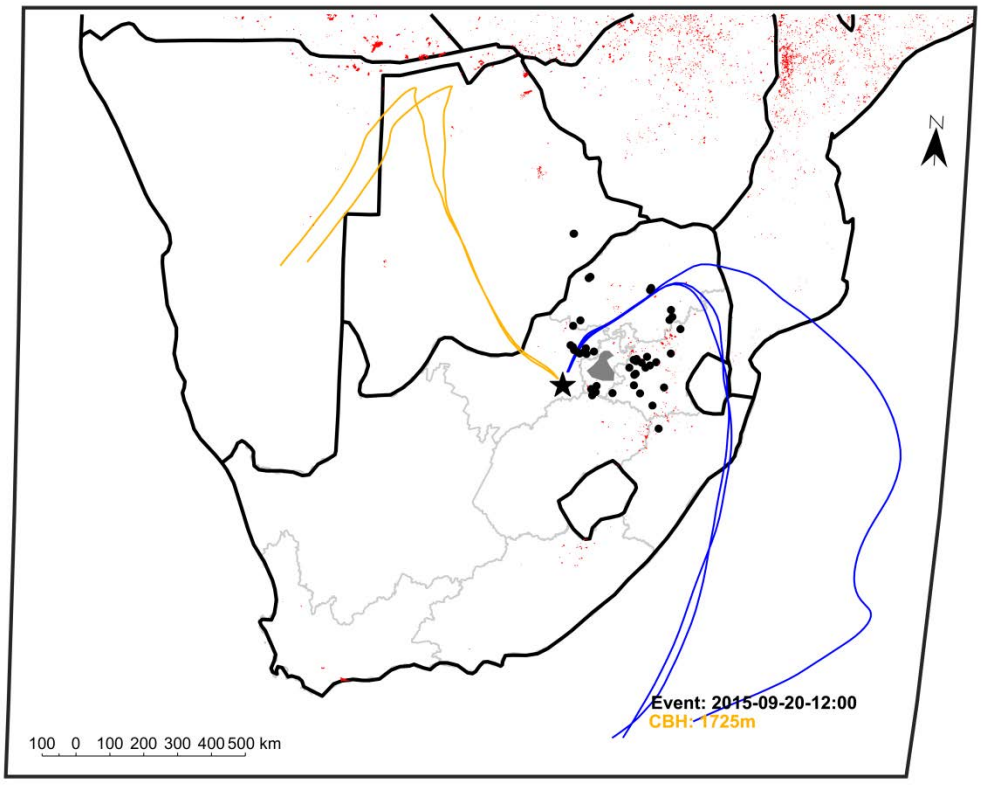

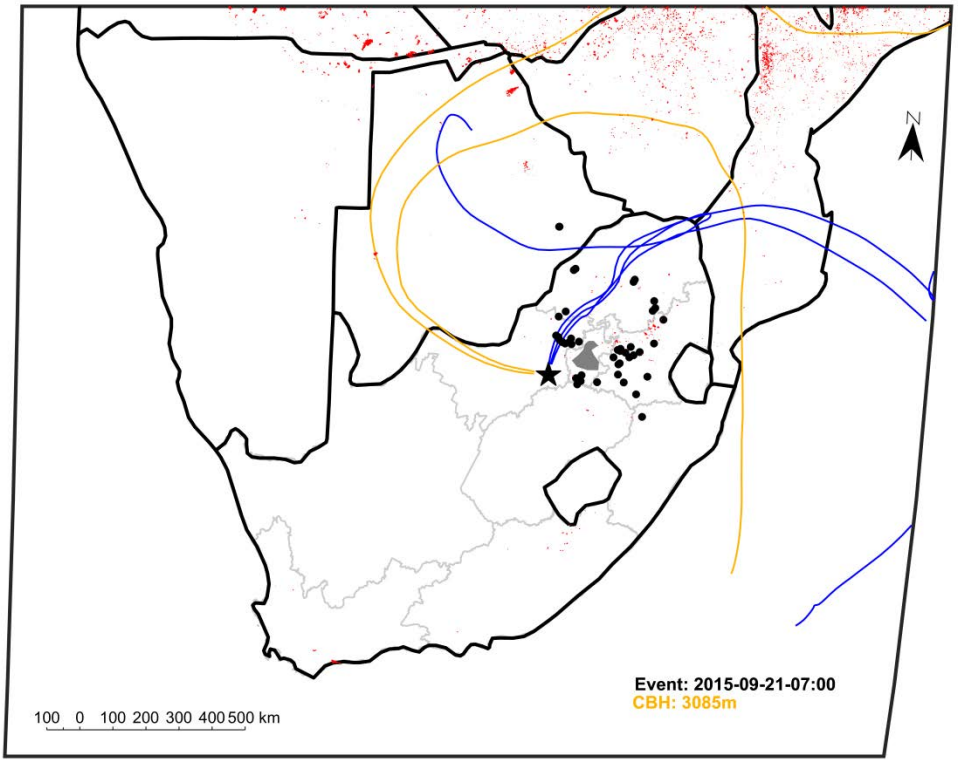

Figure 6.7 Back trajectories at CBH and 100 m a.g.l. for rain events corresponding to open biomass burning on 20 September 2015 (top) and 22 September 2015 (bottom).

6.7 Summary & Conclusion

The statistical analyses in Chapter 5 proved insightful in determining certain relationships between the rainwater chemistry, the air mass history and the ambient measurements. However, certain phenomena in the rainwater chemistry could not be clearly defined by statistical methods, as reported in Chapter 5 only. These exceptions and events related to effects determined in Chapter 5 were explored in this chapter as case studies. In addition, these case studies explored how rain events that were grouped in the same clusters could be related to different chemical compositions or air mass history. The influence of the anthropogenic source region on rainwater chemistry at Welgegund, as determined in Chapters 4 and 5, was confirmed. The influence of below-cloud scavenging on rain chemistry at Welgegund was highlighted by investigating the chemical composition of successive rain events associated with similar air mass histories. A case study also revealed the impact of pollution build-up due to strong low-level inversion layers that can result in higher loading of ionic species in rainwater that is not explicitly related to the air mass history alone. In addition, the relationship between higher ionic concentrations and higher rain intensity, as suggested by statistical analyses, was also supported by case studies comparing the rain events with the maximum and highest average rain intensities to the rain events with the lowest average rain intensity. Finally, although the open biomass burning and wet seasons in South Africa generally do not coincide, the impact of open biomass burning was also indicated, while it was also suggested that long-range transport of species associated with open biomass burning could influence rain chemistry in the South African interior. The case studies reveal the advantages of CBH measurements and sampling of rainwater at a comprehensively equipped site in order to relate air mass histories to the variability of rainwater chemistry. The case studies again reflect the complexity of the atmospheric equilibrium maintained through deposition processes and the necessity of understanding the factors influencing the rainwater chemistry.

Chapter 7

Project Evaluation

In this concluding chapter, the main findings presented in the three results chapters are reviewed in light of the objectives of this study stated in Chapter 1. The successes and limitations of this study are evaluated, followed by future perspectives and recommendations stemming from this study.

7.1 Assessment of Study

The aim of this study was to identify and determine the influence of large scale factors governing the chemical composition of rainwater and wet deposition at a regional background site in South Africa. A novel technique for relating rain chemistry to air mass history was explored in this study. The general aim of this study was successfully achieved through the specific objectives indicated in Chapter 1. Below, the study is assessed in view of each of these objectives.

1. Determine the chemical composition of rainwater, as well as sulfur- (S) and nitrogen (N) wet deposition fluxes at the Welgegund atmospheric monitoring station over the period of three rain seasons, while also relating wet deposition chemistry at Welgegund to the other South African sites where wet deposition studies were conducted.

This objective was met by determining the chemical composition of rainwater and related wet deposition fluxes for 119 rain samples successfully collected at Welgegund from December 2014 to April 2018. 89% of all rains samples collected passed the data quality objectives (DQO) of the World Meteorological Organisation (WMO), which well exceeded the WMO percentage total precipitation (%TP) acceptance range, i.e. %TP ≥ 70% (WMO, 2004). Sulfate (SO_4^{2-}) and nitrate (NO_3^-) were determined to be the major chemical components in rainwater at Welgegund, with S and N wet deposition determined to be 4.38 S kg.ha^{-1}.y^{-1} and 4.48 N kg.ha^{-1}.y^{-1}, respectively. In comparison to the four other South African sites operated within the Deposition of Biogeochemically Important Traces Species (DEBITS) network, SO_4^{2-} dominated rainwater chemistry at Welgegund, with volume weighted mean (VWM) concentrations of SO_4^{2-} being in the same order as the VWM levels thereof determined at two sites within proximity of industrial activities in the Mpumalanga Highveld and the Vaal Triangle. NO_3^-, the second most abundant

species in rain at Welgegund, also had levels comparable to the industrially influenced sites. S- and N deposition were, however, lower at Welgegund than at the two industrially influences sites due to lower average annual rainfall depths at Welgegund (Conradie et al., 2016). Rainwater was determined to be acidic with an average pH of 4.80, which compared to the pH of rain at the two rural background sites. The relatively higher pH of rain at Welgegund compared to the two industrially influences sites can be attributed to increased neutralisation mainly due to increased levels of Ca^{2+} and aged air masses impacting Welgegund. Seasonal variability in the chemical composition of rainwater could also be related to changes in meteorological conditions and source strengths. It was also successfully indicated that open biomass burning did not significantly influence rain chemistry at Welgegund, which was attributed to peak open biomass burning season not corresponding to the wet season in this region. Rain at Welgegund was successfully contextualised with other sites in South Africa where wet deposition studies were previously conducted (Conradie et al., 2016, Mphepya et al., 2004, 2006), while Welgegund was also successfully positioned as a future site to study wet deposition within the newly formed International Network to study Deposition and Atmospheric composition in Africa (INDAAF) network.

2. Determine the major sources of ionic species at Welgegund through empirical and explorative statistical methods

Spearman correlations and principal component analyses revealed correlations between certain ionic species that are related to specific emission sources. Sources identified with explorative statistical analyses included anthropogenic (industrial)-, marine-, crustal-, agricultural- and biomass burning sources, while empirical calculations (Keene et al., 1986) were successfully employed to estimate source contributions. Anthropogenic sources were estimated to have the largest influence on rain chemistry at Welgegund, which was ascribed to the regional influence of large point sources in the north-eastern South African interior and the aging of air masses through the anticyclonic recirculation over the interior. The large influence from crustal sources compared to the other South African sites could be attributed to air mass movement over the arid region to the west of Welgegund, which included the Karoo and Kalahari. Influence from air masses moving over the oceans bordering South Africa was also substantial. A relatively small contribution was determined from open biomass burning contribution, which was ascribed to the wet season not coinciding with the open biomass burning season as mentioned above. In general, the contribution of different sources on chemical composition at Welgegund was similar to the source contributions estimated for the two industrially influenced sites in South Africa (Conradie et al., 2016, Mphepya, 2004, 2006). Although explorative statistical analyses and empirical calculations were useful to determine source contributions to the chemical composition of rain at Welgegund, limitations

associated with these methods are recognised (Conradie et al., 2016, Mphepya et al., 2004, 2006). Therefore, in an effort to further explore the influences of different sources on rain chemistry at Welgegund, cloud-base height measurements were combined with rain chemistry monitoring in order to relate air mass history to the chemical composition of rain.

3. Develop a novel method to relate below-cloud air mass history and air mass history associated with precipitating clouds to the rainwater chemistry at Welgegund.

Although back trajectory analyses are commonly used in atmospheric chemistry studies to associate the chemical composition of the atmosphere to the influence of sources, several uncertainties are associated with air mass history at cloud height during a precipitation event. Therefore, in this study a novel method was developed to relate air mass history with the chemical composition of rain. This method employed ceilometer measurements conducted at Welgegund to determine cloud base height at the exact time a rain event occurred, while the time at which a rain event started was determined with rain intensity meters. This method enabled calculation of back trajectories at cloud base height (CBH) in order to determine the influence of air mass history associated with the precipitating cloud. Back trajectories were also determined at an arrival height of 100 m above ground level (a.g.l.) in order to establish the influence of below-cloud scavenging.

4. Conduct an advanced assessment of large scale factors influencing chemical composition of rain in the South African interior by relating individual rain events to *in situ* measurements conducted at Welgegund and to air mass history associated with precipitating clouds (CBH) and with the below-cloud air masses (100 m a.g.l.) through statistical clustering analyses; and determine whether using crude back trajectories is a viable method to relate air mass history to the variability in rainwater chemistry.

The novel method developed to relate air mass histories to rain chemistry was successfully subjected to advanced statistical analyses. Hierarchical clustering analyses (HCA) was performed in order to relate rainwater chemistry to air mass history and the ancillary measurements following two approaches, i.e. (1) clustering based on the chemical composition of rainwater, and (2) clustering according to the air mass history at 100 m a.g.l. and at CBH. Air mass history was related to predefined source regions, which included a relatively clean western sector, two anthropogenic source regions to the east and oceanic regions.

Clustering according to chemical composition resulted in a three cluster solution that grouped rain events according to low, medium and high volume weighted mean (VWM) concentrations. High VWM concentrations of chemical compounds were associated with air masses arriving at

100 m a.g.l. that had passed over the anthropogenic source regions. The statistical analyses revealed statistically significant covariance of higher rainwater VWM concentrations to pH and SO_2 concentrations. Although other pollutant concentrations showed some correlation to the rainwater composition, it is noteworthy that nitrogen oxides (NO_x), PM_{10}, equivalent black carbon (eBC), ozone (O_3) and carbon monoxide (CO) concentrations did not show statistically significant covariance with rainwater chemistry. A significant positive correlation between rain intensity and rainwater chemistry was determined through possible increased scavenging efficiency of species, such as SO_4^{2-}, through higher intensity rain events (Hall, 2003; Bae et al., 2006; Kulshrestha et al., 2009; Karev et al., 2010; González and Aristizábal, 2012). Air mass histories at 100 m a.g.l. could be related the rainwater chemistry in this approach.

In the second clustering approach, residence time of air masses over different source regions for air mass history at 100 m a.g.l. related to the variability in rainwater chemistry. The influence of anthropogenic activities, the clean western background sector and oceans was evident in the ionic composition. Clustering according to air mass history at CBH did not reveal particular correlations between air mass history and rainwater chemistry. Therefore, it seemed from statistical analyses of ionic composition and air mass history at CBH and 100 m a.g.l. that below-cloud scavenging played a more significant role than the microscale cloud processes in rain chemistry in this part of South Africa.

Inter-relation between the three-cluster solutions determined with the different approaches in this study confirmed the relationship between the ionic composition and air mass history at 100 m a.g.l. It is concluded that 96h-back trajectory analyses of the well-mixed boundary layer air masses presented nuances with the influence of the progression of synoptic patterns over southern Africa on air flow and are considered to provide a good method to estimate the synoptic scale effects, such as the anticyclonic recirculation, ageing of air masses, prominent inversion layers and pollution build-up, on the variability of rainwater chemistry.

Although statistical analyses were successfully employed in this study to relate chemical composition of rainwater to air mass history, they also highlighted the complexity associated with correlating rain chemistry to sources of chemical species. In addition, this study also indicated limitations associated with statistical analyses of the entire datasets. Therefore, the influences of different source regions, below-cloud scavenging, rain intensity and pollution build-up were further explored through specific case studies.

5. Relate the rainwater chemistry to rain event day synoptic patterns.

Rain events were grouped according to the main synoptic patterns associated with rain events at Welgegund in order to determine the influence of the type of convection on rain chemistry. Surface synoptic charts and infrared satellite images were used to categorize rain events into three groups, namely tropical-temperate surface trough conditions, surface trough conditions with a coastal low pressure, and surface trough conditions with temperate westerly wave disturbances. Events associated with coastal low pressures had the highest VWM, lowest total rainfall depth, and the highest average CO, O_3, eBC and PM_{10} concentrations. Westerly wave conditions were associated with rain events with the lowest VWM, lowest rain intensity, wind speed and PM_{10} concentrations and highest RH. Surface trough related events had the highest SO_4^{2-} concentration which was neutralised through the high concentrations of Ca^{2+} and NH_4^+. These events were also related to the highest rainfall intensities, wind speed, rainfall depth and measured EC, and SO_2 and NO_x concentrations.

In these groups it was evident that the type of uplift and rainfall could influence the rainwater chemistry. Events associated with strong uplift and high rainfall intensity had increased VWM concentrations possibly due to higher scavenging efficiency, however, these events also had the largest rainfall depth effectively diluting the rainwater concentrations. Westerly wave disturbances, with low rainfall intensities, high relative humidity and low rainfall depth had the lowest VWM concentrations. Although the type of convection can be associated with the statistically significant meteorological variables such as pressure, RH, wind speed, temperature, difference in average CBH and rain intensity as determined in the HCA approaches, there are large uncertainties to the mesoscale effects on rainwater chemistry. These include feedback effects, inflow and outflow related to the cloud, the position of convection, and interactions with other storm systems and different environments that could not be determined in the scope of this study. It was concluded that the relationship between the synoptic progression and rainwater chemistry can be better described through the use of back trajectory analyses.

6. Perform specific case studies of rain events in order to further assess the influence of air mass history at cloud base height (in-cloud scavenging) and below clouds (below-cloud scavenging) on rain chemistry.

Case studies were conducted in order to support statistical clustering analyses and also further investigate the influence of factors not clearly revealed through statistical analyses. The influence of the anthropogenic source regions on chemical composition of rainwater was substantiated. The role of below-cloud scavenging on rain chemistry could also be supported in case studies for successive rain events. Case studies also presenting the effect of below-cloud scavenging were

performed for rain events during the dry, winter months when pollution build-up is enhanced through factors relating to the synoptic scale such as prominent low-level inversion layers and ageing of air masses through anticyclonic recirculation. Events with air mass history at both heights arriving from different regions were compared. A comparison was also made between rain events with air masses at both heights arriving from the relatively clean sector and from the eastern anthropogenic source regions and from opposing directions. The relationship between rain intensity and ionic concentrations were further explored by presenting case studies on the events with the highest maximum and average rain intensity compared to the events with the lowest average rain intensity. The influence of long-range transport of air masses passing over open biomass burning was evident in two case studies. Back trajectory analyses were again confirmed to provide a useful method in determining the effect and to some degree the extent of the influence of air mass history at different arrival heights on the variability in rainwater chemistry.

7. Final project assessment remark

The advanced statistical analysis conducted in this study in conjunction with the case studies presented, clearly indicate the advantages associated with the novel method developed in this study to relate rain chemistry with air mass history through determining cloud base height associated with rain events. In addition, the value of performing rain monitoring at a comprehensively equipped atmospheric measurement site is also highlighted. This study clearly shows the benefit of including Welgegund as a ~~–s~~upersite" in the INDAAF network focussing on deposition studies.

7.2 Other Project Limitations

Certain rain events were associated with local and regional power outages due to high intensity thunderstorms that are common over the Highveld (Hart et al., 2010; 2013; Tyson and Preston-Whyte, 2017). Notwithstanding this limitation, data coverage of ~90% of rain events can be considered excellent. In addition, the Welgegund monitoring station is also subject to typical failures of instrumentation associated with operating such a comprehensive monitoring station. Some uncertainty to the rain intensity measurements were assumed, such as wind induced loss of precipitation volume, however, measurements from two instruments correlated well and were combined in this study. Some uncertainties can also be associated with the exact CBH during the onset of a rain event due to certain assumptions made, such as only using the lowest CBH measured with the ceilometer. In most instances when multiple CBHs were measured, differences between the CBHs were small (Costa-Surós et al., 2013). Limitations were also encountered with

the availability of meteorological data in the GDAS database utilised for back trajectory calculations, although more than sufficient back trajectories could be calculated. In addition, the uncertainty associated with back trajectories, generally estimated to be between 15 to 30% (Stohl and Koffi, 1998; Stohl et al., 2002), was limited by compiling three back trajectories for each rain event. Surface synoptic charts were employed in assessing the synoptic pattern and type of convection on the rain event days. This was a possible method due to the highest measured CBH being below 5 km, which could still be considered to be in the boundary layer. However, classification of rain events according to synoptic charts and infrared satellite images was subjective. The mesoscale factors that could influence rainwater chemistry are numerous and complex and it was therefore not able to conclusively relate synoptic patterns directly to rainwater chemistry. These factors could include the position of convection in relation to the monitoring site, feedback effects of outflow and inflow of storm systems, interaction with secondary or other storm systems and wind shear. Although this study attempted to assess the effects of air mass history at the precipitating cloud base height, there are microscale and mesoscale factors associated with the cloud environments that could not be evaluated in this study.

7.3 Future Perspectives

In view of the major findings in this study, as well as successes and shortcomings described, the following future perspectives are suggested for continued research.

It is recommended that the spatial and temporal resolutions of wet deposition studies in southern Africa are increased. Comparison of rain chemistry at Welgegund with the other South African DEBITS sites indicated large differences between sites, which highlights the importance of regionally representative spatial information. The rain measurements at Welgegund also reflected large inter-annual variabilities in annual rainfall depths as observed at the other South African DEBITS sites, which also signifies the importance of continued long-term measurements of precipitation chemistry. The impacts of regional and global changes in meteorological patterns on the rain could be better quantified through long-term monitoring. Muthige et al. (2018) determined that global warming up to a critical threshold of 2^{o}C will decrease the frequency of tropical cyclones impacting South Africa. The decrease in tropical cyclones and tropical low pressures is predicted to be associated with decreased rainfall over the Limpopo River basin, which could also affect the rainfall over the Highveld. It is possible that less frequent rain events will result in more pollutant build-up in the South African atmosphere and increased concentrations in rainwater. Heavy grassland grazing activities reduce soil CH_4 uptake and nitrous oxide (N_2O) and CO_2 emissions in a relatively dry environment (<400 mm.yr^{-1}). Nitrogen processes in the soil are sensitive to moisture limitation, which is enhanced under heavy grazing in grassland areas. With a change in

precipitation frequency, depth and patterns, the interaction between grazing and precipitation will alter the grassland-soil greenhouse gas balance (Tang et al., 2019). Although Hg is not analysed in this study, some strong correlations have been found between SO_4^{2-}, NO_3^- and NH_4^+ to Hg in rainwater sampled in Nepal. The correlation in their study was attributed to biomass burning, fossil fuel and poor quality coal combustion sources (Tripathee et al., 2019), which are sources that influence Welgegund and other regions in South Africa. Continued long-term measurements of rain chemistry will also reflect general changes in atmospheric chemistry associated with fluctuations in anthropogenic activities and the impacts of mitigation strategies.

Although hierarchical clustering analysis was successfully employed in this study, it is also recommended that future studies consider other advanced statistical methods, such as positive matrix factorisation from which more accurately source contributions to the ionic composition could be determined. In addition, clustering air masses through methods as described by Pérez et al. (2017), for instance, could also improve clustering analysis. Other input parameters could also be considered in future studies such as satellite cloud height measurements (Costa-Surós et al., 2013), while upper atmospheric conditions could also be included.

Future studies could also consider to combine wet deposition studies with dry deposition, i.e. gaseous species and atmospheric aerosols at Welgegund, in order to determine total deposition of chemical species. At present, micrometeorological measurements of SO_2 and NO_2 are conducted at Welgegund from which accurate dry deposition velocities for these gases will be determined for the first time in South Africa. Furthermore, it is also recommended that intensive soil measurement and vegetation surveys are conducted at Welgegund in order to establish the buffering capacity and critical loads in this region. Without this information, the impact of atmospheric deposition on the environment cannot be completely and precisely quantified.

Appendix A

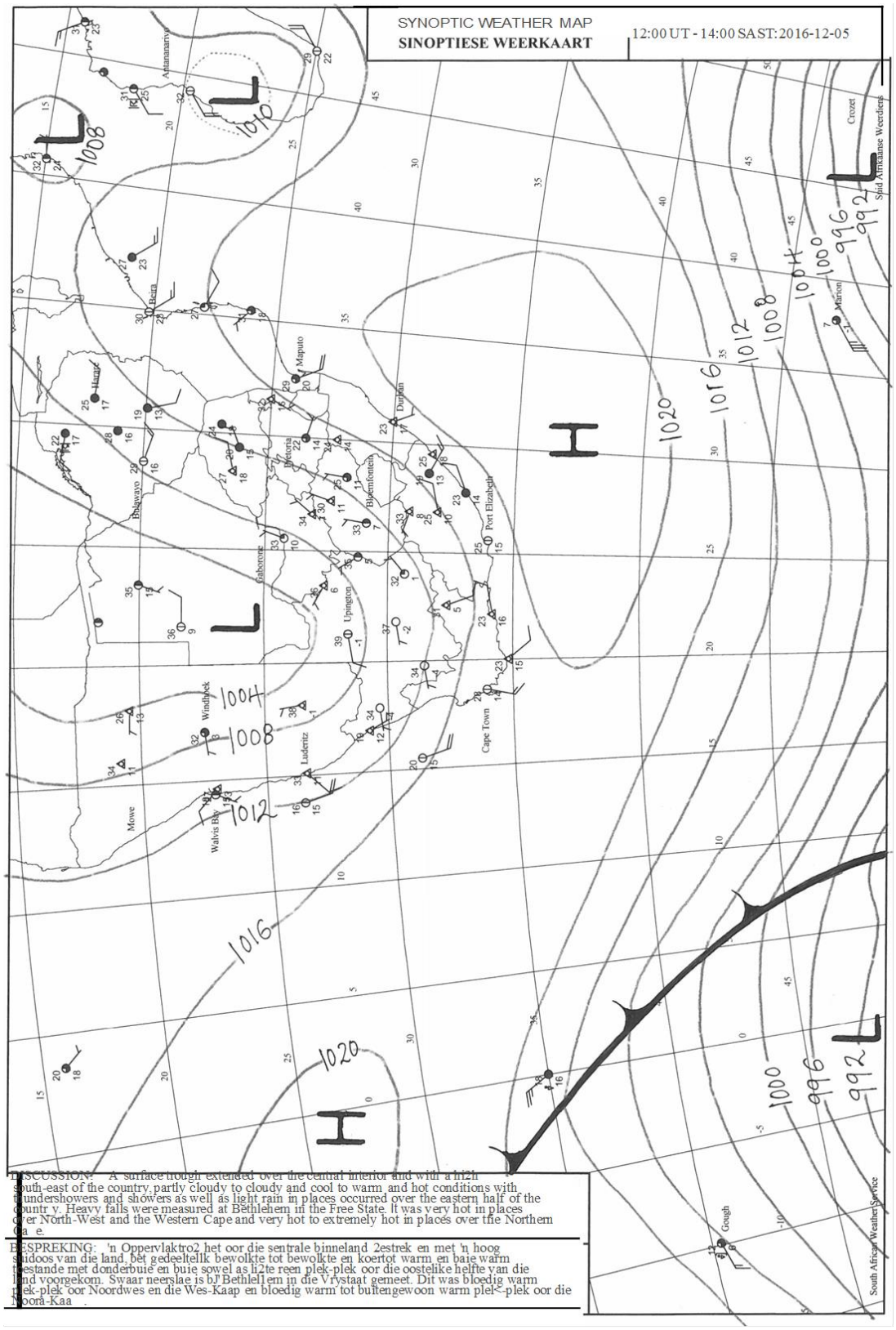

Figure A1(a) Example of a synoptic pattern for a rain event on 5 December 2016, grouped in the surface trough group in Chapter 5.4 (SAWS, 2019).

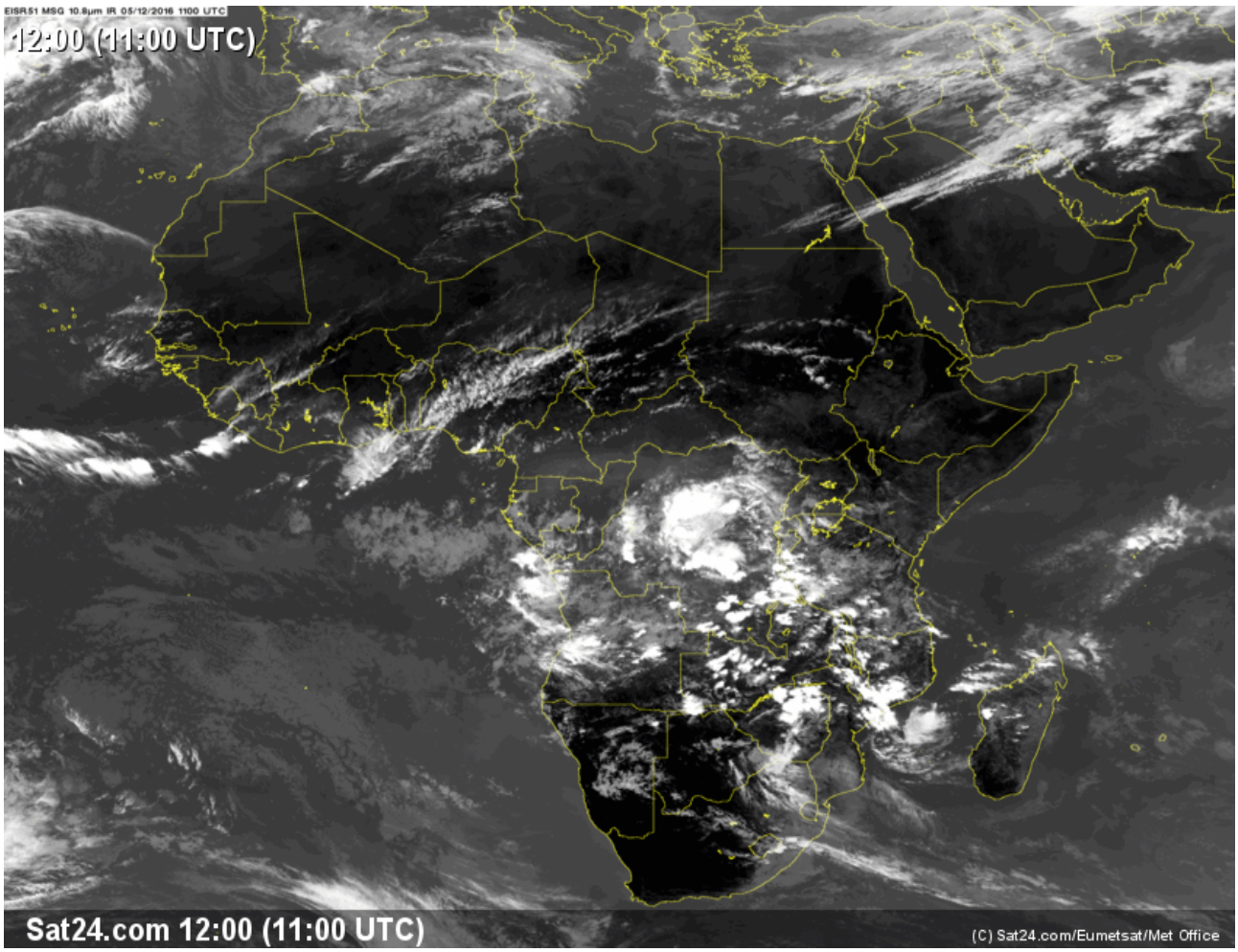

Figure A1(b) Example of an IR satellite image for a rain event on 5 December 2016, grouped in the surface trough group in Chapter 5.4 (EUMETSAT, 2019).

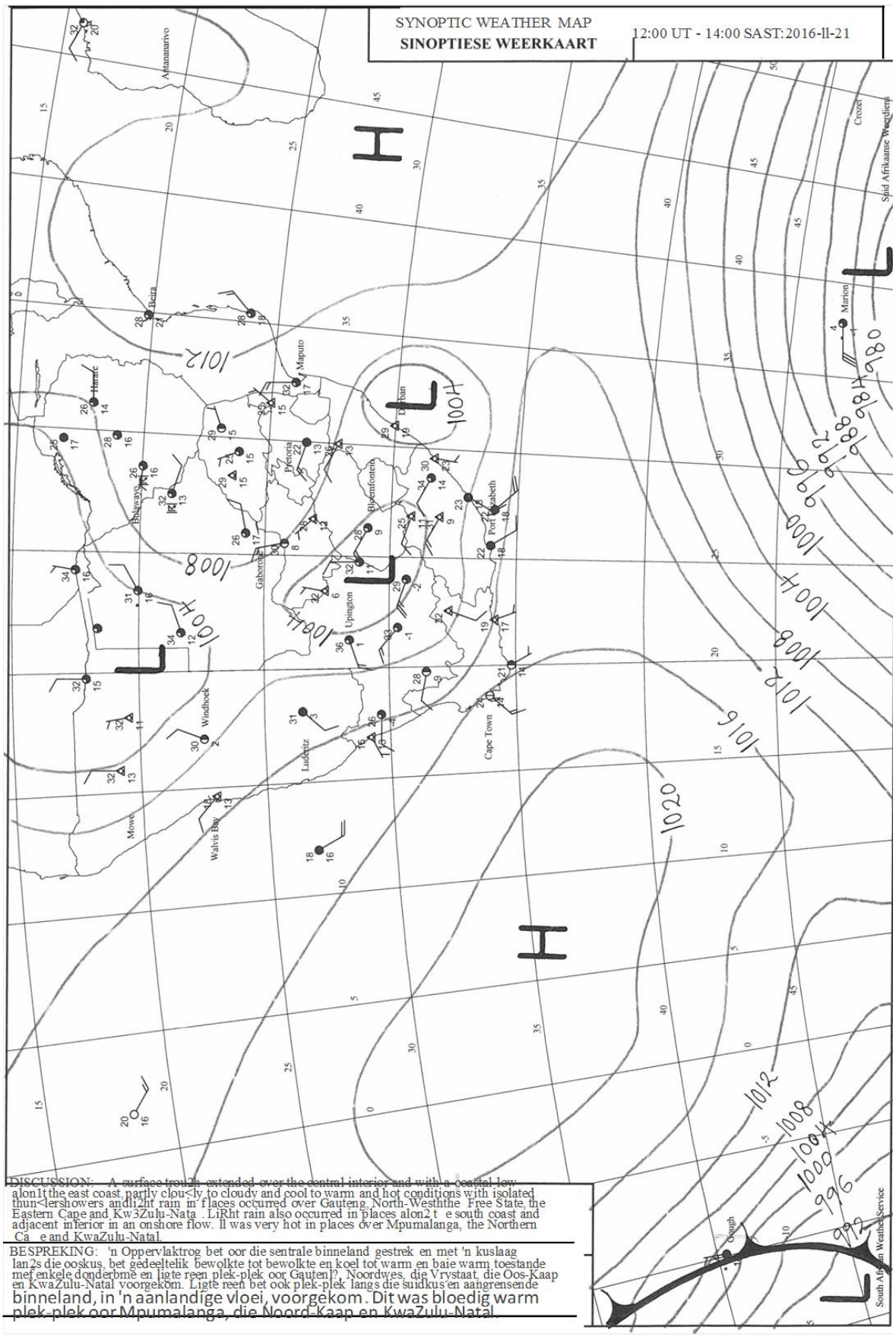

Figure A2(a) Example of a synoptic pattern for a rain event on 21 November 2016, grouped in the surface trough with a coastal low pressure group in Chapter 5.4 (SAWS, 2019).

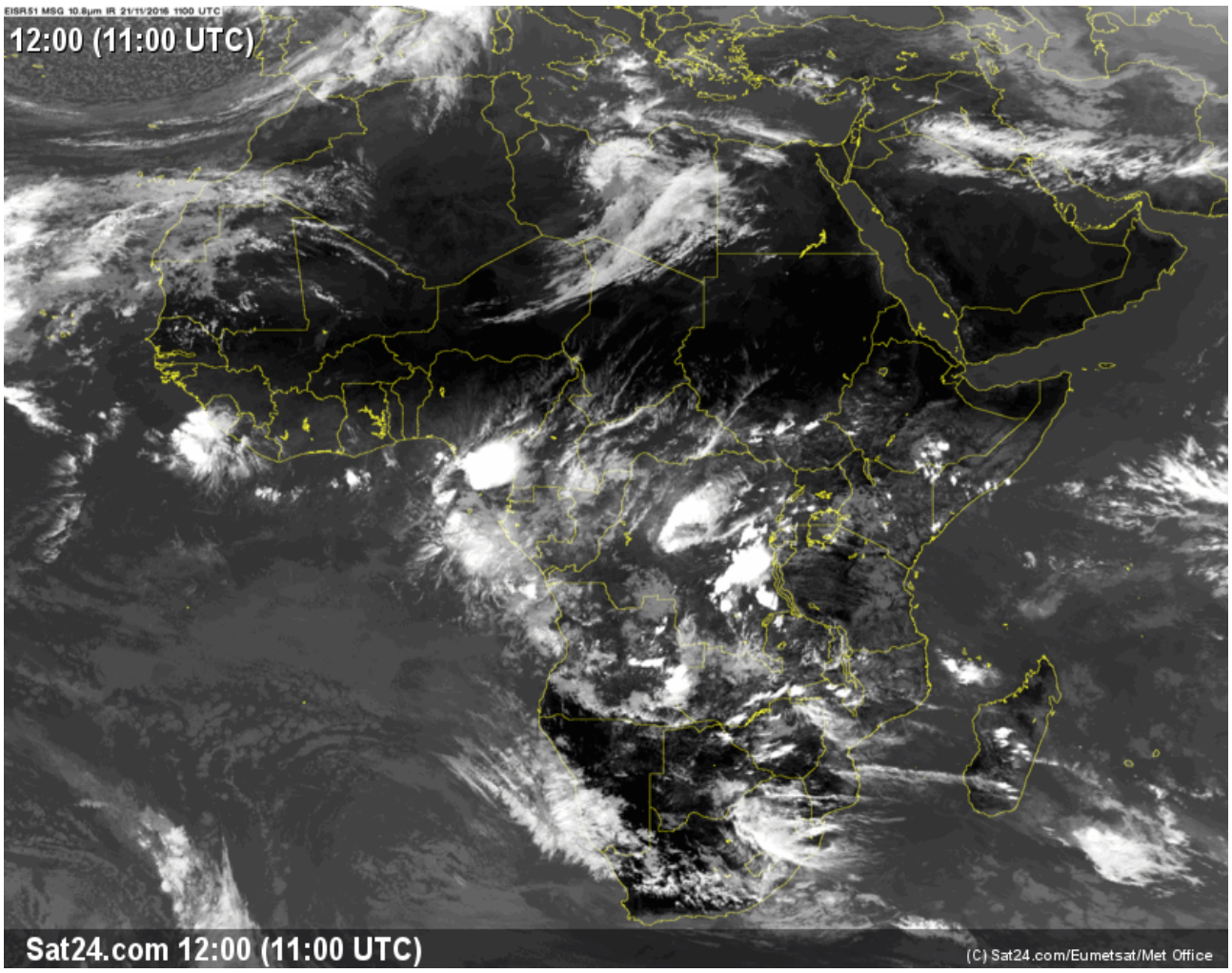

Figure A2(b) Example of an IR satellite image for a rain event on 21 November 2016, grouped in the surface trough with a coastal low pressure group in Chapter 5.4 (EUMETSAT, 2019).

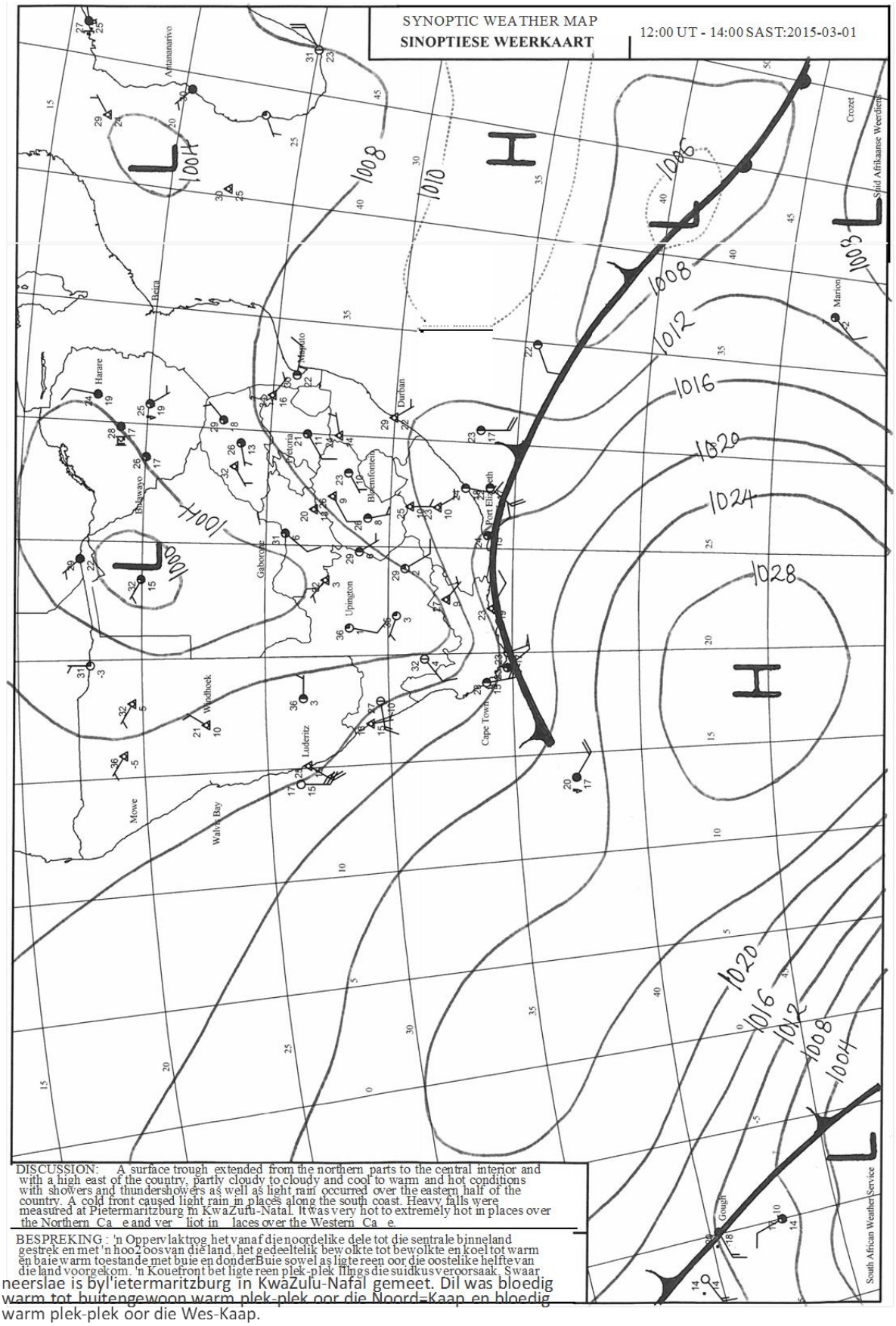

Figure A3(a) Example of a synoptic pattern for a rain event on 1 March 2015 grouped in the surface trough with a westerly wave group in Chapter 5.4 (SAWS, 2019).

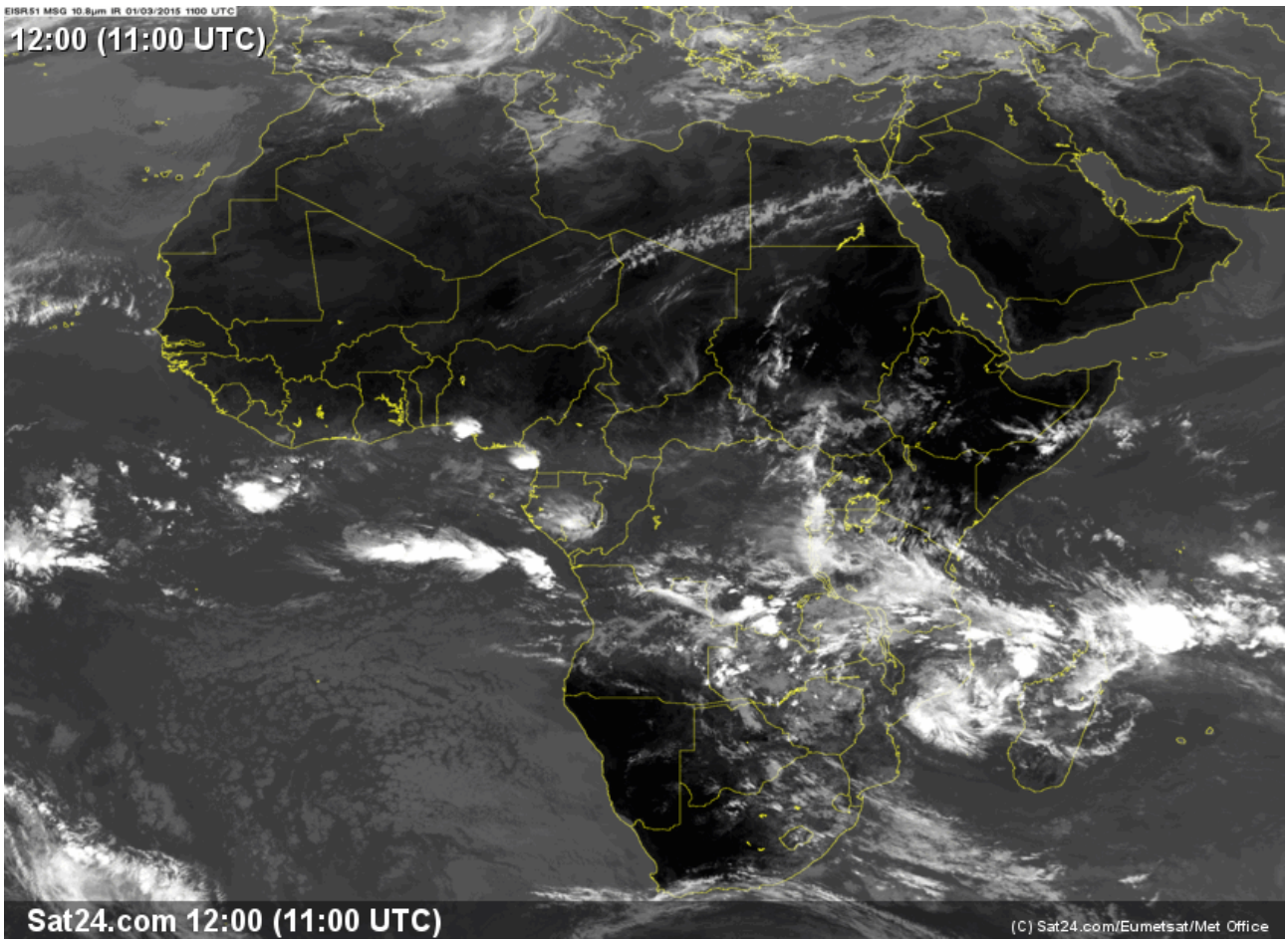

Figure A3(b) Example of an IR satellite image for a rain event on 1 March 2015, grouped in the surface trough with a westerly wave group in Chapter 5.4 (EUMETSAT, 2019).

Appendix B

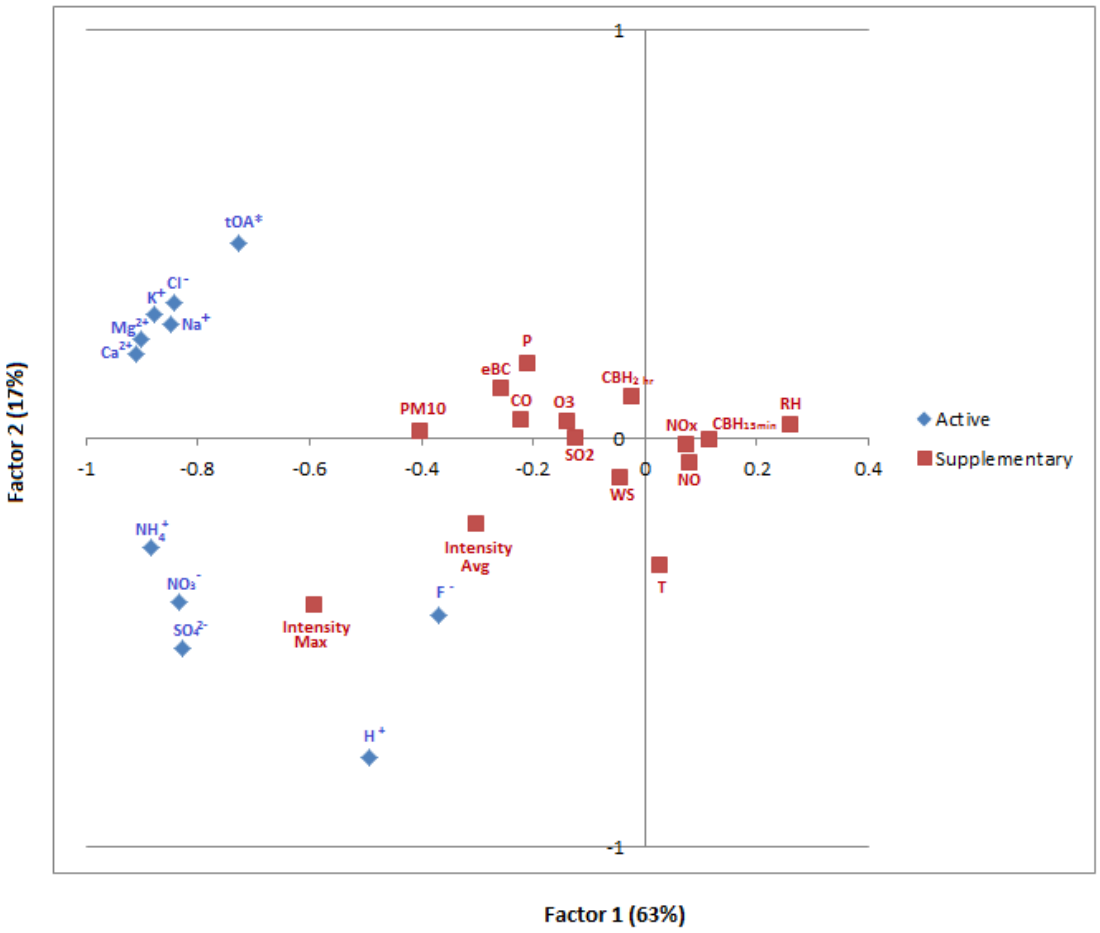

Figure B1 Score plot from the principal component analysis on the rainwater ionic composition (active) and ancillary measurements (supplementary) without rotation of the axes that explain 80% of the variance. Diagonally opposed variables have inverse relationships, while variable grouped together correlate positively. Increasing distance from the origin indicates increased effect of the variable on the variance.

Appendix C

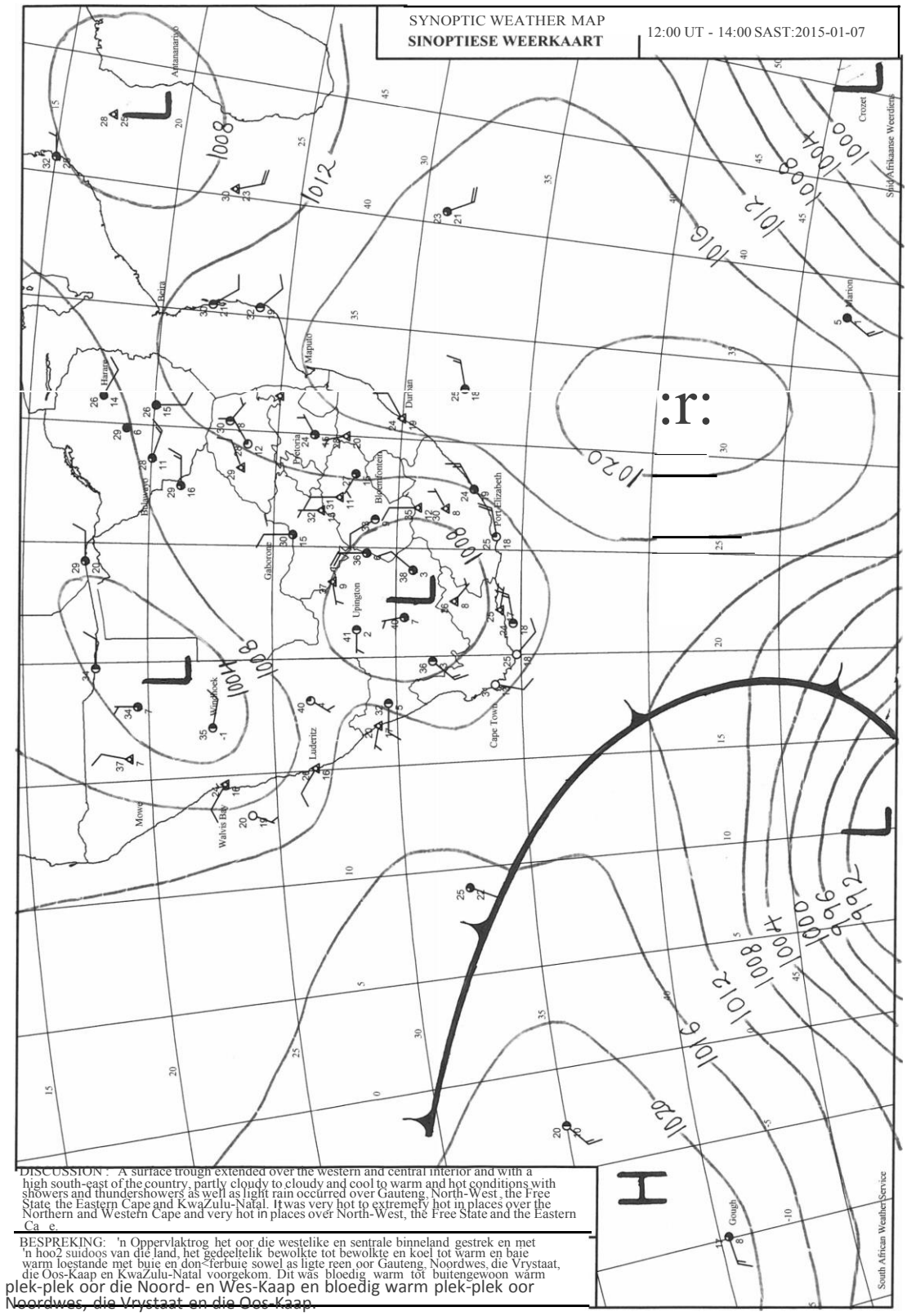

Figure C1(a) Synoptic chart associated with the rainfall event with the highest maximum rain intensity on 7 January 2015 (SAWS, 2019).

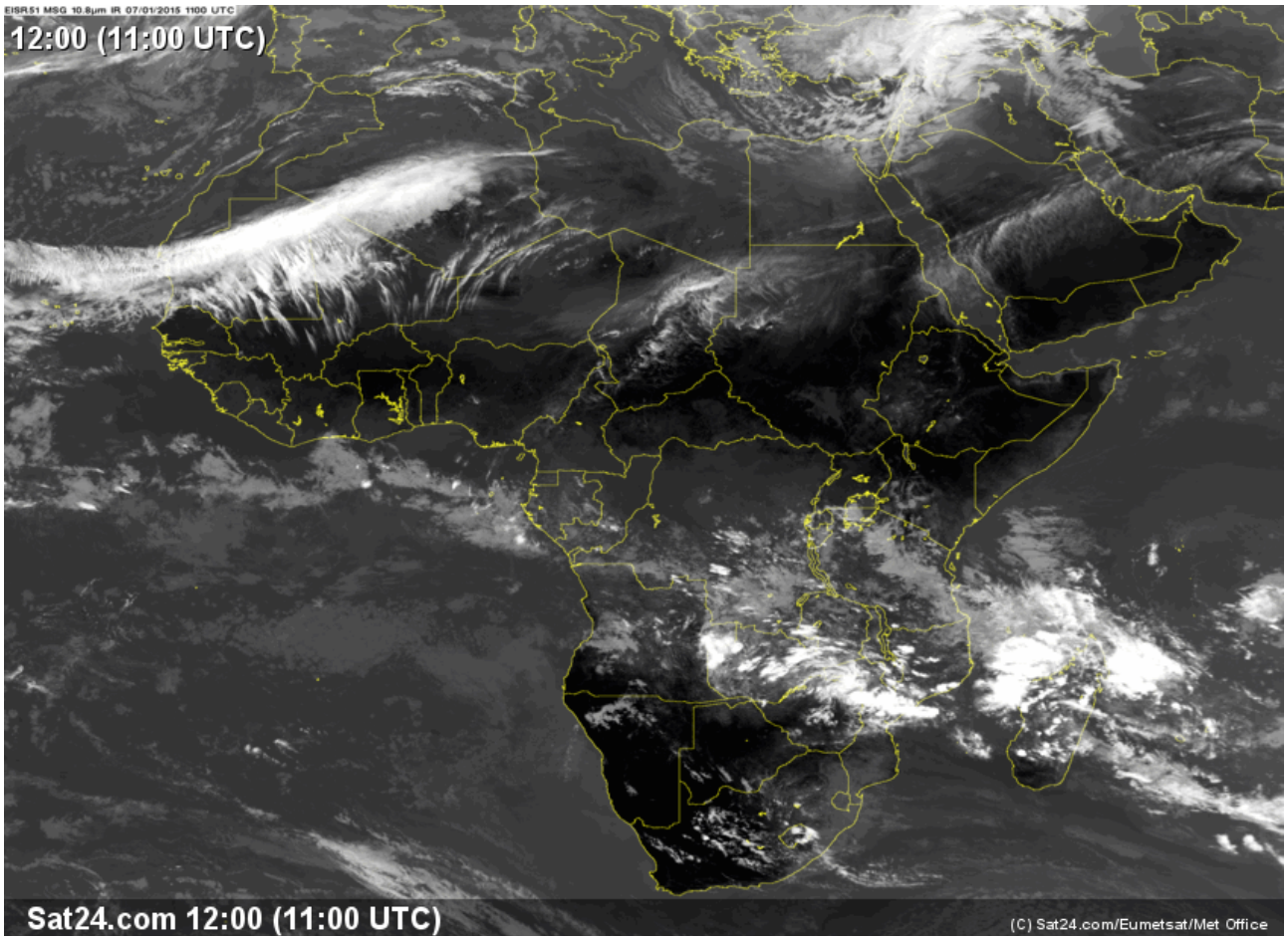

Figure C1(b) The IR satellite image for the rain event associated with the highest maximum rain intensity on 7 January 2015 (EUMETSAT, 2019).

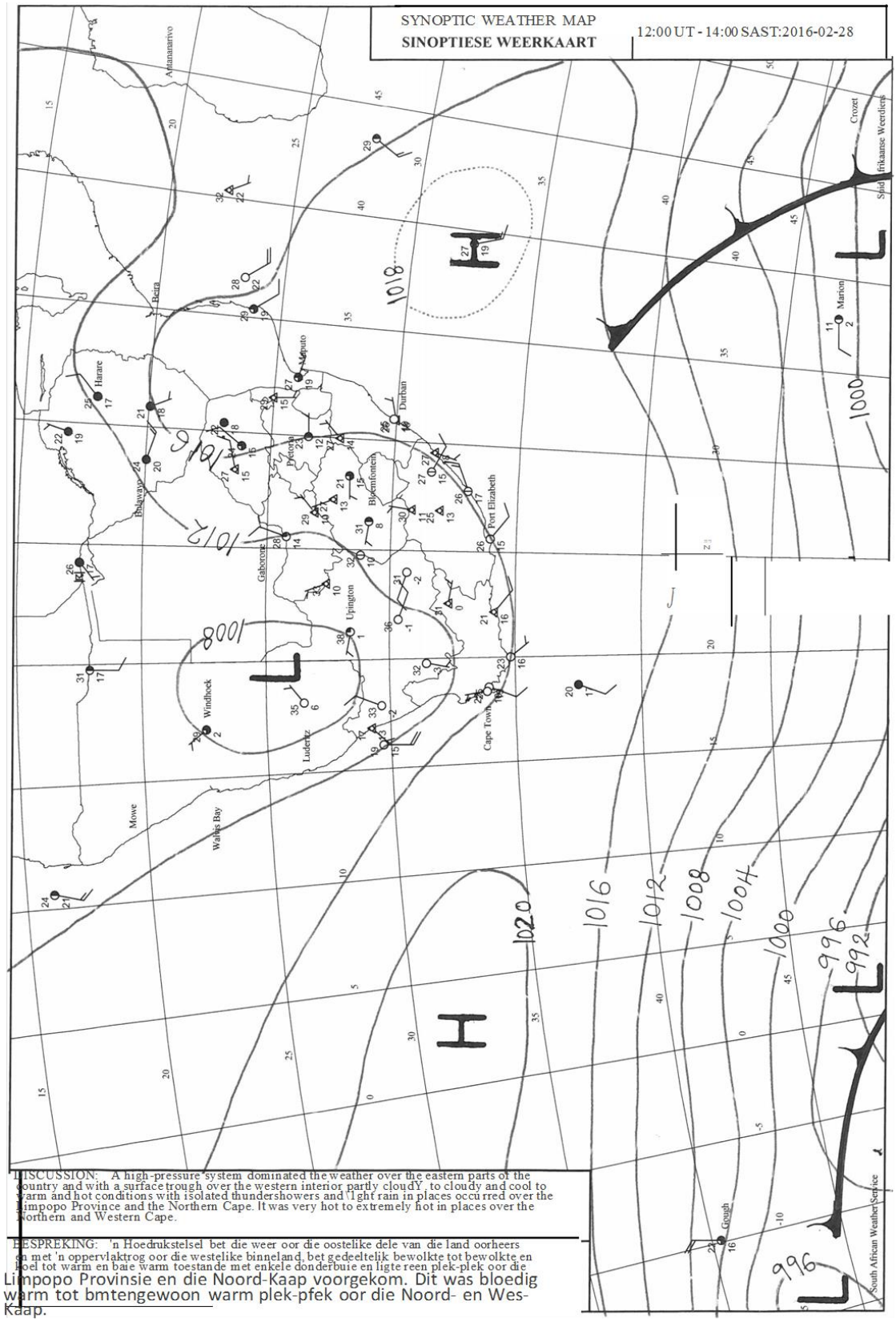

Figure C2(a) Synoptic chart associated with the rainfall event with the highest average rain intensity on 28 February 2016 (SAWS, 2019).

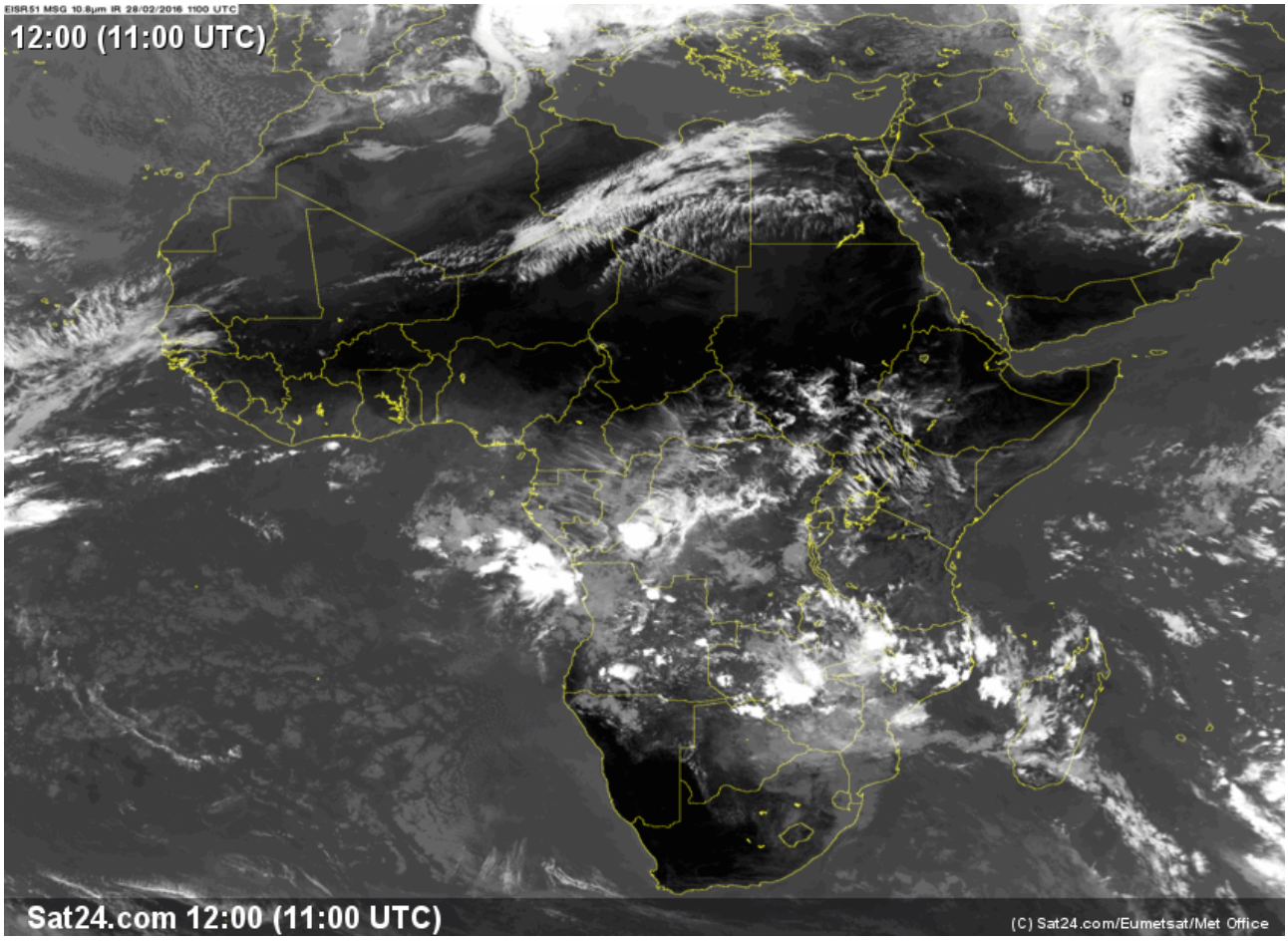

Figure C2(b) The IR satellite image for the rain event associated with the highest average rain intensity on 28 February 2016 (EUMETSAT, 2019).

Bibliography

ABRAHAM, F. 1974. *Homogeneous nucleation theory: The pretransition theory of vapor condensation,* NY and London, Academic Press. 278.

ABER, J. D., NADELHOFFER, K. J., STEUDLER, P. & MELILLO, J. M. 1989. Nitrogen saturation in northern forest ecosystems. BioScience, 39, 378-286.

ADEWUYI, Y. G., CHO, S.-Y., TSAY, R.-P. & CARMICHAEL, G. R. 1984. Importance of formaldehyde in cloud chemistry. *Atmospheric Environment (1967),* 18**,** 2413-2420.

ADON, M., GALY-LACAUX, C., YOBOUÉ, V., DELON, C., LACAUX, J. P., CASTERA, P., GARDRAT, E., PIENAAR, J. J., AL OURABI, H., LAOUALI, D., DIOP, B., SIGHA-NKAMDJOU, L., AKPO, A., TATHY, J. P., LAVENU, F. & MOUGIN, E. 2010. Long term measurements of sulfur dioxide, nitrogen dioxide, ammonia, nitric acid and ozone in Africa using passive samplers. *Atmospheric Chemistry and Physics,* 10**,** 7467-7487.

AIKAWA, M., HIRAKI, T. & MUKAI, H. 2014. Precipitation chemistry and ozone and sulfate concentrations in the ocean atmosphere observed by the multi-year cruising in East Asia and West Oceania (35^{o}N-35^{o}S, 100-135^{o}E) in August and September. *Journal of Atmospheric Chemistry,* 71**,** 65-78.

AIUPPA, A., BELLOMO, S., ALESSANDRO, W. D., FREDERICO, C., FERM, M. & VALENZA, M. 2004. Volcanic plume monitoring at Mount Etna by diffusive (passive) sampling. *Journal of Geophysical Research,* 109**,** 1-11.

AKPO, A. B., GALY-LACAUX, C., LAOUALI, D., DELON, C., LIOUSSE, C., ADON, M., GARDRAT, E., MARISCAL, A. & DARAKPA, C. 2015. Precipitation chemistry and wet deposition in a remote wet savanna site in West Africa: Djougou (Benin). *Atmospheric Environment,* 115**,** 110-123.

AL-KHASHMAN, O. A. 2009. Chemical characteristic of rainwater collected at a western site of Jordan. *Atmospheric Research,* 91**,** 53-61.

AURELA, M., BEUKES, J. P., VAN ZYL, P. G., VAKKARI, V., TEINILÄ, K., SAARIKOSKI, S. & LAAKSO, L. 2016. The composition of ambient and fresh biomass burning aerosols at a savannah site, South Africa. *South African Journal of Science,* 112**,** 8.

BAE, S. Y., JUNG, C. H. & KIM, Y. P. 2006. Development and evaluation of an expression for polydisperse particle scavenging coefficient for the below-cloud scavenging as a function of rain intensity using the moment method. *Journal of Aerosol Science,* 37**,** 1507-1519.

BANERJEE, D. 2008. Study of precipitation chemistry over an industrial city. *International Journal of Envrionmental Science and Technology,* 5**,** 331-338.

BATOR, A. & COLLETT JR, J. L. 1997. Cloud chemistry varies with drop size. *Journal of Geophysical Research: Atmospheres,* 102**,** 28071-28078.

BEARD, K. V., BRINGI, V. N. & THURAI, M. 2010. A new understanding of raindrop shape. *Atmospheric Research,* 97**,** 396-415.

BEUKES, J. P., VENTER, A. D., JOSIPOVIC, M., VAN ZYL, P. G., VAKKARI, V., JAARS, K., DUNN, M., & LAAKSO, L. 2015. Automated Continuous Air Monitoring, Comprehensive Analytical Chemistry, 70, 183-208.

BEUKES, J. P., VAKKARI, V., VAN ZYL, P. G., VENTER, A. D., JOSIPOVIC, M., JAARS, K., TIITTA, P., KULMALA, M., WORSNOP, D., PIENAAR, J. J., VIRKKULA, A. & LAAKSO, L. 2013. Source region plume characterisation of the interior of South Africa as observed at Welgegund. *Clean Air Journal,* 23, 7-10.

BRANDT, C. & VAN ELDIK, R. 1995. Transition metal-catalyzed oxidation of sulfur(iv) oxides. Atmospheric-relevant processes and mechanisms. *Chemical Reviews,* 95**,** 119-190.

BRIMBLECOMBE, P. 2003. Aqueous phase chemistry of the troposphere. *In:* HEWITT, C. N. & JACKSON, A. (eds.) *Handbook of atmospheric science: Principles and applications.* Oxford: Blackwell Science. 211-227.

BRIMBLECOMBE, P. & DAWSON, G. 1984. Wet removal of highly soluble gases. *Journal of atmospheric chemistry,* 2**,** 95-107.

BRYSON, C. T. 1988. Effects of rainfall on foliar herbacides applied to seedling Johnsongrass (*sorghum halepense)*. *Weed Technology,* 2**,** 153-158.

CAIRNCROSS, B. 2004. *Field guide to rocks and minerals of southern Africa,* Cape Town, SA, Struik Nature. 292.
CAMPOS, E. F., ZAWADZKI, I., PETITDIDIER, M. & FERNÁNDEZ, W. 2006. Measurement of raindrop size distributions in tropical rain at Costa Rica. *Journal of Hydrology,* 328**,** 98-109.
CAPE, J. N., SMITH, R. I., FOWLER, D., BESWICK, K. & CHOULARTON, T. 2015. Long-term trends in rain and cloud chemistry in a region of complex topography. *Atmospheric Research,* 153**,** 335-347.
CHAFE, Z. A., BRAUER, M., KLIMONT, Z., VAN DINGENEN, R., MEHTA, S., RAO, S., RIAHI, K., DENTENER, F. & SMITH, K. R. 2014. Household cooking with solid fuels contributes to ambient PM2. 5 air pollution and the burden of disease. *Environmental health perspectives,* 122**,** 1314-1320.
CHAMEIDES, W. L. 1986. Possible role of NO3 in the nighttime chemistry of a cloud. *Journal of Geophysical Research: Atmospheres,* 91**,** 5331-5337.
CHAN, M. N., CHOI, M. Y., NG, N. L. & CHAN, C. K. 2005. Hygroscopicity of Water-Soluble Organic Compounds in Atmospheric Aerosols: Amino Acids and Biomass Burning Derived Organic Species. *Environmental Science & Technology,* 39**,** 1555-1562.
CHAPMAN, E. G., GUSTAFSON, W. I., EASTER, R. C., BARNARD, J. C., GHAN, S. J., PEKOUR, M. S. & FAST, J. D. 2009. Coupling aerosol-cloud-radiative processes in the WRF-Chem model: Investigating the radiative impact of elevated point sources. *Atmospheric Chemistry and Physics,* 9**,** 945-964.
CHATE, D., MURUGAVEL, P., ALI, K., TIWARI, S. & BEIG, G. 2011. Below-cloud rain scavenging of atmospheric aerosols for aerosol deposition models. *Atmospheric Research,* 99**,** 528-536.
CHATE, D. M. 2005. Study of scavenging of submicron-sized aerosol particles by thunderstorm rain events. *Atmospheric Environment,* 39**,** 6608-6619.
CHATE, D. M. 2011. Below-thunderstorm rain scavenging of urban aerosols in the health hazardous modes. *Natural Hazards,* 56**,** 81-91.
CHATE, D. M. & PRANESHA, T. S. 2004. Field studies of scavenging of aerosols by rain events. *Aerosol Science,* 35**,** 695-706.
CHEN, S., JIANG, N., HUANG, J., ZANG, Z., GUAN, X., MA, X., LUO, Y., LI, J., ZHANG, X. & ZHANG, Y. 2019. Estimations of indirect and direct anthropogenic dust emission at the global scale. *Atmospheric Environment,* 200**,** 50-60.
CHENG, Y., ENGLING, G., HE, K.-B., DUAN, F.-K., MA, Y.-L., DU, Z.-Y., LIU, J.-M., ZHENG, M. & WEBER, R. J. 2013. Biomass burning contribution to Beijing aerosol. *Atmospheric Chemistry and Physics,* 13**,** 7765-7781.
CHILOANE, K. E., BEUKES, J. P., VAN ZYL, P. G., MARITZ, P., VAKKARI, V., JOSIPOVIC, M., VENTER, A. D., JAARS, K., TIITTA, P., KULMALA, M., WIEDENSOHLER, A., LIOUSSE, C., MKHATSHW, G. V., RAMANDH, A. & LAAKSO, L. 2017. Spatial, temporal and source contribution assessments of black carbon over the northern interior of South Africa. Atmospheric Chemistry and Physics, 17, 6177-6196.
CHRISTNER, B. C., CAI, R., MORRIS, C. E., MCCARTER, K. S., FOREMAN, C. M., SKIDMORE, M. L., MONTROSS, S. N. & SANDS, D. C. 2008. Geographic, seasonal, and precipitation chemistry influence on the abundance and activity of biological ice nucleators in rain and snow. *PNAS,* 105**,** 18854-18859.
CHVÌLA, B., SEVRUK, B. & ONDRAS, M. 2005. The wind-induced loss of thunderstorm precipitation measurements. *Atmospheric Research,* 77**,** 29-38.
CIESIN 2010. Columbia University, United Nations Food and Agriculture Programme (FAO), and Centro Internacional de Agricultura Tropical (CIAT), 2005, Gridded Population of the World: Future Estimates (GPWFE). *Center for International Earth Science Information Network CIESIN.* Palisades, NY: Socioeconomic Data and Applications Center (SEDAC), Columbia University.
COHEN, J. 1988. *Statistical Power Analysis for the Behavioral Sciences,* New York, NY, Routledge Academic. 559.
COLLETT JR, J., OBERHOLZER, B. & STAEHELIN, J. 1993. Cloud chemistry at Mt Rigi, Switzerland: dependence on drop size and relationship to precipitation chemistry. *Atmospheric Environment. Part A. General Topics,* 27**,** 33-42.

COLLETT, K. S., PIKETH, S. J. & ROSS, K. E. 2010. An Assessment of the atmospheric nitrogen budget on the South African Highveld. *South African Journal of Science,* 106 9.
CONNELL, D. W. 2005. *Basic concepts of environmental chemistry,* Boca Raton, FL, Taylor & Francis Group. 480.
CONRADIE, E. H., VAN ZYL, P. G., PIENAAR, J. J., BEUKES, J. P., GALY-LACAUX, C., VENTER, A. D. & MKHATSHW, G. V. 2016. The chemical composition and fluxes of atmospheric wet deposition at four sites in South Africa. *Atmospheric Environment,* 2016, 113-131.
COSTA-SURÓS, M., CALBÓ, J., GONZÁLEZ, J. A. & MARTIN-VIDE, J. 2013. Behavior of cloud base height from ceilometer measurements. *Atmospheric Research,* 127**,** 64-76.
CRITCHFIELD, H. J. 1983. *General climatology,* New Jersey, Prentice Hall. 453.
ĆURIĆ, M., JANC, D. & VUČKOVIĆ, V. 2006. Seeding agent dispersion within convective cloud as simulated by a 3-D numerical model. *Meteorology and Atmospheric Physics,* 92**,** 205-216.
ĆURIĆ, M., JANC, D., VUČKOVIĆ, V. & KOVAČEVIĆ, N. 2009. An inadvertent transport of the seeding material as a result of cloud modification. *Meteorology and atmospheric physics,* 105**,** 157-165.
DAMBREVILLE, C., HALLET, S., NGUYEN, C., MORVAN, T., GERMON, J.-C. & PHILIPPOT, L. 2006. Structure and activity of the denitrifying community in a maize-cropped field fertilized with composted pig manure or ammonium nitrate. FEMS microbiology ecology, 56, 119-131.
DE BOER, G., HASHINO, T. & TRIPOLI, G. J. 2010. Ice nucleation through immersion freezing in mixed-phase stratiform clouds: theory and numerical simulations. *Atmospheric Research,* 96**,** 315-324.
DELMAS, R. 1981. Contribution a l'etudedes forets equatoriales commesources naturelles de derives soufres atmospheriques. *PhD Thesis, Universite Paul Sabatier de Toulouse, Toulose, France*.
DEMOTT, P. J., MÖHLER, O., STETZER, O., VALI, G., LEVIN, Z., PETTERS, M. D., MURAKAMI, M., LEISNER, T., BUNDKE, U., KLEIN, H., KANJI, Z. A., COTTON, R., JONES, H., BENZ, S., BRINKMANN, M., RZESANKE, D., SAATHOFF, H., NICOLET, M., SAITO, A., NILLIUS, B., BINGEMER, H., ABBATT, J., ARDON, K., GANOR, E., GEORGAKOPOULOS, D. G. & SAUNDERS, C. 2011. Resurgence in ice nuclei measurement research. *Bulletin of the American Meteorological Society,* 92**,** 1623-1635.
DENTENER, F., DREVET, J., LAMARQUE, J. F., BEY, I., EICKHOUT, B., FIORE, A. M., HAUGLUSTAINE, D., HOROWITZ, L. W., KROL, M., KULSHRESTHA, U. C., LAWRENCE, M., GALY-LACAUX, C., RAST, S., SHINDELL, D., STEVENSON, D., VAN NOIJE, T., ATHERTON, C., BELL, N., BERGMAN, D., BUTLER, T., COFALA, J., COLLINS, B., DOHERTY, R., ELLINGSEN, K., GALLOWAY, J. N., GAUSS, M., MONTANARO, V., MULLER, J. F., PITARI, G., RODRIGUEZ, J., SANDERSON, M., SOLMON, F., STRAHAN, S., SHULTZ, M., SUDO, K., SZOPA, S. & WILD, O. 2006. Nitrogen and sulfur deposition on regional and global scales: A multimodel evaluation. *Global Biogeochemical Cycles,* 20. 21.
DHITAL, S. & RAUN, W. R. 2016. Variability in optimum nitrogen rates for maize. *Agronomy Journal,* 108**,** 2165-2173.
DRAXLER, R. R. & HESS, G. D. 2004. Description of the HYSPLIT_4 modeling system. *NOAA Tech Memo***,** 24.
DUSEK, U., FRANK, G. P., HILDEBRANDT, L., CURTIUS, J., SCHNEIDER, J., WALTER, S., CHAND, D., DREWNICK, F., HINGS, S., JUNG, D., BORRMANN, S. & ANDREAE, M. O. 2006. Size matters more than chemistry for cloud-nucleating ability of aerosol particles. 1375-1378.
EBY, G. N. 2004. *Principles of environmental geochemistry,* Belmont, CA, Brooks/Cole. 514.
EKMAN, A. M. L., ENGSTRÖM, A. & SÖDERBERG, A. 2011. Impact of two-way aerosol-cloud interaction and changes in aerosol size distributionon simulated aerosol-induced deep convective cloud sensitivity. *Journal of Atmospheric Sciences,* 68**,** 685-698.
ELLIS, S. M. & STEYN, H. S. 2003. Practical significance (effect sizes) versus or in combination with statistical significance (p-values). *Management Dynamics: Journal of the Southern African Institute for Management Scientists,* 12**,** 51-53.

EMEIS, S., SCHAFER--, K., MUNKEL--, C., FRIEDL, R. & SUPPAN, P. 2012. Evaluation of the interpretation of ceilometer data with RASS and radiosonde data. *Boundary-Layer Meteorology,* 143**,** 25-35.
ENGELMANN, R. J. 1965. The calculation of precipitation scavenging. Richland, Washington: Batelle-Northwest: Pacific Northwest Laboratory.
ENGELMANN, R. J. 1971. Scavenging prediction using ratios of concentrations in air and precipitation. *Journal of Applied Meteorology,* 10**,** 493-497.
EPA 1999. United States Environmental Protection Agency. Atmospheric deposition of sulfur and nitrogen compounds. *National air quality and emissions trends report.* 237.
EPA 2008. United States Envrionmental Protection Agency. Integrated science assessment for sulfur oxides- health criteria. 479.
EUMETSAT 2019. Monitoring weather and climate from space. http://pics.eumetsat.int/viewer/index.html; http://www2.sat24.com/history.aspx?culture=en [Accessed 27 May 2019]
EVANS, C. D., MONTEITH, D. T., FOWLER, D., CAPE, J. N. & BRAYSHAW, S. 2011. Hydrochloric acid: an overlooked driver of environmental change. Environmental science & technology, 45, 1887-1894.
FEDKIN, N. M., LI, C., DICKERSON, R. R., CANTY, T. & KROTKOV, N. A. 2019. Linking improvements in sulfur dioxide emissions to decreasing sulfate wet deposition by combining satellite and surface observations with trajectory analysis. *Atmospheric Environment,* 199**,** 210-223.
FEINGOLD, G., COTTON, W. R., KREIDENWEIS, S. M. & DAVIS, J. T. 1999. The impact of giant cloud condensation nuclei on drizzle formation in stratocumulus: Implications for cloud radiative properties. *Journal of the atmospheric sciences,* 56**,** 4100-4117.
FELTRACCO, M., BARBARO, E., KIRCHGEORG, T., SPOLAOR, A., TURETTA, C., ZANGRANDO, R., BARBANTE, C. & GAMBARO, A. 2019. Free and combined L- and D-amino acids in Arctic aerosol. *Chemosphere,* 220**,** 412-421.
FIELDS, S. 2004. Global nitrogen: cycling out of control. National Institue of Environmental Health Sciences.
FINLAYSON-PITTS, B. J. & PITTS, J. N., JNR 2000. *Chemistry of the upper and lower atmosphere: Theory, experiments and applications,* California, Academic Press. 969.
FLEMING, Z. L., MONKS, P. S. & MANNING, A. J. 2012. Review: Untangling the influence of air-mass history in interpreting observed atmospheric composition. *Atmospheric Research***,** 1-39.
FORBES, P. 2012. Particle emissions from household fires in South Africa. *WIT Transactions on***,** 445-456.
FREIMAN, M. T. & TYSON, P. D. 2000. The thermodynamic structure of the atmosphere over South Africa: Implications for water vapour transport. *Water SA,* 26**,** 153-158.
FUENTES, J. D., CHAMECKI, M., NASCIMENTO DOS SANTOS, R. M., VON RANDOW, C., STOY, P. C., KATUL, G., FITZJARRALD, D., MANZI, A., GERKEN, T. & TROWBRIDGE, A. 2016. Linking meteorology, turbulence, and air chemistry in the Amazon rain forest. Bulletin of the American Meteorological Society, 97, 2329-2342.
GALLOWAY, J. N., SAVOIE, D. L., KEENE, W. C. & PROSPERO, J. M. 1993. The temporal and spatial variability of scavenging ratios for nss sulfate, nitrate, methanesulfonate and sodium in the atmosphere over the North Atlantic Ocean. *Atmospheric Environment,* 27A**,** 235-250.
GALY-LACAUX, C., LAOUALI, D., DESCROIX, L., GOBRON, N. & LIOUSSE, C. 2009. Long term precipitation chemistry and wet deposition in a remote dry savanna site in Africa (Niger). *Atmospheric Chemistry and Physics,* 9**,** 1579-1595.
GARSTANG, M., TYSON, P. D., SWAP, R., EDWARDS, M., KÅLLBERG, P. & LINDESAY, J. A. 1996. Horizontal and vertical transport of air over southern Africa. *Journal of Geophysical Research: Atmospheres (1984–2012),* 101**,** 23721-23736.
GESAMP 1985. Atmospheric transport of contaminants into the Mediterranean region. *In:* (UNEP), U. N. E. P. (ed.) *Regional Seas Reports and Studies.*
GIERENS, R., HENRIKSSON, S., JOSIPOVIC, M., VAKKARI, V., VAN ZYL, P. G., BEUKES, J. P., WOOD, C. R. & O'CONNOR, E. J. 2019. Observing continental boundary-layer structure

and evolution over the South African savannah using a ceilometer. *Theoretical and Applied Climatology,* 136**,** 333-346.
GONG, W., DASTOOR, A. P., BOUCHET, V. S., GONG, S., MAKAR, P. A., MORAN, M. D., PABLA, B., MÉNARD, S., CREVIER, L. P., COUSINEAU, S. & VENKATESH, S. 2006. Cloud processing of gases and aerosols in a regional air quality model (AURAMS). *Atmospheric Research,* 82**,** 248-275.
GONZÁLEZ, C. M. & ARISTIZÁBAL, B. H. 2012. Acid rain and particulate matter dynamics in a mid-sized Andean city: Th effect of rain intensity on ion scavenging. *Atmospheric Environment,* 60**,** 164-171.
GOVERNMENT GAZETTE REPUBLIC OF SOUTH AFRICA 2007. National Environmental Management: Air Quality Act, 2004 (No.39 of 2004), Declaration of the Highveld as Priority Area in Terms of Section 18(1) of the National Environmental Management: Air Quality Act, 2004 (Act No. 39 of 2004). *In:* AFFAIRS, D. O. E. (ed.). Republic of South Africa: Deparment of Environmental Affairs.
GOVERNMENT GAZETTE REPUBLIC OF SOUTH AFRICA 2009. National Environmental Management: Air Quality Act, 2004 (Act No.39 of 2004), Vaal Triangle Airshed Priority Area Air Quality Management Plan. *In:* TOURISM, D. O. E. A. A. (ed.). Republic of South Africa.
GOVERNMENT GAZETTE REPUBLIC OF SOUTH AFRICA 2015. National Environmental Management: Air Quality Act, 2004 (No.39 of 2004), Waterberg Bojanala Priority Area Air Quality Plan. *In:* AFFAIRS, D. O. E. (ed.).
GRAEDEL, T. E. & CRUTZEN, P. J. 1993. *Atmospheric change: An earth system perspective,* New York, W.H. Freeman and Company.
GREAVER, T. L., SULLIVAN, T. J., HERRICK, J. D., BARBER, M. C., BARON, J. S., COSBY, B. J., DEERHAKE, M. E., DENNIS, R. L., DUBOIS, J.-J. B., GOODALE, C. L., HERLIHY, A. T., LAWRENCE, G. B., LIU, L., LYNCH, J. A. & NOVAK, K. J. 2012. Ecological effects of nitrogen and sulfur air pollution in the US: what do we know? *Frontiers in Ecology and the Environment,* 10**,** 365-372.
GROSJEAN, D. 1989. Organic acids in southern California air: Ambient concentrations, mobile source emissions, in situ formation and removal processes. *Environmental Science & Technology,* 23**,** 1506-1514.
HADI, D. A., CROSSLEY, A. & CAPE, J. N. 1994. Particulate and dissolved organic carbon in cloud water in southern Scotland. *Environmental Pollution,* 88**,** 299-306.
HALL, B. D. 2003. Atmospheric removal processes. *In:* HEWITT, C. N. & JACKSON, A. (eds.) *Handbook of atmospheric science: Principles and applications.* Oxford: Blackwell Science. 649.
HALSALL, C. J. 2003. Regional-scale pollution problems. *In:* HEWITT, C. N. & JACKSON, A. (eds.) *Handbook of atmospheric science: Principles and applications.* Oxford: Blackwell Science. 649.
HARRISON, M. S. J. 1984. The annual rainfall cycle over the central interior of South Africa. *South African Geographical Journal,* 66**,** 47-64.
HARRISON, M. S. J. 1986. *A synoptic climatology of South African rainfall variations.* PhD, University of Witwatersrand.
HART, N. C., REASON, C. J. & FAUCHEREAU, N. 2013. Cloud bands over southern Africa: seasonality, contribution to rainfall variability and modulation by the MJO. *Climate dynamics,* 41**,** 1199-1212.
HART, N. C. G., REASON, C. J. C. & FAUCHEREAU, N. 2010. Tropical-extratropical interactions over Southern Africa: Three cases of heavy summer season rainfall. *Monthly Weather Review,* 138**,** 2608-2623.
HEGG, D. A. & HOBBS, P. V. 1981. Cloud water chemistry and the production of sulfates in clouds. *Atmospheric Environment (1967),* 15**,** 1597-1604.
HELAS, G. & PIENAAR, J. J. 1996. Biomass burning emissions. *In:* HELD, G., GORE, B. J., SURRIDGE, A. D., TOSEN, G. R., TURNER, C. R. & WALMSLEY, R. D. (eds.) *Air pollution and its impacts on South African Highveld.* Cleveland: Environmental Scientific Association. 12-15.

HELD, G., SCHEIFINGER, H., SNYMAN, G. M., TOSEN, G. R. & ZUNCKEL, M. 1996. The climatology and meteorology of the highveld. *In:* HELD, G., GORE, B. J., SURRIDGE, A. D., TOSEN, G. R., TURNER, C. R. & WALMSLEY, R. D. (eds.) *Air pollution and its impacts on the South African Highveld.* Cleveland: Environmental Scientific Association. 60-71.

HIRSIKKO, A., VAKKARI, V., TIITTA, P., MANNINEN, H. E., GAGNÉ, S., LAAKSO, H., KULMALA, M., MIRME, A., MIRME, S., MABASO, D., BEUKES, J. P. & LAAKSO, L. 2012. Characterisation of sub-micron particle number concentrations and formation events in the western Bushveld Igneous Complex, South Africa. *Atmospheric Chemistry and Physics,* 12**,** 3951-3967.

HOFFMANN, E. H., TILGNER, A., WOLKE, R., BÖGE, O., WALTER, A. & HERRMANN, H. 2018. Oxidation of substituted aromatic hydrocarbons in the tropospheric aqueous phase: kinetic mechanism development and modelling. *Physical Chemistry Chemical Physics,* 20**,** 10960-10977.

HOLMES, C. D., KRISHNAMURTHY, N. P., CAFFREY, J. M., LANDING, W. M., EDGERTON, E. S., KNAPP, K. R. & NAIR, U. S. 2016. Thunderstorms increase mercury wet deposition. *Environmental Science & Technology,* 50**,** 9343-9350.

HOSIOKANGAS, J., RUUSKANEN, J. & PEKKANEN, J. 1999. Effects of soil dust episodes and mixed fuel sources on source apportionment of PM10 particles in Kuopio, Finland. *Atmospheric Environment,* 33**,** 3821-3829.

HUANG, X., ZHANG, J., LUO, B., LUO, J., ZHANG, W. & RAO, Z. 2019. Characterization of oxalic acid-containing particles in summer and winter seasons in Chengdu, China. Atmospheric Environment, 198, 133-141.

IPCC 2013. Intergovernmental Panel on Climate Change. Climate Change 2013: The physical science basis. *In:* STOCKER, T. F., QIN, D., PLATTNER, G.-K., TIGNOR, M. M. B., ALLEN, S. K., BOSCHUNG, J., NAUELS, A., XIA, Y., BEX, V. & MIDGLEY, P. M. (eds.) *Contribution of Working Group I to the Fifth Assessment Report of the Intergovernmental Panel on Climate Change.* Cambridge, UK and New York, NY, USA. 1535.

IRIBARNE, J. & CHO, H. 1989. Models of cloud chemistry. *Tellus B: Chemical and Physical Meteorology,* 41**,** 2-23.

JAARS, K., BEUKES, J. P., VAN ZYL, P. G., VENTER, A. D., JOSIPOVIC, M., PIENAAR, J. J., VAKKARI, V., AALTONEN, H., LAAKSO, H., KULMALA, M., TIITTA, P., GUENTHER, A., HELLÉN, H., LAAKSO, L. & HAKOLA, H. 2014. Ambient aromatic hydrocarbon measurements at Welgegund, South Africa. *Atmospheric Chemistry and Physics Discuss,* 14**,** 4189-4227.

JAARS, K., VAN ZYL, P. G., BEUKES, J. P., HELLÉN, H., VAKKARI, V., JOSIPOVIC, M., VENTER, A. D., RÄSÄNEN, M., KNOETZE, L., CILLIERS, D. P., SIEBERT, S. J., KULMALA, M., RINNE, J., GUENTHER, A., LAAKSO, L. & HAKOLA, H. 2016. Measurements of biogenic volatile organic compounds at a grazed savannah-grassland-agriculture landscape in South Africa. *Atmospheric Chemistry and Physics*.15665-15688.

JACKSON, A. V. 2003. Sources of air pollution. *In:* HEWITT, C. N. & JACKSON, A. (eds.) *Handbook of atmospheric science: Principles and applications.* Oxford: Blackwell Science. 124-155.

JOHNSON, D. B. 1982. The role of giant and ultragiant aerosol particles in warm rain initiation. *Journal of Atmospheric Sciences,* 39**,** 448-460.

JOHNSON, R. A. & WICHERN, D. W. 2007. *Applied multivariate statistical analysis,* New Jersey, Pearson Prentice Hall. 773.

JOSIPOVIC, M., ANNEGARN, H. J., KNEEN, M. A., PIENAAR, J. J. & PIKETH, S. J. 2011. Atmospheric dry and wet deposition of sulphur and nitrogen species and assessment of critical loads of acidic deposition exceedance in South Africa. *South African Journal of Science,* 107. 1-10.

KANAYO, J., NDUKA, C. & ORISAKWE, O. E. 2010. Precipitation chemistry and occurence of acid rain over the oil-producing Niger Delta region of Nigeria. *The Scientific World,* 10**,** 528-534.

KAREV, A. R., LEE, D. I., YOU, C. H. & UYEDA, H. 2010. Variations in raindrop size distributions observed in mid-latitude ocean clouds during the East-Asian summer monsoon. *Atmospheric Research,* 96**,** 65-78.

KARYDIS, V. A., TSIMPIDI, A. P., BACER, S., POZZER, A., NENES, A. & LELIEVELD, J. 2017. Global impact of mineral dust on cloud droplet number concentration. *Atmospheric Chemistry and Physics,* 17**,** 5601-5621.

KAUFMAN, Y. J., ICHOKU, C., GIGLIO, L., KORONTZI, S., CHU, D. A., HAO, W. M., LI, R.-R. & JUSTICE, C. O. 2003. Fire and smoke observed from the Earth Observing System MODIS instrument - products, validation, and operational use. *International Journal of Remote Sensing,* 24**,** 1765-1781.

KAUFMAN, Y. J. & NAKAJIMA, T. 1993. Effect of Amazon smoke on cloud microphysics and albedo-analysis from satellite imagery. *Journal of Applied Meteorology,* 32**,** 729-744.

KAWAMURA, K., KASUKABE, H. & BARRIE, L. A. 1996. Source and reaction pathways of dicarboxylic acids, ketoacids and dicarbonyls in arctic aerosols: one year of observations. *Atmospheric Environment,* 30**,** 1709-1722.

KEENE, W. C., PSZENNY, A. A., GALLOWAY, J. N. & HARTLEY, M. E. 1986. Sea-salt corrections and interpretation of constituent ratios in marine precipitation. *Journal of Geophysical Research,* 91**,** 6647-6658.

KELLEY, K. & SWEENEY, D. 2005. Tillage and urea ammonium nitrate fertilizer rate and placement affects winter wheat following grain sorghum and soybean. Agronomy journal, 97, 690-697.

KHAIN, A. P., ROSENFELD, D., POKROVSKY, A., BLAHAK, U. & RYZHKOV, A. 2011. The role of CCN in precipitation and hail in a mid-latitude storm as seen in simulations using a spectral (bin) microphysics model in a 2D dynamic frame. *Atmospheric Research,* 99**,** 129-146.

KHAIN, A. P. & SEDNEV, I. 1999. Effects of cloud-aerosol interaction on cloud-microphysics, precipitation formation and size distribution of atmospheric aerosol: Numerical experiments with a spectral microphysics cloud model. *Atmospheric Research,* 52. 195-220.

KOCH, D. & DEL GENIO, A. D. 2010. Black carbon semi-direct effects on cloud cover: review and synthesis. *Atmospheric Chemistry and Physics,* 10**,** 7685-7696.

KONWAR, M., MAHESKUMAR, R. S., KULKARNI, J. R., FREUD, E., GOSWAMI, B. N. & ROSENFELD, D. 2012. Aerosol control on depth of warm rain in convective clouds. *Journal of Geophysical Research,* 117**,** 10.

KOREN, I., DAGAN, G. & ALTARATZ, O. 2014. From aerosol-limited to invigoration of warm convective clouds. *Science,* 344**,** 1143-1146.

KRAUSS, T., BRUINTJES, R. & VERLINDE, J. 1987. Microphysical and radar observations of seeded and nonseeded continental cumulus clouds. *Journal of climate and applied meteorology,* 26**,** 585-606.

KRUG, E. C. & FRINK, C. R. 1983. Acid rain on acid soil: a new perspective. *Science,* 221**,** 520-525.

KULMALA, M., JOSIPOV, M., VAKKARI, V., WORSNOP, D., PIENAAR, J. J., BEUKES, J. P., JAARS, K., LAAKSO, L., VENTERIC, A. D. & TIITTA, P. 2013. Source region plume characterisation of the interior of South Africa as observed at Welgegund. *Clean Air Journal= Tydskrif vir Skoon Lug,* 23**,** 7-10.

KULSHRESTHA, U. C., REDDY, L. A. K., SATYANARAYANA, J. & KULSHRESTHA, M. J. 2009. Real-time wet scavenging of major chemical constituents of aerosols and rol of rain intensity in Indian region. *Atmospheric Environment,* 43**,** 5123-5127.

LAAKSO, L., VAKKARI, V., VIRKKULA, A., LAAKSO, H., BACKMAN, J., KULMALA, M., BEUKES, J. P., VAN ZYL, P. G., TIITTA, P., JOSIPOVIC, M., PIENAAR, J. J., CHILOANE, K., GILARDONI, S., VIGNATI, E., WIEDENSOHLER, A., TUCH, T., BIRMILI, W., PIKETH, S., COLLETT, K., FOURIE, G. D., KOMPPULA, M., LIHAVAINEN, H., DE LEEUW, G. & KERMINEN, V.-M. 2012. South African EUCAARI measurements: seasonal variation of trace gases and aerosol optical properties. *Atmospheric Chemistry and Physics,* 12**,** 1847-1864.

LABAN, T. L., VAN ZYL, P. G., BEUKES, J. P., VAKKARI, V., JAARS, K., BORDUAS-DEDEKIND, N., JOSIPOVIC, M., THOMPSON, A. M., KULMALA, M. & LAAKSO, L. 2018. Seasonal influences on surface ozone variability in continental South Africa and implications for air quality. *Atmospheric Chemistry and Physics*.

LACAUX, J., TATHY, J. & SIGHA, L. 2003. Acid wet deposition in the tropics: two case studies using DEBITS measurements.

LAKENS, D. 2013. Calculating and reporting effect sizes to facilitate cumulative science: a practical primer for t-tests and ANOVAs. *Frontiers in Psychology* [Online]. [Accessed 863 4].

LAMB, D. & CHEN, J. P. 1990. A modeling study of the effects of ice-phase microphysical processes on trace chemical removal efficiencies. *Atmospheric Research,* 25**,** 31-51.

LAOUALI, D., GALY-LACAUX, C., DIOP, B., DELON, C., ORANGE, D., LACAUX, J. P., AKPO, A., LAVENU, F., GARDRAT, E. & CASTERA, P. 2012. Long term monitoring of the chemical composition of precipitation and wet deposition fluxes over three Sahelian savannas. *Atmospheric Environment,* 50**,** 314-327.

LASKIN, A., SMITH, J. S. & LASKIN, J. 2009. Molecular Characterization of Nitrogen-Containing Organic Compounds in Biomass Burning Aerosols Using High-Resolution Mass Spectrometry. *Environmental Science & Technology,* 43**,** 3764-3771.

LI, J., WU, K., LI, F., CHEN, Y., HUANG, Y. & FENG, Y. 2017. Effects of latent heat in various cloud microphysics processes on autumn rainstorms with different intensities on Hainan Island, China. *Atmospheric Research,* 189**,** 47-60.

LI, Y., BARTH, M. C. & STEINER, A. L. 2019. Comparing turbulent mixing of atmosheric oxidants across model scales. *Atmospheric Environment,* 199**,** 88-101.

LI, Y., WANG, Y., DING, A., LIU, X., GUO, J., LI, P., SUN, M., GE, F. & WANG, W. 2011. Impact of long-range transport and under-cloud scavenging no precipitation chemistry in East China. *Environmental Science and Pollution Research,* 18**,** 1544-1554.

LIKENS, G. E., DRISCOLL, C. T. & BUSO, D. C. 1996. Long-term effects of acid rain: Response and recovery of a forest ecosystem. *Science,* 272**,** 244-246.

LIU, B., KANG, S., SUN, J., ZHANG, Y., XU, R., WANG, Y., LIU, Y. & CONG, Z. 2013. Wet precipitation chemistry at a high-altitude site (3,326 m a.s.l.) in the southeastern Tibetan Plateau. *Environmental Science and Pollution Research,* 20**,** 5013-5027.

LIU, W., HE, X., PANG, S. & ZHANG, Y. 2017. Effect of relative humidity on O3 and NO2 oxidation of SO2 on a-Al2O3 particles. *Atmospheric Environment,* 167**,** 245-253.

LOMPAR, M., ĆURIĆ, M., ROMANIC, D., ZOU, L. & LIANG, H. 2018. Precipitation enhancement by cloud seeding using the shell structured TiO2/NaCl aerosol as revealed by new model for cloud seeding experiments. *Atmospheric research,* 212**,** 202-212.

LOURENS, A. S. M., BEUKES, J. P., VAN ZYL, P. G., FOURIE, G. D., BURGER, J. W., PIENAAR, J. J., READ, C. E. & JORDAAN, J. H. 2011. Spatial and temporal assessment of gaseous pollutants in the Highveld of South Africa. *South African Journal of Science,* 107**,** 8.

LOURENS, A. S. M., BUTLER, T. M., BEUKES, J. P., VAN ZYL, P. G., BEIRLE, S., WAGNER, T. K., HEUE, K.-P., PIENAAR, J. J., FOURIE, G. D. & LAWRENCE, M. G. 2012. Re-evaluating the NO2 hotspot over the South African Highveld. *South African Journal of Science,* 108**,** 6.

LU, J., GE, X., LIU, Y., CHEN, Y., XIE, X., OU, Y., YE, Z. & CHEN, M. 2019. Significant secondary organic aerosol production from aqueous-phase processing of two intermediate volatility organic compounds. *Atmospheric Environment,* 211**,** 63-68.

LUO, H., JIANG, B., LI, F. & LIN, W. 2019. Simulation of the effects of sea-salt aerosols on the structure and precipitation of a developed tropical cyclone. *Atmospheric Research,* 217**,** 120-127.

LUTGENS, F. K. & TARBUCK, E. J. 1982. *The atmosphere: an introduction to meteorology,* New Jersey, Prentice-Hall. 478.

LYNN, B. H., KHAIN, A. P., DUDHIA, J., ROSENFELD, D., POKROVSKY, A. & SEIFERT, A. 2005a. Spectral (bin) microphysics coupled with a mesoscale model (MM5). Part I: Model description and first results. *American Meteorological Society,* 133**,** 44-58.

LYNN, B. H., KHAIN, A. P., DUDHIA, J., ROSENFELD, D., POKROVSKY, A. & SEIFERT, A. 2005b. Spectral (bin) microphysics coupled with a mesoscale model (MM5). Part II: Simulation of a CaPE rain event with a squall line. *American Meteorological Society,* 133**,** 59-71.

MAHLABA, J. S., KEARSLEY, E. P. & KRUGER, R. A. 2011. Effect of fly ash characteristics on the behaviour of pastes prepared under varied brine conditions. *Minerals Engineering,* 24**,** 923-929.
MARTINEZ, D. & GORI, E. G. 1999. Raindrop size distributions in convective clouds over Cuba. *Atmospheric Research,* 52**,** 221-239.
MARZUKI, KOZU, T., SHIMOMAI, T., HASHIGUCHI, H., RANDEU, W. L. & VONNISA, M. 2010. Raindrop size distributions of convective rain over equatorial Indonesia during the first CPEA campaign. *Atmospheric Research,* 96**,** 645-655.
MATHER, G. K. 1991. Coalescence enhancement in large multicell storms caused by the emissions from a Kraft paper mill. *Journal of Applied Meteorology,* 30**,** 1134-1146.
MCCARTHY, T. & RUBIDGE, B. 2005. *The story of Earth and life: A southern African perspective on a 4.6 billion-year journey,* Cape Town, Struik. 333.
MCFIGGANS, G., ARTAXO, P., BALTENSPERGER, U., COE, H., FACCHINI, C., FEINGOLD, G., FUZZI, S., GYSEL, M., LAAKSONEN, A., LOHMANN, U., MENTEL, T. F., D.M., M., O'DOWD, C. D., SNIDER, J. R. & WEINGARTNER, E. 2005. The effect of physical and chemical aerosol properties on wam cloud droplet activation. *Atmospheric Chemistry and Physics,* 5**,** 8507-8646.
MCGRANAHAN, G. & MURRAY, F. (eds.) 2003. *Air pollution & health in rapidly developing countries,* VA: Earthscan. 227.
MEKIC, M., LIU, J., ZHOU, W., LOISEL, G., CAI, J., HE, T., JIANG, B., YU, Z., LAZAROU, Y. G. & LI, X. 2019. Formation of highly oxygenated multifunctional compounds from cross-reactions of carbonyl compounds in the atmospheric aqueous phase. *Atmospheric Environment***,** 117046.
MENZ, F. C. & SEIP, H. M. 2004. Acid rain in Europe and the United States: an update. *Environmental Science & Policy,* 7**,** 253-265.
METH, O. 2018. New satellite data reveals the world's largest air pollution hotspot is Mpumalanga-South Africa. Greenpeace. https://www.greenpeace.org/africa/en/press/4202/new-satellite-data-reveals-the-worlds-largest-air-pollution-hotspot-is-mpumalanga-south-africa/ [Accessed 29 October 2019].
MICHAELIDES, S., LEVIZZANI, V., ANAGNOSTOU, E., BAUER, P., KASPARIS, T. & LANE, J. E. 2009. Precipitation: Measurement, remote sensing, climatology and modelling. *Atmospheric Research,* 94**,** 512-533.
MOGALE, M. & DYSON, L. L. 2017. Continental tropical low-pressure systems and their associated rainfall over the Highveld of South Africa using self-organizing maps. 62-65.
MOGANELWA, A. 2013. *International technology transfer to accomplish process engineering designs for power plants. MEng. [Unpublished].* MSc in Engineering Management, University of Johannesburg.
MOHNEN, V. A. & KADLECEK, J. A. 1989. Cloud chemistry research at Whiteface Mountain. *Tellus B,* 41**,** 79-91.
MOODY, J. L. & SAMSON, P. J. 1989. The influence of atmospheric transport on the precipitation chemistry at two sites in the midwestern United States. *Atmospheric Environment,* 23**,** 2117-2132.
MPHEPYA, J. N., GALY-LACAUX, C., LACAUX, J. P., HELD, G. & PIENAAR, J. J. 2006. Precipitation chemistry and wet deposition in Kruger National Park, South Africa. *Journal of Atmospheric Chemistry* 53**,** 169-183.
MPHEPYA, J. N., PIENAAR, J. J., GALY-LACAUX, C., HELD, G. & TURNER, C. R. 2004. Precipitation chemistry in semi-arid areas of southern Africa: A case study of a rural and an industrial site. *Journal of Atmospheric Chemistry,* 47**,** 1-24.
MÜLLER, S., SZAKÁLL, M., MITRA, S. K., DIEHL, K. & BORRMANN, S. 2013. Shapes and oscillations of raindrops with reduced surface tensions: Measurements at the Mainz vertical wind tunnel. *Atmospheric Research,* 119**,** 38-45.
MUTHIGE, M. S., MALHERBE, J., ENGLEBRECHT, F., GRAB, S., BERAKI, A., MAISHA, T. R. & VAN DER MERWE, J. 2018. Projected changes in tropical cyclones over the South West Indian Ocean under different extents of global warming. *Environmental Research Letters,* 13**,** 065019.

NATIONAL ACADEMIES OF SCIENCES ENGINEERING AND MEDICINE 2016. *The Future of Atmospheric Chemistry Research: Remembering Yesterday, Understanding Today, Anticipating Tomorrow,* Washington, DC, The National Academies Press. 226.
NEL, A. & COBBING, J. R. D. 2019. South Africa. *Encyclopaedia Brittanica.* Encyclopaedia Brittanica, inc. https://www.britannica.com/place/South-Africa [Accessed 24 November 2019].
NEWELL, R. E., KIDSON, J. W., VINCENT, D. G. & BOER, G. J. 1972. *The general circulation of the tropical atmosphere and interactions with extratropical latitudes,* Cambridge, MIT Press. 258.
NISHIJO, M., NAKAGAWA, H., MORIKAWA, Y., TABATA, M., SENMA, M., MIURA, K., TAKAHARA, H., KAWANO, S., NISHI, M., MIZUKOSHI, K., KIDO, T. & NOGAWA, K. 1995. Mortality of inhabitants in an area polluted by cadmium: 15 year follow up. *Occupational and Environmental Medicine,* 52**,** 181-184.
ORUÉ, M. R., GAIERO, D. & KIRSCHBAUM, A. 2019. Seasonal characteristics of the chemical composition of rainwaters from Salta city, NW Argentina. *Environmental Earth Sciences,* 78. 16.
ÖZSOY, T., TÜRKER, P. & ÖRNEKTEKIN, S. 2008. Precipitation chemistry as an indicator of urban air quality in Mersin, North-Eastern Mediterranean Region. *Water Air Soil Pollution,* 189**,** 69-83.
PAPO, G. T. 2014. *Assessment of South African coals in a bubbling fluidised bed combustion testing facility.* MSc Eng, University of Witwatersrand.
PARK, S.-S., SIM, S. Y., BAE, M.-S. & SCHAUER, J. J. 2013. Size distribution of water-soluble components in particulate matter emitted from biomass burning. *Atmospheric Environment,* 73**,** 62-72.
PAULIQUEVIS, T., LARA, L. L., ANTUNES, M. L. & ARTAXO, P. 2012. Aerosol and precipitation chemistry measurements in a remote site in Central Amazonia: the role of biogenic contribution. *Atmospheric Chemistry and Physics,* 12**,** 4987-5015.
PENKETT, S. A., JONES, B. M. R., BRICE, K. A. & EGGLETON, A. E. J. 1978. The importance of atmospheric ozone and hydrogen peroxide in oxidising sulphur dioxide in cloud and rainwater. *Atmospheric Environment,* 13**,** 123-137.
PÉREZ, I. A., SÁNCHEZ, M. L., GARCÍA, M. A. & PARDO, N. 2017. Boundaries of air mass trajectory clustering: key points and applications. *International Journal of Environmental Science and Technology,* 14**,** 653-662.
PIETERS, R. 2007. *An assessment of dioxins, dibenzofurans and PCBs in the sediments of selected freshwater bodies and estuaries in South Africa.* Doctor of Philosophy, North-West University, Potchefstroom Campus.
PIKETH, S., ANNEGARN, H. & TYSON, P. 1999. Lower tropospheric aerosol loadings over South Africa: The relative contribution of aeolian dust, industrial emissions, and biomass burning. *Journal of Geophysical Research: Atmospheres,* 104**,** 1597-1607.
PIKETH, S. & PRANGLEY, A. R. 1999. Trajectory climatology of transboundary transport from the highveld. *Eskom Report.* Cleveland. 24.
POSSANZINI, M., BUTTINI, P. & DI PALO, V. 1988. Characterization of a rural area in terms of dry and wet deposition. *Science of the Total Environment,* 74**,** 111-120.
PRESTON-WHYTE, R. A. & TYSON, P. D. 1988. *The atmosphere and weather of southern Africa,* Cape Town, SA, Oxford University Press. 374.
PRETORIUS, I., PIKETH, S. J., BURGER, R. & NEOMAGUS, H. 2015. A perspective on South African coal fired power station emissions. *Journal of Energy in Southern Africa,* 26. 27-40.
PRUPPACHER, H. R. & KLETT, J. D. 1997. *Microphysics of clouds and precipitation*, Reidel. 954.
QA/SAC-AMERICAS. 2018. *The Quality Assurance Science Activity Centre - Lab Intercomparison Study Data* [Online]. World Meteorological Organisation Global Atmospheric Watch. Available: http://www.qasac-americas.org/lis/700152/57/rings [Accessed 18 January 2018 2018].
RAKOV, V. A. & UMAN, M. A. 2003. *Lightning: physics and effects,* Cambridge, UK, Cambridge University Press. 687.
RÄSÄNEN, M., AURELA, M., VAKKARI, V., BEUKES, J. P., TUOVINEN, J. P., VAN ZYL, P. G., JOSIPOVIC, M., VENTER, A. D., JAARS, K., SIEBERT, S. J., LAURILA, T., RINNE, J. &

LAAKSO, L. 2017. Carbon balnace of a grazed savanna grassland ecosystem in South Africa. *Biogeosciences,* 14**,** 1039-1054.
RAUBER, R. M., OLTHOFF, L. S., RAMAMURTHY, M. K. & KUNKEL, K. E. 2000. The relative importance of warm rain and melting processes in freezing precipitation events. *American Meteorological Society,* 39**,** 1185-1195.
RAUBER, R. M. & TOKAY, A. 1991. An explanation for the existence of supercooled water at the top of cold clouds. *Journal of Atmospheric Sciences,* 48**,** 1005-1023.
REN, Q. & ZHAO, C. 2012. NOx and N2O Precursors from Biomass Pyrolysis: Nitrogen Transformation from Amino Acid. *Environmental Science & Technology,* 46**,** 4236-4240.
REYNOLDS, B., FOWLER, D. & THOMAS, S. 1996. Chemistry of cloud water at an upland site in mid-Wales. *The Science of the Total Environment,* 188**,** 115-125.
ROBERTS, G., WOOSTER, M. & LAGOUDAKIS, E. 2009. Annual and diurnal african biomass burning temporal dynamics. *Biogeosciences,* 6**,** 849-866.
ROBERTS, J. S. 2003. Dew point temperature. *In:* HELDMAN, D. R. (ed.) *Encyclopedia of agricultural, food, and biological engineering.* New York, NY: Marcel Dekker. 1208.
RODHE, H., DENTENER, F. & SCHULZ, M. 2002. The global distribution of acidifying wet deposition. Environmental Science & Technology, 36, 4382-4388.
RODRIGUEZ, C. A. M., DA ROCHA, R. P. & BOMBARDI, R. 2010. On the development of summer thunderstorms in the city of São Paulo: Mean meteorological characteristics and pollution effect. *Atmospheric Research,* 96**,** 477-488.
ROSENFELD, D., RUDICH, Y. & LAHAV, R. 2001. Desert dust suppressing precipitation— A possible desertification feedback loop. *Proceedings of the National Academy of Sciences of the United States of America,* 98**,** 5975-5980.
ROSENFELD, D., SHERWOOD, S., WOOD, R. & DONNER, L. 2014. Climate effects of aerosol-cloud interactions. *Science,* 343**,** 379-380.
ROSENFELD, D. & WOODLEY, W. L. 2000. Convective clouds with sustained highly supercooled liquid water down to-37.5C. *Nature,* 405**,** 440-442.
ROSENFELD, D., WOODLEY, W. L., KHAIN, A. P., COTTON, W. R., CARRIO, G., GINIS, I. & GOLDEN, J. H. 2012. Aerosol effects on microstructure and intensity of tropical cyclones. *Bulletin of the American Meteorological Society***,** 987-1001.
ROSS, K., PIKETH, S., BRUINTJES, R., BURGER, R., SWAP, R. & ANNEGARN, H. 2003. Spatial and seasonal variations in CCN distribution and the aerosol-CCN relationship over southern Africa. *Journal of Geophysical Research: Atmospheres,* 108. 18.
ROUAULT, M., ROY, S. S. & BALLING JR, R. C. 2013. The diurnal cycle of rainfall in South Africa in the austral summer. *International Journal of Climatology,* 33**,** 770-777.
ROY, D. P., BOSCHETTI, L., JUSTICE, C. O. & JU, J. 2008. The collection 5 MODIS burned area product - Global evaluation by comparison with the MODIS active fire product. *Remote Sensing of Environment,* 112**,** 3690-3707.
SANGER, L. J., BILLETT, M. F. & CRESSER, M. S. 1996. The effect of precipitation chemistry upon anion and cation fluxes from the surface layer of ombrotrophic mires in the UK. *Journal of Applied Ecology,* 33**,** 754-772.
SANTACHIARA, G., DI MATTEO, L., PRODI, F. & BELOSI, F. 2010. Atmospheric particles acting as ice forming nuclei in different size ranges. *Atmospheric Research,* 96**,** 266-272.
SAWS. 2017. *Historical rainfall maps* [Online]. South African Weather Service. Available: http://www.weathersa.co.za/climate/historical-rain-maps; http://www.weathersa.co.za/home/historicalrain [Accessed 26 February 2018].
SAWS. 2019. *South African Weather Service (SAWS)* [Online]. Available: http://www.weathersa.co.za/observations/synoptic-charts; http://www.weathersa.co.za/home/historicalsynoptic [Accessed 2019].
SCHINDLER, D. W. 1988. Effects of acid rain on freshwater ecosystems. *Science,* 239**,** 149-157.
SCHLESINGER, W. H. & HARTLEY, A. E. 1992. A global budget for atmospheric NH 3. *Biogeochemistry,* 15**,** 191-211.
SCHMELLER, G. & GERESDI, I. 2019. Study of interaction between cloud microphysics and chemistry using coupled bin microphysics and bin aqueous chemistry scheme. *Atmospheric Environment,* 198**,** 366-380.

SCHREUDER, D. 2006. Technologies for emissions reduction in the metallurgical and chemical process industries. *International Platinum Conference 'Platinuim Surges Ahead.* The Southern African Institute of Mining and Metallurgy. 181-190.
SCHWAB, J. J., CASSON, P., BRANDT, R., HUSAIN, L., DUTKEWICZ, V., WOLFE, D., DEMERJIAN, K. L., CIVEROLO, K. L., RATTIGAN, O. V., FELTON, H. D. & DUKETT, J. E. 2016. Atmospheric chemistry measurements at Whiteface Mountain, NY: Cloud water chemistry, precipitation chemistry, and particulate matter. *Aerosol and Air Quality Research,* 16**,** 841-854.
SCHWARTZ, S., BENKOVITZ, C. & GUO, G. 2002. Aerosol influence on cloud microphysics examined by satellite measurements and chemical transport modeling. *Journal of the Atmospheric Sciences,* 59**,** 714-725.
SCORGIE, Y. 2012. *Urban air quality management and planning in South Africa.* PhD in Environmental Science, University of Johannesburg.
SEINFELD, J. H. & PANDIS, S. N. 2006. Atmospheric chemistry and physics: From air pollution to climate change. 2 ed. NJ: John Wiley & Sons. 1152.
SEVRUK, B. 1996. Adjustment of tipping-bucket precipitation gauge measurements. *Atmospheric Research,* 42**,** 237-246.
SHALLCROSS, D. E., WANG, K. Y. & DIMMER, C. H. 2003. Biogeochemical cycles and residence times. *In:* HEWITT, C. N. & JACKSON, A. (eds.) *Handbook of atmospheric science: Principles and applications.* Oxford: Blackwell Science. 90-123.
SHEN, Z., ZHANG, L., CAO, J., TIAN, J., LIU, L., WANG, G., ZHAO, Z., WANG, X., ZHANG, R. & LUI, S. 2012. Chemical composition sources, deposition fluxes of water-soluble inorganic ions obtained from precipitation chemistry measurements collected at an urban site in northwest China. *Journal of Environmental Monitoring,* 14**,** 3000-3008.
SIMPSON, L. & DYSON, L. L. 2018. Severe weather over the Highveld of South Africa during November 2016. *Water SA,* 44**,** 75-85.
STATSOFT, I. 2006. SATISTICA (data analysis software system). 7.1 ed.
STEFELS, J., STEINKE, M., TURNER, S., MALIN, G. & BELVISO, S. 2007. Environmental constraints on the production and removal of the climatically active gas dimethylsulphide (DMS) and implications for ecosystem modelling. *Biogeochemistry,* 83**,** 245-275.
STEIN, A. F., DRAXLER, R. R., ROLPH, G. D., STUNDER, B. J. B., COHEN, M. D. & NGAN, F. 2015. NOAA's HYSPLIT atmospheric transport and dispersion modeling system. *American Meteorological Society***,** 2059-2077.
STERN, D. I. 2006. Reversal of the trend in global anthropogenic sulfur emissions. Global Environmental Change, 16, 207-220.
STOHL, A. 1998. Computation, accuracy and applications of trajectories - A review and bibliography. *Atmospheric Environment,* 32**,** 947-966.
STOHL, A., ECKHARDT, S., FORSTER, C., JAMES, P., SPICHTINGER, N. & SEIBERT, P. 2002. A replacement for simple back trajectory calculations in the interpretation of atmospheric trace substance measurements. *Atmospheric Environment,* 36**,** 4635-4648.
STOHL, A. & KOFFI, N. E. 1998. Evaluation of trajectories calculated from ECMWF data against constant volume balloon flights during ETEX. *Atmospheric Environment,* 32**,** 4151-4156.
SUN, M., WANG, Y., WANG, T., FAN, S., WANG, W., LI, P., GUO, J. & LI, Y. 2010. Cloud and the corresponding precipitation chemistry in south China: Water-soluble components and pollution transport. *Journal of Geophysical Research,* 115**,** D22303.
SWARTZ, J. 2019. Long-term trends of ambient gaseous concentrations at South African DEBITS sites and wet deposition at Cape Point. Doctor of Philosophy in Environmental Sciences with Chemistry, North-West University.
SZAKÁLL, M., MITRA, S. K., DIEHL, K. & BORRMANN, S. 2010. Shapes and oscillations of falling raindrops- A review. *Atmospheric Research,* 97**,** 416-425.
TAKENAKA, N., DAIMON, T., UEDA, A., SATO, K., KITANO, M., BANDOW, H. & MAEDA, Y. 1998. Fast oxidation reaction of nitrite by dissolved oxygen in the freezing process in the tropospheric aqueous phase. *Journal of Atmospheric Chemistry,* 29**,** 135-150.

TANG, S., WANG, K. Y., XIANG, Y., TIAN, D., WANG, J., LIU, Y., CAO, B., GUO, D. & NIU, S. 2019. Heavy grazing reduces grassland soil greenhouse gas fluxes: A global meta-analysis. *Science of the Total Environment,* 654**,** 1218-1224.
TANG, Y., HAN, Y., MA, X. & LIU, Z. 2018. Elevated heat pump effects of dust aerosol over Northwestern China during summer. *Atmospheric Research,* 203**,** 95-104.
TERBLANCHE, D., MITTERMAIER, M., BURGER, R., PIKETH, S. & BRUINTJES, R. 2000. The Aerosol Recirculation and Rainfall Experiment (ARREX): an initial study on aerosol-cloud. *South African Journal of Science,* 96.
THOMPSON, D. G., STEPHENSON, G. R., SOLOMON, K. R. & SKEPASTS, A. V. 1984. Persistence of (2,4-dichlorophenoxy)acetic acid and 2-(2,4-dichlorophenoxy)propionic acid in agricultural and forest soils of northern and southern Ontario. *Journal of Agricultural and Food Chemistry,* 32**,** 578-581.
TIITTA, P., VAKKARI, V., CROTEAU, P., BEUKES, J. P., VAN ZYL, P. G., JOSIPOVIC, M., VENTER, A. D., JAARS, K., PIENAAR, J. J., NG, N. L., CANAGARATNA, M. R., JAYNE, J. T., KERMINEN, V.-M., KOKKOLA, H., KULMALA, M., LAAKSONEN, A., WORSNOP, D. & LAAKSO, L. 2014. Chemical composition, main sources and temporal variability of PM1 aerosols in southern African grassland. *Atmospheric Chemistry and Physics,* 14. 1909-1927.
TOST, H., JÖCKEL, P., KERKWEG, A., POZZER, A., SANDER, R. & LELIEVELD, J. 2007. Global cloud and precipitation chemistry and wet deposition: tropospheric model simulations with ECHAM5/MESSy1. *Atmospheric Chemistry and Physics,* 7**,** 2733-2757.
TRIPATHEE, L., GUO, J., KANG, S., PAUDYAL, R., HUANG, J., SHARMA, C. M., ZHANG, Q., CHEN, P., GHIMIRE, P. S. & SIGDEL, M. 2019. Saptial and temporal distribution of total mercury in atmospheric wet precipitation at four sites from the Nepal-Himalayas. *Science of the Total Environment,* 655**,** 1207-1217.
TYSON, P. D., GARSTANG, M. & SWAP, R. 1996. Large-scale recirculation of air over southern Africa. *Journal of Applied Meteorology,* 35**,** 2218-2236.
TYSON, P. D. & PRESTON-WHYTE, R. A. 2017. *The Weather and Climate of Southern Africa,* Cape Town, South Africa, Oxford University Press. 408.
UCHIYAMA, R., OKOCHI, H., OGATA, H., KATSUMI, N. & NAKANO, T. 2019. Characteristics of trace metal concentration and stable isotopic composition of hydrogen and oxygen in "urban-induced heavy rainfall" in downtown Tokyo, Japan; The implication of mineral/dust particles on the formation of summer heavy rainfall. *Atmospheric Research,* 217**,** 73-80.
UIJLENHOET, R. & STRICKER, J. N. M. 1999. A consistent rainfall parameterization based on the exponential raindrop size distribution. *Journal of Hydrology,* 218**,** 101-127.
UNIDO 2018. Competitive industrial performance report 2018. In: ORGANIZATION, U. N. I. D. (ed.) Biennial CIP report. 2018 ed.
URONE, P. P. 2001. *College physics,* California, Brooks/Cole. 893.
VAISALA 1999. Ceilometer CT25K User's Guide. *In:* VAISALA (ed.).
VAKKARI, V., BEUKES, J. P., LAAKSO, H., MABASO, D., PIENAAR, J. J., KULMALA, M. & LAAKSO, L. 2013. Long-term observations of aerosol size distributions in semi-clean and polluted savannah in South Africa. *Atmospheric Chemistry and Physics,* 13**,** 1751-1770.
VAKKARI, V., KERMINEN, V. M., BEUKES, J. P., TIITTA, P., ZYL, P. G., JOSIPOVIC, M., VENTER, A. D., JAARS, K., WORSNOP, D. R. & KULMALA, M. 2014. Rapid changes in biomass burning aerosols by atmospheric oxidation. *Geophysical Research Letters,* 41**,** 2644-2651.
VAKKARI, V., TIITTA, P., JAARS, K., CROTEAU, P., BEUKES, J. P., JOSIPOVIC, M., KERMINEN, V. M., KULMALA, M., VENTER, A. D. & VAN ZYL, P. G. 2015. Reevaluating the contribution of sulfuric acid and the origin of organic compounds in atmospheric nanoparticle growth. *Geophysical Research Letters,* 42**,** 10,486-10,493.
VENTER, A. D., VAKKARI, V., BEUKES, J. P., VAN ZYL, P. G., LAAKSO, H., MABASO, D., TIITTA, P., JOSIPOVIC, M., KULMALA, M., PIENAAR, J. J. & LAAKSO, L. 2012. An air quality assessment in the industrialised western Bushveld Igneous Complex, South Africa. *South African Journal of Science,* 108**,** 10.

VENTER, A. D., VAN ZYL, P. G., BEUKES, J. P., JOSIPOVIC, M., HENDRIKS, J., VAKKARI, V. & LAAKSO, L. 2017. Atmospheric trace metals measured at a regional background site (Welgegund) in South Africa. *Atmospheric Chemistry and Physics,* 17**,** 4251-4263.

VET, R., ARTZ, R. S., CAROU, S., SHAW, M., RO, C. U., AAS, W., BAKER, A., BOWERSOX, V. C., DENTENER, F., GALY-LACAUX, C., HOU, A., PIENAAR, J. J., GILLETT, R., FORTI, M. C., GROMOV, S., HARA, H., KHODZER, T., MAHOWALD, N. M., NICKOVIC, S., RAO, P. S. P. & REID, N. W. 2014. A global assessment of precipitation chemistryand deposition of sulfur, nitrogen, sea salt, base cations, organic acids, acidity and pH, and phosphorus. *Atmospheric Environment*. 3-100.

WALKER, S. & TSUBO, M. 2003. Estimation of rainfall intensity for potential crop production on clay soil with in-field water harvesting practices in a semi-arid area. Bloemfontein, South Africa: Water Research Commission. 113.

WALLACE, J. M. & HOBBS, P. V. 2006a. Atmospheric Chemistry. *In:* DMOWSKA, R., HARTMANN, D. & ROSSBY, H. T. (eds.) *Atmospheric Science: An introductory survey.* Canada: Elsevier.465.

WALLACE, J. M. & HOBBS, P. V. 2006b. Cloud Microphysics. *In:* DMOWSKA, R., HARTMANN, D. & ROSSBY, H. T. (eds.) *Atmospheric Science: An Introductory Survey.* Canada: Elsevier. 465.

WALLACE, J. M., HOBBS, P. V., MCMURDIE, L. & HOUZE, R. A. 2006. Weather Systems. *In:* DMOWSKA, R., HARTMANN, D. & ROSSBY, H. T. (eds.) *Atmospheric Science: An Introductory Survey.* Canada: Elsevier. 465.

WELGEGUND. 2018. *Welgegund measurement station* [Online]. Available: http://www.welgegund.org/site-description [Accessed 12 March 2019].

WESTERVELT, D., PIERCE, J. & ADAMS, P. 2014. Analysis of feedbacks between nucleation rate, survival probability and cloud condensation nuclei formation. *Atmospheric Chemistry and Physics,* 14**,** 5577-5597.

WEX, H., STRATMANN, F., TOPPING, D. & MCFIGGANS, G. 2008. The Kelvin versus the Raoult Term in the Köhler Equation. *Journal of the Atmospheric Sciences,* 65**,** 4004-4016.

WMO 2004. Manual for the GAW Precipitation chemistry programme. *In:* WATCH, W. M. O. G. A. (ed.). 182.

XU, D., GE, B., WANG, Z., SUN, Y., CHEN, Y., JI, D., YANG, T., MA, Z., CHENG, N. & HAO, J. 2017. Below-cloud wet scavenging of soluble inorganic ions by rain in Beijing during the summer of 2014. *Environmental Pollution,* 230**,** 963-973.

XU, Z., WU, Y., LIU, W. J., LIANG, C. S., JI, J., ZHAO, T. & ZHANG, X. 2015. Chemical composition of rainwater and the acid neutralizing effect at Beijing and Chizhou city, China. *Atmospheric Research,* 164-165**,** 278-285.

YANG, F., TAN, J., SHI, Z. B., CAI, Y., HE, K., MA, Y., DUAN, F., OKUDA, T., TANAKA, S. & CHEN, G. 2012. Five-year record of atmospheric precipitation chemistry in urban Beijing, China. *Atmospheric Chemistry and Physics,* 12**,** 2025-2035.

YAO, Z. T., JI, X. S., SARKER, P. K., TANG, J. H., GE, L. Q., XIA, M. S. & XI, Y. Q. 2015. A comprehensive review on the applications of coal fly ash. Earth-Science Reviews, 141, 105-121.

YIN, Y., LEVIN, Z., REISIN, T. G. & TZIVION, S. 2000. The effects of giant cloud condensation nuclei on the development of precipitation in convective clouds—A numerical study. *Atmospheric research,* 53**,** 91-116.

ZHANG, L., MICHELANGELI, D. V., DJOUAD, R. & TAYLOR, P. A. 2006a. Modeling studies of the sulfur cycle in low-level, warm stratiform clouds. *Atmospheric research,* 80**,** 187-217.

ZHANG, L., VET, R. & MICHELANGELI, D. V. 2006b. Numerical investigation of gas scavenging by weak precipitation. *Journal of Atmospheric Chemistry,* 53**,** 203-231.

ZHANG, Y., KANG, S., LI, C., CONG, Z. & ZHANG, Q. 2012. Wet deposition of precipitation chemistry during 2005-2009 at a remote site (Nam Co Station) in central Tibetan Plateau. *Journal of Atmospheric Chemistry,* 69**,** 187-200.

ZHAO, B., LIOU, K. N., GU, Y., LI, Q., JIANG, J. H., SU, H., HE, C., TSENG, H. L. R., WANG, S., LIU, R., QI, L., LEE, W. L. & HAO, J. 2017. Enhanced PM2.5 pollution in China due to aerosol-cloud interactions. *Scientific Reports,* 7. 1-11.

ZHAO, S., YU, Y., HE, J., YIN, D. & WANG, B. 2015. Below-cloud scavenging of aerosol particles by precipitation in a typical valley city, northwestern China. *Atmospheric Environment,* 102**,** 70-78.
ZUNCKEL, M., ROBERTSON, L., TYSON, P. & RODHE, H. 2000. Modelled transport and deposition of sulphur over Southern Africa. *Atmospheric Environment,* 34**,** 2797-2808.